Assessing key physical properties of the Rotorua, Kaharoa and Taupō tephras for their potential use in hydroponics

A thesis presented in partial fulfilment of the requirements for the degree of

Master of Science

In

Earth Science

At Massey University, Manawatū,

New Zealand.

Susan McLachlan

2024

Abstract

Food security is an increasing concern as global populations grow and fertile land availability decreases. Hydroponics, where plants are grown in a soilless medium or nutrient solution, is a potential method of securing food supplies. Understanding the physical and chemical properties of growth media is important as they influence plant growth and productivity. Pumice, a vesicular lightweight material produced by volcanic eruptions, is used in some areas as a growth medium due to its ability to support plant growth. This natural resource is abundant in New Zealand but currently underutilised. The Taupō and Okataina Volcanic Centres (TVC and OVC) in the Central North Island have produced vast volumes of pyroclastic material in the last >60,000 years. This study focused on some of their youngest eruptives, the Kaharoa (OVC), Rotorua (OVC) and Taupō Y (TVC) tephras, to assess their suitability as hydroponic growth media.

Samples of the Kaharoa, Rotorua, Taupō Y2 and Y5 deposits and the commercially available Daltons pumice were characterised for grain size then split into hydroponic grades of 1-4 mm and 4-8 mm. The physical properties were used to define relationships between volcanological and hydroponic parameters. Componentry of the grades and pumice clast morphology, texture, density, and porosity were characterised. Vertical variations in the Rotorua and Taupō tephra profiles reflect changes in the eruption plume, degassing and/or conduit processes during the eruption. Settling velocities are reflected in lateral changes in pumice clast shape, size, and density in the Kaharoa deposits.

The hydroponic parameters water holding capacity (WHC), bulk density and total porosity were found to be closely related to clast density and porosity and generally fall within the range of the tested hydroponic media. However, tephra WHC was generally lower than that of the hydroponic media. The low bulk density of the tephras particularly the 4-8 mm grade make them a relatively light material, however, their low WHC may limit their usefulness as a growing medium or require more frequent or alternate methods of irrigation. The higher bulk density and WHC of the 1-4 mm grade means it is likely to be better suited for many species.

Acknowledgments

I would like to sincerely thank my supervisors Dr. Anke Zernack and Prof. Gert Lube who have provided ideas, support, guidance, and feedback throughout this work. This work, from the concept through selecting sample locations and field work, laboratory work and the writing of the report would not have been possible without your help.

I would like to thank Dr. Anke Zernack, Prof. Jonathan Proctor, Matapura Ellison and Ron McLachlan for assistance with funding applications, and the Graduate Women Manawatū (GWM) Charitable Trust and Te Rūnanaga o Ngāi Tahu for their financial assistance and support.

Thank you to Dr Anja Moebis for your time, assistance, and tutelage in the Laboratory. You have gone above and beyond in picking up the pieces.

I would like to thank Ian Furkert and Shannon Mills for their help, assistance, and support in the Laboratory.

Landowners Charlotte Mogg and TW Moore for allowing access to quarries on their properties.

Thank you to Anne McLachlan for their help with proofreading this report.

Thank you to my employer Jonathan Findon for allowing me the time I needed to complete this thesis.

A big thanks must go to my close family including my husband Steve Madgwick and children Lachlan and Evelyn Fasher and friends who have encouraged and supported me throughout this thesis. Your love and support have been invaluable.

Without the support and assistance of so many wonderful people this work would not have been completed.

Table of Contents

List of Figures

List of Tables

List of abbreviations

Volcanics

HLVZ	Haroharo Linear Vent Zone
OVC	Okataina Volcanic Centre
TLVC	Tarawera Linear Vent Zone
TVC	Taupō Volcanic Centre
TVZ	Taupō Volcanic Zone
PDC	Pyroclastic Density Currents

Volcanic Parameters

Gradistat Calculations

Φ1	Cumulative proportions
Φ5	Cumulative proportions
Φ16	Cumulative proportions
Φ 50	Cumulative proportions
Φ75	Cumulative proportions
Φ84	Cumulative proportions
Φ95	Cumulative proportions
Mz	Mean
Sk	Skewness
K	Kurtosis

Air Space & Bulk Density

As	Air space
Vw	Water volume (ml)
Vs	Sample volume (ml)
Db	Sample bulk density (g/cm^3)
Md	Mass of dry sample

Particle Densities

Vg	Clast volume (accessed by gas)
Vc	Sample chamber volume
Vr	Reference chamber volume
P1	First pressure
P2	Second pressure
dc	Skeletal density
Mg	Mass of clast
de	Envelope density (clast bulk density)
Vb	Bulk volume of clast
ds	Solid / total density
Mp	Mass of crushed clast
Φc	Connected porosity
Φi	Isolated porosity
Φt	Total porosity

Hydroponic Parameters

ω	Water holding capacity
Mw	Mass of wet sample
Md	Mass of dry sample
Mc	Mass of container
ωSP	Gravimetric water content at stress point.
ωPWP	Gravimetric water content at permanent wilting point.
ωt	Total water holding capacity
ωr	Readily water holding capacity.

1 Introduction

1.1 Research Problem

Increasing global population, urban expansion, loss of production land, soil degradation, increased resource consumption, more extreme weather due to climate change and a reduction in freshwater means that food security is an increasing concern globally (Wilson & Houghton (2004) as cited in Kennard et al., 2020; Kriewald et al., 2019). By using hydroponic food cultivation, food security may be increased and when grown locally can also reduce the costs and impacts of food transport (Kennard et al., 2020; Kriewald et al., 2019). Hydroponic food production involves growing plants without soil in a growth medium or water based nutrient solution (Kennard et al., 2020). This involves delivering macro- and micro-nutrients directly to the roots via water, allowing plants to be grown closer together, out of season, or in locations currently unsuitable for agriculture (Schafer, 2020).

Grown hydroponically root-water nutrient interactions are maximised, resulting in greater growth rates as plants do not need to grow the protective tissues they require in soil (Volder & van Iersel, 2019). However, there are disadvantages such as higher costs to set up and run, the greater skill levels required to manage the system, and environmental impacts from nutrient solution or growth media disposal after use, particularly in open systems (Morgan, 2021).

Hydroponic systems may be open where the nutrient solution is disposed of after use or closed where the solution is collected for reuse (Jones, 2005; Morgan, 2021). Hydroponic systems may involve suspending plant roots in water (also referred to as hydroculture) or growing plants in a substrate or growth medium to support the plants root system (Morgan, 2021; Schafer, 2020). Most growers prefer a porous substrate with substrates currently in use including rockwool, peat, coir and pumice or combinations of these (Schafer, 2020). Further classification of a hydroponic system is based on the method in which nutrients are supplied, these include drip irrigation, ebb and flow, capillary fed, continuous flow or aeroponic misting (Morgan, 2021).

The physical and chemical properties of hydroponic growth media influence their ability to supply oxygen and water to roots (Bar-Tal et al., 2019). Physical properties such as the size and shape of

particles, bulk density and porosity are important in determining a medium's ability to provide the stability and support the plant requires, absorb and retain water to allow nutrient delivery to roots, while allowing for air circulation and drainage and preventing root damage from temperature extremes (Bar-Tal et al., 2019; Gizas & Savvas, 2007; Likitlersuang et al., 2022; PureHydroponics, 2023; Volder & van Iersel, 2019).

Growth media may be synthetic (polyurethane, polystyrene, or polyester fleece), organic (peat, coconut coir, wood fibre or sawdust), or inorganic, which may be natural and unmodified (pumice, sand, scoria, tuff) or processed (expanded clay, perlite, vermiculite, zeolite, foamed glass and rockwool) (Bar-Tal et al., 2019; Kennard et al., 2020; Schafer, 2020). Disadvantages of organic materials include compaction and environmental implications such as habitat destruction, reduction in species diversity, release of greenhouse gases during processing and transport, and disposal of used media to land fill (Carlile et al., 2019). Inorganic materials may also have environmental implications due to manufacturing and disposal methods (Kennard et al., 2020).

The properties of traditional growth medians such as coconut husk / coir from around the world are well researched (Altland et al., 2011; Gizas & Savvas, 2007). A growth medium with a low bulk density and high porosity is required in hydroponics to ensure water and air can be provided to the plant (Wallach, 2019). Pumice is an inert inorganic material consisting of vesicular volcanic glass with a low density of 0.4-0.8 g/cm^3 and a high total porosity of 70-85 vol.% formed during a volcanic eruption (Bar-Tal et al., 2019); this gives it the ability to store air and water. Due to being inert, nutrient supply to the plant can be controlled. Additionally, it retains its structure, can be reused many times and can be disposed of without causing environmental pollution (Bar-Tal et al., 2019; Marinou et al., 2013).

Pumice properties vary between volcanic centres and eruptions, resulting in a range of pumice types in the Taupō Volcanic Zone (TVZ) in the Central North Island of New Zealand. Numerous large explosive eruptions in the TVZ over the past >2Ma have resulted in many different pumice types from 8 eruption centres (Cole et al., 1995; Pittari et al., 2021; Wilson et al., 1995). It is

currently an underutilised natural resource in NZ and iwi are increasingly interested in utilising the pumice resources found in their rohe.

The use of pumice in hydroponics has been studied in practice by several authors (Gizas & Savvas, 2007; Marinou et al., 2013; Papadopoulos et al., 2008; Pérez-Urrestarazu et al., 2019; Raviv et al., 1999; Sahin et al., 2005). Marinou et al. (2013) compared strawberry growth in pumice, sawdust, and coco soil, while Sahin et al. (2005) compared strawberry growth. Gizas and Savvas (2007) investigated gypsophilis, rose, cucumber and lettuce growth in differing proportions of pumice. Pérez-Urrestarazu et al. (2019) studied the use of pumice in vertical greening walls and Raviv et al. (1999) compared the growth of roses in tuff and pumice from Italy and Greece. All studies found growth was improved in smaller pumice grades, or a mix which included pumice.

In the Bay of Plenty, pumice from local sand quarries is already being used by nurseries in the By of Plenty (BOP) for growing and propagation. Furthermore, pumice derived as a by-product from sand mining is marketed by suppliers such as Daltons and Ausperl in various grade sizes as a growing medium and horticultural product for the home garden. However, no systematic studies of the unique hydroponic properties of New Zealand pumice were identified during this research.

1.2 Research Aims

This thesis focuses on pumice derived from two active calderas (Taupō and Okataina) in the TVZ, which have erupted frequently during the last 60,000 years producing vast volumes of pyroclastic material. The physical properties of pumice from some of the youngest eruptions from the Taupo, Haroharo and Tarawera volcanic centres are compared to assess the suitability for their use in hydroponics.

The principal aims are:

1. To define the physical properties of three young pumice deposits in the Central North Island of New Zealand, namely the Rotorua, Kaharoa and Taupō Y2 and Y5 tephras.
2. To establish relationships between their volcanological and hydroponic properties.
3. To compare these parameters with those of coir and a commercially available pumice currently in use in the Central North Island and with locally sourced harakeke.
4. Determine the suitability of the three tested pumice types as growth media.

1.3 Thesis Structure

Introduction

The introduction discusses the research problem identified and why this research has been undertaken. The research aims of the study are set.

Hydroponics

This section contains an introduction to hydroponics and why hydroponics food production is important for the future. The properties and sources of growth media are discussed along with the use of pumice as a growth medium.

Evolution and Volcanic Products of the Taupō Volcanic Zone

This section provide background on the Taupō Volcanic Zone (TVZ), the Okataina Volcanic Centre (OVC) and the Taupō Volcanic Centre (TVC). The Rotorua (15.6ka), Kaharoa (0.7ka) and Taupō (1.8ka) tephras and related literature are introduced based on existing literature.

Methodology

This section sets out sample collection and preparation and the methods used to analyse the volcanological and hydroponic properties of the tephras and hydroponic media.

Results

Results from analyses of the volcanological and hydroponic properties of the tephras are provided in text and/or graphical form as relevant to the data.

Discussion

The discussion comprises three parts: Firstly, the differences of tephra units from the same eruption and between eruptions are discussed in the context of existing literature. Secondly, the hydroponic properties of the tephras are discussed. Finally, the relationships between the tephras and the supplied hydroponic media are discussed.

Conclusion

The conclusion links back to the research aims and provides a summary and concluding remarks of this thesis. Areas requiring further investigation or study are suggested.

2 Literature review

2.1 Hydroponics

Due to growing populations, urban expansion, lack of green spaces in densely populated areas, degradation of soils, an increase in extreme weather events and decreasing freshwater resources, food security is becoming an increasing concern (Kennard et al., 2020; Pérez-Urrestarazu et al., 2019). Growing food hydroponically, where plants are grown without soil and nutrients are delivered directly to the roots via water may help address these food security issues (Kennard et al., 2020; Schafer, 2020). Additionally, growing plants hydroponically in vertical systems on buildings is an option for increasing green space (Pérez-Urrestarazu et al., 2019).

Hydroponics involves growing plants without the use of soil, usually in a porous substrate or growth medium such as peat, coir, and pumice that both, supports and allows for delivery of nutrients directly to the root system (Morgan, 2021; Schafer, 2020). This maximises root, water, and nutrient interactions, improves water and fertiliser efficiency and avoids many soilborne diseases (Morgan, 2021; Volder & van Iersel, 2019). This approach improves the yield and quality of crops and plants can be grown closer together and/or out of season or in greenhouses for areas unsuitable for agriculture (Morgan, 2021; Schafer, 2020). However, capital and running costs are higher compared to traditional methods and require an increase in grower skills to manage the system (Morgan, 2021).

To allow for plant protection and greater control over the growing environment most hydroponic systems use a greenhouse or other structure (such as shade houses in hotter climates) for crop protection (Morgan, 2021; Schafer, 2020). These systems can range in size, type and complexity from small systems on benches covered with plastic to large systems in warehouses with carbon dioxide regulation and artificial lighting to further increase crop growth and yield throughout the year (Morgan, 2021).

Hydroponic systems are classified by the way in which nutrients are delivered and may be closed where the nutrient solution is collected and reticulated for reuse or open where the nutrient solution is discarded after use (Jones, 2005; Morgan, 2021).

Closed systems include the Ebb and flow (flood and drain) system that periodically floods the root system with a nutrient solution (ebb) which drains into a reservoir to be reticulated for reuse (Figure 2.1a) (Growace, 2023). The Nutrient Film Technique (NFT) is similar to ebb and flow and involves using a pump to deliver nutrient solutions to roots; any unused solution is collected and returned to the pump reservoir for reuse (Figure 2.1b) (Jones, 2005). Capillary systems move a nutrient solution between two areas providing subsurface irrigation; the movement of the solution as it enters and leaves the rootzone increases gas exchange (Figure 2.1c) (Capillary Flow, 2023).

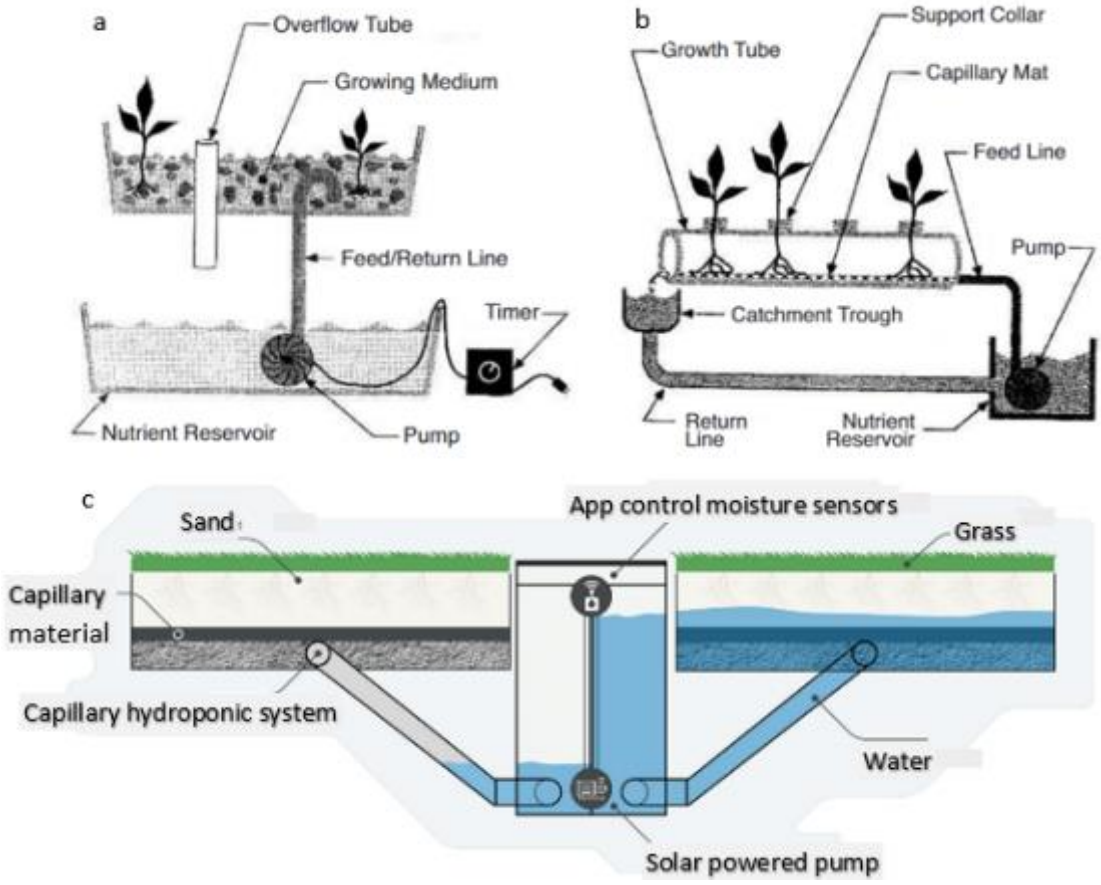

Figure 2.1: Hydroponic systemsa. Ebb and flow system; b. Typical NFT arrangement in which unused solution is returned to the reservoir (image from Jones, 2005); c. Capillary flow system (image from Capillary Flow, 2023).

Open systems include using drip/pass-through irrigation where a drip tube to the base of the plant is inserted next to the plant and any excess nutrient solution drains through holes in the base of the container (Figure 2.2) (Jones, 2005).

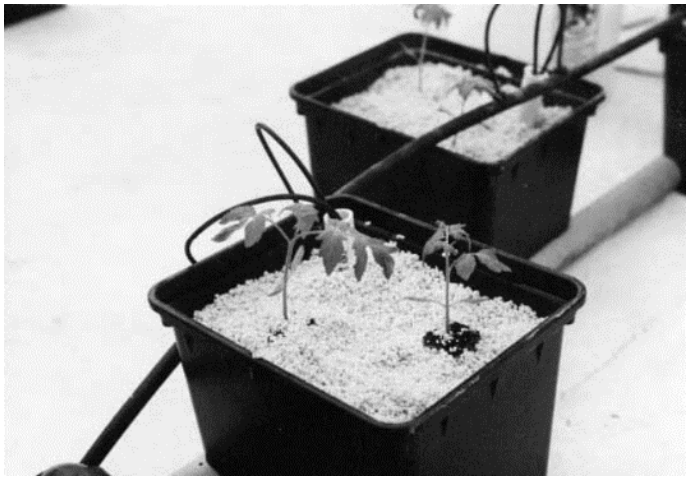

Figure 2.2: Drip/pass through irrigation where tubes deliver a nutrient solution to the plants (image from Jones, 2005).

2.1.1 Growth media

Hydroponic media are selected based on their physical and chemical properties, which determine their ability to provide oxygen, water, and nutrients to roots (Bar-Tal et al., 2019; Gizas & Savvas, 2007; Papadopoulos et al., 2008; Sahin et al., 2005; Wallach, 2019). High porosity in growth media enables roots to easily access water and oxygen and a low bulk density reduces mechanical impedance to root growth while increasing the ease of handling (Bar-Tal et al., 2019; Likitlersuang et al., 2022; Papadopoulos et al., 2008; Volder & van Iersel, 2019). How a growth media preforms varies under different conditions, as such they may be formulated from different ingredients to provide for the specific needs of a species and/or conditions (Pérez-Urrestarazu et al., 2019). Growth media may be organic, inorganic or synthetic, each having advantages and disadvantages (Bar-Tal et al., 2019; Kennard et al., 2020; Pérez-Urrestarazu et al., 2019; Schafer, 2020).

Synthetic growth media are processed materials and include polyurethane, polystyrene, polyester fleece, expanded clay, perlite, vermiculite, zeolite, foamed glass and rockwool (Bar-Tal et al., 2019; Kennard et al., 2020; Pérez-Urrestarazu et al., 2019; Schafer, 2020). The production, use and/or disposal of synthetic media may present environmental or health and safety implications. Life cycle analysis of perlite, a light weight porous media that is formed by grinding and heating hydrated rhyolitic volcanic rock, suggests that the energy used in its production presents significant environmental impacts (Bar-Tal et al., 2019). Rockwool is produced by spinning and drawing molten basalt and was originally produced as an insulation material for the

construction industry (Bar-Tal et al., 2019). It has since been successfully utilised as a growth substrate. However, it can only be used for up to three crop cycles before disposal to landfill, generating high volumes of decomposable waste and presenting a significant environmental concern (Bar-Tal et al., 2019). Additionally, exposure to rockwool fibres may cause eye, skin and respiratory track irritation and is listed as possibly carcinogenic to humans (Occupational Safety and Health Service, 1994).

Inorganic growth media are natural, unmodified materials such as pumice, sand, scoria, tuff (Bar-Tal et al., 2019; Kennard et al., 2020; Pérez-Urrestarazu et al., 2019; Schafer, 2020). These materials maintain their physical characteristics (bulk density, water holding capacity and hydraulic conductivity) over time allowing for repeated use. However, they have little cation exchange capacity (Pérez-Urrestarazu et al., 2019). Extraction of these materials may present environmental issues, however due to being inert disposal generally does not, and some materials such as sand may be repurposed in the construction industry (Bar-Tal et al., 2019; Kennard et al., 2020).

Organic growth media such as peat, sphagnum moss, coir, wood fibre, sawdust and manure have historically been used in combination with soil or inorganic materials to grow plants in containers (Carlile et al., 2019). These materials have excellent water holding capacities and some cation exchange capabilities but tend to degrade, leading to compaction and reduced aeration (Altland et al., 2011; Carlile et al., 2019; Kennard et al., 2020; Pérez-Urrestarazu et al., 2019). The sourcing of organic materials may also result in the release of sequestered carbon, habitat destruction, groundwater degradation, reductions in species diversity and the release of greenhouse gases during processing, transport, and disposal (Carlile et al., 2019; Kennard et al., 2020).

By mixing inorganic and organic media together advantages of both media may be retained, such as coarse particle sizes aiding with aeration, improved water retention and cation exchange (Kennard et al., 2020). Inorganic materials are also used on their own, with perlite and rockwool being the most common due to their availability, low cost, and physical and chemical characteristics (Kennard et al., 2020).

2.1.2 Pumice in Horticulture

In hydroponics the physical properties of a growth medium are influenced by grain size distribution which aids in determining the internal geometry, porosity and fluid interaction and thus the behaviour of the medium (Wallach, 2019). Pumice is a naturally occurring inorganic material that is common in some parts of the world including the Central North Island of New Zealand (Barker et al., 2021; Lowe, 2016; Walker, 1981a; Wilson & Rowland, 2016). It is a vesicular aluminosilicate volcanic glass formed by the expansion of gases when pressure is released during a volcanic eruption, resulting in a lightweight, low density (0.4-0.8 g/cm^3), inert material with a total porosity of 70-85vol.% (Bar-Tal et al., 2019; Papadopoulos et al., 2008). The type and magnitude of the eruption together with fragmentation, transport and deposition processes influence the grain size distribution of volcanic material (Jutzeler et al., 2012).

As pumice is inert the supply of nutrients to the plant can be controlled (Marinou et al., 2013). It also retains its structure without decomposing or compacting, which helps maintain substrate structure, and can be reused multiple times (Bar-Tal et al., 2019). Another advantage of pumice is that it is a natural product and can be disposed of without causing environmental pollution (Bar-Tal et al., 2019). As pumice increases aeration and drainage it is usually added to other media at 10 – 20 vol% (Altland et al., 2011). A 2004 study in Turkey that compared mixing different ratios and grades of pumice with soil found that the addition of 45 vol% of 4-8 mm grade pumice produced the best plant growth in strawberry plants (Sahin et al., 2005). Other studies indicated that the addition of pumice to Douglas Fir Bark decreased total porosity and available water but increased bulk density (Altland et al., 2009; Altland et al., 2011).

Raviv et al. (1999) found in a study of tuff and pumices from Italy and Greece that pumice had a low water holding capacity compared to media such as stone wool, perlite or organic media and this could affect the uptake of nutrients and water by the roots (c.f. Papadopoulos et al., 2008). A study by Pérez-Urrestarazu et al. (2019) that compared pumice, expanded clay and perlite for use in vertical living walls found that although pumice resulted in slightly better performance lighting was the largest influence on plant performance.

Studies by Gizas and Savvas (2007) found that gypsophilia and cucumber gave higher yields when grown in 0-2 mm or 0-4 mm grades of pumice with relatively low air-filled porosity over plants grown in 0-8 mm or 4-8 mm grades while lettuce and rose had a weaker response to the different grain sizes.

Marinou et al. (2013) compared pure and mixed sawdust, coco soil and pumice substrates to determine their performance as a growth media in the cultivation of strawberries (*Fragaria x ananassa).* The addition of pumice to sawdust altered the aeration and water balance of the sawdust. Additionally, when pumice was mixed with either the sawdust or coco soil the mixes produced up to 34% more plant growth than a substrate composed of 100% pumice. Plant yield was increased, and fruit numbers were c. 50% greater for plants grown in a sawdust and pumice mix compared to those grown in the other media tested.

2.2 Evolution and Volcanic Products of the Taupō Volcanic Zone

2.2.1 Taupō Volcanic Zone

The Taupō Volcanic Zone (TVZ) is a 300 km long (200 km on land), 60 km wide NNE-SSW trending rift system located at the southern end of the c. 2,800 km Tonga-Kermadec arc system (Barker et al., 2021; Miller et al., 2022; Sas et al., 2021; Wilson et al., 1995; Wilson & Rowland, 2016). The TVZ began forming 2 Ma as a result of the westward subduction of the Pacific Plate under the Australia Plate at the Hikurangi Margin (Figure 2.3) (Barker et al., 2021; Cole et al., 1995; Miller et al., 2022; Wilson et al., 1995; Wilson & Rowland, 2016). The subduction has induced rifting, faulting (a 15-20 km-wide zone known as the Taupō Fault Belt) and volcanism in the region (Cole et al., 2010; Sas et al., 2021; Thompson et al., 2015; Wilson & Rowland, 2016).

Crustal thinning due to the rifting has resulted in an elevated rate of magma emplacement and decompression of the mantle (Sas et al., 2021). This has produced andesitic volcanism with associated composite cone volcanoes in the northeast and southwest of the TVZ and a 125 km long section of rhyolitic volcanism with caldera volcanoes in the central region (Barker et al., 2021; Wilson & Rowland, 2016).

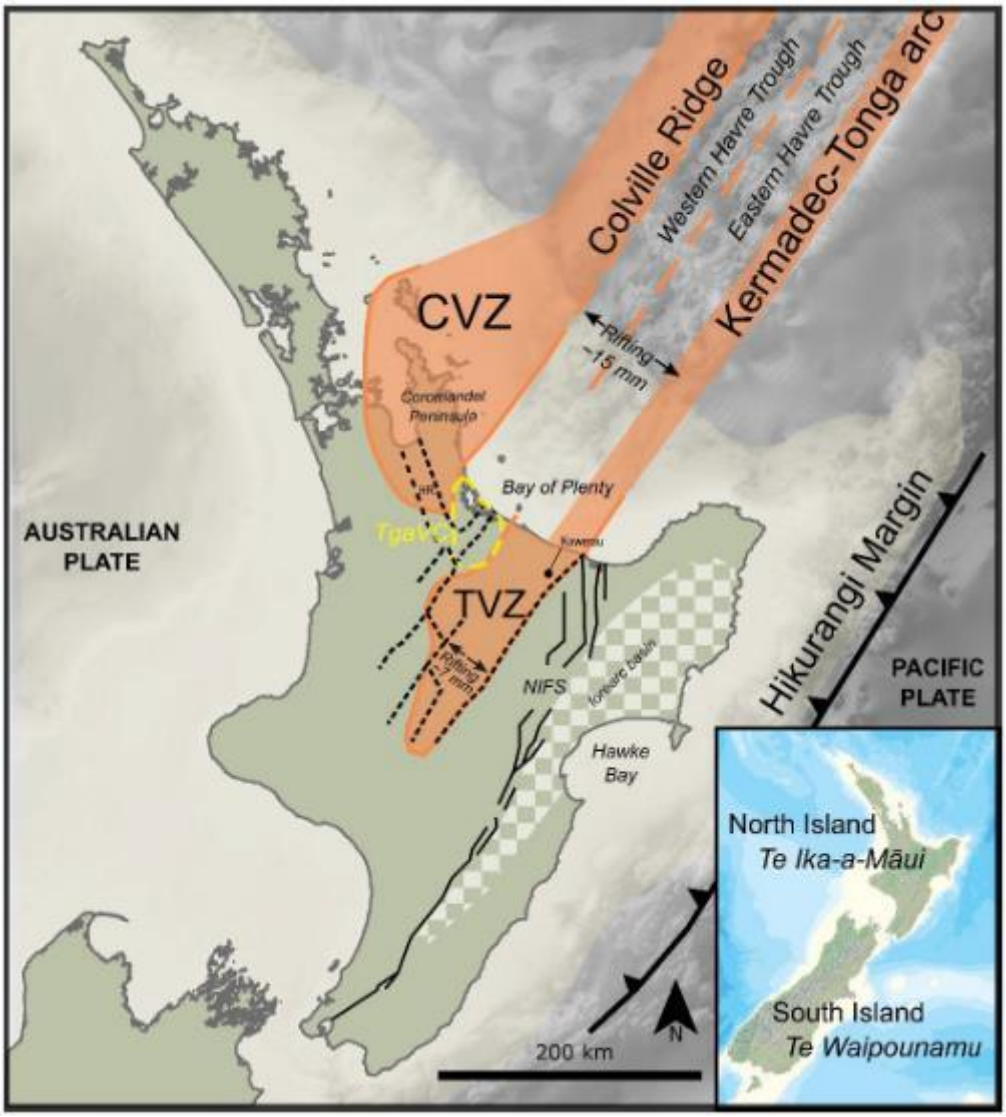

Figure 2.3: Map of the North Island of New Zealand indicating the location of the Hikurangi Margin and offshore and onshore rifting. TVZ = Taupō Volcanic Zone; CVZ = Coromandel Volcanic Zone, remnant of an older volcanic arc; TgaVC = Tauranga Volcanic Centre; NIFS = North Island Fault System, with major faults represented by solid black lines (image from Prentice, 2023).

Of the eight caldera forming centres located within the TVZ (Figure 2.4), only the Okataina (OVC) and Taupō Volcanic Centres (TVC) are considered active. The OVC is the most recently active caldera and contains the Haroharo and Tarawera linear vent zones (HLVZ and TLVZ, respectively), which are marked by a series of vents that run in a generally northeast to southwest direction (Cole et al., 2010). The last eruption from the OVC occurred on 10 June 1886 from Mt Tarawera (Cole et al., 2014; Cole et al., 2010; Miller et al., 2022). The TVC was last active 1800 years ago when the c. 232 CE with the Taupō eruption which produced the Y1-Y7 Units (Houghton et al., 2010; Lowe & Pittari, 2021a; Smith & Houghton, 1995; Wilson, 1985).

The Old TVZ refers to activity which occurred 2-0.35 Ma and most of the resulting deposits have either been removed by erosion or are inaccessible due to burial at depths of 1-3 km. The Young TVZ encompasses activity from 350 – 61 Ka (Figure 2.4) (Chambefort et al., 2014; Cole et al., 1995; Prentice, 2023; Wilson & Rowland, 2016) with the Whakamaru group ignimbrites separating the deposits of the Old from the Young TVZ (Chambefort et al., 2014; Wilson et al., 1995; Wilson & Rowland, 2016).

The Modern TVZ is the largest and most productive rhyolitic system (silicic) on Earth and describes activity since the Rotoiti eruption for which the former age of c. 61Ka (Figure 2.5) (Wilson et al., 1995) has been revised to c. 45 Ka (Danišík et al., 2012). Frequent large volumes of rhyolitic magma amounting to c. 15-20,000 km^3 and small amounts of basaltic magma have been erupted from the Okataina and Taupō Volcanic Centres (Figure 2.4) (Cole et al., 2014; Danišík et al., 2012; Miller et al., 2022; Sas et al., 2021; Smith et al., 2006; Wilson et al., 1995; Wilson et al., 2007).

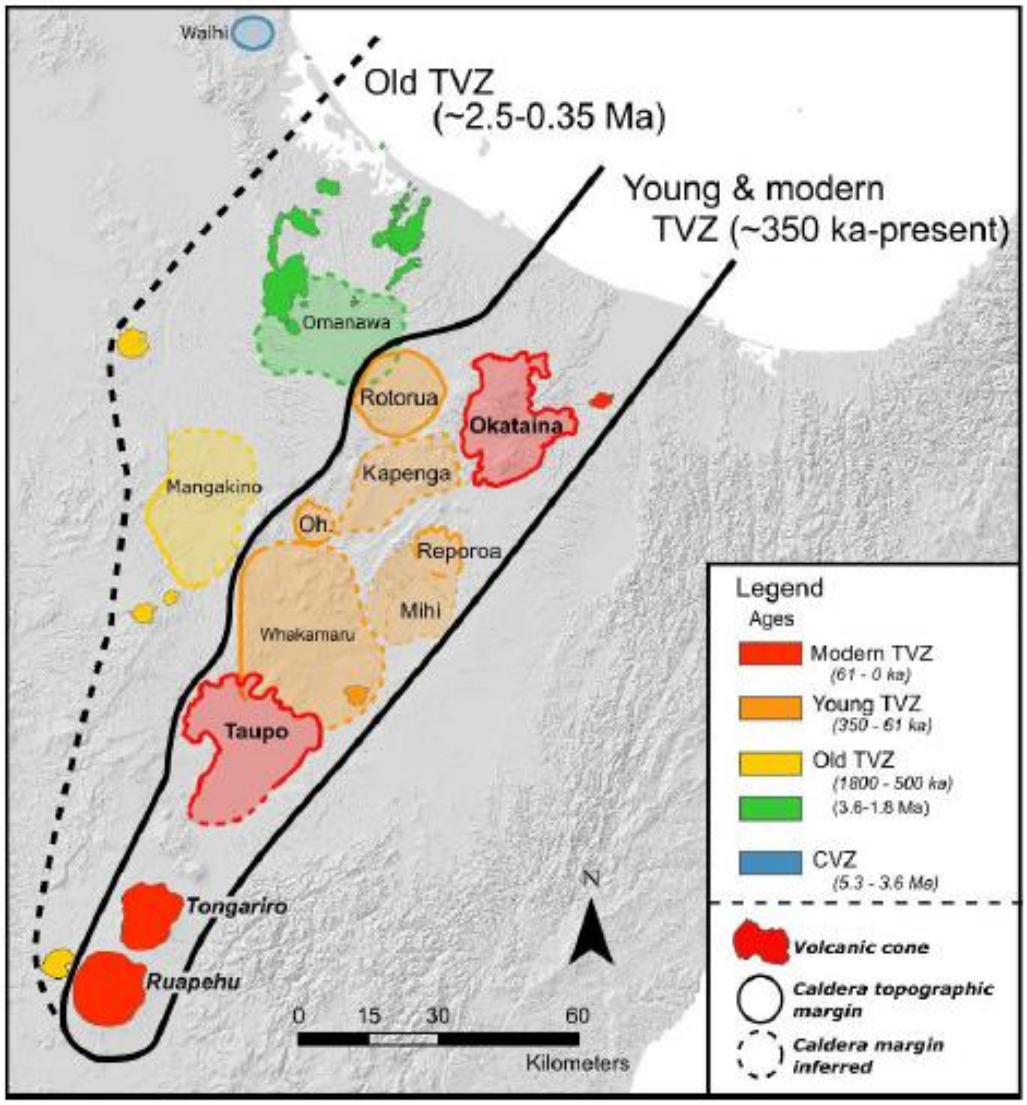

Figure 2.4: Map indicating the location of the Old TVZ during which the Mangakino caldera (shown in yellow) was active and New TVZ during which the Rotorua, Kapenga, Ohakuri (Oh), Reporoa, Mihi, Whakamarua calderas were active. The Modern TVZ encompasses the active Okataina and Taupō Volcanic Centres (Cole et al., 2014; Cole et al., 2010; Wilson et al., 1995) (image from Prentice, 2023).

Rhyolitic volcanism in the region has occurred in three main forms: (1) large pyroclastic eruptions (involving 30 or more than 300 km^3 of magma) that formed calderas and produced voluminous ignimbrites, (2) smaller pyroclastic eruptions (from vents within existing calderas) with associated fall and flow deposits and (3) dome-building eruptions (< 10 km^3) (Wilson et al., 1995). Both, large and small pyroclastic eruptions have been produced from the OVC and TVC with between 0.01 and 500 km^3 of magma being ejected (Figure 2.5 and Table 2.1) (Wilson et al., 1995).

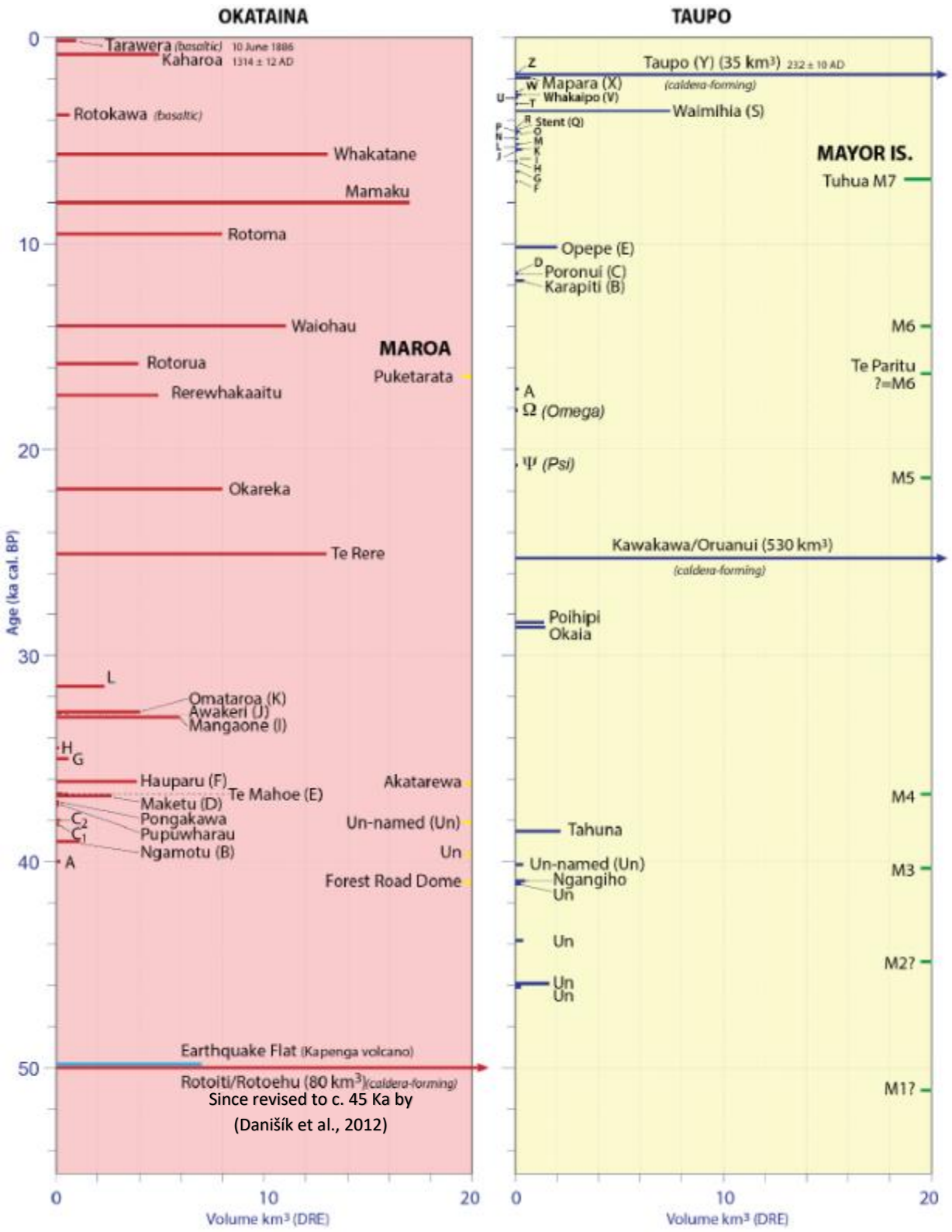

Figure 2.5: Stratigraphic relationship of tephras including ages and volumes (DRE) from the Okataina and Taupō Volcanic Centres since c. 55 Ka with Maroa included in yellow on the right of the Okataina chart and Mayor Is included in green on the right side of the Taupō chart. The Rotoiti Eruption date has been revised to c. 45 Ka by Danišík et al. (2012) (image from Lowe & Balks, 2019).

Table 2.1: Ages and generalised descriptions of the main rhyolitic tephras deposited in the Rotorua-Galatea area since the c. 25 Ka Kawakawa/Oruanui eruption from the Taupō Volcanic Centre (from Lowe & Balks, 2019).

Name (source)*	Date or age¶	Description
Tarawera Tephra (Tr) (Tarawera)	10 June 1886	Comprises basaltic scoria (Tarawera Scoria) with occasional rhyolite clasts and/or fine greyish brown 'muddy' ash (Rotomahana Mud). Mud was dispersed more widely than the scoria.
Kaharoa Tephra (Ka) (Tarawera)	1314 ± 12 AD (636 ± 12 cal yr BP)	Fine to coarse white to grey ash, with occasional dense pumice, rhyolite, obsidian and basalt lapilli. Contains abundant biotite.
Taupo Tephra (also known as Unit Y) (Tp) (Taupo)	232 ± 10 AD (1718 ± 10 cal yr BP)	Creamy coloured coarse ash with plentiful shower-bedded pumice lapilli (crushable). Ignimbrite unit always associated with charcoal fragments.
Whakatane Tephra (Wk) (Haroharo)	5526 ± 145 cal yr BP	Shower-bedded pale yellow coarse ash, overlying a fine to coarse rhyolitic (pale grey) ash. Rich in cummingtonite. Reddish-brown uppermost horizon (sometimes with basaltic Rotokawau tephra c. 4 cal ka).
Mamaku Tephra (Ma) (Haroharo)	7940 ± 257 cal yr BP	Loose, coarse yellowish-brown pumice ash grading into a weakly shower-bedded coarse ash/lapilli.
Rotoma Tephra (Rm) (Haraharo)	9423 ± 120 cal yr BP	Shower-bedded fine grey to yellowish brown ash with coarse ash layers, cummingtonite. Marked by a dark Ah horizon at top, sometimes with charcoal, or podzolised.
Waiohau Tephra (Wh) (Tarawera)	14,009 ± 155 cal yr BP	Grey fine and coarse shower-bedded ash. Distinctive v. fine cream ash layer at the base. Usually has well developed yellowish-brown or greyish upper soil horizon. Deposited a few centuries before late-glacial cool episode (NZce-3) in NZ-CES§.
Rotorua Tephra (Rr) (Okareka embayment)	15,635 ± 412 cal yr BP	Shower-bedded pumiceous yellowish lapilli or blocks (gravel). Occasional rhyolitic lithics. Deposited at start of late-glacial mild episode (NZce-4) in NZ-CES§.
Rerewhakaaitu Tephra (Rk) (Tarawera)	17,496 ± 462 cal yr BP	Yellowish-brown ash grading down into tephric loess. Contains abundant biotite. Marks transition from Last Glacial to post-glacial conditions (Termination I); reafforestation occurred soon after deposition.
Okareka Tephra (Ok) (Tarawera)	21,858 ± 290 cal yr BP	Yellowish brown ash contains abundant biotite. Typically encased in yellowish to olive brown tephric loess. Deposited just before stadial A (NZce-6) NZ-CES§.
Te Rere Tephra (Te) (Haroharo/Okareka)	25,171 ± 964 cal yr BP	Yellowish-brown ash (typically encased in yellowish to olive brown tephric loess).
Kawakawa Tephra (Kk) (also known as Oruanui) (Taupo)	25,358 ± 162 cal yr BP	Olive brown to pale yellowish brown ash (typically encased in yellowish to olive brown tephric loess). Deposited just before interstadial D (NZce-9) in NZ-CES§.

2.2.2 Okataina Volcanic Centre

The c. 700 km^2 OVC is the most recently active caldera in the TVZ. It is located in the northeast of the central TVZ at an offset in the Taupō Rift where crustal extension occurs at a rate of 12mm/yr (Cole et al., 2010; Miller et al., 2022; Thompson et al., 2015). The most recent rhyolitic activity was the 1315 CE Kaharoa eruption (Leonard et al., 2002; Lowe et al., 1998; Nairn et al., 2001;

Nairn et al., 2004), which was followed by the basaltic Plinian Tarawera eruption on June 10, 1886, that formed a 17 km long fissure (Cole et al., 2014; Cole et al., 2010; Miller et al., 2022; Rowe et al., 2021; Walker et al., 1984).

The OVC is a depression formed from multiple phases of caldera collapse that have been filled with ignimbrites, extruded domes, pyroclastic deposits, and lakes (Cole et al., 2014). Its northwestern and southeastern boundaries are fault controlled (Cole et al., 2010). The caldera comprises two active vent zones, the Haroharo and Tarawera Linear Vent Zones (HLVZ & TLVZ) that have formed with a northeast / southwest orientation (Figure 2.6) (Cole et al., 2010) due to southwest rifting of the Whakatane segment and northeast rifting of the Kapenga segment (the Whakatane and Ngakuru grabens).

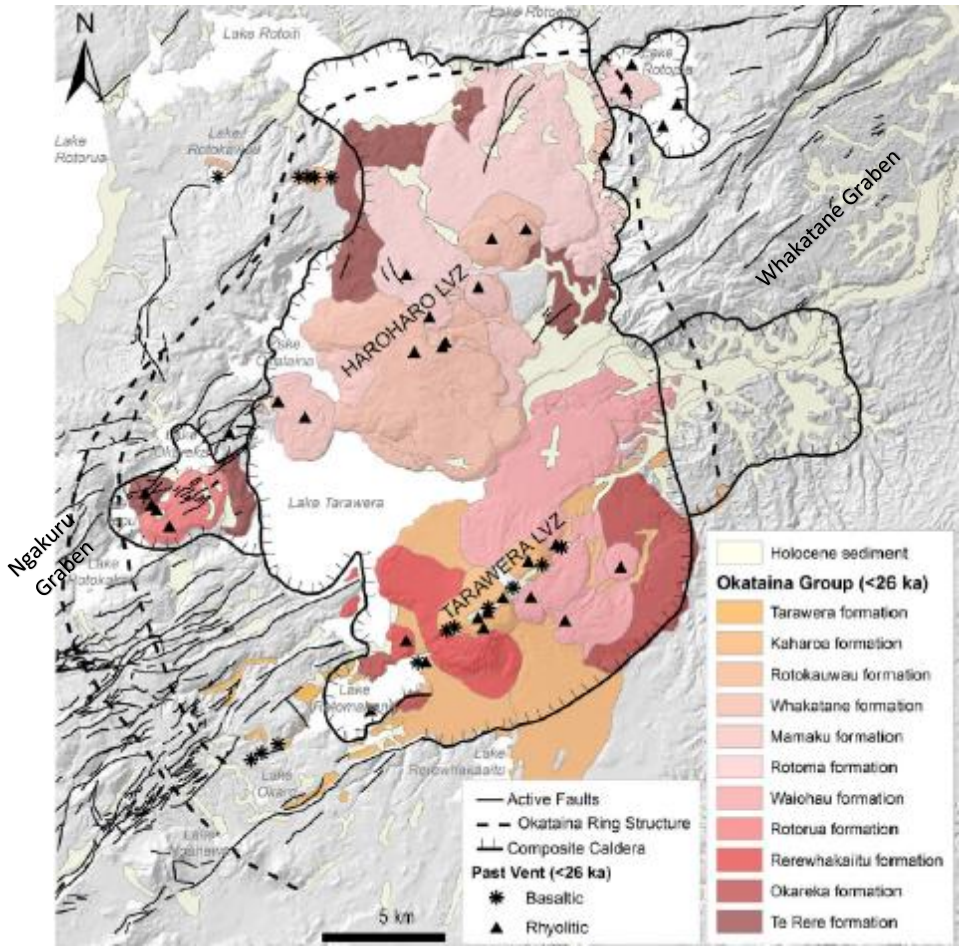

Figure 2.6: Map of the OVC showing eruptions deposit since 26 Ka, the caldera boundary and the Haroharo and Tarawera linear vent zones. The Whakatane Graben is to the northeast and the Ngakuru Graben is to the southwest (Thompson et al., 2015)

Over the past c. 625 ka there have been at least three caldera-forming events with dome-building activity occurring between each event (Cole et al., 2014; Thompson et al., 2015). The eruption of the Utu Ignimbrite between c. 550-557 ka (Cole et al., 2010; Smith et al., 2006; Thompson et al., 2015) caused caldera collapse in the southern OVC (Cole et al., 2014). At c. 322 ka the eruption of the Matahina Ignimbrite resulted in a caldera collapse in the northern OVC, followed at c. 45 ka by the eruption of the Rotoiti Ignimbrite causing a caldera collapse in the northern OVC (Cole et al., 2010; Thompson et al., 2015). In addition, a possible minor collapse in southern OVC could have occurred when the Kawerau Ignimbrite was erupted at c. 33 ka (Cole et al., 2014).

The c. 45 ka Rotoiti Eruption began with a basaltic Sub-Plinian eruption (<0.5 km^3) followed by a rhyolitic Plinian eruption (c. 100 km^3) and caldera collapse (Shane et al., 2005; Thompson et al., 2015). A further 12 eruptions over 10-12 Kyr until c. 31 Ka deposited the Mangaone Subgroup (MgSg) consisting of pyroclastic units, further modifying the caldera prior to a period of quiescence (Cole et al., 2010; Jurado-Chichay & Walker, 2001; Thompson et al., 2015).

Activity returned from 26 Ka with the record including 9 rhyolitic Plinian eruptions (5 eruptions from HLVZ and 4 eruptions from TLVZ) totalling >85 km^3 magma volume. Seven of the eruptions have tapped different magmas along the vent zones (Cole et al., 2010; Sas et al., 2021; Smith et al., 2006; Thompson et al., 2015). Typically, the eruptions occurred in three stages over months to several years, beginning with a phreatomagmatic, hydrothermal, or basaltic explosion, followed by rhyolitic Plinian explosions and then dome extrusion (Thompson et al., 2015). Two basaltic eruptions also occurred during this time; the 3.7 Ka Rotokawau basaltic maar eruption in the northwest of the OVC and the 1886 CE Tarawera basaltic Plinian eruption from Mt. Tarawera in the TLVZ (Thompson et al., 2015). All Plinian eruptions have produced widespread tephra deposits (Thompson et al., 2015).

2.2.2.1 Haroharo Volcanic Complex

The Haroharo linear vent zone (HLVZ) is a 27 x 3 km NE-SW trending dome complex with a series of vents in the north of the OVC (Cole et al., 2014; Sas et al., 2021; Smith et al., 2006). The vent orientation runs parallel to the tectonic structure of the area and appears to be a continuation of the Ngakuru Graben axis (Sas et al., 2021) (Figure 2.6).

The 800 m-high Haroharo Dome Complex has developed since 25-26 ka from effusive activity during 5 major eruptions (Cole et al., 2014; Smith et al., 2006). Each eruption has involved numerous vents with younger lava flows covering older vents (Smith et al., 2006). Intermittent explosive activity resulted in the rhyolitic domes and lava flows being interbedded with pyroclastic flows and fall deposits (Cole et al., 2014). Activity began at the southern end of the HLVZ with the 25 ka Te Rere and 15.8 ka Rotorua eruptions. However, Kilgour and Smith (2008) infer these to have erupted from the Okareka Embayment in the southwest of the OVC (Smith et al., 2006). These events were followed by the 9.5 ka Rotoma, the 8.1 ka Mamaku and the 5.6 ka Whakatane eruptions from the centre and northern end of the HLVZ (Figure 2.5 and Table 2.1) (Smith et al., 2006). Revised dates were provided by Lowe et al. (2013): Te Rere 25,171 ± 964 cal. yr. BP; Rotorua 15,635 ± 412 cal. yr. BP; Rotoma 9423 ± 120 cal. yr. BP; Mamaku 7940 ± 257 cal. yr. BP and Whakatane 5526 ± 145 cal. yr. BP. The eruptions from the central and northern HLVZ have involved vents that were spread over 12 km, with the Rotoma and Whakatane episodes tapping multiple magmas (Smith et al., 2006).

2.2.2.2 Tarawera Volcanic Complex

The 8 km-long Tarawera linear vent zone (TLVZ) runs parallel to the NNE-SSW trending rift system of the TVZ and is potentially a continuation of the Whakatane Graben (Figure 2.6) (Cole et al., 2014; Sas et al., 2021). The dome complex formed from extruded lava domes and flows, Plinian eruptions and pyroclastic flows from the Okareka (21,858 ± 290 cal. yr. BP); Rerewhakaaitu (17,496 ± 462 cal. yr. BP); Waiohau (14,009 ± 155 cal. yr. BP) and the 1314 ± 12 Kaharoa eruptions (Figure 2.5 and Table 2.1) (Lowe et al., 2013; Nairn et al., 2001; Speed et al., 2002). The basaltic Plinian Tarawera eruption in 1886 created a fissure through the dome complex that extends 17 km from Waimangu to Mt Tarawera (Carey et al., 2007).

The Rerewhakaaitu Eruption resulted in Plinian fall deposits across the Central North Island and the extrusion of lava domes and flows (Shane et al., 2007). This was followed by the Waiohau eruption with at least 15 episodes, during which the early eastern dome was extruded, this was followed by the Plinian phases (Speed et al., 2002).

The most recent rhyolitic eruption from the TLVZ was the 1315 CE Kaharoa Eruption that erupted 4-5 km^3 of magma from an 8 km-long chain of 7 vents (Cole et al., 2014; Leonard et al., 2002; Nairn et al., 2005; Nairn et al., 2001; Shane et al., 2007). The eruption sourced magma c. 6-7 km beneath the Earth's surface and was triggered by repeated basalt intrusions (Cole et al., 2014; Leonard et al., 2002; Nairn et al., 2005; Nairn et al., 2001; Nairn et al., 2004; Shane et al., 2007). Initial Plinian falls were dispersed in narrow lobes to the southeast (Nairn et al., 2005). Later tephra falls fell to the north while a small lava dome was extruded (Nairn et al., 2005). During the final phase of the eruption three large domes were extruded over a c. 5-year period (Nairn et al., 2005; Nairn et al., 2001).

The 10 June 1886 Tarawera Eruption is the most recent of four documented basaltic Plinian eruptions (Carey et al., 2007; Walker et al., 1984). During the eruption at least 50 vents, aligned along a northeast trending 17 km fissure of the TLVZ into the Rotomahana Basin, erupted c. 0.8 km^3 DRE (2.0 km^3 tephra volume) of basaltic magma (Carey et al., 2007; Shane et al., 2007). This dispersed scoria up to 150 km and ash up to 230 km east of the vent of over a c. 5-hour period (Houghton et al., 2004). Eyewitness accounts indicate there was increased geothermal activity at Lake Rotomahana and a 30 cm-high wave on Lake Tarawera on 1 June 1886 while earthquakes of increasing intensity began an hour before the eruption started (Carey et al., 2007). The eruption began at the northeast end of the domes with explosive activity which migrated to the southwest across the domes and to Rotomahana where pyroclastic density currents swept out radially for 4-6 km (Carey et al., 2007).

2.2.3 Taupō Volcanic Centre

The TVC is located c. 60 km south-southwest of the OVC in the southern part of the Central TVC and is considered the most frequently active rhyolitic volcano in the world (Lowe & Balks, 2019; Potter et al., 2015). The caldera is c. 50 km across, 300-500 m deep (Wilson et al., 1984) and overlaps the now largely buried Whakamaru caldera structure to the north that was formed between 350-320 ka by the eruption of ignimbrites and fall deposit (Muirhead et al., 2022; Sutton et al., 1995). It is partly occupied by Lake Taupō with a shoreline of 193 km, a width of c. 35 km (Grzelewski, 2009) and an area of c.600 km^2 (Wilson et al., 1984) that conceals most of the young vent sites and caldera collapse areas (Figure 2.7) (Barker et al., 2021).

Since 65 ka TVC has produced voluminous eruptions, including the youngest super-eruption on Earth, the c. 25.5 ka Kawakawa/Oruanui Eruption that generated 430 km^3 of fall deposits, 320 km^3 of pyroclastic density-current deposits (mostly non-welded ignimbrite) and c. 420 km^3 of primary intracaldera material, a total equivalent to 530 km^3 DRE (dense rock equivalent) of magma (Allan et al., 2017; Cole et al., 1998; Sutton et al., 1995; Wilson, 2001; Wilson et al., 2006). This eruption formed a caldera in the northern half of present-day Lake Taupō, while the southern half of the lake is believed to be a tectonically controlled half graben that may predate the Kawakawa/Oruanui Eruption (Cole et al., 1998; Muirhead et al., 2022; Sutton et al., 1995). Many of the vents associated with the TVC are located in the eastern portion of the caldera with rhyolitic domes surrounding the lake and extending from Marotiri in the north to Maunganamu in the south and most domes and vents being aligned NE to SW with the Taupō Fault Belt (Figure 2.7) (Cole et al., 1998; Muirhead et al., 2022).

Twenty-eight post-Kawakawa/Oruanui eruptions have been identified (Wilson, 1993). The first three; labelled ψ, Ω and A were dacitic and erupted from the north of Lake Taupō c. 20.5-17 ka; while the Puketarata Eruption c. 16 ka was from a dome northeast of these (Barker et al., 2021; Brooker et al., 1993). The 25 rhyolitic eruptions since c. 12 ka occurred in 3 periods (B-E, F-W and X-Z) from overlapping vents (Barker et al., 2021; Sutton et al., 1995; Wilson, 1993), including a large number of explosive events with wide a range of volumes (Figure 2.5 above) from focused vent locations (Barker et al., 2021; Wilson, 1993). During the larger eruptions (B, E, S and Y) vent location, eruption intensity and wind direction varied, and eruption styles included the generation of pyroclastic density currents and phreatomagmatic activity when magma interacted with water (Barker et al., 2021). Obsidian lithics comprised in smaller eruptives are indicative of potential dome extrusion (Barker et al., 2021).

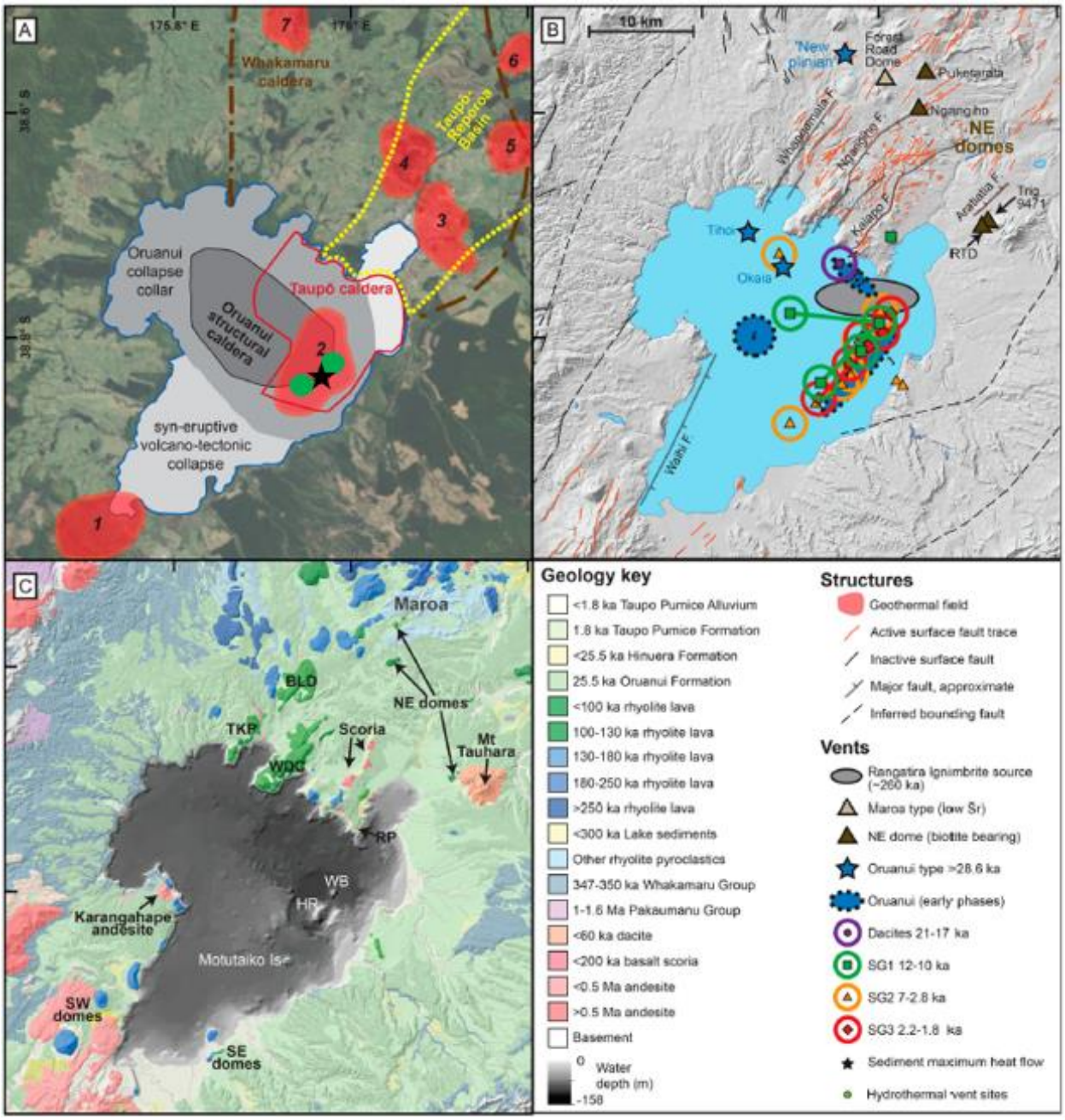

Figure 2.7: Maps of the Taupō Volcanic Centre. A. Caldera outlines (Leonard et al., 2010) including from south to north Tokaanu hydrothermal area (1), Lake Taupō (2), Tauhara volcano and geothermal system (3), Wairakei geothermal system (4), Rotokawa geothermal system (5), Ngatamariki geothermal system (6) and Mokai geothermal system (7); the green circles are hydrothermal vents discovered by (De Ronde et al., 2002) and the black star mark the highest lake sediment heat flow from (Whiteford, 1996). B. Vent sites and faults from Barker et al. (2015). C. Geology and bathymetry of Lake Taupō; the rhyolite ages as shown in the key have some overlap as rhyolite ages of the dome complexes have been simplified by (Leonard et al., 2010). WDC = Whakaroa Dome Complex, TKP = Te Kauwae Point, BLD = Ben Lomond Dome, HR = Horomatangi Reefs and WB = Waitahanui Bank (image from Barker et al., 2021).

The most recent activity at this centre was the Taupō (Y) eruption c. 1,800 years ago (232 CE), the largest eruption since the Kawakawa/Oruanui event (Sutton et al., 1995). The eruption discharged c. 35 km^3 of DRE magma (Muirhead et al., 2022) and consisted of three phreatomagmatic (Y1, Y3 and Y4), two Plinian fall deposits (Y2 and Y5), and a widespread non-welded ignimbrite (Y6) (Cole et al., 1998; Froggatt, 1981; Houghton et al., 2010; Houghton et al., 2014; Lowe & Pittari, 2021a; Smith & Houghton, 1995; Walker, 1980, 1981a, 1981b; Wilson, 1985, 1993; Wilson & Walker, 1985). Further caldera collapse in the northeast portion of the current lake is inferred to have accompanied this eruption (Davy & Caldwell, 1998; Sutton et al., 1995).

2.2.4 Plinian Eruptions and their Products

Volcanism in the Central TVZ is dominated by large, often caldera-forming explosive eruptions. These so-called Plinian eruptions, named after Pliny the Younger who witnessed the 79 CE eruption of Mount Vesuvius in Italy, are defined as those that produce a sustained convection plume of pyroclasts and gas rising >25 km above sea level (Blake, 2021). The fragmented volcanic material is ejected at a rate of 10^6 to 109 kg/sec up to 55 km into the stratosphere (Cioni et al., 2015; Fisher & Schmincke, 1984; Pyle, 2015; Walker, 1981a; Wilson et al., 1995). At these heights the plume spreads out into an umbrella shape and are dispersed by stratospheric winds to produce fall deposits of pumice and ash with volumes ranging from 1 to >3000 km^3 covering areas of c. 500 km^2 to 50,000 km^2 (Cioni et al., 2015; Fisher & Schmincke, 1984; Walker, 1981a). When magma eruption rates exceed the plume's ability to rise convectively the plume becomes unstable resulting in partial or complete collapse, which in turn generates a pyroclastic density current (PDC) (Dufek et al., 2015; Walker, 1981a). Pyroclastic density current deposits are typically found proximal to the vent and may alternate with fall deposits if the plume collapses in repeating cycles (Dufek et al., 2015).

Tephra is the fragmented material ejected from the vent into the atmosphere during a volcanic eruption (Siebert et al., 2015). The resulting pyroclastic deposits comprise of a high content of juvenile particles (pumice and glass shards), free crystals (phenocrysts separated from magma during the explosion) and lithics (pre-existing solid rock fragments) (Fisher & Schmincke, 1984; Walker, 1981a). Tephra particles are classified based on grain size: ash (<2mm), lapilli (2-64mm) and bombs or blocks (>64 mm).

Settling velocities of the erupted pyroclasts determine the distribution and sorting of the deposit (Fisher & Schmincke, 1984). Those with high settling velocities like bombs or blocks follow a ballistic trajectory, whereas those with a lower settling velocity are transported by turbulent suspension within the eruption cloud and atmospheric winds (Fisher & Schmincke, 1984). The suspended fragments fall according to their settling velocity relative to the energy within the eruption cloud and wind strength to produce fall deposits, the dispersal of which is strongly influenced by wind conditions (Fisher & Schmincke, 1984). As a result, the thickness of a fall deposit and the grain size of the clasts decrease exponentially away from the source vent depending on the volume of erupted material, mass eruption rate, height of the eruption column, wind speed and direction, and magma fragmentation mechanism (Houghton & Carey, 2015; Walker, 1981a).

Differing settling velocities of deposit components result in overlapping grain sizes and variations in overall composition of a deposit between locations (Fisher & Schmincke, 1984). Rhyolitic Plinian fallout deposits generally consist of angular pumice lapilli with layers (discrete or with gradational contacts) of lithic fragments where bedding is defined by grain size and composition (Fisher & Schmincke, 1984). Due to the continuity of the discharge these deposits tend to be homogenous and well sorted throughout the deposit thickness (Walker, 1981a).

Subvolcanic processes such as crystallisation, differentiation, migration, degassing and the properties of the magma involved in the eruption determine the bulk chemical and mineralogical composition of the resulting juvenile tephra particles (pumice and glass shards), while gas content and fragmentation processes influence their texture, shape, size, and porosity (Arculus, 2021; Branney et al., 2021).

This study investigates deposits that are produced by eruptions of various sized from three different volcanic sources and thus comprise a range of different pumice types with diverse compositions, crystal contents, densities, and porosities. The studied pyroclastic deposits are: (1) the 1315 CE Kaharoa Tephra erupted from the Tarawera Volcanic Centre (Hogg et al., 2003; Nairn et al., 2004; Shane et al., 2008); (2) the Rotorua Tephra which erupted in two phases from the Haroharo Volcanic Complex c. 15.6 ka (c.f., Kilgour & Smith, 2008; Lowe et al., 2013; Shane et al.,

2008; Smith et al., 2006; Wilson & Walker, 1985); and subunits Y2 and Y5 which were produced by the 232 CE Taupō Y eruption c.1.8ka (c.f., Hogg et al., 2012; Lowe & Pittari, 2021a; Smith et al., 2005; Wilson, 1993; Wilson & Walker, 1985).

2.2.4.1 Rotorua Tephra 15.6 ka

The 15,635 ± 412 cal. yr BP (Lowe et al., 2013) Rotorua Eruption from the HLVZ (Smith et al., 2006) involved two phases which sequentially tapped two distinct silicic bodies beneath the Okaraka Embayment (Kilgour & Smith, 2008; Shane et al., 2008). The first phase was an explosive Plinian phase, which deposited the multi-bedded Rotorua Ash fall deposit to the northeast (Kilgour & Smith, 2008). This was followed by an effusive eruption of relatively gas-poor magma and dome-building of the second phase (Kilgour & Smith, 2008).

All phase 1 units (T1) have a northwest dispersal direction as shown in Figure 2.8, while dispersal of phase 2 pyroclastic deposits is in a southeast direction. Combining the proximal and distal data from Lowe (1988), Sandiford et al. (2001) and Shane and Hoverd (2002) the whole-deposit dispersal of phase 1 of the eruption is shown in Figure 2.9 (Kilgour & Smith, 2008).

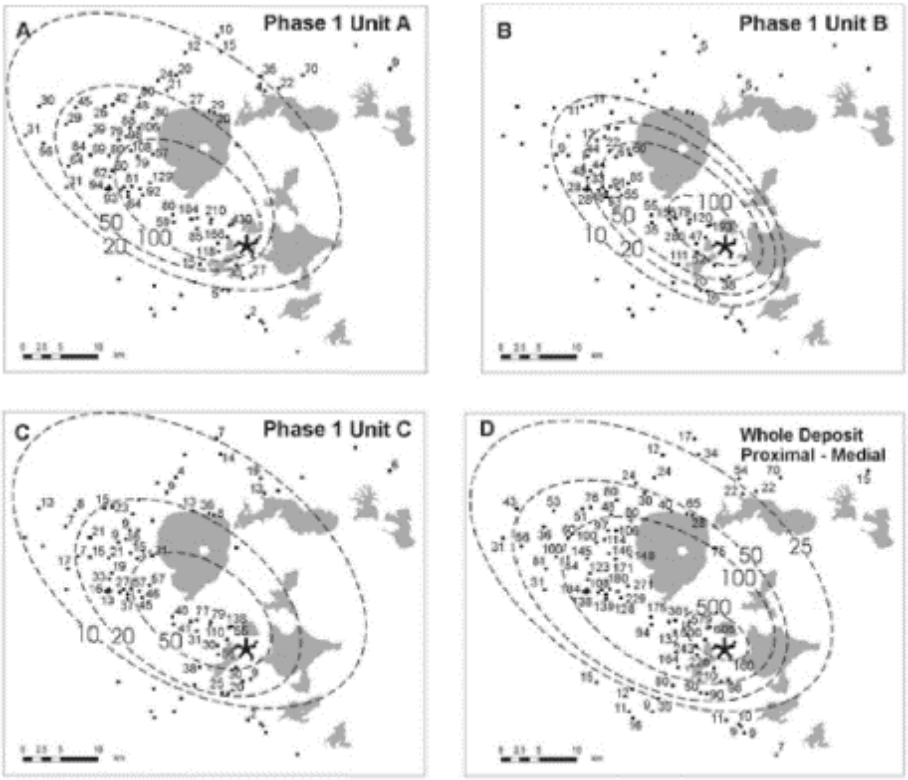

Figure 2.8: Rotorua phase 1 (T1) subunit isopach maps (A, B and C) and the whole proximal deposit (D). Thickness contours are in centimetres and the black star indicates the vent location (image from Kilgour & Smith, 2008).

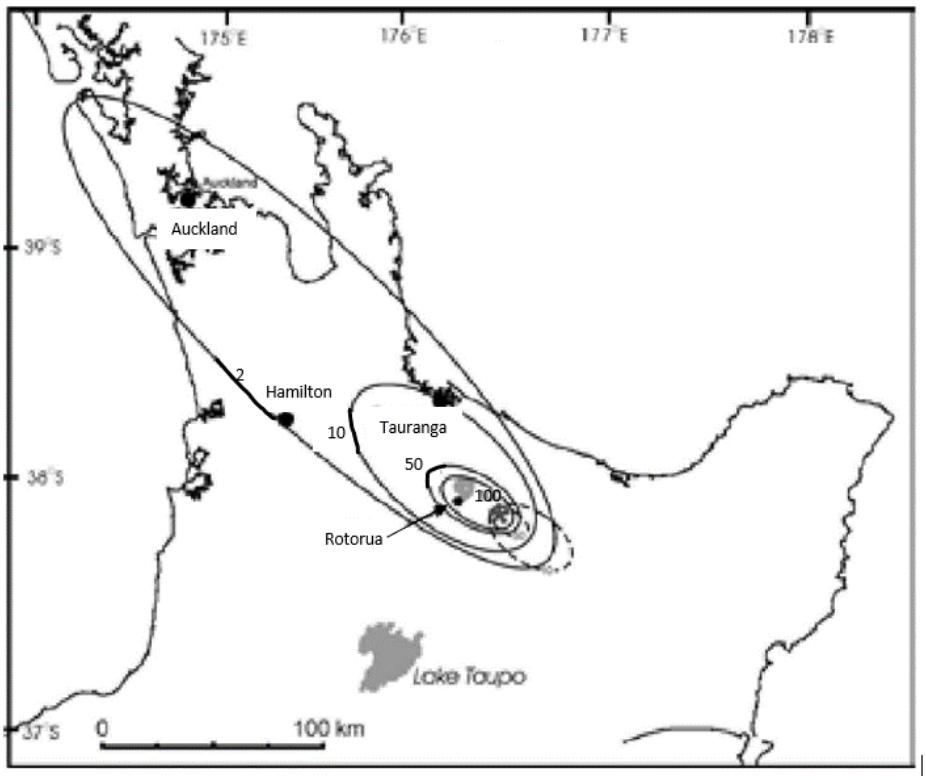

Figure 2.9: Total Isopach map of Phase 1 (shown solid) and phase 2 (shown dashed) deposits with contour thicknesses given in centimetres (image adapted from Kilgour & Smith, 2008).

The Rotorua Ash is a fall deposit bedded at centimetre-scale, that changes to a three-bed subdivision at distances > 10 km from the vent (Figure 2.11) (Kilgour & Smith, 2008). The basal unit consists of coarse to very coarse, typically reversely graded lapilli (bed A) overlain by bedded medium lapilli (bed B) that show both reverse and normal grading (Kilgour & Smith, 2008) (Figure 2.10). The upper unit (bed C) is massive, comprising fine lapilli and ash with a chemical composition that differs from the lower beds and is indicative of a relatively degassed magma source (Kilgour & Smith, 2008). The proximal explosive Plinian phase deposits (T1) are dominated by low-K_2O/high-CaO pumice lapilli containing orthopyroxene + hornblende + augite with rare high-K_2O (>4wt.%) and low-CaO (<0.9wt%) biotite-bearing lapilli. The phase 2 pyroclastic deposits (T2) that overlay the T1 deposits close to the source vent have abundant biotite and high-K_2O/low-CaO compositions (Shane et al., 2008).

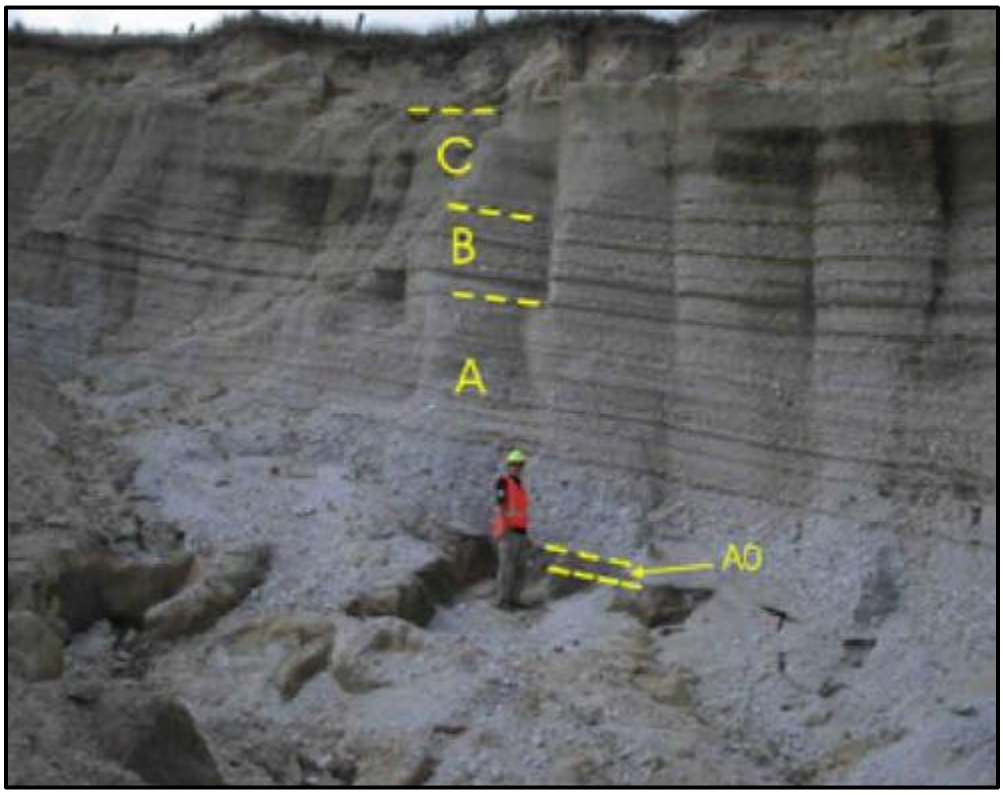

Figure 2.10: Image from Kilgour and Smith (2008) indicating Units A, B and C divisions.

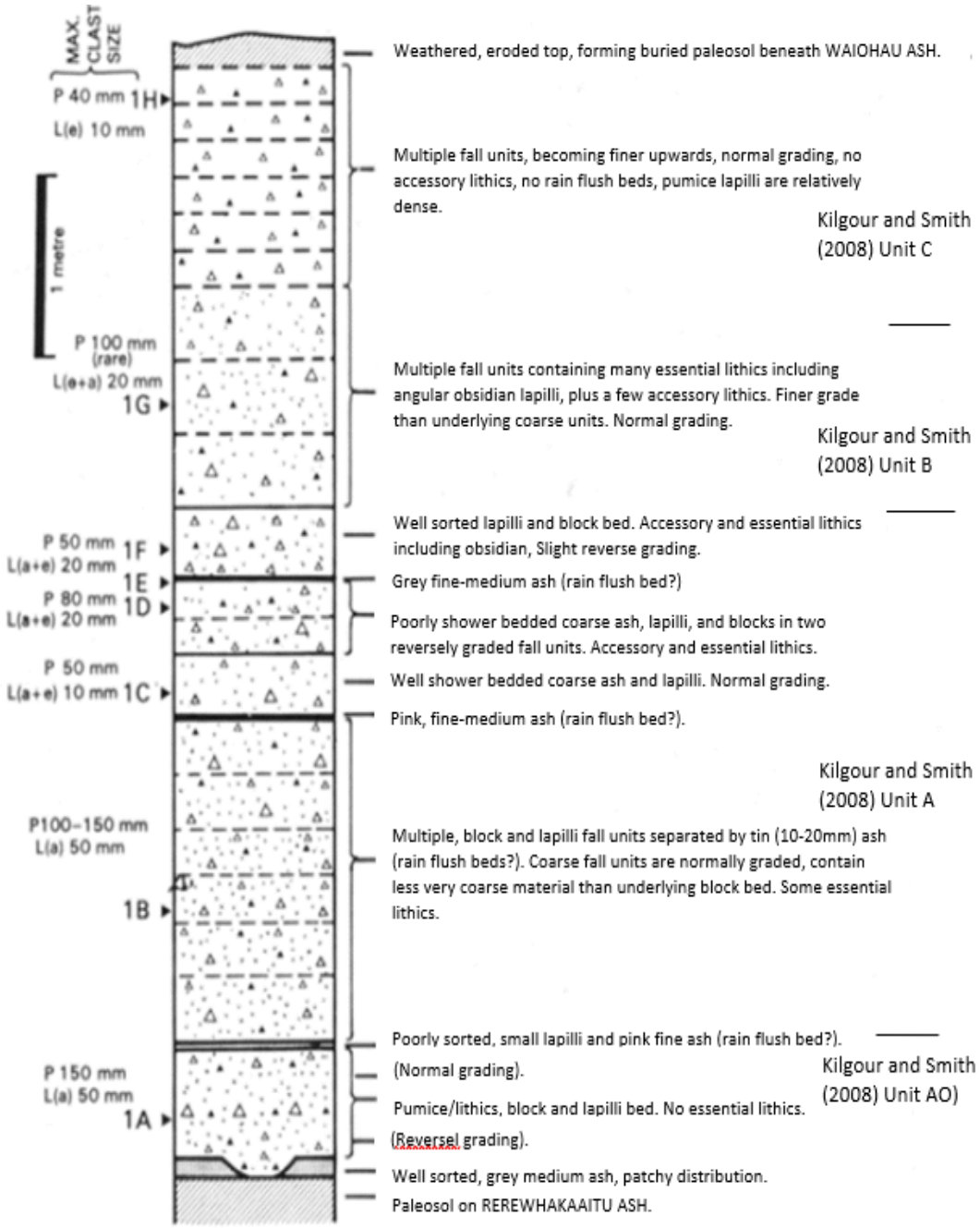

Figure 2.11: Stratigraphy of the Rotorua Tephra at a pumice quarry on Okareka Loop Rd (image from Nairn, 1980), Units from (Kilgour & Smith, 2008).

Most of the Rotorua eruptive are comprised of vesicular pumice clasts, however, a small number of clasts show varying stages of vesicle collapse (Kilgour & Smith, 2008). Therefore, pumice clasts which may be vesicular or dense along with wall rock lithics, obsidian and crystals make up the deposit. The abundance of dense juvenile clasts increases towards the top of the T1 deposits as grain size decreases (Kilgour & Smith, 2008). Lithics in T1 units are mostly rhyolitic lava and the

crystal component consists of plagioclase, quartz, hypersthene, hornblende and biotite (Kilgour & Smith, 2008). Vesicularity of the juvenile clasts is c. 75% in beds A and B, decreasing to between c. 65 and 45% in bed C, while the vesicularity of the T2 juvenile clasts ranges from 50 to 20% (Kilgour & Smith, 2008).

2.2.4.2 Kaharoa 1315 CE

The c. 1315 CE Kaharoa Eruption (Lowe et al., 2013; Todde, 2022) from the TLVZ is the most recent rhyolitic event in New Zealand (Shane et al., 2008). The deposit was first described by Grange (1929, 1937) as a tephra derived from Mt. Tarawera with subsequent work focusing on deposit structure, stratigraphy, petrology, and the bi-lobate distribution (Cole, 1970a, 1970b; Nairn & Beanland, 1989; Nairn et al., 2001; Pullar & Birrell, 1973; Pullar et al., 1973; Sahetapy-Engel et al., 2014; Todde, 2022).

The eruption deposited a total at least 9.1 km^3 DRE during two stages (Sahetapy-Engel et al., 2014) and covered an area of >30,000 km^2 of the north and east of the North Island with pyroclastic deposits (Figure 2.12) (Hogg et al., 2003; Nairn et al., 2004; Shane et al., 2008).

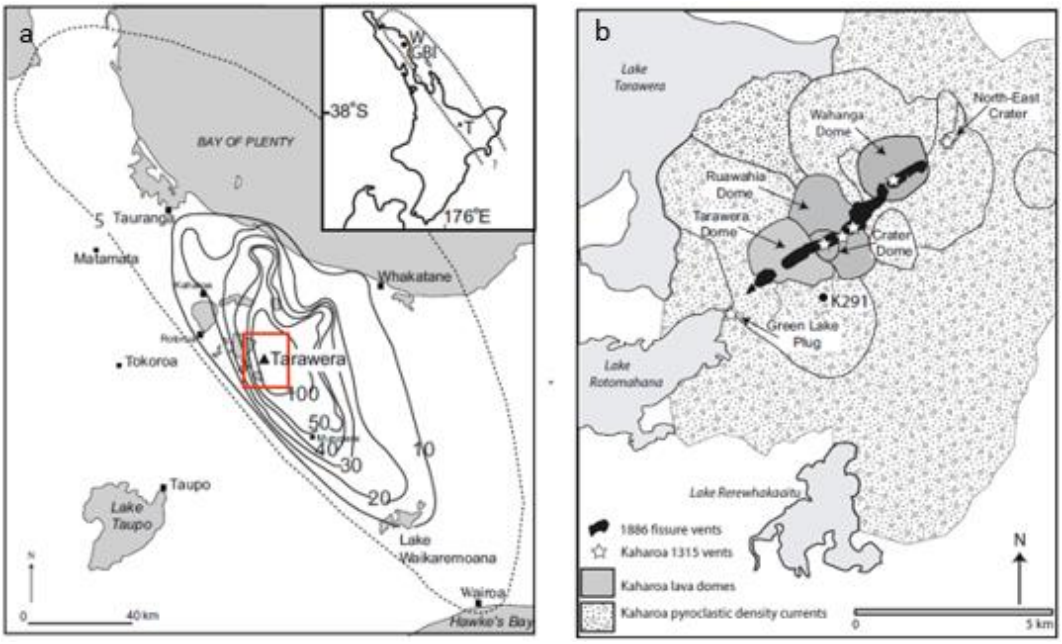

Figure 2.12: a. Isopach map of the Kaharoa fall deposit over the North Island, after Pullar and Birrell (1973), contour thicknesses are in centimetres, dashed line indicates the 5 cm isopach. Inset shows the 2 cm isopach outline. Red box indicates area shown in image b. b. Sketch of Tarawera showing lava domes, PDC deposits and source vents (white stars) for the Kaharoa eruption; the Kaharoa fall deposit covers the entire area (Image from Sahetapy-Engel et al., 2014).

The initial eruption involved up to 13 sub-Plinian to Plinian explosions (Sahetapy-Engel et al., 2014) from at least seven vents along 8 km of the TLVZ from the Green Lake Plug vent in the southwest to the Northeast Crater (Nairn et al., 2001; Todde, 2022). The first seven explosions produced lapilli fall units to the southeast, the subsequent six explosions deposited lapilli fall units to the north and northwest. These fall units are interbedded with massive ash layers derived from pyroclastic density currents (Cole et al., 2014; Nairn et al., 2001; Sahetapy-Engel et al., 2014; Shane et al., 2008; Todde, 2022). A period of dome building followed during which the Tarawera, Ruawahia and Wahanga lava domes were emplaced accompanied by block and ash flows which formed fans to the south and southeast of the Tarawera and Ruawahia domes and south of the Wahanga Dome (Cole et al., 2014; Nairn et al., 2001; Sahetapy-Engel et al., 2014; Shane et al., 2008; Todde, 2022). More than 7.3 km^3 DRE was erupted during initial explosive stages with the whole eruption releasing a total of at least 9.1 km^3 DRE (Sahetapy-Engel et al., 2014).

The Kaharoa pumice is a light-coloured high silica (c. 76 % SiO_2) rhyolite with biotite crystals that has a lower vesicularity (30-50 %) and higher density than other Holocene tephras in New Zealand (Leonard et al., 2002; Sahetapy-Engel et al., 2014). Two rhyolite juvenile components were identified by Nairn et al. (2004); T1: the low-Zr, low-Sr, high-Rb type of the early Plinian explosions, which were deposited to the southeast (Units A-H) (Figure 2.13) (Leonard et al., 2002; Nairn et al., 2001); and T2: the high-Zr, high-Sr, low-Rb type of the later explosions, which were deposited to the north and northwest (Units L-M) (Figure 2.13) and form the domes (Leonard et al., 2002; Nairn et al., 2001). Nairn et al. (2001) identified all units as containing: lithics (mostly rhyolitic) clasts, the largest of which (c. 1 m) are associated with ballistic impact craters close to source; basalt clasts up to 1 cm in diameter and often coated in rhyolite (Leonard et al., 2002; Nairn et al., 2001); and rhyolite pumice.

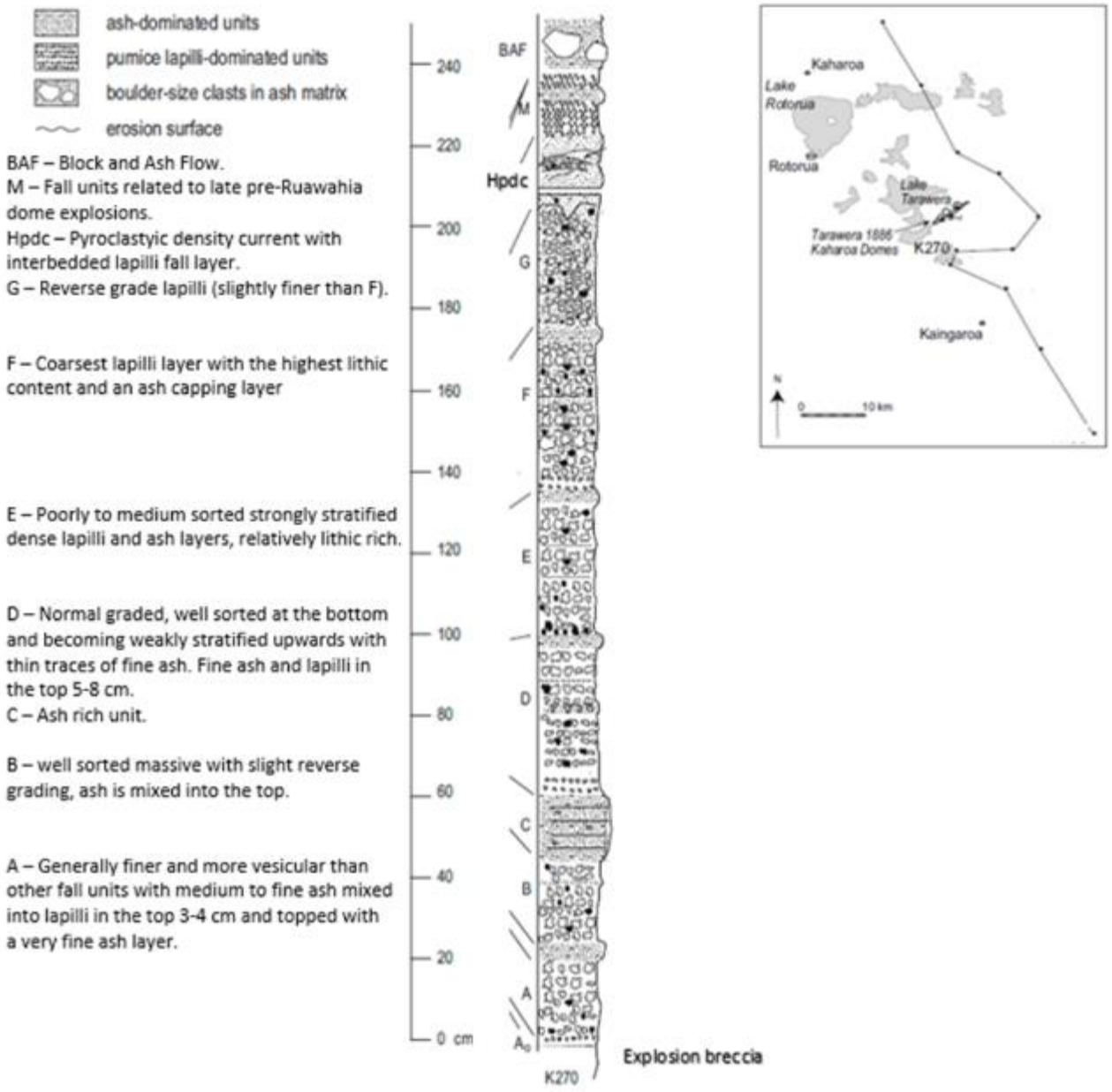

Figure 2.13: Kaharoa Tephra stratigraphy at K270 (801 Ashpit Rd) as shown on the inset map (Column and descriptions from Sahetapy-Engel et al., 2014)

2.2.4.3 Taupō 232 CE

The Taupō (Y) eruption occurred from a lineation of vents in the north-east of present-day Lake Taupō. These vents are now covered by the Horomatangi and Waitahanui reefs (c.f. Figure 2.7) (Houghton et al., 2010). The eruption was the largest globally in the last 2000 years (Houghton et al., 2010; Walker, 1980), producing a total eruptive magma volume of at least 35 km^3 DRE, equivalent to c. 105 km^3 of bulk pyroclastic material (Wilson, 1993; Wilson & Walker, 1985). It

comprised seven phases (Y1-Y7) (Figure 2.15) that produced two dry Plinian fall deposits (the Hatepe Pumice/Y2 and Taupō Plinian Pumice/Y5) (Figure 2.15), three phreatomagmatic fall deposits (the initial ash/Y1, the Hatepe Ash/Y3 and Rotongaio Ash/Y4), multiple intraplinian ignimbrites, a widespread ignimbrite (the Taupō ignimbrite/Y6) and a final effusive dome growing stage (Y7) (previously known as eruption Z) which created the Horomatangi and Waitanui reefs (Figure 2.14) (Houghton et al., 2010; Walker, 1980, 1981b; Wilson & Walker, 1985).

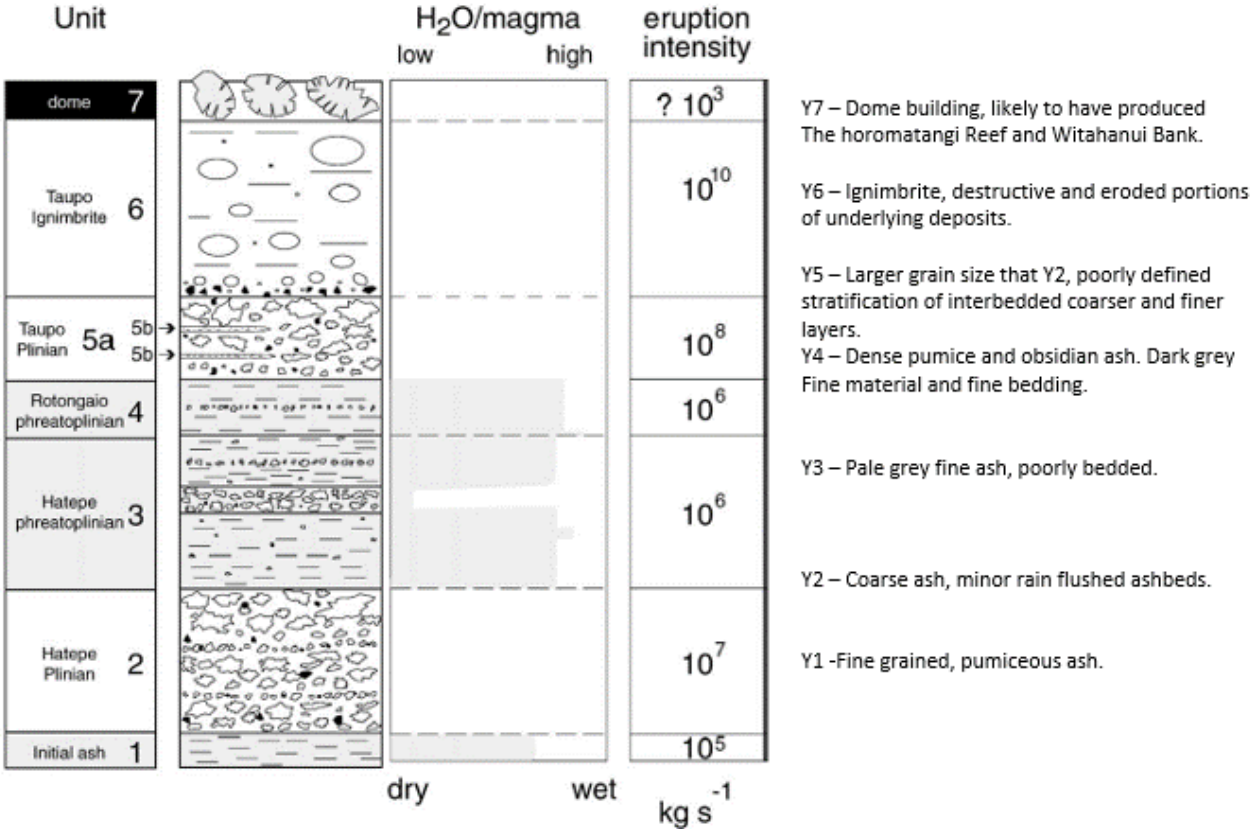

Figure 2.14: Eruptive products from the 232 CE Taupō Y Eruption as modelled by Houghton et al. (2010) after Wilson and Walker (1985), relative deposit thicknesses are not to scale. Descriptions adapted from (Houghton et al., 2010; Smith & Houghton, 1995); Wilson and Walker (1985).

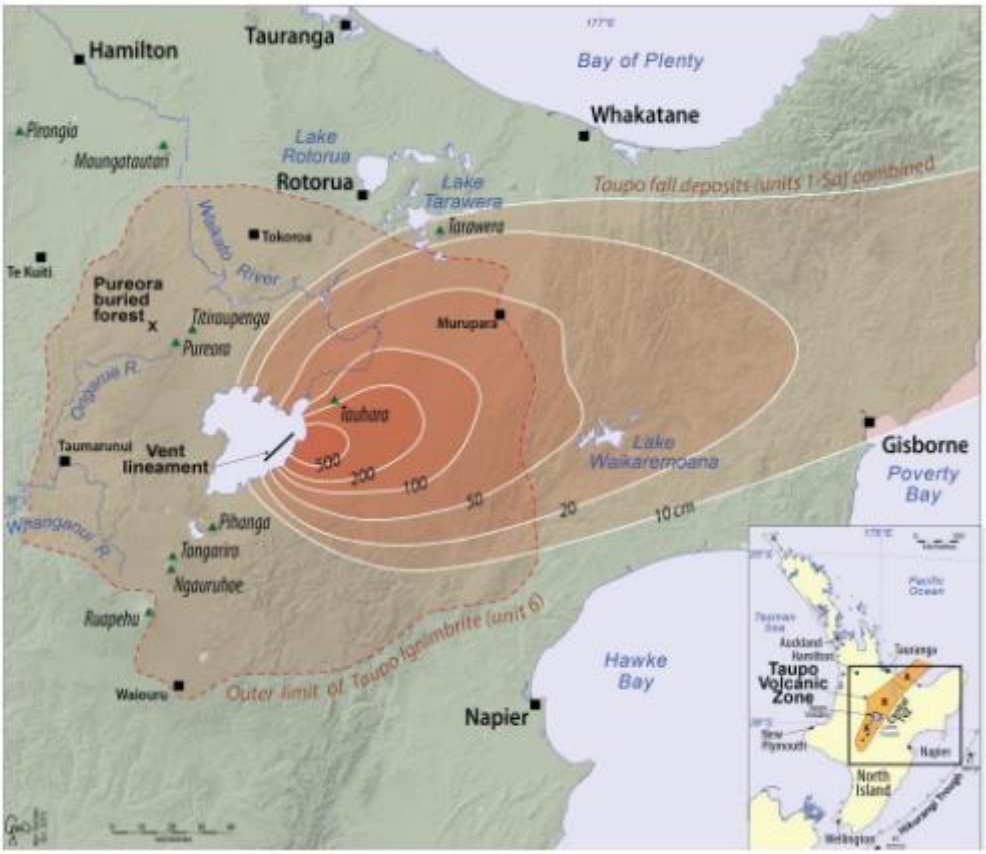

Figure 2.15: The isopaches of the Taupō fall deposits are indicated with solid white lines, the extent of the Taupō Ignimbrite (Y6) is shown with a dashed line (image from Lowe & Balks, 2019).

2.2.4.3.1 Taupō Y2 (Hatepe Pumice)

The Y2 fall deposit (Hatepe pumice) represents the second phase of the Taupō eruption. The deposit has a volume of 2.3 km^3 as calculated by isopach data or 6 km^3 as calculated by crystal mass method (Tapscott, 2023; Walker, 1981b), and reaches thicknesses of more than 2 m near the vent and has a dispersal distance of c. 140 km to the east coast of the North Island (Wilson, 1993).

The Y2 deposit at a location 20 km from the vent has a thickness of 146 cm with sharp contacts to the underlying Y1 and overlying Y3 units (Walters, 2020). The unit is dominated by pumice lapilli, massive with moderate to poor sorting, however, general reverse grading is seen in the upper 60% of the unit; and weak banding occurs at cm scale due to local fining and coarsening is present in the unit (Walters, 2020).

The deposit represents a shift to magmatic activity with sharp contacts to the underlying Y1 and overlying Y3 units (at a location c. 20 km from the vent) (Lowe & Pittari, 2021a; Walters, 2020). It is a uniform, faintly bedded and well sorted deposit, comprising relatively coarse pumice that is highly to extremely vesicular with low crystal content, minor amounts of dense juvenile clasts, and no ash beds with the exception of rain flush beds (Lowe, 2021; Tapscott, 2023; Wilson, 1993; Wilson & Walker, 1985). Textures within the deposit range from sheared to equant shaped bubbles, with higher density pumice displaying more bubble deformation than lower density pumice (Houghton et al., 2010; Walker, 1981b). The vesicularity of pumice within the Y2 deposit ranges from 68-87% with a mean of 76% (Houghton et al., 2010).

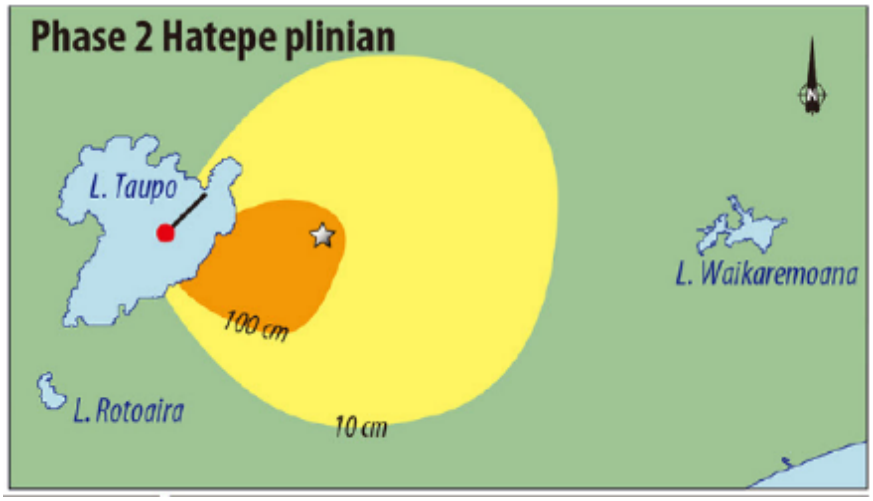

Figure 2.16: Map of the Y2 (Hatepe) fall deposit, based on Wilson & Houghton (2004) as cited in Lowe and Pittari (2021a); the red dot indicates the vent location at the end of the 9 km long NE-SW lineament in Lake Taupō.

2.2.4.3.2 Taupō Y5 (Taupō Plinian Pumice)

The Y5 fall deposit (Taupō Plinian Pumice) with a volume of between 7.7 km^3, as calculated using various isopach data, to c. 23-24 km^3 as calculated by mass balance calculations, was produced by a plinian eruption (Walker, 1980; Wilson, 1993). The Y5 deposit is widely dispersed the deposit reaching the coastline at c. 220 km to the east with 80% of the deposit being deposited further out to sea (Lowe & Pittari, 2021a; Walker, 1980; Wilson, 1993). The deposit has a maximum thickness of 1.8–2.1 m 20 km downwind of the vent and thins slowly (Figure 2.17) (Walker, 1980). The eruption plume is estimated to have reached heights of between c. 35-40 km (Houghton et al., 2014) and 50-55 km, with the eruptive phase lasting c. 6-17 hours (Lowe & Balks, 2019; Walker, 1980).

The Y5 deposit consists of 26 stratigraphic units of coarse pumice interbedded with intraplinian PDC deposits near the source. These units display changes in grain size, pumice morphology and lithic content (Walker, 1980; Wilson & Walker, 1985). At c. 20 km northeast of the source along SH5 the unit is 82 cm thick with a sharp basal contact and a distinct colour change to orange-brown from the grey-brown of the Y4 unit below (Tapscott, 2023). At this location the Y5 unit can be divided into a 30 mm thick unit dominated by very fine ash with fine lapilli and lithics with a gradational upper contact, overlain by ash-poor medium lapilli (Tapscott, 2023). In general, sorting improves with distance from the vent with an unusually low-density pumice being the major component of the deposit (Walker, 1980). Appreciable amounts of glass shards only occur in size classes < ¼ mm (Walker, 1980) and the very few lithic clasts are interpreted as being recycled from the vent walls (Wilson, 1993).

A wide range of vesicle sizes are found in the deposit with large equant vesicles formed by the merging of smaller vesicles (Houghton et al., 2010). Localised shear is seen in higher density clasts where finely vesicular deformed material surrounds clusters of large vesicles, while in lower density clasts large vesicles are surrounded by small bubbles (Houghton et al., 2010). The vesicularity of the Y5 deposit ranges from 68-85% with a mean of 79% (Houghton et al., 2010).

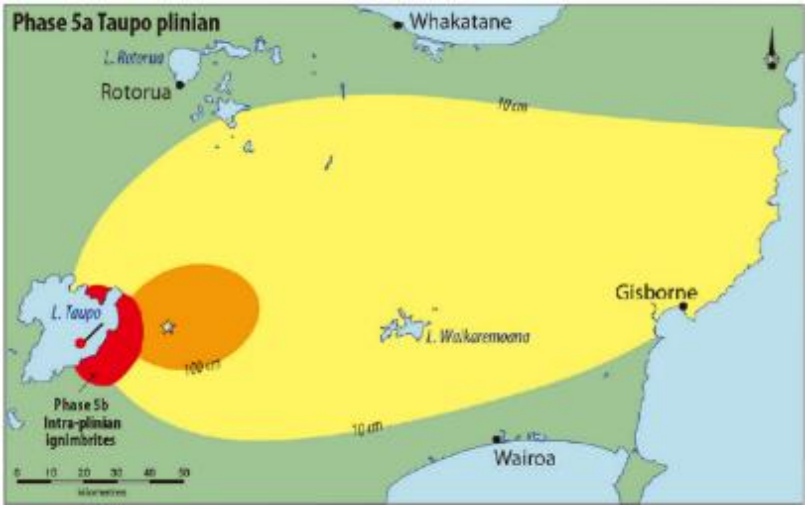

Figure 2.17: Map of the Y5 (Taupō) fall deposit, based on Wilson & Houghton (2004) as cited in Lowe and Pittari (2021a); the red dot indicates the vent location at the end of the 9 km long NE-SW lineament in Lake Taupō.

2.2.4.3.3 Taupō Fluvially Reworked Pumice

Fall deposits are classed as primary volcaniclastics by some (e.g., Manville et al., 2009) although the appropriate nomenclature has been highly debated (e.g., Cas & Wright, 1987; Fisher, 1961; Sohn & Sohn, 2019; White & Houghton, 2006). When these primary volcaniclastics are mobilised or reworked by a mass transport process such as flowing water, they become secondary volcaniclastics (Manville et al., 2009; Sohn & Sohn, 2019). These secondary volcaniclastic deposits are characterised by sedimentary features such as inverse grading, rafted pumices, and hydraulic sorting (settling by grain density) (Manville et al., 2009; Manville et al., 1999). Additionally, as material is transported by fluvial processes particle roundness increases due to abrasion as they collide with other particles (Szabó, 2015).

Large Plinian eruptions such as the 232 CE Taupō event cover the surrounding landscape in vast volumes of loose pyroclastic deposits, with intense reworking of the unconsolidated material affecting drainage networks for years to decades following the eruption (Manville et al., 2009). This has been observed following the eruption of Mount St. Helens in 1980 (Major & Mark, 2006; Major et al., 2000) and at Pinatubo in 1991 (Newhall & Punongbayan, 1996) with duration and extent of the sedimentary response varying between events depending on volume, nature, and distribution of the pyroclastic deposits as well as the local climate and topography (Manville & Wilson, 2004). In addition to the long-term landscape response, the sudden influx of large volumes of sediment can also have more immediate consequences as the material can form dams blocking pre-existing catchments thus creating potentially large lakes. Syn- or post-eruptive failure of these dams results in breakout floods that can release a large amount of water quickly (e.g., Hodgson & Nairn, 2005; Macías et al., 2004; Manville & Hodgson, 2010; Manville et al., 1999; Park & Schmincke, 2020; Schmincke et al., 1999; Smith, 1991a).

A breakout flood occurred when a 30-40 m dam of nonwelded ignimbrite produced by the 232 CE Taupō eruption and blocking the caldera outlet failed, releasing c. 20 km^3 of water into the Waikato River (Manville et al., 1999). This resulted in a 12 km spillway and fluvially reworked secondary volcaniclastic deposits including fan deposits, boulder lags, fine grained, laminated slack water deposits, and erosional and aggradation features extending c. 232 km downstream

of Lake Taupō (Manville, 2002; Manville et al., 1999; Manville & Wilson, 2004; Wilson & Walker, 1985).

The sedimentary response to the 232 CE Taupō eruption has not been limited to the Waikato River system. During the eruption volcanic deposits blocked and/or aggraded in drainage systems over c. 20,000 km^2 around the vent (Smith, 1991a). This caused long term sedimentary responses in catchments throughout the Waikato, the Bay of Plenty and Hawkes Bay (Manville et al., 2009; Segschneider, Landis, Manville, et al., 2002) including Lake Taupō and adjacent areas (Riggs et al., 2001; Smith, 1991b; White et al., 2001), Lake Reporoa and the Reporoa Basin (Manville, 2001, 2002), the Rangitaiki, Mohaka and Ngaruroro Rivers (Segschneider, Landis, Manville, et al., 2002; Segschneider, Landis, White, et al., 2002).

3 Methodology

3.1 Sampling Methods

Sample sites of the primary deposits were selected based on previous knowledge of the a) volcanic origin, type, and age of the tephra (to include young, primary deposits from 2 calderas and 3 different volcanic complexes with different densities, porosities, and mineralogical compositions), b) the locations (proximal versus distal), c) the suitability of the exposure, and d) the accessibility of the site. The Rotorua Tephra was split into three packages based on known differences in sedimentary characteristics and properties of juvenile particles. Samples were collected from the Y2 and Y5 units of the Taupō tephra, lapilli fall units of the medial Kaharoa and distal Kaharoa tephra.

3.2 Lab Work Methods

Samples were processed in the laboratories at Massey University to determine the volcanological and horticultural properties of the individual tephras. The parameters for two key hydroponic grades (1-4 mm and 4-8 mm) were also assessed.

Bulk density, air space, total water holding capacity, permanent wilting point and pH were determined from bulk samples of the hydroponic grades, which represent the most commonly grain size classes in hydroponic cultivation and propagation. Porosity and particle density were determined for individual pumice clasts of the samples.

3.2.1 Grain Size Distribution

Bulk samples were assessed for grain size distribution by a combination of wet and dry sieving. The fractions greater than 0 ϕ (phi) (1 mm) were weighted and the fractions less than 0 ϕ were analysed using a laser particle analyser. These methods are outlined below.

3.2.1.1 Wet Sieving

Wet sieving washes and separates the finer particles from coarser material (Advantech Mfg., 2001). Pumice samples were washed with water during wet sieving to separate smaller particles from larger particles including those which may have adhered to or embedded into the vesicles

of larger pumice clasts. Water is used during the process to prevent breakage of the pumice clasts.

Ideally a tower of sieve fractions is used, and water added to wash the sample through. However, in this instance samples were passed through a single -2 ϕ (4 mm) mesh sieve until the water ran clear. The resultant fraction of >-2 ϕ was transferred to containers and oven dried. The <-2 ϕ fraction was placed into buckets and left overnight to allow sediment to settle, the water was subsequently siphoned off and the samples oven dried.

3.2.1.2 Dry Sieving

The dried samples were then hand sieved through a stack of 7 sieves of decreasing mesh size in full phi (ϕ) increments as indicated in Table 3.1 below. Material with an axis smaller than the mesh size passes through to the lower sieve. To ensure all the appropriate size fraction passed through the sieve, each sieve was brushed. The samples were then collected, labelled, weighed and the proportions of each fraction calculated as weight percentages.

Table 3.1: Mesh Sizes in phi and mm used for dry sieving.

Sieve Mesh Size (ϕ)	Sieve Mesh Size (mm)
-6	64
-5	32
-4	16
-3	8
-2	4
-1	2
0	1

3.2.1.3 Laser Particle Analysis

A Laser Particle Analyser such as the Horiba Partica LA 950V2 Laser Scattering Particle Size Distribution Analyser (LPA or PSDA) uses laser diffraction of two light sources; one red (long wavelength to measure coarser particles) and one blue (short wavelength to measure finer particles) (HORIBA Ltd, 2023) to measure particle sizes from 0.01-3000 µm (3 mm).

To prepare for laser particle analysis, the <0 ϕ (1 mm) fraction of the sieved sample was passed through a riffle splitter to split the samples. Three sub samples of the split sample were analysed in the LPA using the Fraunhofer method which ignores particles smaller than 9 ϕ (1.95 µm) (clays). The Fraunhofer method was used because each mineral has its own refractive index, however the samples in this report contain a mixture of minerals.

3.2.1.4 Gradistat Calculations

The weight percentages calculated from sieving and the LAP data were entered into the Gradistat program to calculate the overall grain-size distribution and statistics (by weight) based on Folk and Ward (1957). These are calculated in both geometric (log-normal distribution with metric size values) and logarithmic scales (log-normal distribution with phi size values) using moment and graphical parameters (Blott & Pye, 2001). In the graphical method emphasis is placed on the central portion of the grain size curve with values outside 95% and 5% of the distribution being ignored (Blott & Pye, 2001). The logarithmic statistics of the graphical method used in this study are:

Graphic mean:

$$Mz = \frac{\Phi 16 + \Phi 50 + \Phi 84}{3}$$

Equation 1: Graphic mean (Folk & Ward, 1957).

Graphic standard deviation (sorting) describes the spread around the mean (Blott & Pye, 2001) and is calculated as:

$$\sigma 1 = \frac{\Phi 84 - \Phi 16}{4} + \frac{\Phi 95 - \Phi 5}{6.6}$$

Equation 2: Graphic standard deviation (Folk & Ward, 1957).

Graphic skewness is the symmetry of the distribution where fine skew (also known as positive or left skew) indicates more finer clasts and coarse skew (also known as negative or right skew) indicates more coarser clasts. Graphic skewness is calculated as:

$$Sk = \frac{\Phi 16 + \Phi 84 - 2\Phi}{2(\Phi 84 - \Phi 84)} + \frac{\Phi 5 + \Phi 95 - 2\Phi 50}{2(\Phi 95 - \Phi 5)}$$

Equation 3: Graphic skewness (Folk & Ward, 1957).

Kurtosis is the degree of concentration of the grains relative to the mean, where values greater than 1.0 indicate a strongly peaked (leptokurtic) distribution (Blott & Pye, 2001). Kurtosis is calculated as:

$$K = \frac{\Phi 95 - \Phi 5}{2.44(\Phi 75 - \Phi 5)}$$

Equation 4: Kurtosis (Folk & Ward, 1957).

Median = 50
Mode = the most frequently occurring grain size/s (by weight retained), where the sample is bimodal, two modes are given.

3.2.2 Volcanological Properties

A minimum of 300 grains were selected from both size fractions of each sample.

3.2.2.1 Pumice Morphologies and textures

The shape, textures, vesicularity and vesicle shapes of the pumice clasts from the componentry subsamples were assessed.

3.2.2.1.1 Clast Shape

Clast shape was assessed by visual inspection of pumice clasts from the componentry analysis subsamples and comparisons made against Figure 3.1.

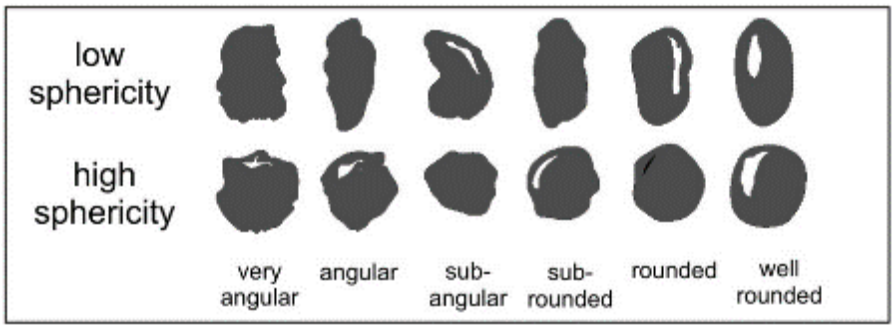

Figure 3.1: Clast shape (image from Geologyistheway, 2023)

3.2.2.1.2 Bubble textures

Macrotextures of dominant pumice types were assessed by visual inspection of clasts from the componentry subsamples. The classifications used in this study are based on bubble textures and banding, which indicate magma mixing prior to cooling (Wright et al., 2011).

3.2.2.1.3 Vesicularity

Houghton and Wilson (1989) proposed a vesicularity index of six classes derived from the arithmetic mean of 30 juvenile clasts and the vesicularity range as the total spread of values. Here macro-vesicularity was assessed visually.

Table 3.2: Vesicularity Index defined by Houghton and Wilson (1989).

% Vesicularity	Description
0-5	Non-vesicular
5-20	Incipiently vesicular
20-40	Poorly vesicular
40-60	Moderately vesicular
60-80	Highly vesicular
>80	Extremely vesicular

3.2.2.2 Componentry

Component analysis was performed on subsamples of the sieved samples, which were combined into hydroponic size classes as defined in Table 3.3. Subsamples contained a minimum of 300 grains to provide a representative componentry count and were obtained by manual quartering of the sample. The proportions of crystals, juvenile pyroclasts and lithics from each combination were determined. The juvenile grains were separated into different pumice types (as described below in the clast morphology section) and glass shards. The lithics were separated into hydrothermally altered material (altered by the interaction with hydrothermal fluids), heat altered material (altered by heat), recycled volcaniclastics and accidental lithics (basement or country rock).

Table 3.3: Combined grain size fractions used for componentry analysis.

Grain Size Fraction	Combination (ϕ)	Combination (mm)
1-4 mm	0Φ + -1 ϕ	1 + 2 mm
4-8 mm	-2 ϕ	4 mm

3.2.2.3 Particle Density

Skeletal and total density were measured using a Ultrapycnometer 1000 (a He-Pycnometer) and Envelope density was measured using a GeoPyc 1360.

Although a population of 30 clasts is usually adequate to construct a density histogram, the density means and standard deviations of 10 clasts is almost identical to those for 30 clasts (Houghton & Wilson, 1989), thus 10 clasts per sample were measured.

3.2.2.3.1 Skeletal Density

Skeletal density is the mass of a clast divided by the volume of the clast including the closed pores (pores within the clast) that are not accessible from the exterior of the clast (skeletal or apparent volume) (Figure 3.2B) (Webb, 2001).

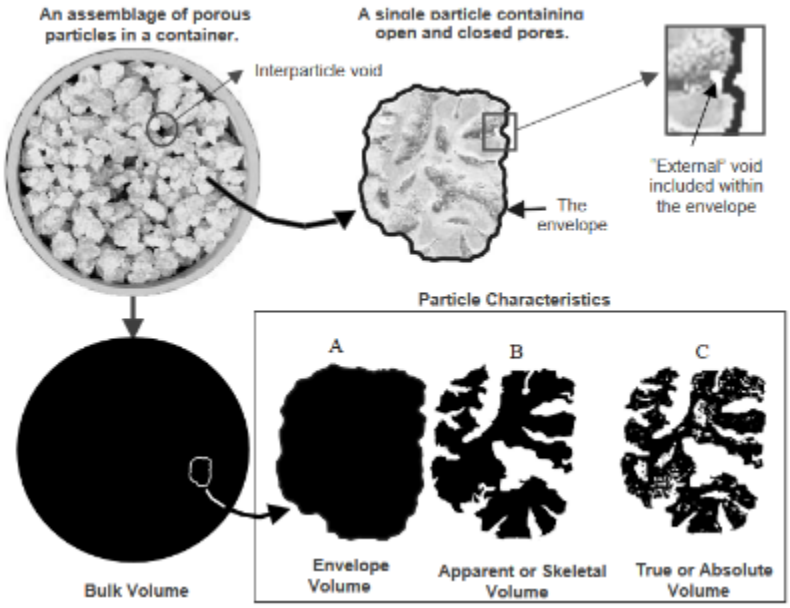

Figure 3.2: Volume types used in particle density calculations, the black areas of the particles in the box at the bottom of the image are analogous to volume. A is the envelope volume of the particle; B is the skeletal volume which contains the envelope volume less the external and open pore volume; C is the True volume and is the envelope volume less open and closed pores (image from Webb, 2001).

Skeletal density was measured in the Ultrapycnometer 1000 by using Archimedes' principle of fluid displacement and Boyle's law of volume pressure relationships. The instrument comprises two chambers. A sample (a pumice clast) of a known weight is placed in a chamber which is then pressurised with nitrogen to fill the connected pore space in the sample; the second chamber is a reference chamber of a fixed volume. A valved pathway between chambers admits nitrogen from the pressurised sample chamber into the reference chamber and transducers (pressure measuring devices) measure the change in pressure as the helium equalises between the chambers.

The calculation used when the sample chamber is pressurised first is:

$$Vg = Vc + \frac{Vr}{1 - \frac{P1}{P2}}$$

Equation 5: Sample volume equation.

Where Vg is the skeletal volume of the clast; Vc is the sample chamber volume; Vr is the reference chamber volume; P1 is the first pressure and P2 is the second pressure.

Skeletal density was calculated as:

$$dc = \frac{Mg}{Vg}$$

Equation 6: Skeletal density equation.

Where dc is the skeletal density; Mg is the mass of the clast and Vg is the skeletal volume of the clast as calculated above.

3.2.2.3.2 Envelope Density

Envelope density is the mass of a clast divided by volume including accessible small pores and cavities (envelope volume) (Figure 3.2A above) (Micromeritics Instrument Corporation, 2023; Webb, 2001). To measure the envelope density the clasts were placed in a GeoPyc 1360 pycnometer which determines volume and density by using displacement of a quasi-fluid called DryFlo (small rigid spheres with high flowability). The weight of the clast is entered into the GeoPyc 1360 and the DryFlo is placed in a chamber and a zero-depth run performed. The sample is then placed in the DryFlo which is then consolidated around the clast in the GeoPyc 1360, and

the displacement measured to give volume and envelope density (Micromeritics Instrument Corporation, 2023).

$$de = \frac{Mg}{Vb}$$

Equation 7: Envelope density equation.

Where de is the envelope density; Mg is the mass of the clast and Vb is the volume of the clast as calculated above.

3.2.2.3.3 Solid Density

Solid density (true density) is the mass of a clast divided by the total volume of the clast (without pores) (Figure 3.2C above). Solid density was measured in the Ultrapycnometer 1000 (a He-pycnometer) as above in Section 3.2.2.3.1, however the clast was crushed to remove intra-clast pore spaces and re-weighed prior to being placed in the chamber.

The calculation used when the sample chamber is pressurised first is:

$$Vp = Vc + \frac{Vr}{1 - \frac{P1}{P2}}$$

Equation 8: Sample volume equation.

Where Vp is the volume of the crushed clast; Vc is the sample chamber volume; Vr is the reference chamber volume; P1 is the first pressure and P2 is the second pressure.

Solid density was calculated as:

$$ds = \frac{Mp}{Vp}$$

Equation 9: Solid density equation.

Where ds is the solid density; Mp is the mass of the crushed clast and Vp is the volume of the crushed clast as calculated above.

3.2.2.4 Porosity of Pumice Clasts

The proportion of macropores is important for gas exchange, and water and nutrient absorption (Marinou et al., 2013). By using the bulk volume (Vb) as calculated by the GeoPyc 1360 pycnometer (Section 3.2.2.3.2), the volume of the clast determined by flowing gas (Vs) as calculated by the Ultrapycnometer 1000 (Section 3.2.2.3.1), and the solid density (ds) (Section

3.2.2.3.3), the total (bulk) porosity (Φt), connected porosity (Φc) and isolated porosity (Φi) were calculated.

3.2.2.4.1 Total Porosity

Total porosity is the total pore volume in a pumice clast, expressed as a percentage or fraction of the total volume (Wallach, 2019) or as porosity units. Although total porosity is related to envelope density, the envelope density cannot be used to calculate the total porosity if the pores are closed as occurs in pumice (Wallach, 2019).

Porosity is calculated from the bulk volume and solid density derived above (Sections 3.2.2.3.3). The calculation used is:

$$\Phi t = 1 - \left(\frac{Vb}{ds}\right) 100$$

Equation 10: Total porosity equation.

Where Φt is the total porosity, Vb is the bulk volume and ds is the solid density.

3.2.2.4.2 Connected Porosity

Connected or effective porosity is the intra-clast pore space through which an uninterrupted path exists between the edges of a clast and is calculated as:

$$\Phi c = \left(\frac{Vb - Vg}{Vb}\right) 100$$

Equation 11: Connected porosity equation.

Where Φc is the connected porosity, Vb is the bulk volume and Vg is the clast volume.

3.2.2.4.3 Isolated Porosity

Isolated porosity is the amount of intra-clast pore space that is not accessible to water and air (it is trapped within the clast) and is calculated as:

$$\Phi i = \Phi t - \Phi c$$

Equation 12: Isolated porosity equation.

Where Φi is the isolated porosity, Φt is the total porosity and Φc is the connected porosity.

3.2.3 Hydroponic Properties

3.2.3.1 pH

pH of the water used in the air space calculations (section 3.2.3.3 below) was measured using a litmus test paper. For the hydroponic media where organic material was incorporated, the water was left in the sample and the pH tested the following day and again 3 days later.

3.2.3.2 Bulk Density

Bulk density of an assemblage of particles (in this case hydroponic pumice particle classes) is the ratio of the mass of the solids to the bulk volume and is measured in kg/m^3, g/L (Blok et al., 2019) or g/cm^3 (Wallach, 2019). The bulk density is determined by the weight of a known volume of a material (Blok et al., 2019). If more than one component is in a media then the characteristics of all components contribute to the bulk density (Bar-Tal et al., 2019; Wallach, 2019).

To measure bulk density (db) a dry sub sample of the hydroponic media samples and the 1-4 mm and 4-8 mm fractions of the pumice samples were weighed and poured into a measuring cylinder. The cylinder was tapped five times and the sample volume measured; this was repeated five times and the average volume used in the calculation of bulk density by applying the following calculation:

$$Db = \frac{Md}{Vs}$$

Equation 13: Bulk density equation.

Where Db is bulk density of the sample in g/cm^3; Md is the dry weight in g; and Vs is sample volume is in cm^3.

3.2.3.3 Total Porosity, Free Air Space and Water Holding Capacity of the Bulk Medium

Water holding capacity can be measured volumetrically or gravimetrically. We have calculated the volumetric water holding capacity as this also provides total porosity and free air space for each sample and is generally used in hydroponics. Gravimetric water holding capacity has also been calculated as this provides information regarding stress point and permanent wilting point and is usually used to assess soils.

3.2.3.3.1 Volumetric Water Holding Capacity

To estimate volumetric water holding capacity (q) a container of known volume (with taped holes at the bottom) was filled with dry sub sample of the hydroponic media samples and the 1-4 mm and 4-8 mm fractions of the pumice samples; the container was then tapped 5 times. Water was then added to the container using a measuring cup until the medium was just covered with a thin film of water. The amount of water required to cover the sample was recorded and this volume used to calculate the total porosity (Pt) of the bulk sample using the equation:

$$Pt = \left(\frac{Vw}{Vs}\right)100$$

Equation 14: Total porosity of the bulk medium.

Where Pt is the total porosity of the bulk sample; Vw is the water volume in millilitres (ml); and Vs is sample volume in millilitres (ml).

Once the medium was saturated the pot was elevated above a bucket and the tape removed from the holes, allowing the water to drain. When water had finished draining the amount of drained water collected was measured. The drained water is used to calculate the percent of free air space using the equation:

$$As = \left(\frac{Drained\ water}{Total\ volume}\right)100$$

Equation 15: Free air space equation

Where As is the free air space as a percentage, drained water is the volume of collected water, and total volume is the volume of the container.

The volumetric water holding capacity of the medium can be calculated from the free air space and total porosity of the bulk sample:

$$q = Pt - As$$

Equation 16: Volumetric water holding capacity equation.

Where q is the volumetric water holding capacity; Pt is the total porosity of the bulk sample as a percentage; and As is the free air space as a percentage.

3.2.3.3.2 Gravimetric Water Holding Capacity

To estimate the gravimetric water holding capacity (ω), which is the mass of water divided by the mass of solids, subsamples of the pumice and hydroponic media were placed in rings on a 100 kPa (1bar) porous ceramic pressure plate. The ceramic plate had a rubber backing with a copper mesh between the rubber and ceramic plate to create an air gap. The subsamples were wet and left to stand in water overnight to ensure they were saturated. The pressure plate with sub samples was then removed from the water and held in a plastic bag to prevent evaporation. The underside of the plate was connected to a pump to create suction to draw water through the plate and remove it. The top of the pressure plate was at atmospheric pressure and the underside of the pressure plate was maintained at -10 kPa (-0.1 bar); this was regulated by a bubble tower that was attached to the pump. The water from under the pressure plate was trapped before reaching the pump and drained into a collecting flask (Figure 3.3). Once the water stopped dripping into the flask, the subsamples were removed and placed into containers and each subsample weighed while wet. The subsamples were then oven dried at 105°C overnight and reweighed in the morning; the container weight was also recorded.

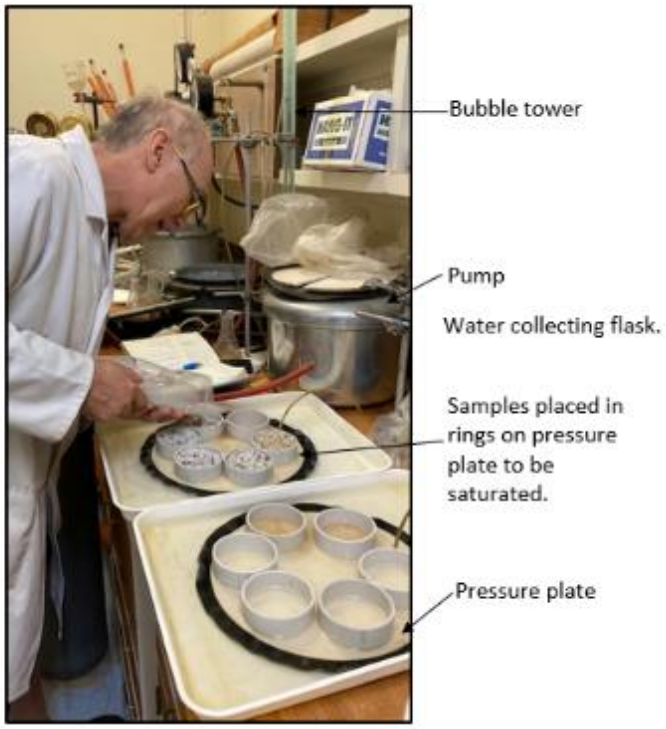

Figure 3.3: Sample preparation for water holding capacity.

To calculate the gravimetric water holding capacity the following equation was used:

$$\omega = (\frac{Mw - Md}{Md - Mc})100 = (\frac{Mwater}{Msample})100$$

Equation 17: Gravimetric water holding capacity equation.

Where ω is the gravimetric water holding capacity, Mw is the mass of the wet subsample, Md is the mass of the dry subsample, Mc is the mass of the container, Mwater is the mass of the water in the subsample and Msample is the dry mass of the subsample.

Volumetric water holding capacity can be linked to the gravimetric water holding capacity as:

$$Vw = \frac{Mwater}{water\ density} \text{ and } Vt = \frac{Msample}{bulk\ density}$$

thus

$$q = (Mwater/Dw)/(Msample/Db)$$

$$q = (Mwater/Msample)(Db/Dw)$$

$$q = \omega(Db/Dw)$$

$$q = \omega * Db$$

Where Dw is water density and is taken to be 1000 kg/m3 or 1 g/ml.

3.2.3.4 Stress Point

To estimate the stress point, subsamples of the pumice and hydroponic media were placed in rings on a 3,000 kPa (3 bar) porous ceramic pressure plate. The ceramic plate had a rubber backing with a copper mesh between the rubber and ceramic plate to create an air gap. The subsamples were wet and left to stand in water overnight to ensure they were saturated. The pressure plate with subsamples was then removed from the water and placed in a 500 kPa (5 bar) pressure vessel. The underside of the plate was connected to a collecting flask via plastic tubing to allow water to drain. Once the water stopped dripping into the flask, the subsamples were removed and placed into containers and each subsample weighed. The subsamples were

then oven dried at 105°C overnight and re-weighed in the morning; the container weight was also recorded. To calculate the gravimetric water content at stress point the following equation was used:

$$\omega SP = (\frac{Mw - Md}{Md - Mc})100 = (\frac{Mwater}{Msample})100$$

Equation 18: Water holding capacity equation.

Where ωSP is the gravimetric water content at stress point, Mw is the mass of the wet subsample, Md is the mass of the dry subsample, Mc is the mass of the container, Mwater is the mass of the water in the subsample and Msample is the dry mass of the subsample.

3.2.3.5 Permanent Wilting Point

To estimate the permanent wilting point, the procedure for estimating stress point (section 3.2.3.4) was repeated, however a 15,000 kPa (15 bar) pressure plate and pressure vessel were used. To calculate the gravimetric water content at permanent wilting point the following equation was used:

$$\omega PWP = (\frac{Mw - Md}{Md - Mc})100 = (\frac{Mwater}{Msample})100$$

Equation 19: Water holding capacity equation.

Where ωPWP is the gravimetric water content at permanent wilting point, Mw is the mass of the wet subsample, Md is the mass of the dry subsample, Mc is the mass of the container, Mwater is the mass of the water in the subsample and Msample is the dry mass of the subsample.

Total Available Water Holding Capacity

The total available water holding capacity (ωt) is the amount of water held in the growth medium between the gravimetric water holding capacity (ω) (Section 3.2.3.3.2) and the permanent wilting point (PWP) (Section 3.2.3.5). The total available water holding capacity is calculated as:

$$\omega t = \omega - \omega PWP$$

Equation 20: Total available water holding capacity equation.

Where ωt is total available water holding capacity, ω is water holding capacity and ωPWP is the gravimetric water content at permanent wilting point.

3.2.3.6 Readily Available Water Holding Capacity

The total available water holding capacity (ωr) is the amount of water held in the growth medium between the gravimetric water holding capacity (ω) (Section 3.2.3.3.2) and the stress point (SP) (Section 3.2.3.5). The readily available water holding capacity is calculated as:

$$\omega r = \omega - \omega SP$$

Equation 21: Readily available water holding capacity equation.

Where ωr is readily available water holding capacity, ω is water holding capacity and ωSP is the gravimetric water content at stress point.

4 Results

4.1 Rotorua Tephra

4.1.1 Field description

Three bulk samples of the Rotorua Tephra were collected on 10 June 2022 from the TW Moore Quarry on Okareka Loop Road (Table 4.1, Figure 4.1). The exposure comprised c. 5m of fine to coarse grained lapilli beds overlain by a c. 1.5 m-thick tephric soil (Figure 4.2a and b). The beds are described in a stratigraphic column (Figure 4.3). The samples were collected from three deposit packages based on visual differences in deposit and pumice clast properties (Figure 4.4). These units represent three phases of the 15.6 ka Rotorua eruption and are similar to those described by Kilgour and Smith (2008) as Units A, B and C. However, in this study, the boundary between RQ-L1-02 and RQ-L1-03 was drawn c. 30 cm above the boundary between Units A and B of Kilgour and Smith (2008). Sample RQ-L1-01 was collected from the lower portion of Unit C, sample RQ-L1-02 was collected from Unit B and sample RQ-L1-03 was collected from the upper section of Unit A and lowermost portion of Unit B (Figure 4.3).

Bulk sample RQ-L1-01 was derived from a poorly sorted, shower bedded, lithic-rich, fine to coarse lapilli deposit. Above the collection point the profile changed to a coarse ash similar to that described as Unit C by Kilgour and Smith (2008). Bulk sample RQ-L1-02 was collected from a very poorly sorted, shower bedded deposit of coarse ash to medium lapilli interbedded with fine lithic-rich ash layers similar to Unit B of Kilgour and Smith (2008). Bulk sample RQ-L1-03 represents a very poorly sorted, shower-bedded deposit made of coarse ash to coarse lapilli with interbedded fine lithic-rich ash layers. This differs from Unit A, which was described by Kilgour and Smith (2008) as being coarse to very coarse typically reverse graded lapilli but is similar to Unit B. This is likely due to the collection location of the bulk samples relative to Kilgour and Smith (2008) Unit A and Unit B boundary.

The differences between Units, A (RQ-L1-03), B (RQ-L1-02) and C (RQ-L1-01) are due to different chemical compositions that indicate the degassed magma source found by Kilgour and Smith (2008) and described by Shane et al. (2008) as magmas T1 and T2 (Figure 4.3). Sample RQ-L1-03 was collected from the T1 deposits which are dominated by low-K_2O/high-CaO lapilli with

orthopyroxene + hornblende + augite (Shane et al., 2008). Sample RQ-L1-02 was collected from the upper section of the T1 deposit which contains rare high-K_20 (>4 wt%) and low-CaO (<0.9 wt%) biotite-bearing lapilli (Shane et al., 2008). Sample RQ-L1-01 was collected from T2 deposits that overlie T1 deposits and contain abundant biotite and high-K_2O/low-CaO Shane et al. (2008).

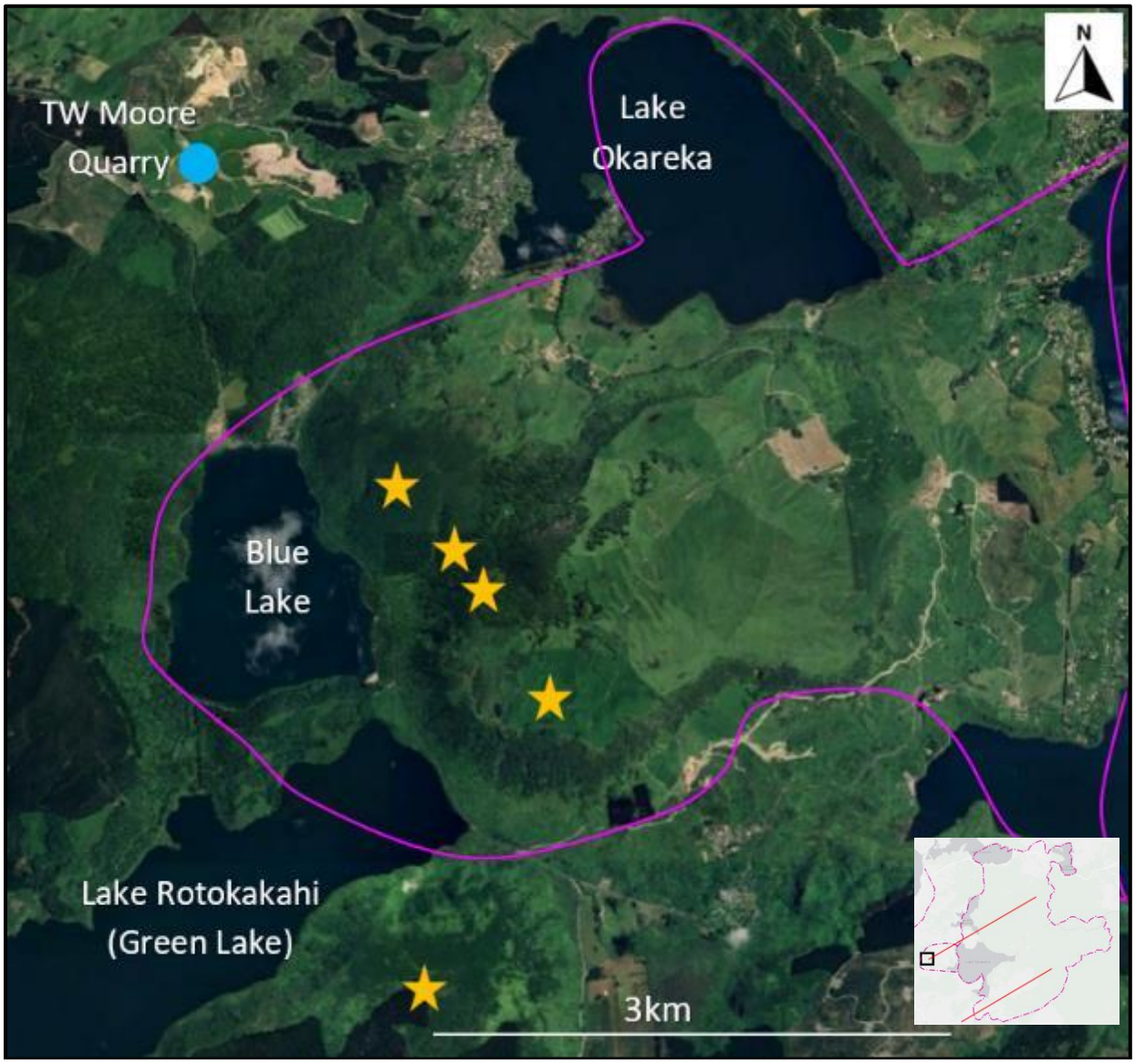

Figure 4.1: Map indicating TW Moore Quarry (blue dot) where the Rotorua samples were collected. Yellow stars indicate the inferred vent locations after Nairn (1980), pink lines indicate approximate boundaries of the Okareka Embayment and OVC (image adapted from Google Earth). Inset Map: Pink lines indicate the OVC and Okareka Embayment, red lines indicate Linear Vent Zones, and the black box shows map location.

Figure 4.2a: The Rotorua Tephra Sample Collection Site at TM Moore Quarry on Okareka Loop Road.

Figure 4.2b: Close-up of the Rotorua Tephra bulk sample packages at TM Moore Quarry.

Table 4.1: Sample Collection Details.

Tephra	Sample Location	Sample #	Sample description	Date collected
Rotorua	TW Moore Quarry, Okareka Loop Rd	RQ L1 01 (Upper section)	Poorly sorted fall deposit of fine-medium lapilli with coarse ash and lithics	10.06.2022
		RQ L1 02 (Middle section)	Medium – coarse lapilli, poorly sorted, some medium – coarse ash, some black lithics	10.06.2022
		RQ L1 03 (Lower section)	Fine – medium lapilli, coarse ash with lithics and ash layers	10.06.2022

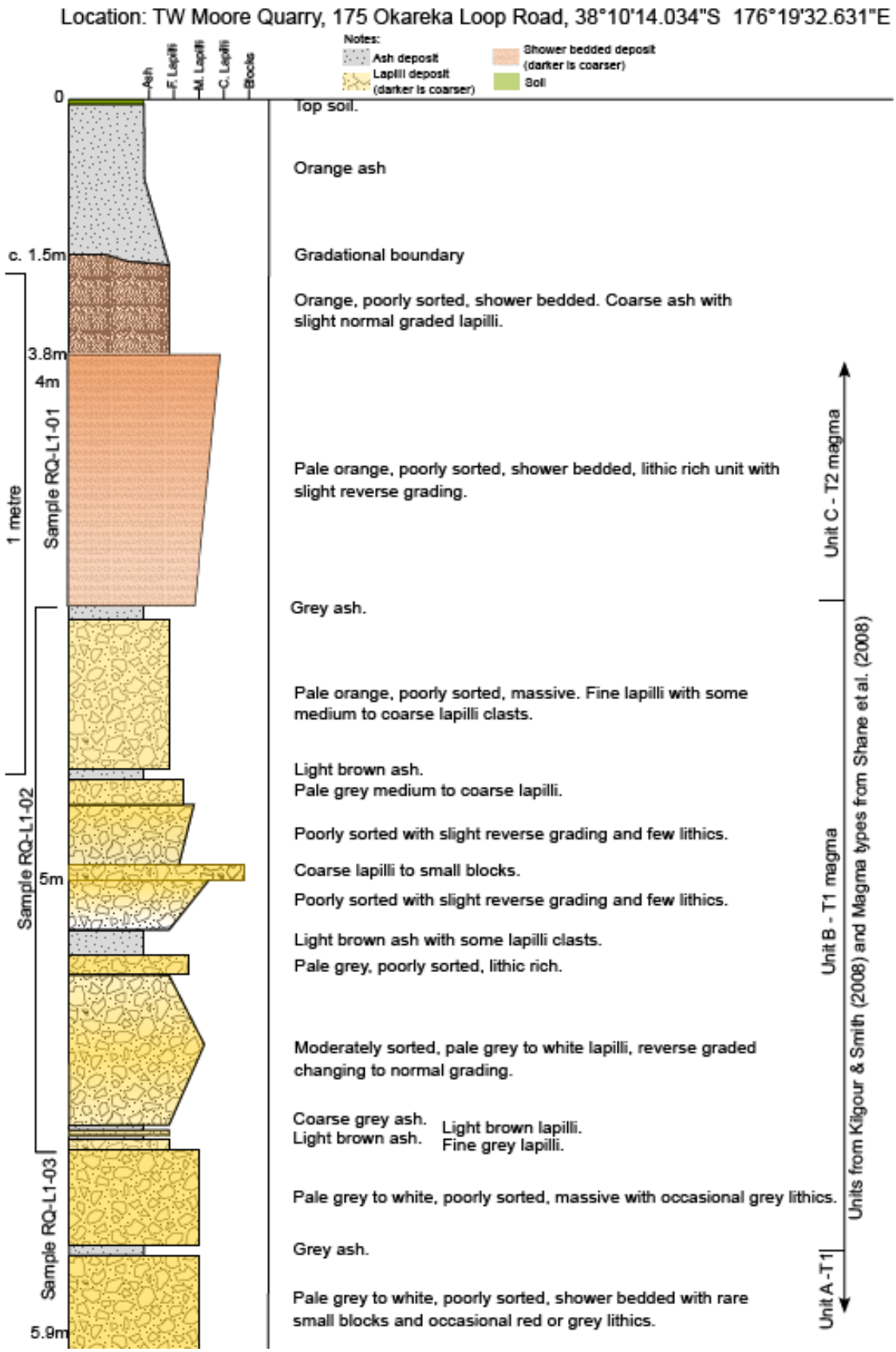

Figure 4.3: TW Moore Quarry Exposure Stratigraphic Column.

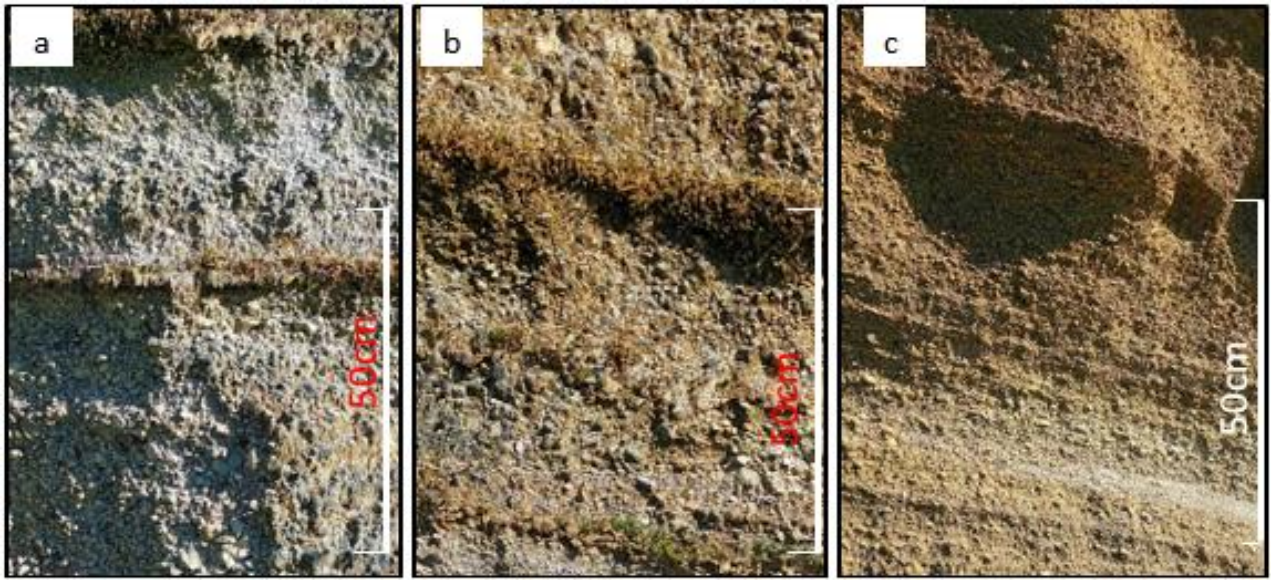

Figure 4.4: Sample collections areas. a. Sample RQ-L1-03; b. Sample RQ-L1-02; c. Sample RQ-L1-01.

4.1.2 Physical Properties

4.1.2.1 Grain size distribution

Grain size distribution classifications are based on statistical parameters that describe the sample. The mean is the average grain size, the median (D_{50}) is the size below which 50% of the particles fall and Mode 1 is the grain size with the highest weight fraction (the largest peak in the graph); a second mode indicates the sample is bimodal. Standard deviation (σ) is the amount of sample within a range from the mean and is used in the calculations of graphic mean, skewness, and kurtosis. D_{10} is defined as the point on the distribution curve below which 10% of the particles fall and D_{90} is the point below which 90% of the particles fall.

Kurtosis and skewness are dimensionless ratios indicating sorting. Kurtosis is a measure of how sharp the curve is and indicates the sorting relationship between the end and centre of the curve; a sharp peak (leptokurtic with values >1.0) suggests better sorting than a flat curve which has a large grain size spread in the centre (platikutic with values <1.0). Skewness indicates the grain spread characteristics, the closer to zero the more symmetrical the curve. Higher values indicate an asymmetrical curve with positive and negative numbers indicating whether the sample is skewed to the left or right. A positive number shows that the sample is skewed to the right with a fine tail to the left, negative values indicate the opposite (López, 2016).

The RQ-L1-01 bulk sample (Figure 4.5a and b) is poorly sorted with a coarse ash (<2 mm) to lapilli (2-64 mm) dominated distribution. The histogram is unimodal and symmetrical with a peak between 0-1 ϕ; a coarse tail extending to -5 ϕ and a long fine tail extending to 8 ϕ. The cumulative curve indicates that there is a steady increase in grain size from -0.4 ϕ to 1.0 ϕ, at 1 ϕ grain size tapers off with a long tail extending to 8 ϕ. D_{10} is -3.20 ϕ and D_{90} is 1.15 ϕ.

The RQ-L1-02 bulk sample (Figure 4.5c and d) is very poorly sorted with a coarse ash to lapilli dominated distribution. The histogram is unimodal and left skewed with a peak between -3 to -4 ϕ. It has a coarse tail extending to -6 ϕ and a long fine tail extending to 9 ϕ. The cumulative curve indicates that there is a steady increase in grain size from -0.5ϕ to 1.0 ϕ, at 1 ϕ grain size tapers off to a long tail extending to 9 ϕ. D_{10} is -4.23 ϕ and D_{90} is 1.11 ϕ.

The RQ-L1-03 bulk sample (Figure 4.5e and f) is very poorly sorted with a coarse ash to lapilli dominated distribution. The histogram is bimodal and left skewed with peaks between -2 to -3 ϕ and > -6 ϕ, with a coarse tail extending to >-6 ϕ and a long fine tail extending to 9 ϕ. The cumulative curve indicates that there is a steady increase in grain size from -0.5 ϕ to 0 ϕ, at 0 ϕ grain size tapers off to a long tail extending to 9 ϕ. D_{10} is -4.81 ϕ and D_{90} is 0.52 ϕ.

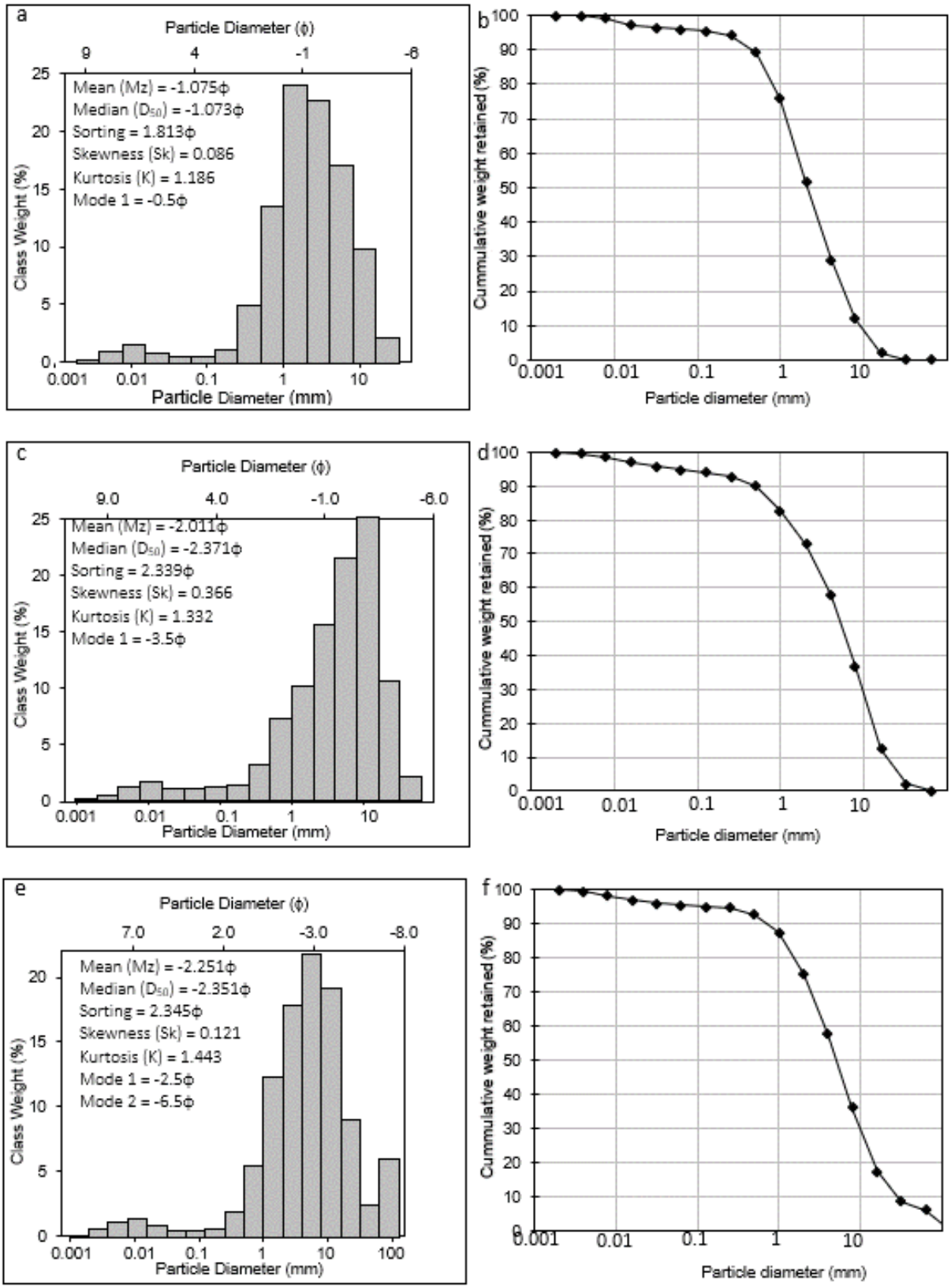

Figure 4.5: Grain size distribution histograms & cumulative curves of RQ-L1-01 (a, b) RQ-L1-02 (c, d) RQ-L1-03 (e, f).

4.1.2.2 Pumice Morphologies and Textures

Between 228 and 361 pumice clasts were assessed.

4.1.2.2.1 Pumice types

The pumice clasts within the samples were assessed visually and separated into four types (Figure 4.6). R.Dense clasts are rounded to subrounded with a uniform texture and are incipiently to poorly vesiculated with equant to slightly elongated vesicles. R.Light clasts are rounded to subrounded with a uniform to frothy texture and are highly to extremely vesiculated with equant to elongated vesicles. R.Angular clasts are subangular to angular with a uniform to fibrous texture and are highly vesiculated with elongated vesicles. R.Banded clasts have a banded texture.

Figure 4.6: Pumice types identified in the Rotorua Tephra, scale bar with 1 mm intervals shown at the bottom of the photos. a. R.Dense, b. R.Light, c. R.Angular and d. R.Banded.

4.1.2.2.2 Clast Shapes

Visual observations of the Rotorua pumice clast shapes indicated that the dominant clast shape was subrounded in all fractions except for RQ-L1-01 1-4 mm in which the dominant shape was

rounded. The samples also contained minor amounts of more angular clasts (Figure 4.7, Table 4.2).

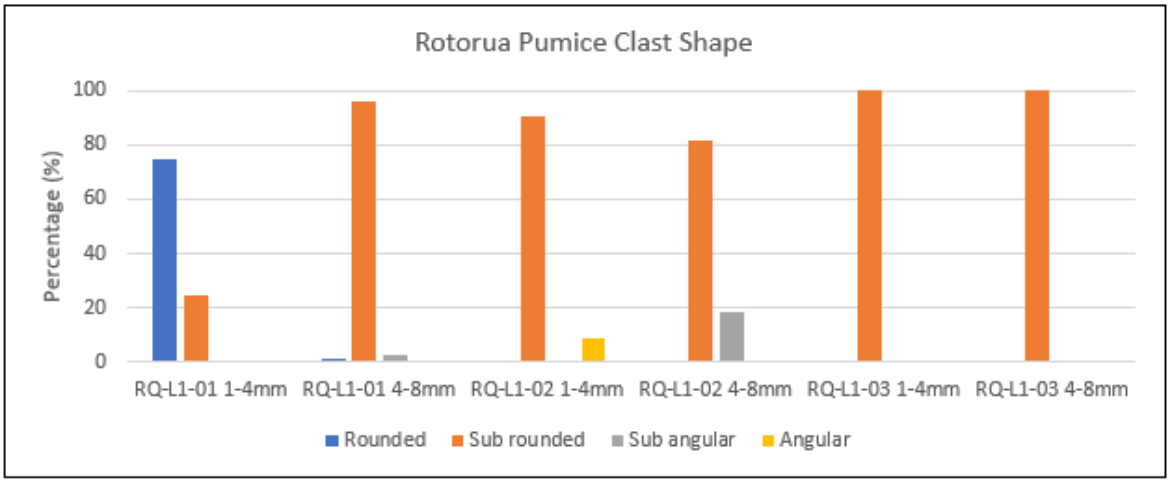

Figure 4.7: Clast shape proportions of the Rotorua samples.

Table 4.2: Morphologies and textures of Rotorua pumice clasts.

Sample	Clast Shape (%)				Clast Texture (%)			Clast Vesicularity (%)					Vesicle Shape (%)		
	Rounded	Sub rounded	Sub angular	Angular	Uniform	Frothy	Fibrous	Incipiently	Poorly	Moderately	Highly	Extremely	Equant	Slightly Elongate	Elongated
RQ-L1-01 1-4mm	74.7	24.9	0.0	0.0	75.1	24.9	0	75.1	0.0	0	24.9	0.0	75.1	0.0	24.9
RQ-L1-01 4-8mm	0.9	96.3	2.8	0.0	97.2	0	2.8	0.0	96.3	0	2.8	0.9	0.0	96.3	3.7
RQ-L1-02 1-4mm	0.8	90.2	0.0	9.0	91.0	0	9.0	0.8	82.1	0	17.1	0.0	9.0	0.0	91.0
RQ-L1-02 4-8mm	0	81.4	18.6	0.0	100	0	0	0	0	97.2	2.8	0.0	15.9	81.4	2.8
RQ-L1-03 1-4mm	0	100	0.0	0.0	100	0	0	0	0	100	0	0	0	100	0
RQ-L1-03 4-8mm	0	100	0.0	0.0	100	0	0	0	0	100	0	0	0	0	100

4.1.2.2.3 Clast Textures

Clast textures are defined as uniform (an almost smooth surface with circular vesicles), frothy (with many circular vesicles) or fibrous where the vesicles are elongated in one direction due to shear during the explosion (Ohashi et al., 2020) and banded.

The dominant texture in all samples is uniform with minor amounts of frothy or fibrous textures present in RQ-L1-01 and RQ-L1-L2 (Table 4.2).

4.1.2.2.4 Clast Vesicularities

The pumice macro-vesicularity as proposed by Houghton and Wilson (1989) (Section 3.2.2.1.3) was visually assessed. Vesicularity decreases towards the top of the profile and increases as clast size increases. In RQ-L1-01 and RQ-L1-02 vesicularity is generally higher in the 4-8 mm fractions than the 1-4 mm fractions (Figure 4.8, Table 4.2). Vesicularity in both size fractions of the RQ-L1-02 sample was similar.

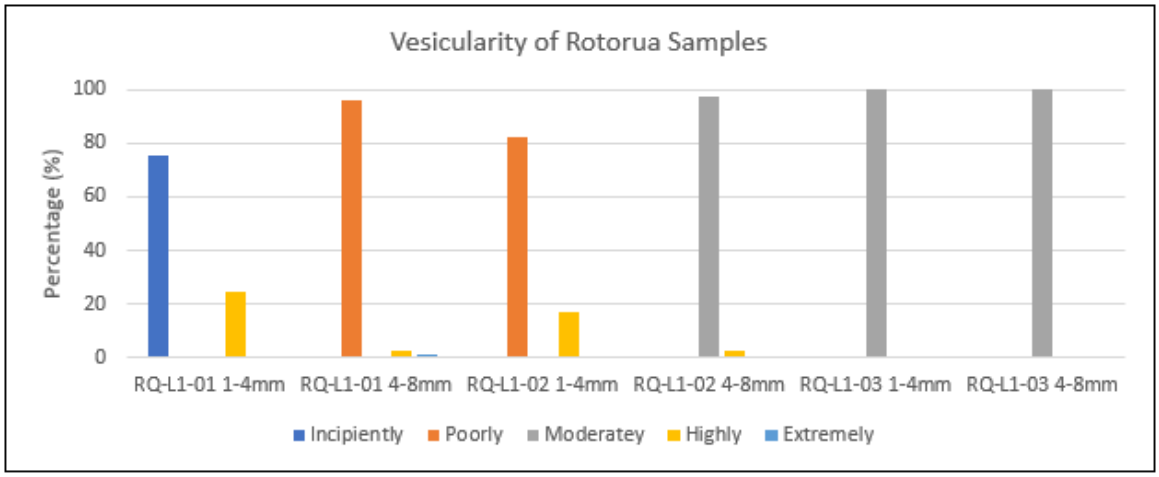

Figure 4.8: Clast vesicularity proportions of the Rotorua samples.

4.1.2.2.5 Vesicle Shapes

Vesicle shape was observed visually. Vesicles are more elongated in RQ-L1-01 and RQ-L1-03 4-8 mm fractions than the corresponding 1-4 mm fractions, whereas the vesicles in RQ-L1-02 1-4 mm were more elongated than those in RQ-L1-02 4-8 mm. The dominant vesicle shape in RQ-L1-01 1-4 mm was equant and in RQ-L1-02 1-4 mm and RQ-L1-03 4-8mm it was elongated; the remaining sample contained predominantly slightly elongated vesicles (Figure 4.9, Table 4.2).

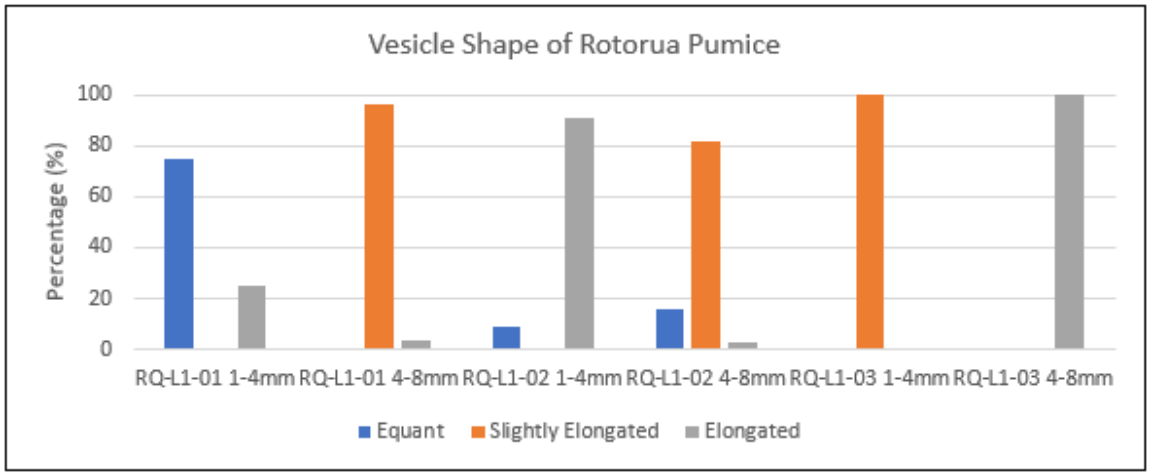

Figure 4.9: Vesicle shape of Rotorua pumice clasts.

4.1.2.3 Componentry

Componentry of volcanic deposits provides information on the nature of the vent and eruption processes. Here, the relative proportions of the various pumice types (described in Section 4.1.2.2.1), accidental lithics, recycled volcaniclastic material, hydrothermally and heat altered material, free, and glass shards were counted. Accidental clasts are country or basement rock lithics. Recycled clasts are recycled volcaniclastic material. Hydrothermal clasts are hydrothermally altered material. Heat clasts are heat altered material. Crystals are crystals formed through volcanics and Glass are glass shards. Analysis was undertaken on a minimum of 300 grains from each of the 1-4 mm and 4-8 mm fractions of each sample.

Pumice contents within the 1-4 mm fractions of the samples decreased by 16.4% towards the top of the stratigraphic profile from 90% in RQ-L1-03 to 73.6% in RQ-L1-01. Pumice contents within the 4-8 mm fractions were generally higher than in the smaller grade and slightly increased by 1.9% towards the top of the profile from 90.4% in RQ-L1-03 to 92.3% in RQ-L1-01 (Figure 4.10, Table 4.3). The dominant pumice type in all samples is R.Dense with slightly higher overall contents in the coarser fraction. A small amount of banded pumice is present in the 1-4 mm fractions of each sample. The proportions of R.Light and R.Angular clasts vary strongly between sample fractions (Figure 4.11, Table 4.3).

Lithics composed of volcaniclastic material, country rock and heat or hydrothermally altered material were found in all Rotorua samples (Figure 4.10, Table 4.3). Lithic contents of the 1-4 mm

and 4-8 mm fractions within a sample were similar, with RQ-L1-02 1-4 mm containing the highest proportion (Figure 4.12, Table 4.3).

The proportion of glass shards in the sample fractions varied greatly from 7.7% in RQ-L1-01 1-4 mm to 0.6% in RQ-L1-02 4-8 mm (Figure 4.10, Table 4.3).

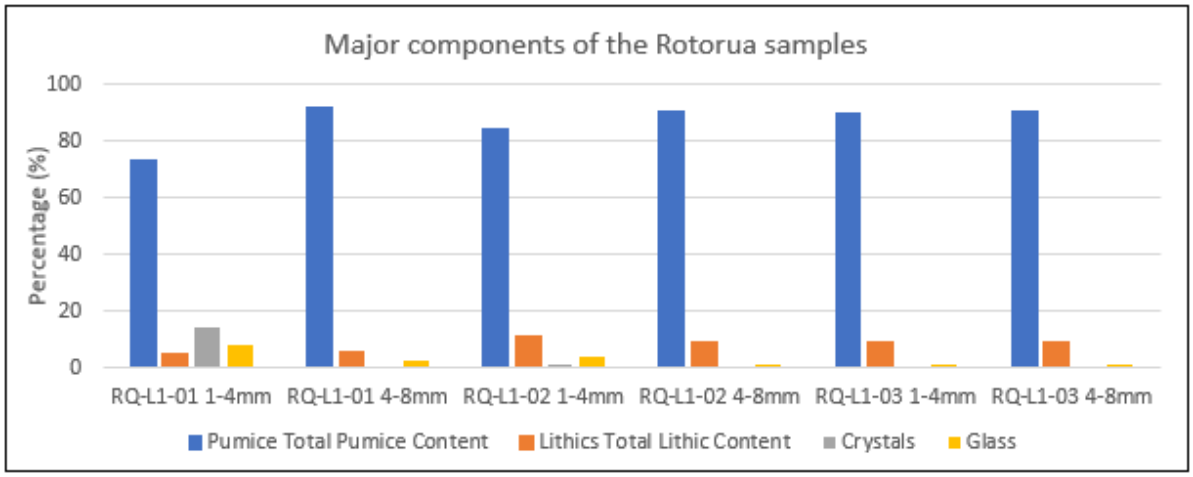

Figure 4.10: Major componentry of the Rotorua Pumice samples.

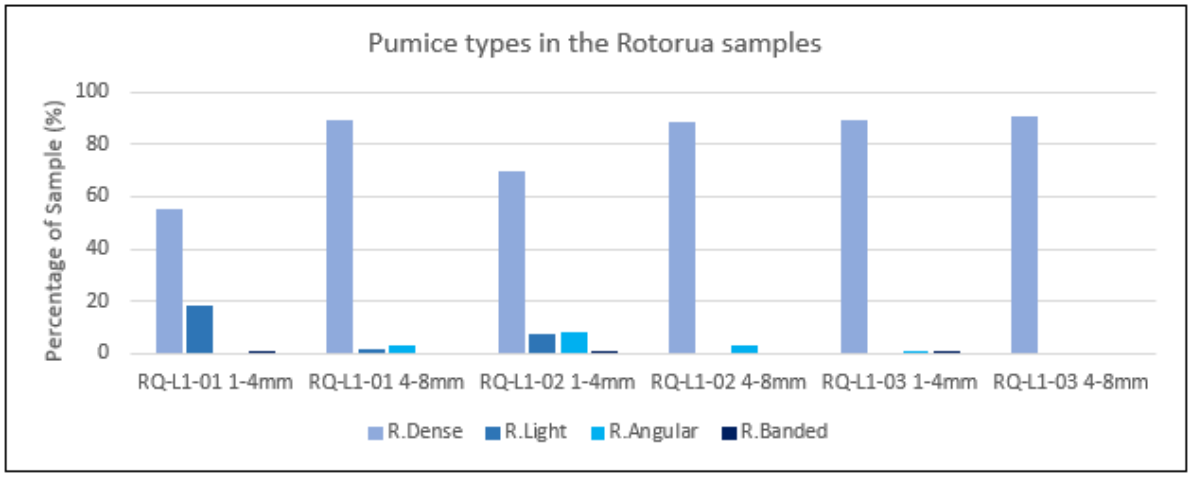

Figure 4.11: Proportions of pumice types in the Rotorua samples.

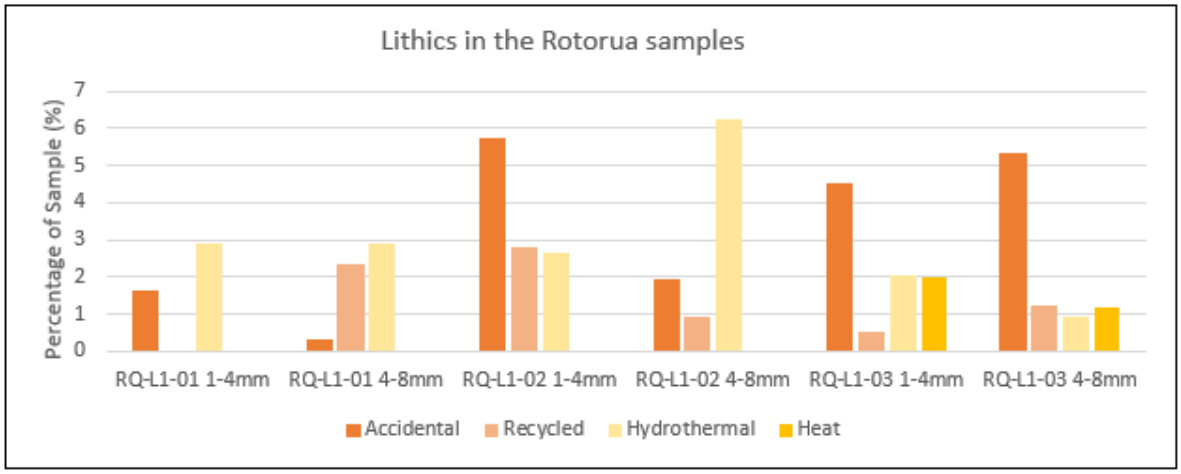

Figure 4.12: Proportions of lithics in the Rotorua samples.

Table 4.3: Componentry of the Rotorua samples.

Sample	Pumice (%)					Lithics (%)					Crystals (%)	Glass (%)
	R.Dense	R.Light	R.Angular	R.Banded	**Total Pumice Content**	Accidental	Recycled	Hydrothermal	Heat	**Total Lithic Content**		
RQ-L1-01 1-4mm	54.8	18.1	0	0.7	**73.6**	1.6	0	2.9	0	**4.5**	**14.2**	**7.7**
RQ-L1-01 4-8mm	88.8	0.9	2.6	0	**92.3**	0.3	2.3	2.9	0	**5.4**	**0**	**2.3**
RQ-L1-02 1-4mm	69.7	6.9	7.6	0.5	**84.6**	5.7	2.8	2.6	0	**11.1**	**0.7**	**3.6**
RQ-L1-02 4-8mm	87.9	0	2.5	0	**90.3**	1.9	0.9	6.2	0	**9.0**	**0**	**0.6**
RQ-L1-03 1-4mm	89.0	0	0.3	0.8	**90.0**	4.5	0.5	2.0	2.0	**9.0**	**0**	**1.0**
RQ-L1-03 4-8mm	90.4	0	0	0	**90.4**	5.3	1.2	0.9	1.2	**8.7**	**0**	**0.9**

4.1.2.4 Particle density and porosity

Particle density is the density of an individual particle, in this case pumice clasts, and excludes the air space between particles included in bulk density calculations. Particle density is important in hydroponics for pedotransfer functions and is used in media porosity calculations (Ruehlmann, 2020).

Due to the clast size required by the Ultrapycnometer 1000 (a He-Pycnometer) and GeoPyc 1360 particle densities and porosities were only calculated for the pumice clasts of the 4-8 mm fractions of samples.

Particle densities generally decrease towards the top of the profile, except for the envelope density of RQ-L1-02 which is slightly higher than that of RQ-L1-03 (Table 4.4, Figure 4.13).

Total porosity reduces slightly towards the top of the profile. The connected and isolated porosities of RQ-L1-01 and RQ-L1-03 are similar. However, the connected porosity of RQ-L1-02 exceeds that of both RQ-L1-01 and RQ-L1-03 and the isolated porosity of RQ-L1-02 is less than both RQ-L1-01 and RQ-L1-03 (Table 4.4, Figure 4.14).

As envelope density decreases the connected and isolated porosities increase, and as skeletal and solid density decreases total porosity also decreases.

Table 4.4: Mean Particle Densities and Porosities of Rotorua Pumice Sample Subsets of 10 Clasts.

	RQ-L1-01 (4-8 mm)		RQ-L1-02 (4-8 mm)		RQ-L1-03 (4-8 mm)	
	Mean	SD (σ)	Mean	SD (σ)	Mean	SD (σ)
Skeletal density (dc)	2.94g/cm^3	0.362	2.87g/cm^3 (10)	0.423	1.83g/cm^3	0.195
Envelope density (de)	1.07g/cm^3	0.313	0.78g/cm^3 (10)	0.04	0.81g/cm^3	0.152
Solid Density (ds)	2.85g/cm^3	0.483	2.77g/cm^3 (10)	0.629	2.23g/cm^3	0.142
Total porosity (Φt)	87.82%	1.57	86.23% (10)	2.54	85.49%	2.03
Connected porosity (Φc)	62.8%	11.56	72.27% (10)	4.40	56.10%	6.73
Isolated porosity (Φi)	24.95%	10.76	13.96% (10)	5.20	29.39%	7.30

Refer Appendices for raw data from which calculations were made.

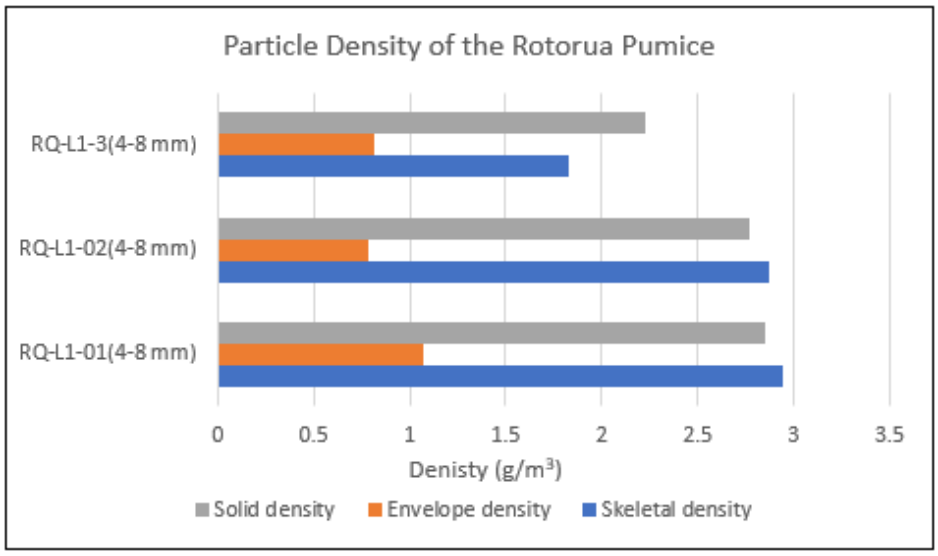

Figure 4.13: Mean particle densities of a subset of the Rotorua samples.

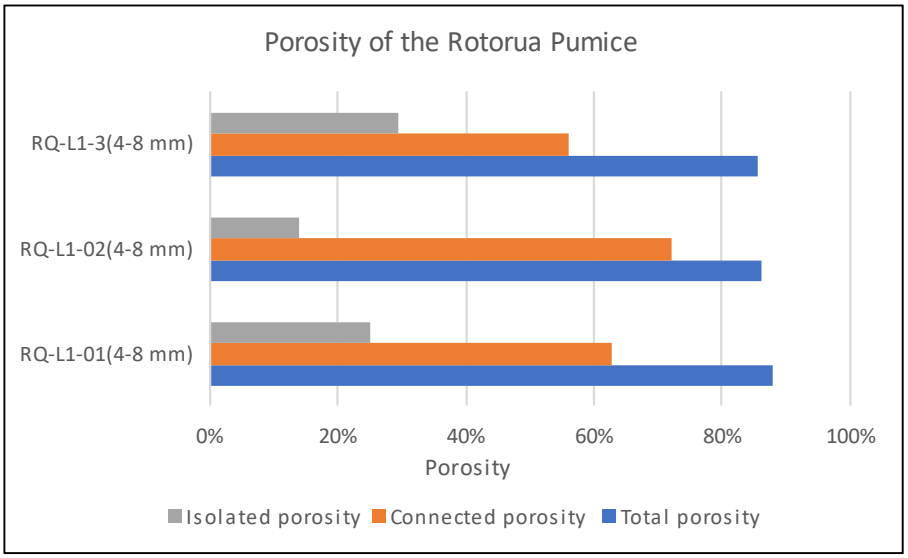

Figure 4.14: Mean porosity of a subset of the Rotorua samples.

4.1.3 Hydroponic Properties

4.1.3.1 Bulk Density, Total Porosity, Free Air Space, pH, and Water Holding Capacity

The bulk density, total porosity, free air space, pH and water holding capacities were measured on a subsample of each size fraction. These parameters are investigated here as they affect plant growth in hydroponics as well as transport and handling of a medium.

In hydroponics bulk density of a growth medium affects the water holding and aeration properties, root penetrability (Bar-Tal et al., 2019) and nutrient transport of a growth media (Wallach, 2019). Media with lower bulk densities tend to be easier to mix and transport than

those with higher bulk densities (Wallach, 2019). Additionally, as the set up for hydroponics often includes beds or pots on a raised stand, a lower bulk density is important for the handling and support of the pots.

Total porosity of the bulk medium is the percentage of inter- and intra-clast pore spaces in the medium that can be filled by water and/or air. Free air space is the percentage of the total volume of the drained medium that is occupied by air. These spaces contain gases that are constantly diffusing to and from the atmosphere. Free air space in a growth medium provides plant roots with the oxygen they require for metabolism and stores carbon dioxide produced by plant respiration before it diffuses back to the atmosphere.

Water holding capacity, also referred to as field capacity, is the amount of water the medium can hold when freely drained. Field capacity was defined in California in 1949 as "*the amount of water held by a soil after excess water has drained away and the rate of downward movement has naturally decreased*". This determines the amount of water and aeration available to plant roots in a growth medium and is related to the pore size distribution and bulk density (Bar-Tal et al., 2019). If growth media are mixed the water holding capacity is determined by the size and distribution of each medium and the new inter- and intra-clast pore spaces created when they are mixed (Bar-Tal et al., 2019).

pH is a measure of the amount of free hydrogen ions (H^+) and hydroxyl ions (OH^-) in an aqueous solution, indicating the solution's acidity or alkalinity (basic). pH ranges from 0 to 14, with 7 being neutral ($H^+ = OH^-$), values below 7 ($H^+ > OH^-$) being acidic and those above being alkaline ($H^+ < OH^-$). pH requirements vary depending on the plant species. The correct pH for a species increases the plant's ability to absorb nutrients and thus the plant's growth rate and overall health are improved (Saaid et al., 2021). The pH for most hydroponically grown crops such as melons, apples, beans, squash, and tomatoes lie between 5.5 and 6, however, others such as blueberries need a lower pH of 4.0 – 5.0.

The bulk density of the 4-8 mm fractions is less than that of the 1-4 mm fractions in the Rotorua samples (Figure 4.15). The bulk density generally increases towards the top of the profile from

0.62 g/cm^3 to 0.74 g/cm^3 in the 1-4 mm fractions and from 0.53 g/cm^3 to 0.68 g/cm^3 in the 4-8 mm fractions, although the RQ-L1-02 4-8 mm fraction was 0.50 g/cm^3.

The greatest range in bulk density between size fractions occurs in the RQ-L1-02 sample (0.16 g/cm^2) and the least in the size fractions of the RQ-L1-01 sample (0.05 g/cm^2) (Figure 4.15).

Total Porosity of the Rotorua pumice varied from 52.58% in RQ-L1-01 1-4 mm to 69.50% in RQ-L1-03 4-8 mm. Free Air Space of the Rotorua pumice fractions ranged from 26.27% in RQ-L1-01 1-4 mm to 42.08% in RQ-L1-03 4-8 mm (Figure 4.15).

Both the gravimetric and volumetric water holding capacities (WHC) were highest in RQ-L1-02 1-4 mm. Generally, the 1-4 mm fractions had a higher WHC than the 4-8 mm fractions. Gravimetric WHC is larger than the volumetric WHC (Figure 4.15, Table 4.5).

Table 4.5: Mean water holding capacities of a subset of the Rotorua samples.

	RQ-L1-01	RQ-L1-02	RQ-L1-03
Volumetric WHC (q) (1-4 mm)	26.31%	29.78%	26.66%
Volumetric WHC (q) (4-8 mm)	18.95%	20.72%	27.42%
Gravimetric WHC (ω) (1-4 mm)	47.72%	69.64%	52.07%
Gravimetric WHC (ω) (4-8 mm)	23.5%	38.89%	36.19%

The pH of all the Rotorua samples was neutral at pH 7.

As free air space decreases the bulk density of the sample increases, while volumetric and gravimetric WHC decreases. As total porosity increases so too does the volumetric WHC (Figure 4.15). The free air space and total porosity of the 1-4 mm fractions is generally lower, and the bulk density, volumetric and gravimetric WHC is generally higher than those of the corresponding 4-8 mm fraction.

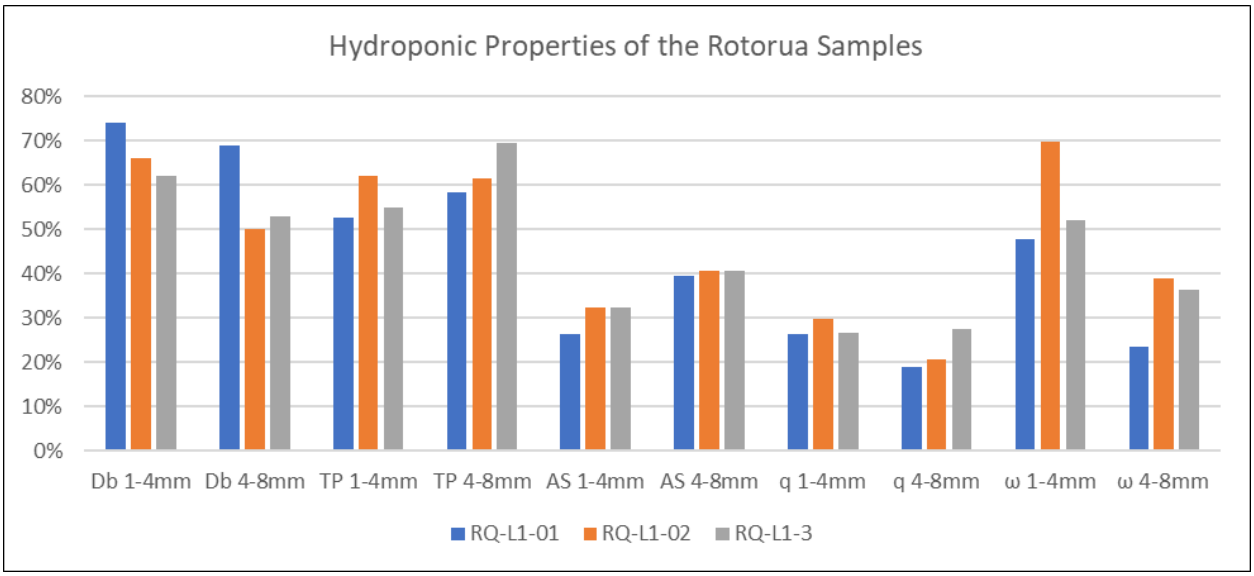

Figure 4.15: The mean hydroponic properties of a subset of the Rotorua samples. Db is bulk density, TP is total porosity, AS is free air space, *q* is volumetric WHC and ω is gravimetric WHC.

4.1.3.2 Stress Point, Permanent Wilting Point, Total Available Water Holding Capacity and Readily Available Water Holding Capacity

The stress point (ωSP) is the water content of the growth medium where evapotranspiration from the plant requires physiological work by the roots to extract water from the growth medium. At this point plant growth is retarded. The permanent wilting point (ωPWP) is the point at which the plant has extracted all the accessible water from the growth medium, at this point the plant will wilt and die if water is not replenished. The ωSP and ωPWP are not well defined and differ between species, but ωSP generally correlates to a water content between -40 and -100 kPa (-0.4 and -1 bar) and ωPWP to a water content at -1,500 kPa (-15bar) (Scotter, n.d.).

The total available water holding capacity (ωt) is the amount of water held by the soil between gravimetric WHC and ωPWP and is the maximum amount of water a medium can hold. The readily available water holding capacity (ωr) is the amount of water held by the soil between gravimetric WHC and ωSP. The ωSP, ωPWP, ωt and ωr are generally calculated for soils and are useful in providing information on the irrigation requirements of soils and crops.

The ωSP of the RQ-L1-03 fractions is generally higher than corresponding fractions of RQ-L1-01 and RQ-L1-02. However, the ωr of the RQ-L1-02 fractions exceeds that of the corresponding fractions of the RQ-L1-01 and RQ-L1-03 fractions (Figure 4.16, Table 4.6).

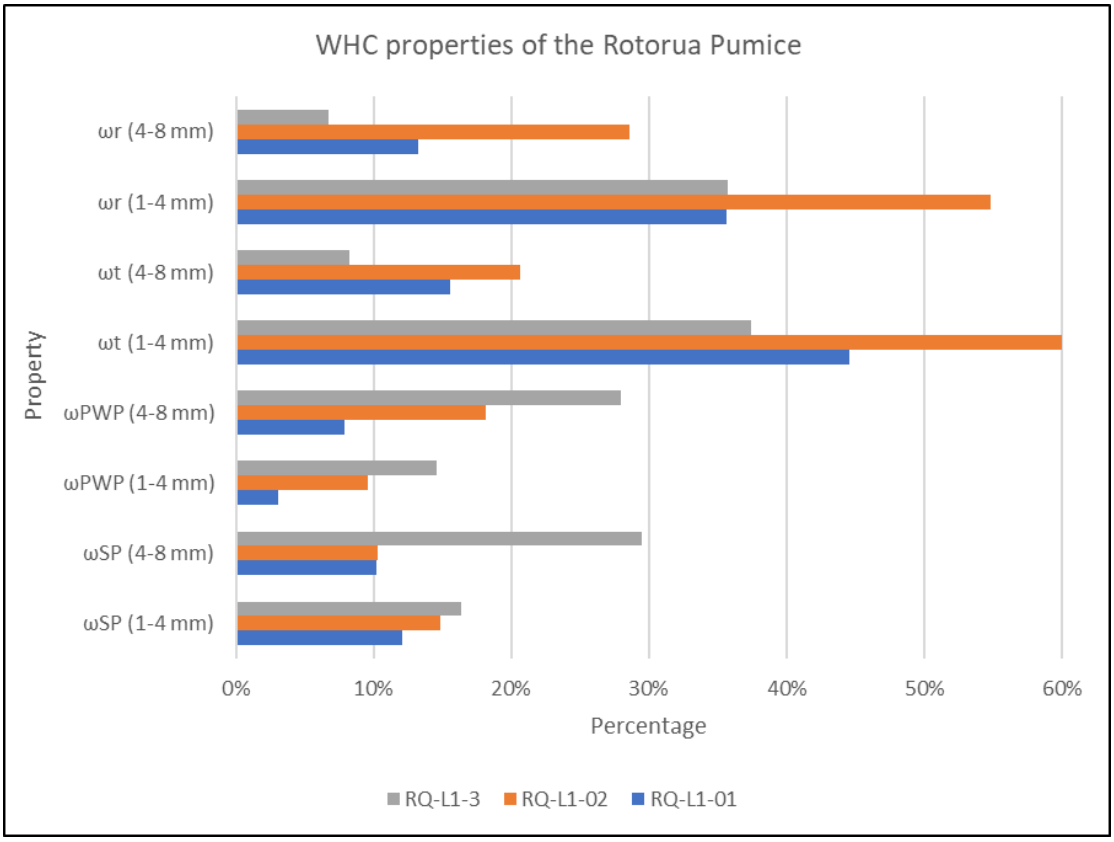

Figure 4.16: Mean water holding properties of a subset of the Rotorua samples.

Table 4.6: Mean ωSP, ωPWP, ωt and ωr of a subset of the Rotorua samples.

	RQ-L1-01	RQ-L1-02	RQ-L1-3
Stress point (ωSP) (1-4 mm)	12.07%	14.81%	16.34%
Stress point (ωSP) (4-8 mm)	10.22%	10.26%	29.47%
Permanent wilting point (ωPWP) (1-4 mm)	3.11%	9.61%	14.63%
Permanent wilting point (ωPWP) (4-8 mm)	7.93%	18.20%	27.95%
Total available water holding capacity (ωt) (1-4 mm)	44.61%	60.02%	37.44%
Total available water holding capacity (ωt) (4-8 mm)	15.57%	20.69%	8.25%
Readily available water holding capacity (ωr) (1-4 mm)	35.66%	54.82%	35.73%
Readily available water holding capacity (ωr) (4-8 mm)	13.29%	28.63%	6.72%

4.2 Kaharoa Tephra

4.2.1 Field description

Two bulk samples (KA01 and KR01) of the 1315 CE Kaharoa tephra were collected 6 February 2023 (Table 4.7). Bulk sample KA01 was collected from a medial location c. 6.5 km south of the vent at 801 Ash Pit Road from an exposure in a quarry. Bulk sample KR01 was collected from a

more distal location c. 10 km south of the vent from a road cutting on Rerewhakaaitu Rd (KR01) (Figure 4.17). Both samples are from the southeast depositional sector where Kaharoa Type 1 compositions (Nairn et al., 2001; Sahetapy-Engel et al., 2014) were deposited.

Figure 4.17: Map indicating the sample location of the Kaharoa samples. KA01 is the medial sample from 801 Ashpit Rd and KR01 is the distal sample from Rerewakaaitu Rd. Yellow stars indicate the seven vent locations active during the Kaharoa Eruption (after Nairn et al. (2001) & Todde (2022)) (image from Google Earth). Inset Map: Pink lines indicate the OVC and Okareka Embayment, red lines indicate Linear Vent Zones, and the black box shows map location.

The Ashpit Road exposure (Figure 4.18a, b & 4.19) is point K270 described by Sahetapy-Engel et al. (2014) and corresponds to the Koa Gully reference section (K291) of Nairn et al. (2001) located c. 5 km to the north. This exposure comprises c. 2.5 m of lapilli and ash beds which overlie the Taupō and Whakatane tephras. The KA01 medial sample was collected from basal units described as Units A and B by Sahetapy-Engel et al. (2014). These units are normally graded, poorly sorted, lithic-rich fine ash to medium lapilli (Figure 4.21a). This differs from the Sahetapy-Engel et al. (2014) description of unit B being a well sorted massive with slight reverse grading and ash mixed into the top of the unit. The basal units are overlain by lithic-rich alternating ash and lapilli beds described by Sahetapy-Engel et al. (2014) as Units C-G and M and underlain by a paleosol above the Whakatane Tephra. Unit M is overlain by a block and ash flow deposit.

The KR01 distal sample was collected from an exposure on Rerewhakaaitu Rd (Figure 4.20a & b) that comprised a single bed in which individual units were not distinguishable. The bed c. 300 mm fine – coarse lapilli unit (Figure 4.21b) overlies the Taupo Tephra and is overlain by the Tarawera scoria and Rotomahana mud (Figure 4.22).

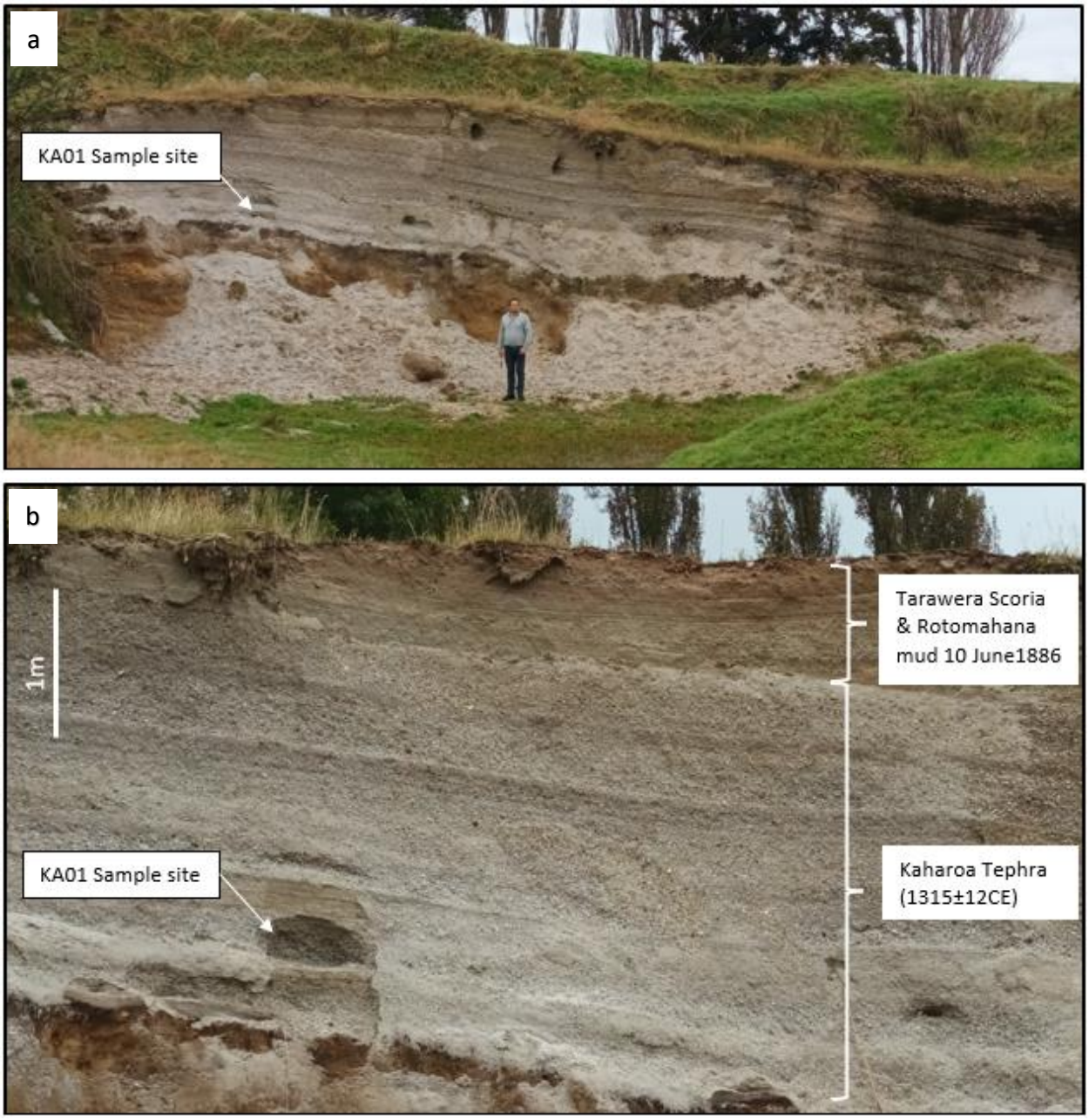

Figure 4.18a: The Kaharoa Tephra (medial) (Sample KA01) Collection Site at 801 Ashpit Road and b. Close up showing sample collection site, Tephras and dates from Lowe (2016).

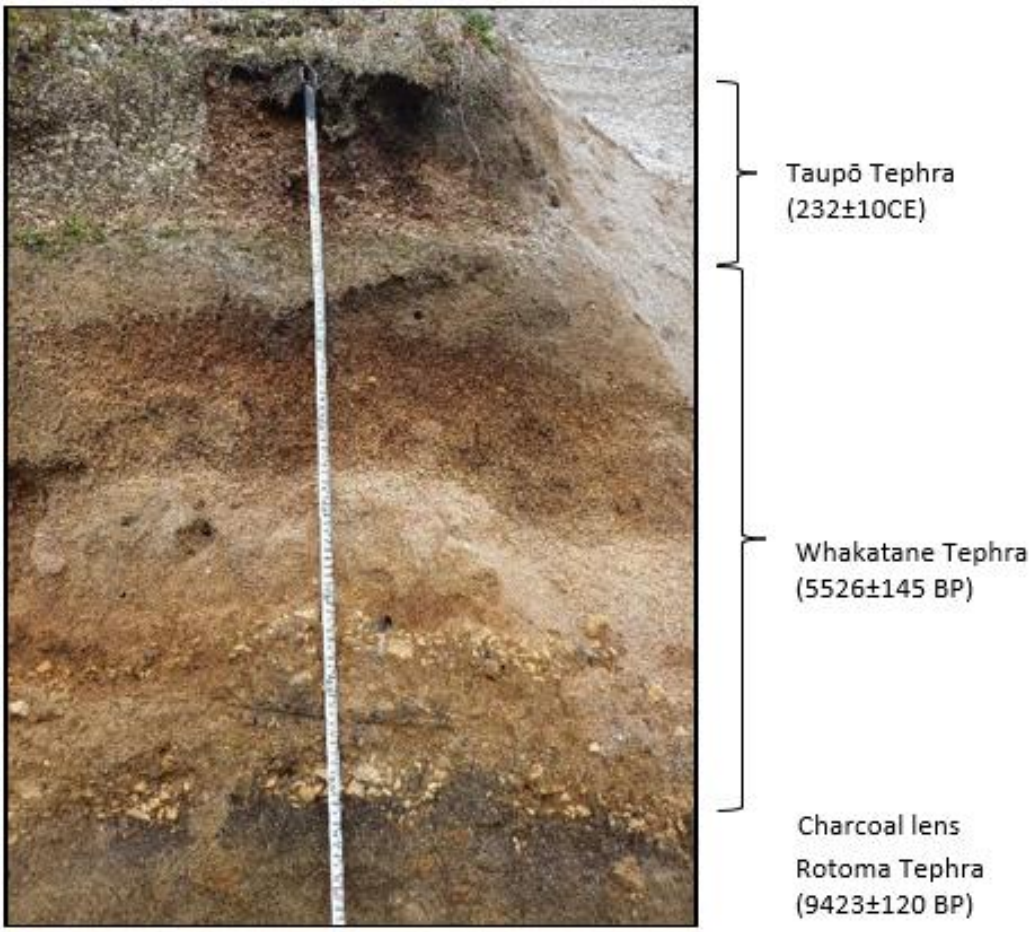

Figure 4.19: Beds underlying the Kaharoa Tephra, Tephras and dates from (Lowe, 2016).

Figure 4.20a: The Kaharoa Tephra (distal) (Sample KR01) Collection Site on Rerewhaaikatu Road and b: the Kaharoa Tephra at road cutting on Rerewhakaaitu Road, Tephras and dates from (Lowe, 2016).

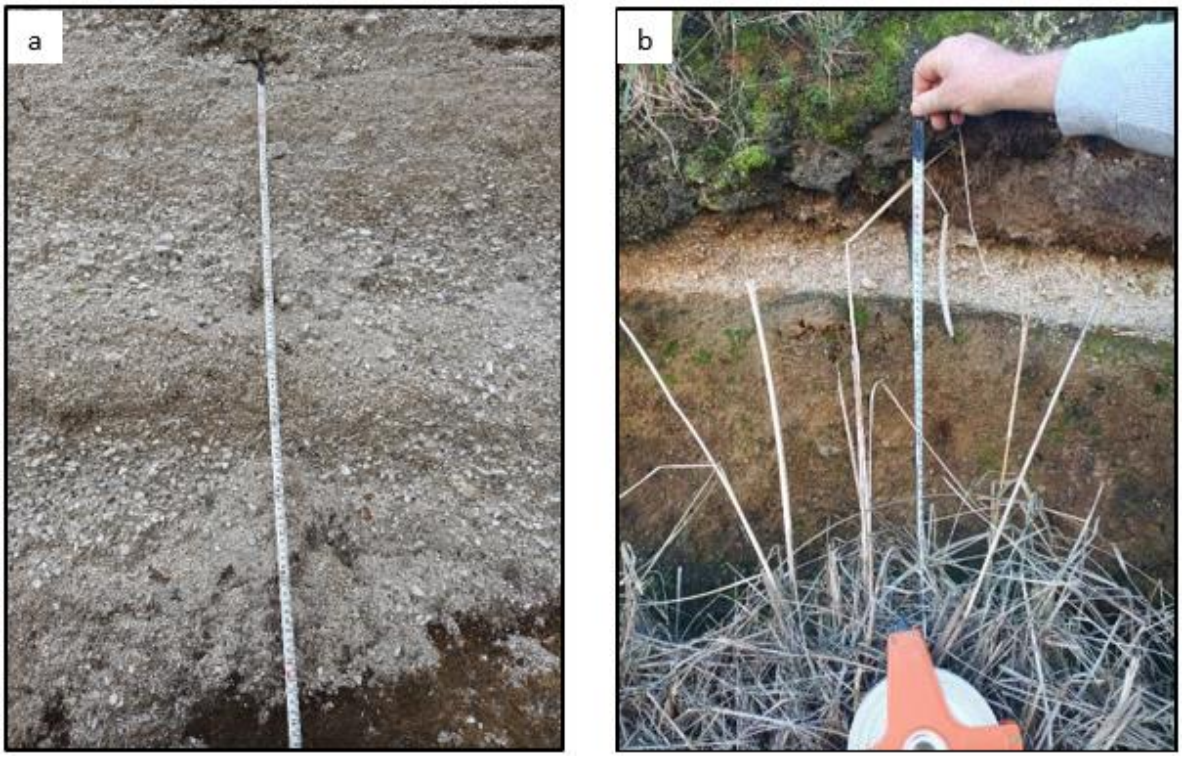

Figure 4.21: Sample collection areas a. Area that Sample KA01 was collected from; b. Area that Sample KR01.

Table 4.7: Sample Collection Details.

Tephra	Sample Location	Sample #	Sample description	Date collected
Kaharoa (Medial)	801 Ashpit Rd	KA01	Medium well sorted lapilli massive with ash layers above and below.	10.06.2022
Kaharoa (distal)	Rerewhakaaitu Rd	KR01	Fine – coarse ungraded lapilli.	06.02.2023

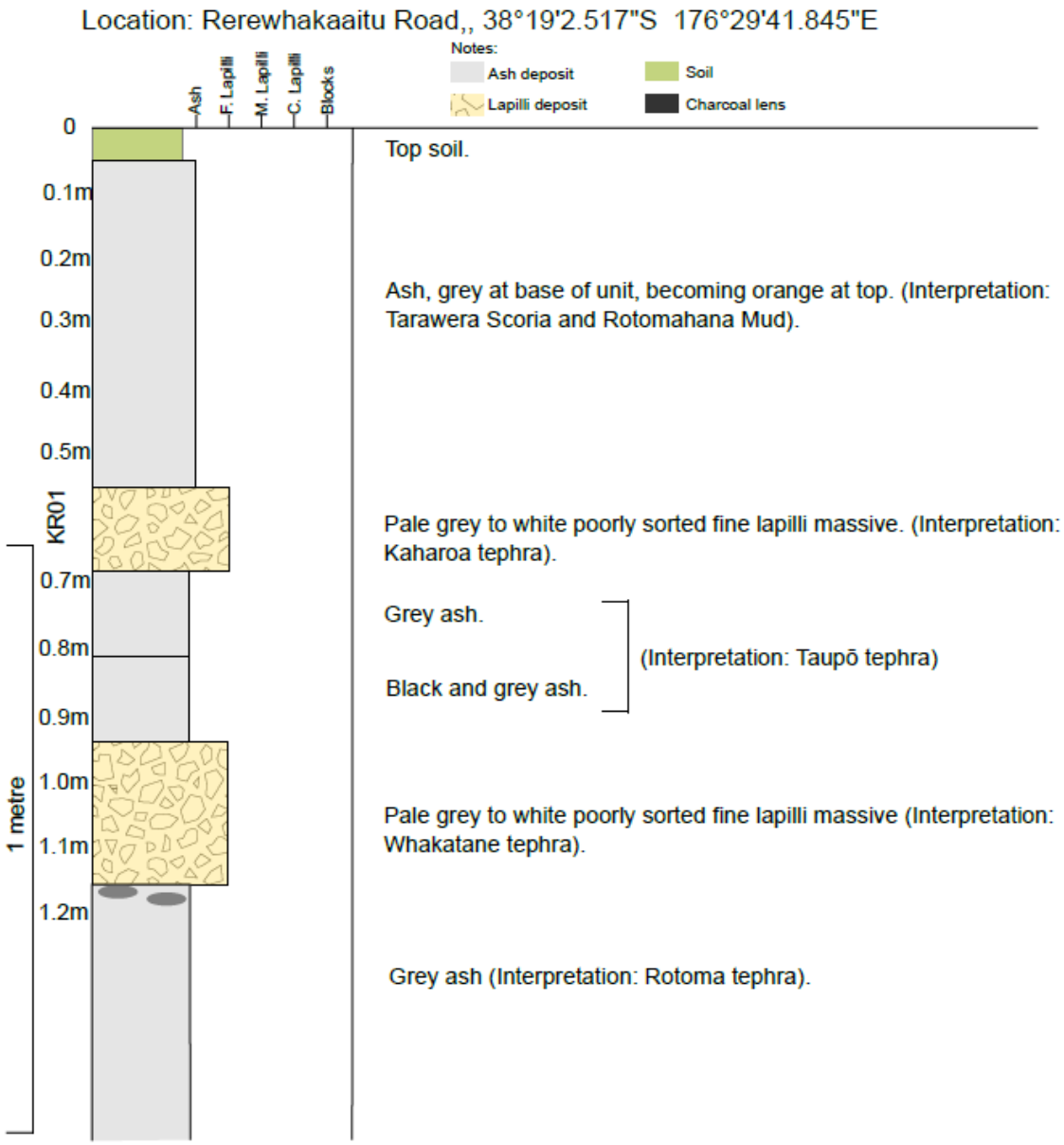

Figure 4.22: KR01, Road Cutting, Rerewhakaaitu Rd Exposure Stratigraphic Column, tephra interpretations after Lowe (2016).

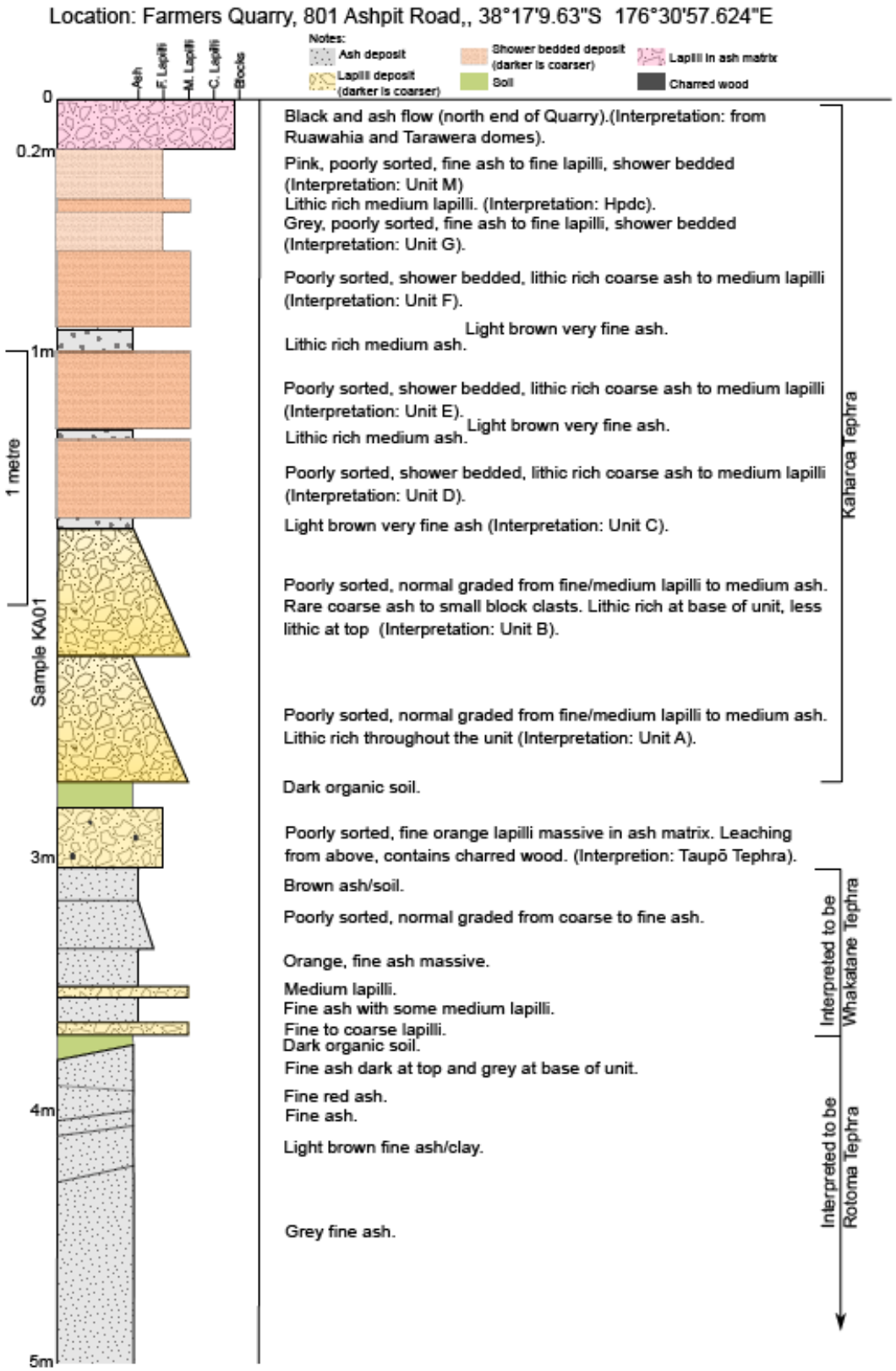

Figure 4.23: Farmers Quarry, 801 Ashpit Rd Exposure Stratigraphic Column, Unit Interpretations after (Sahetapy-Engel et al., 2014) and tephra interpretations after (Lowe, 2016).

4.2.2 Physical Properties

4.2.2.1 Grain size distribution

The KA01 bulk sample (Figure 4.24a and b) is poorly sorted with a coarse ash to lapilli dominated distribution. The histogram is unimodal and left skewed with a peak between -1 ϕ and -2 ϕ, with a coarse tail extending to -5 ϕ and a long fine tail extending to 8 ϕ. The cumulative curve indicates that there is a steady increase in grain size from -0.4 ϕ to 1 ϕ from where grain size tapers off to a long tail that extends to 8 ϕ. D_{10} is -3.28 ϕ and D_{90} is 0.77 ϕ.

The KR01 bulk sample (Figure 4.24c and d) is poorly sorted with a coarse ash to lapilli dominated distribution. The histogram is unimodal and symmetrical with a peak between 0 ϕ and 1, with a coarse tail extending to -5 ϕ and a long fine tail extending to 8 ϕ. The cumulative curve indicates that there is a steady increase in grain size from -0.3 ϕ to 1 ϕ, from where grain size tapers off to a long tail that extends to 8 ϕ. D10 is -2.45 ϕ and D90 is 0.73 ϕ.

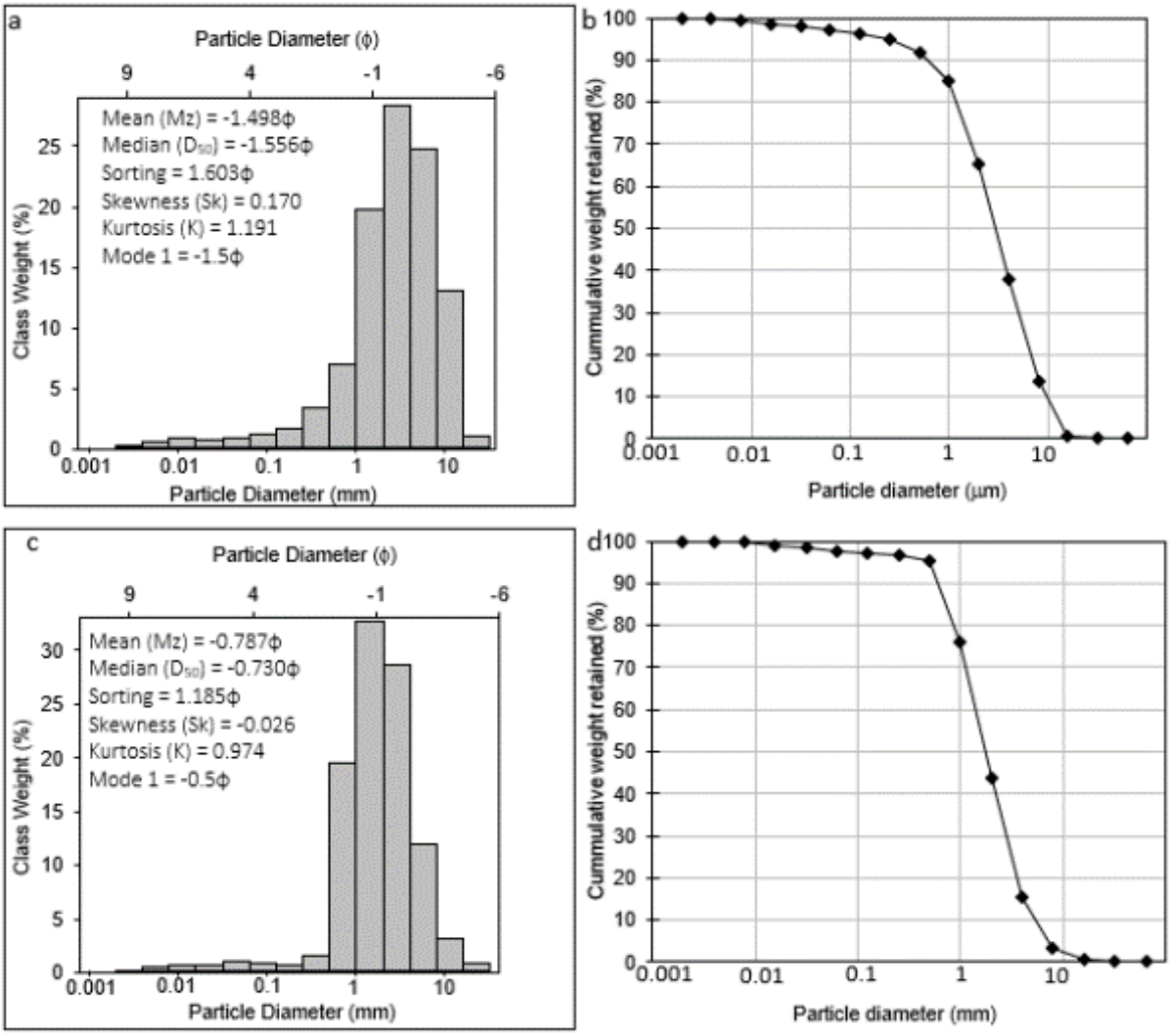

Figure 4.24: Grain size distribution histograms & cumulative curves of KA01 (a, b) and KR01 (c, d).

4.2.2.2 Pumice Morphologies and Textures

The pumice clasts were visually assessed to determine their morphology and textures. Between 297 and 414 pumice clasts were assessed.

4.2.2.2.1 Pumice types

The pumice clasts were observed visually and separated into six types. K.Fibrous pumice clasts (Figure 4.25a) are subrounded with a fibrous texture and are moderately vesiculated with elongated vesicles. K.Subrounded pumice clasts (Figure 4.25b) are subrounded with a uniform texture and are incipiently vesiculated with equant vesicles. K.Dense pumice clasts (Figure 4.25c) are rounded to subrounded with a uniform texture and are incipiently to poorly vesiculated with

equant vesicles. K.Frothy pumice clasts (Figure 4.25d) are subangular with a frothy texture and are highly vesiculated with elongated vesicles. K.Light pumice clasts (Figure 4.25e) are subangular with a fibrous texture and are extremely vesiculated with elongated vesicles. R.Banded pumice clasts (Figure 4.25f) have a banded texture.

Figure 4.25: Pumice types identified in the Kaharoa Tephra, the black lines at the bottom of the photos are at 1mm intervals. a. K.Fibrous, b. K.Subrounded, c. K.Dense, d. K.Frothy, e. K.Light and f. R.Banded.

4.2.2.2.2 Clast Shapes

Visual observations of the Kaharoa samples indicated that the KA01 samples contain predominantly subrounded clasts with minor amounts of rounded clasts. Clast shape in KR01 samples was predominantly subangular with minor subrounded or angular clasts (Figure 4.26, Table 4.8).

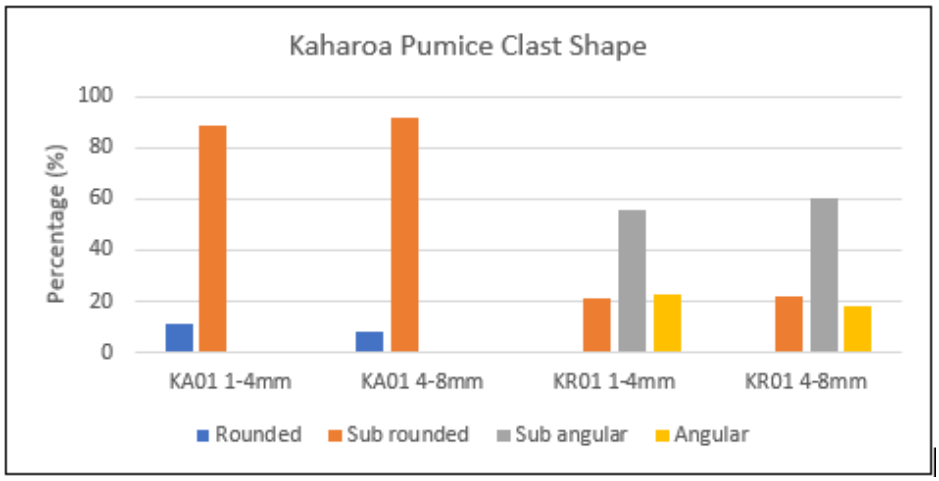

Figure 4.26: Clast shape proportions of the Kaharoa samples.

Table 4.8: Morphologies and textures of Kaharoa pumice clasts

Sample	Clast Shape (%)				Clast Texture (%)			Clast Vesicularity (%)					Vesicle Shape (%)		
	Rounded	Sub rounded	Sub angular	Angular	Uniform	Frothy	Fibrous	Incipiently	Poorly	Moderately	Highly	Extremely	Equant	Slightly Elongate	Elongated
KA01 1-4mm	11.2	88.9	0	0	11.2	0	88.9	11.2	0	88.9	0	0	11.2	0	88.9
KA01 4-8mm	8.2	91.8	0	0	87.5	0	12.5	8.2	0	91.8	0	0	8.2	0	91.8
KR01 1-4mm	0	21.5	56.0	22.5	21.5	56.0	22.5	21.5	0	0	56.0	22.5	21.5	0	78.5
KR01 4-8mm	0	21.9	60.1	17.9	21.9	60.1	17.9	0	21.9	0	60.1	17.9	21.9	0	78.1

4.2.2.2.3 Clast Textures

The dominant texture in KA01 1-4mm was fibrous with minor amounts of uniform clasts; in KA01 4-8mm the dominant texture was uniform with minor amounts of fibrous clasts (Table 4.8).

The dominant texture in KR01 samples was frothy with minor amounts of uniform and fibrous clasts (Table 4.8).

4.2.2.2.4 Clast Vesicularities

Vesicularity in the KA01 samples is similar for both grades, being predominantly moderately vesiculated with remaining clasts being incipiently vesiculated (Figure 4.27, Table 4.8).

Vesicularity in the KA01 samples is similar for both grades, being predominantly highly vesiculated with remaining clasts varying from being incipiently to extremely vesiculated (Figure 4.27, Table 4.8).

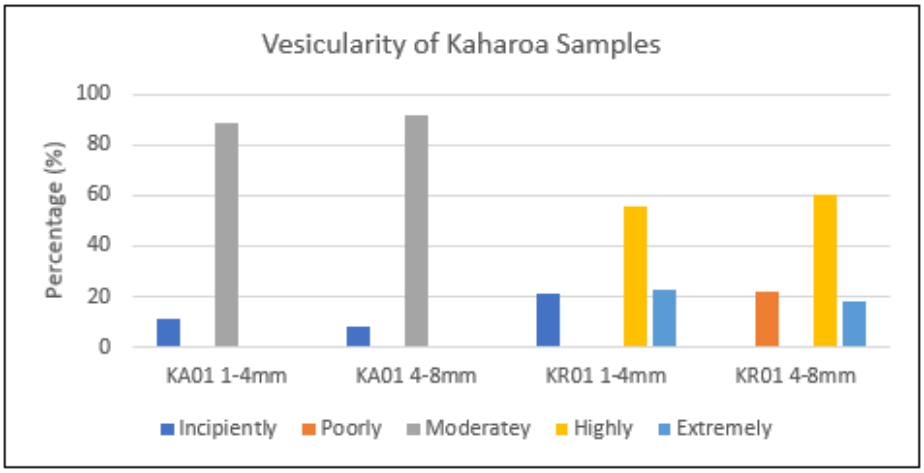

Figure 4.27: Clast vesicularity proportions of the Kaharoa samples.

4.2.2.2.5 Vesicle Shapes

Vesicles in both sizes of the KA01 and KR01 clasts are predominantly elongated with remaining clasts displaying equant vesicle shapes (Figure 4.28, Table 4.8).

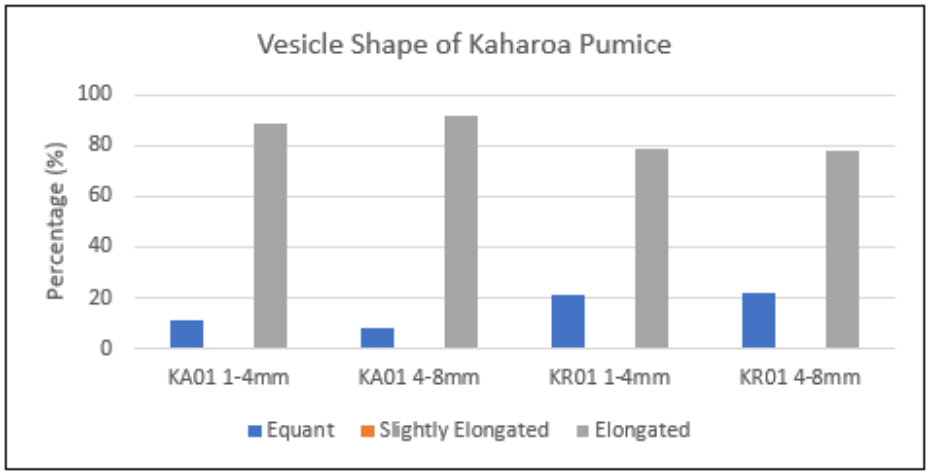

Figure 4.28: Vesicle shape of Kaharoa pumice clasts.

4.2.2.3 Componentry

Pumice contents of the Kaharoa samples increased with distance from the vent, from 91.7% in KA01 1-4 mm to 99.8% in KR01 1-4 mm and from 88.8% KA01 4-8 mm to 99.7% KR01 in 4-8 mm. Glass shards and lithics composed of volcaniclastic material, country rock and hydrothermally altered material were found in KA01 but not in KR01 (Figure 4.29, Table 4.9).

The dominant pumice type in KA01 1-4 mm is K.Fibrous and is K.Subrounded in KA01 4-8 mm accounting for 81.7% of the pumice clasts. In KR01 the dominant pumice type was K.Frothy. Proportions of minor pumice types are present in all samples (Figure 4.30, Table 4.9).

Lithic contents of the 1-4 mm and 4-8 mm fractions within a sample were similar, with KA01 fractions containing more lithics than KR01 fractions (Figure 4.30, Table 4.9).

A single crystal was found in the 1-4 mm fractions of the KA01 and KR01 samples. Glass shards were found in the KA01 samples (Figure 4.29, Table 4.9).

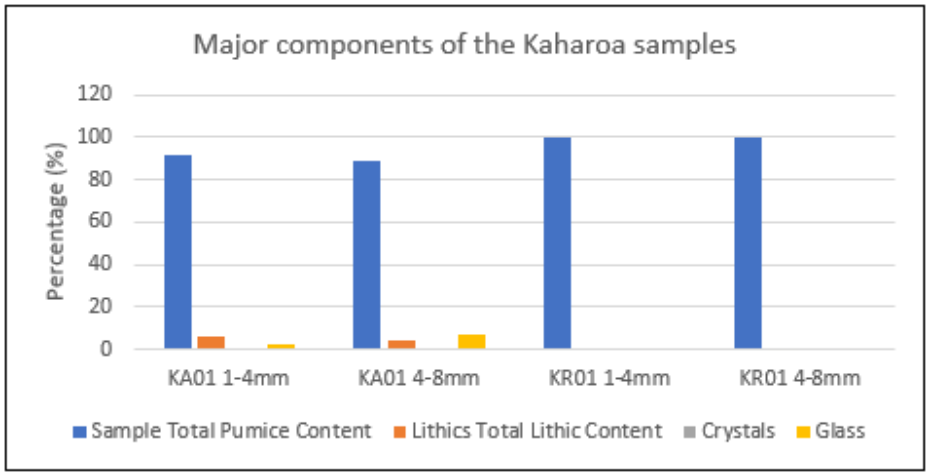

Figure 4.29: Major componentry of the Kaharoa Pumice samples

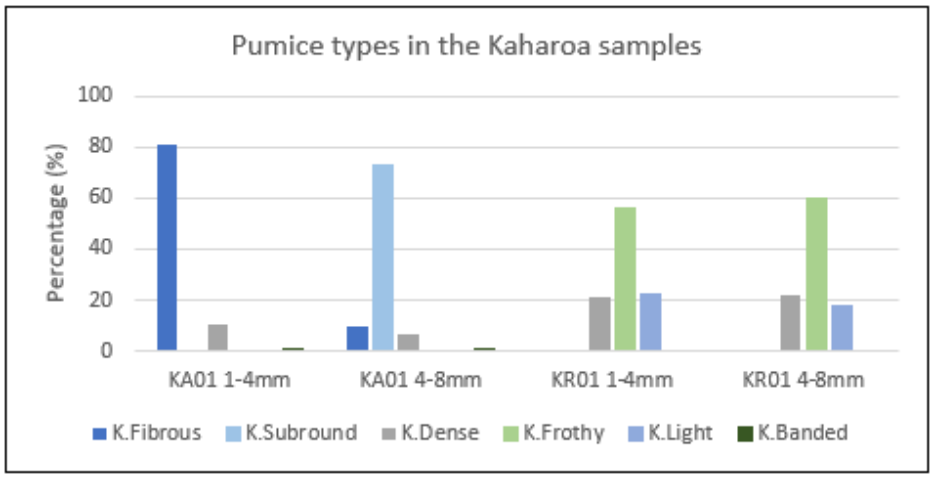

Figure 4.30: Proportions of pumice types in the Kaharoa samples.

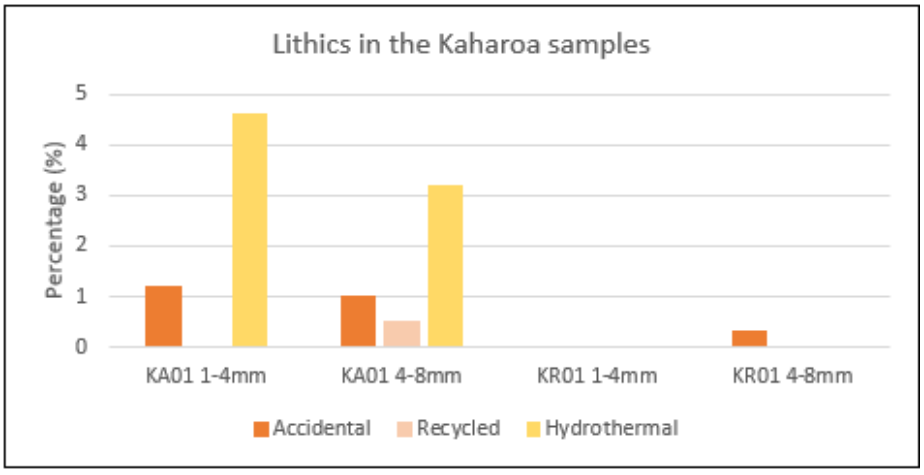

Figure 4.31: Proportions of lithics in the Kaharoa samples.

Table 4.9: Componentry of the Kaharoa samples.

Sample	Pumice (%)							Lithics (%)				Crystals (%)	Glass (%)
	K.Fibrous	K.Subround	K.Dense	K.Frothy	K.Light	K.Banded	**Total Pumice Content**	Accidental	Recycled	Hydrothermal	**Total Lithic Content**		
KA01 1-4mm	81.2	0	10.2	0	0	0.3	**91.7**	1.2	0	4.6	**5.8**	**0.3**	**2.2**
KA01 4-8mm	9.5	72.6	6.6	0	0	0.2	**88.9**	1	0.5	3.2	**4.7**	**0**	**6.6**
KR01 1-4mm	0	0	21.4	55.9	22.4	0	**99.7**	0	0	0	**0**	**0.2**	**0**
KR01 4-8mm	0	0	21.9	59.9	17.9	0	**99.7**	0.3	0	0	**0.3**	**0**	**0**

4.2.2.4 Particle density and porosity

The skeletal, envelope and solid densities of the medial KA01 sample are higher than those of the distal KR01 sample (Table 4.10, Figure 4.32).

The total and isolated porosities of KA01 are greater than that of KR01 with the total porosity of KA01 being 1.85% greater than that of KR01 and the isolated porosity of KA01 being 25.53% greater than that of KR01. However, the connected porosity of KR01 is 23.68% greater than that found in KA01 (Table 4.10, Figure 4.32).

As envelope density decreases the connected porosity increases, however as skeletal and solid density decrease isolated and total porosity also decrease (Table 4.10, Figure 4.32).

Table 4.10: Mean Particle Densities and Porosities of Kaharoa Pumice Sample Subsets of 10 Clasts.

	KA01(4-8 mm)		KR01(4-8 mm)	
	Mean	SD (σ)	Mean	SD (σ)
Skeletal density (dc)	2.04 g/cm^3	0.246	1.85 g/cm^3	0.158
Envelope density (de)	1.17 g/cm^3	0.217	0.60 g/cm^3	0.054
Solid Density (ds)	2.73 g/cm^3	0.237	2.54 g/cm^3	0.237
Total porosity (Φt)	90.43%	1.91	88.58%	1.97
Connected porosity (Φc)	43.61%	7.33	67.29%	3.60
Isolated porosity (Φi)	46.82%	6.39	21.29%	4.29

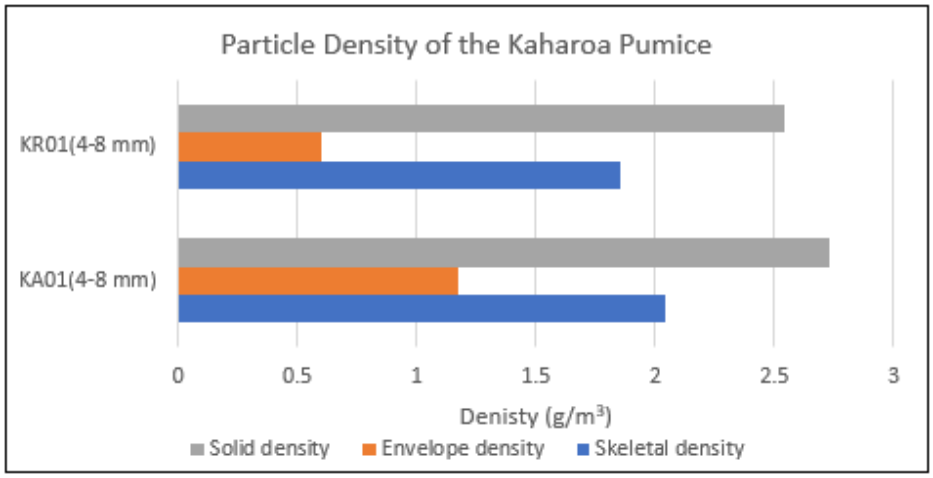

Figure 4.32: Mean Particle Densities of a subset of the Kaharoa samples.

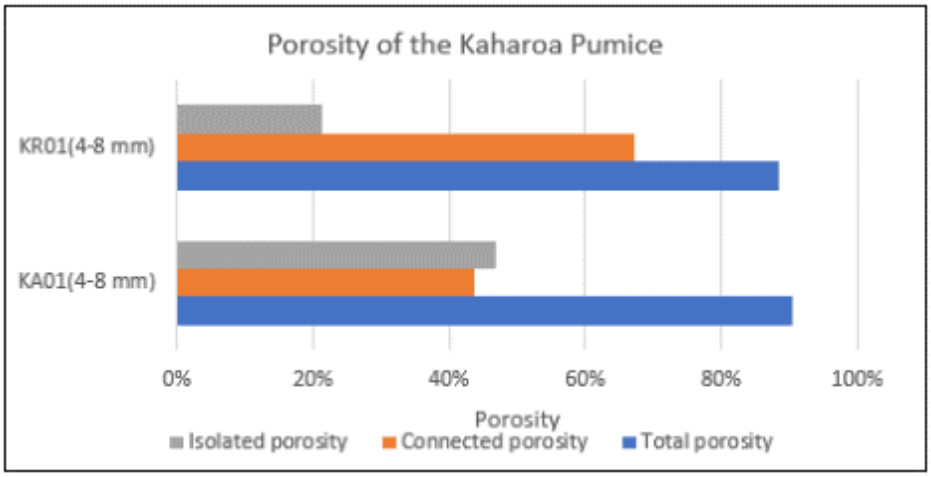

Figure 4.33: Mean Porosity of a subset of the Kaharoa samples.

4.2.3 Hydroponic Properties

4.2.3.1 Bulk Density, Total Porosity, Free Air Space, pH, and Water Holding Capacity

The bulk density of the 4-8mm fractions is slightly less (0.03 g/cm^3) than that of the 1-4mm fractions in both KA01 and KR01 samples. The bulk density is lower in both KR01 fractions than in the corresponding KA01 fractions by 0.38 g/cm^3. This is expected due to heavier particles especially lithics settling closer to the vent (Saxby et al., 2018).

Total Porosity of the Kaharoa pumice fractions ranged from 48.22% in KA01 1-4mm to 64.26% in KR01 4-8mm. Free Air Space ranged from 26.16% in KA01 1-4mm to 44.66% in KR01 4-8mm.

Both the volumetric WHC (q) and gravimetric WHC (ω) of the KR01 fractions were higher than those of the corresponding KA01 fractions. The volumetric WHC (q) of the 1-4 mm fractions were higher than the corresponding 4-8 mm fractions, however, gravimetric WHC (ω) of the 1-4 mm fractions were lower than the corresponding 4-8 mm fractions. Except for KA01 1-4 mm gravimetric WHC is higher than the volumetric WHC (Table 4.11).

Table 4.11: Water holding capacities of a subset of the Kaharoa samples.

	KA01	KR01
Volumetric WHC (q) (1-4 mm)	22.06%	27.56%
Volumetric WHC (q) (4-8 mm)	13.26%	19.60%
Gravimetric WHC (ω) (1-4 mm)	12.83%	42.63%
Gravimetric WHC (ω) (4-8 mm)	20.67%	67.20%

The pH of the 1-4mm fractions of the KA01 and KR01 samples was neutral at pH 7, the 4-8 mm fractions of the KA01 and KR01 samples were slightly acidic at pH 6.5.

As free air space decreases the bulk density of the sample increases, while volumetric and gravimetric WHC decreases. Total porosity increases together with the volumetric and gravimetic WHC (Figure 4.34).

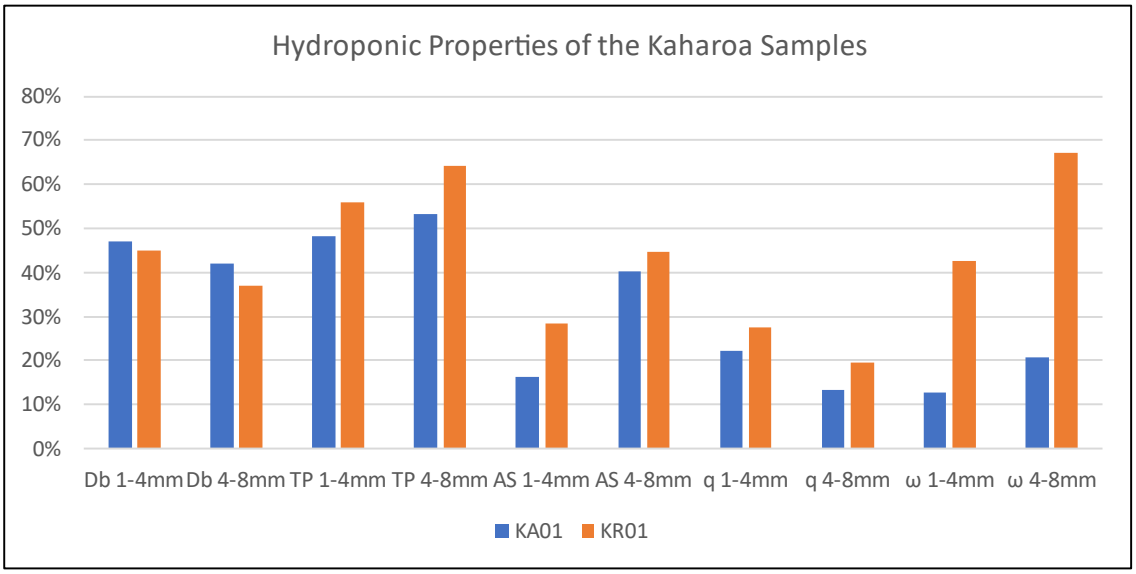

Figure 4.34: The hydroponic properties of a subset of the Kaharoa samples. Db is bulk density, TP is total porosity, AS is free air space, q is volumetric WHC and ω is gravimetric WHC.

4.2.3.2 *Stress Point, Permanent Wilting Point, Total Available Water Holding Capacity and Readily Available Water Holding Capacity*

The ωSP, ωPWP, ωr and ωt of both KR01 fractions are higher than corresponding fractions of KA01 (Figure 4.35, Table 4.12), except for the ωt of KR01 4-8 mm which is a negative value. It is thought likely that the larger clasts of this sample had a small contact area with the plate, leading to either extended drain times or the cessation of drainage via the plate when ωPWP was being measured. If this has occurred, then this is a function of the physical properties of the sample rendering the analytical method unsuitable in this case (Figure 4.35, Table 4.12).

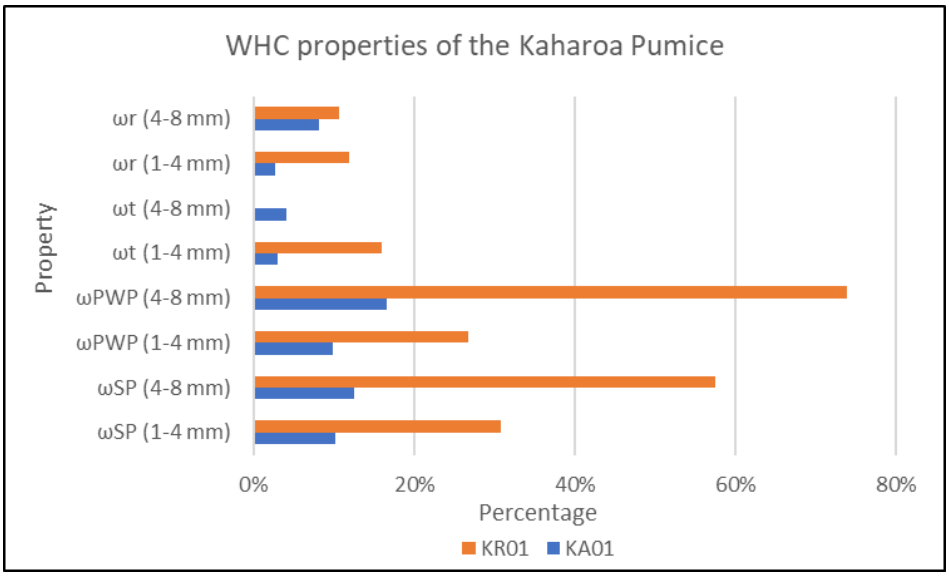

Figure 4.35: WHC properties of a subset of the Kaharoa samples (the negative ωt value for KR01 4-8 mm has been removed for clarity).

Table 4.12: ωSP, ωPWP, ωt and ωr of a subset of the Kaharoa samples.

	KA01	KR01
Stress point (ωSP) (1-4 mm)	10.18%	30.77%
Stress point (ωSP) (4-8 mm)	12.50%	57.50%
Permanent wilting point (ωPWP) (1-4 mm)	9.81%	26.70%
Permanent wilting point (ωPWP) (4-8 mm)	16.56%	74.00%
Total available water holding capacity (ωt) (1-4 mm)	3.02%	15.93%
Total available water holding capacity (ωt) (4-8 mm)	4.11%	-5.77%
Readily available water holding capacity (ωr) (1-4 mm)	2.65%	11.86%
Readily available water holding capacity (ωr) (4-8 mm)	8.17%	10.73%

4.3 Taupō Tephra

4.3.1 Field description

Due to the sudden road closure of State Highway 5 (SH5) following Cyclone Gabrielle reference samples collected earlier by Dr. Anke Zernack were used for this study (Table 4.13). The exposure on SH5 c. 20 km is northeast of the vent (Figure 4.36); this location is the type section for the Taupō eruption sequence (Wilson, 1993) and referred to as Exposure E by Tapscott (2023) and Location 2 by Walters (2020). Once the road SH5 was reopened the sample collection site was visited on 11 May 2023.

The sample location on SH5 (Figure 4.37) comprised a c. 4 m-thick exposure of 5 Taupō eruption units (Figure 4.39). The field descriptions of the units in this study are similar to those described by Walters (2020) (Y2) and Tapscott (2023) (Y5). The Taupō Y2 unit at the base of the exposure is a pale grey to white, poorly sorted medium lapilli bed (Figure 4.38a). This is similar to that described by Walters (2020) but differs from Wilson and Walker (1985) who describe the unit as non-graded and well sorted. The Taupō Y2 unit is overlain by Y3, a unit of cemented ash and lapilli beds overlain by the Y4 unit of dark grey bedded ash. The Taupō Y5 unit overlies Y4 and comprises two pale grey to white, poorly sorted fine – coarse lapilli beds with an intercalated c. 10 cm coarse ash bed. At base of Y5 is a shower bedded ash to fine lapilli bed corresponding to the 30 mm (E-2) basal unit with gradational contact (E-3) described by Tapscott (2023). The upper section of Y5 corresponds with E-4 described by Tapscott (2023). Unit Y5 is overlain by the orange ignimbrite that is referred to as Y6 (Figure 4.39).

Figure 4.36: Map indicating the sample location of the Taupō Y2 and Y5 samples on State Highway 5. Vent lineament and approximate vent locations after (Houghton et al., 2010) and (Lowe & Pittari, 2021b) (image from Google Earth).

Figure 4.37: The Taupō Tephra (samples Taupō Y2 and Taupō Y5) Collection Site at c.1144-1148 SH5.

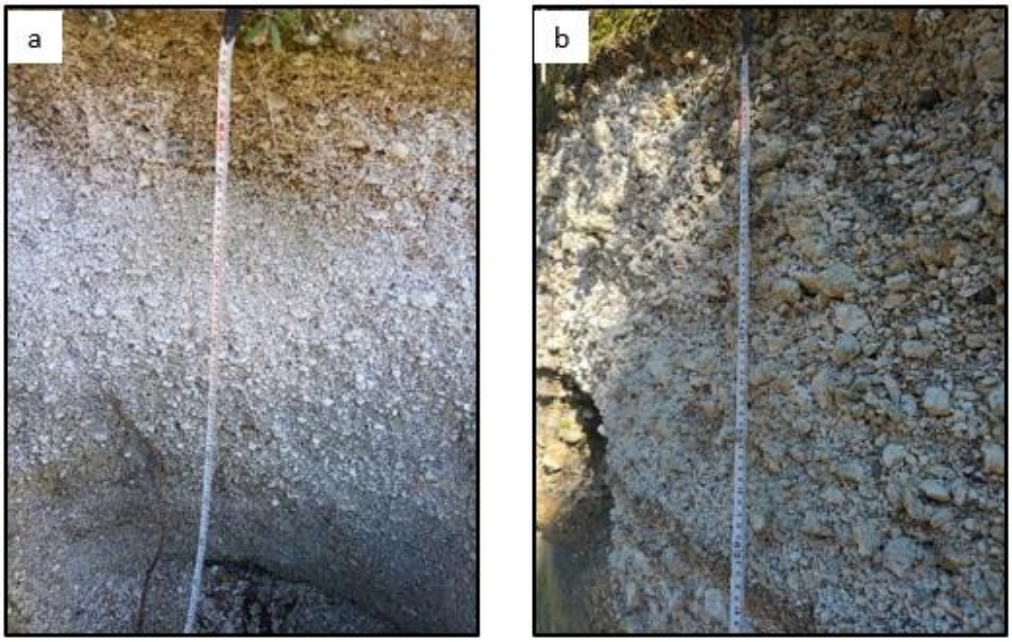

Figure 4.38: Taupō sample collection areas a. Taupō Y2; b. Taupō Y5.

Table 4.13: Sample Collection Details.

Tephra	Sample Location	Sample #	Sample description	Date collected
Taupō Y2	c.1144-1148 SH5	Taupō Y2	White, poorly sorted fine to medium lapilli.	Previously collected
Taupō Y5	c.1144-1148 SH5	Taupō Y5	White, lithic rich, poorly sorted fine to coarse lapilli. Shower bedded at the base of the unit.	Previously collected

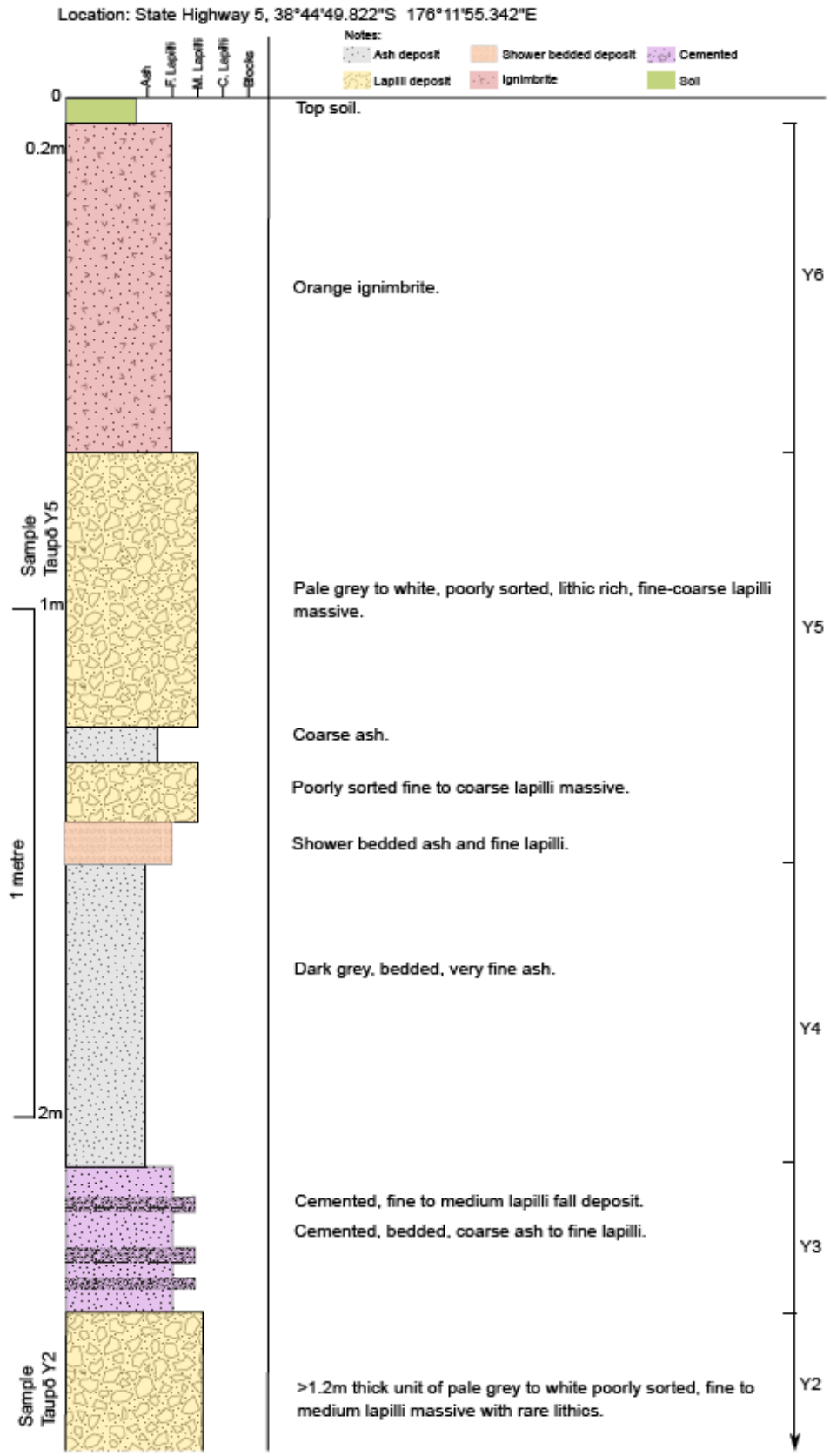

Figure 4.39: Road Cutting, SH5 Exposure Stratigraphic Column.

4.3.2 Physical Properties

4.3.2.1 Grain size distribution

The Taupō Y2 bulk sample (Figure 4.40a and b) is poorly sorted with a coarse ash to lapilli dominated distribution. The histogram is unimodal and symmetrical with a peak between -1 ϕ and -2 ϕ, a coarse tail extending to -5 ϕ and a long fine tail extending to 8 ϕ. The cumulative curve indicates that there is a steady increase in grain size from -0.4 ϕ to 1 ϕ from where grain size tapers off to a long tail that extends to 8 ϕ. D_{10} is -3.57 ϕ and D_{90} is -0.02 ϕ.

The Taupō Y5 bulk sample (Figure 4.40c and d) is poorly sorted with a coarse ash to lapilli dominated distribution. The histogram is unimodal and left skewed with a peak between -3 ϕ and -4 ϕ, and a coarse tail extending to -6 ϕ and a long fine tail extending to 8 ϕ. The cumulative curve indicates that there is a steady increase in grain size from -0.6 ϕ to -1 ϕ from where grain size tapers off to a long tail that extends to 8 ϕ. D_{10} is -5.08 ϕ and D_{90} is 0.77 ϕ.

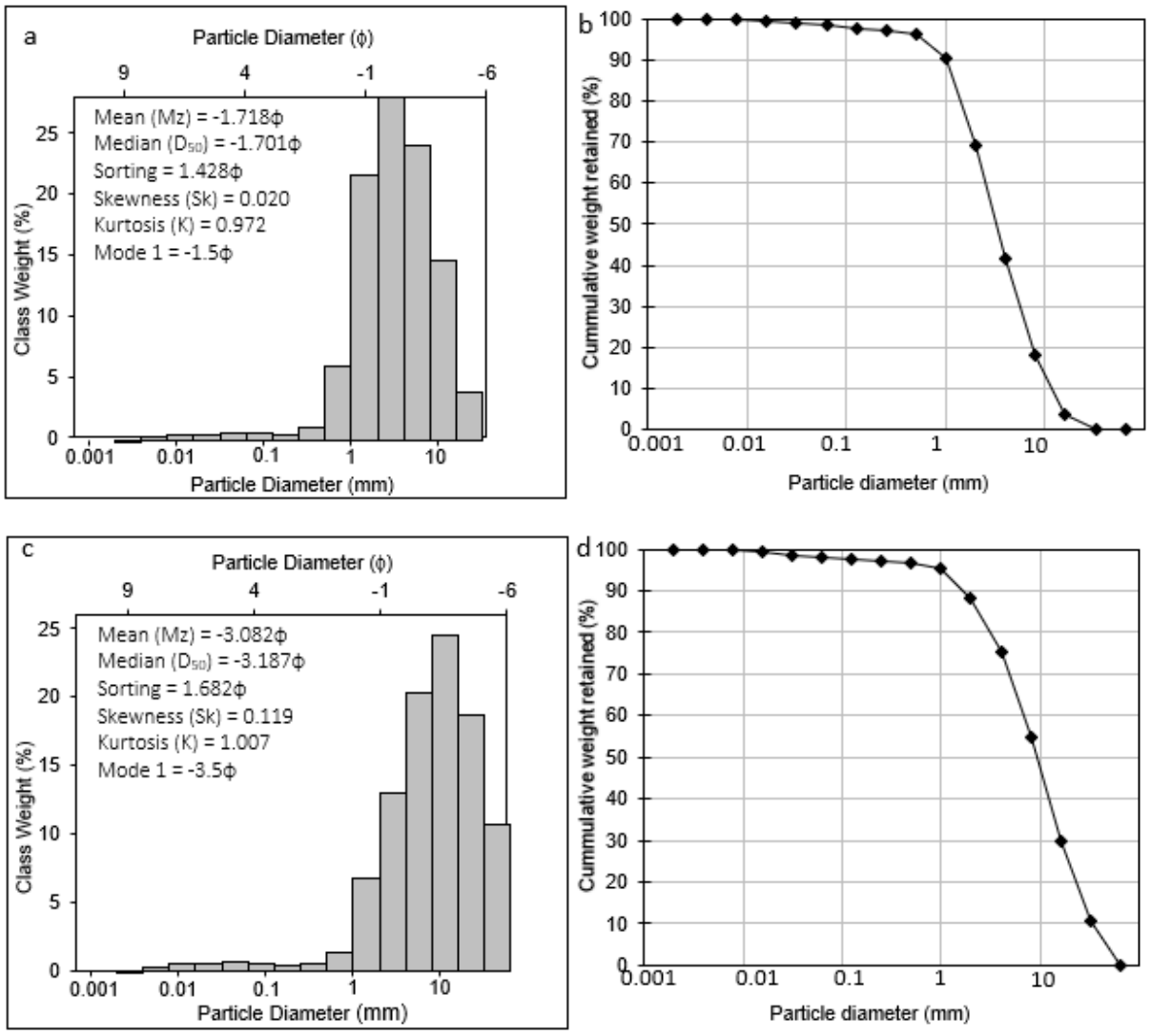

Figure 4.40: Grain size distribution histograms & cumulative curves of Taupō Y2 (a, b) and Taupō Y5 (c, d).

4.3.2.2 Pumice Morphologies and Textures

The pumice clasts were visually assessed to determine their morphology and textures. Between 294 and 371 pumice clasts were assessed.

4.3.2.2.1 Pumice types

The pumice clasts were separated into four types. T.Uniform pumice clasts (Figure 4.41a) are subrounded with a uniform texture and are highly vesiculated with equant vesicles. T.Fibrous pumice clasts (Figure 4.41b) are subangular to angular with a fibrous texture and are highly vesiculated with elongated vesicles. T.Rounded pumice clasts (Figure 4.41c) are rounded to

subrounded with a uniform texture and are moderately vesiculated with equant vesicles. T.Banded pumice clasts (Figure 4.41d) have a banded texture.

Figure 4.41: Pumice types identified in the Taupō Tephras, the black lines at the bottom of the photos are at 1mm intervals. a. T.Uniform, b. T.Fibrous, c. T.Rounded and d. T.Banded.

4.3.2.2.2 Clast Shapes

Visual observations of the Taupō samples clast shapes showed that the Taupō Y2 and Taupō Y5 samples were predominantly subrounded with minor amounts of angular clasts (Figure 4.42, Table 4.14).

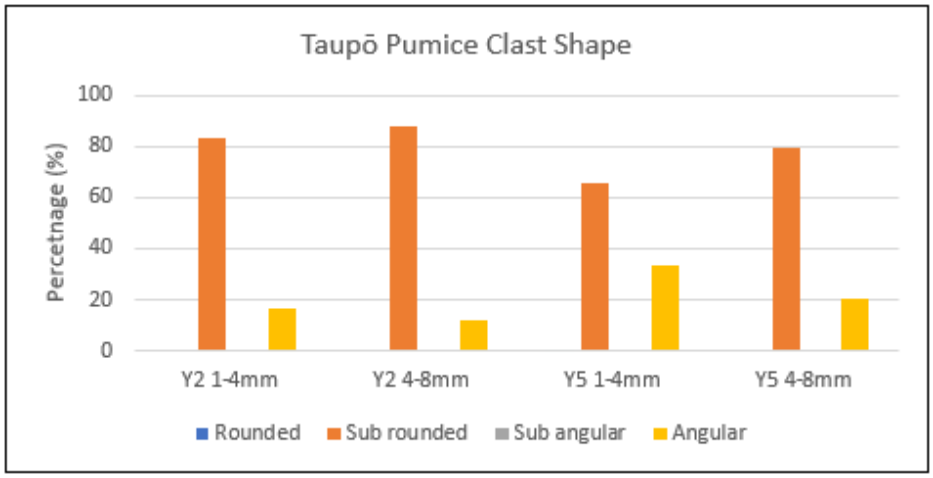

Figure 4.42: Clast shape proportions of the Taupō samples.

Table 4.14: Morphologies and textures of Taupō pumice clasts.

Sample	Clast Shape (%)				Clast Texture (%)			Clast Vesicularity (%)					Vesicle Shape (%)		
	Rounded	Sub rounded	Sub angular	Angular	Uniform	Frothy	Fibrous	Incipiently	Poorly	Moderately	Highly	Extremely	Equant	Slightly Elongate	Elongated
Y2 1-4mm	0	83.6	0	16.4	83.6	0	16.4	0	0	0.7	99.3	0	83.6	0	16.4
Y2 4-8mm	0	88.1	0	11.9	88.1	0	11.9	0	0	0.0	100.0	0	88.1	0	11.9
Y5 1-4mm	0.8	65.5	0	33.7	76.9	0	23.1	0	0	76.9	23.1	0	76.9	0	23.1
Y5 4-8mm	0	79.1	0.6	20.3	79.1	0	20.9	0	0	79.1	20.9	0	79.1	0	20.9

4.3.2.2.3 Clast Textures

The dominant texture of pumice clasts in all samples is uniform with minor amounts of fibrous clasts (Table 4.14).

4.3.2.2.4 Clast Vesicularities

The Taupō Y2 samples are highly vesiculated and the Taupō Y5 samples are predominantly moderately vesiculated with minor amounts of highly vesiculated clasts (Figure 4.43, Table 4.14).

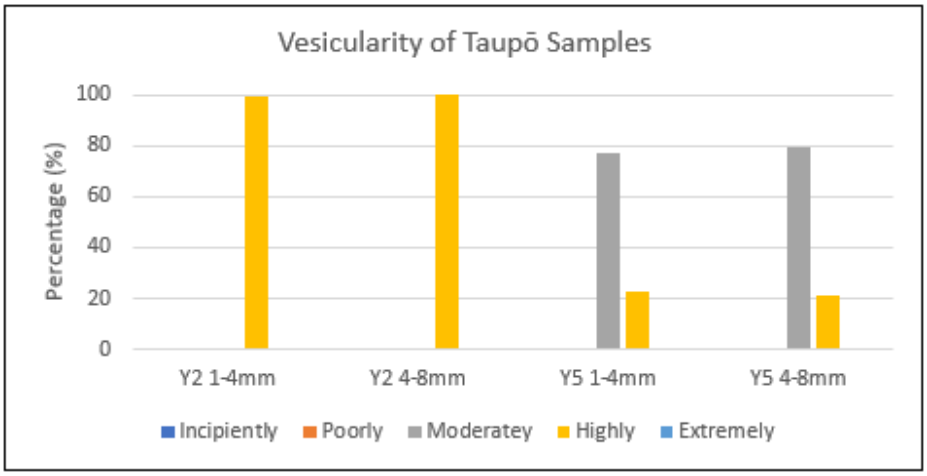

Figure 4.43: Clast vesicularity proportions of the Taupō samples.

4.3.2.2.5 Vesicle Shapes

The Taupō Y2 and Taupō Y5 clasts are predominantly equant with remaining clasts containing elongated vesicles (Figure 4.44, Table 4.14).

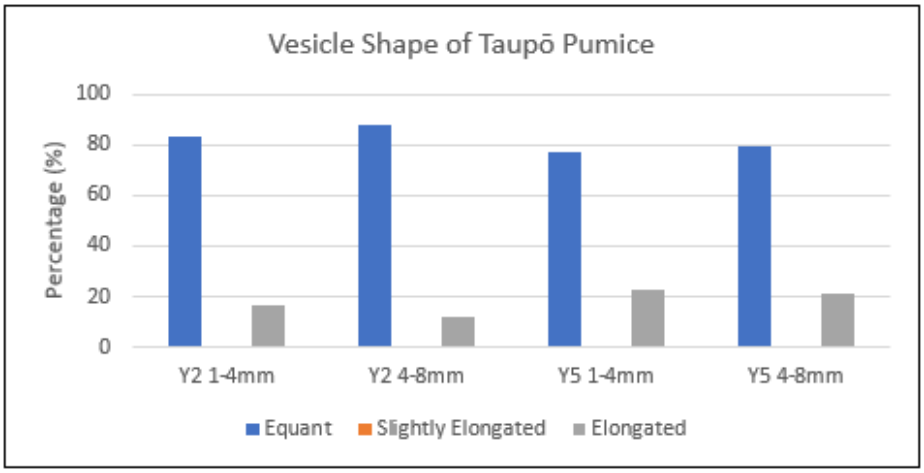

Figure 4.44: Vesicle shape of Taupō pumice clasts.

4.3.2.3 Componentry

Pumice contents in Taupō Y2 size fractions were similar at 96.1% (1-4 mm) and 97.1% (4-8 mm). Pumice proportions in Taupō Y5 1-4 mm were lower than for the Taupō Y5 4-8 mm (87.7% compared to 98.2%) (Figure 4.45, Table 4.15). Minor amounts of glass shards, crystals and lithics composed of volcaniclastic material, country rock and hydrothermally altered material made up the remainder of the samples (Figure 4.45, Table 4.15).

The dominant pumice type of the Taupō Y2 sample was T.Uniform with minor amounts of T.Fibrous and T.Banded clasts. The dominant pumice type in the Taupō Y5 sample was T.Rounded with minor amounts of T.Fibrous and T.Banded clasts (Figure 4.46, Table 4.15).

Lithic contents of the Taupō Y5 1-4 mm sample was higher than that found in both Taupō Y2 and Taupō Y5 4-8 mm samples (Figure 4.47, Table 4.15).

Minor amounts of crystals and glass are in the 1-4 mm fractions of the Taupō samples (Figure 4.45, Table 4.15), and a minor amount of glass was in the Taupō Y2 4-8 mm sample (Figure 4.45, Table 4.15).

Walters (2020) found that free crystals of plagioclase, pyroxene, quartz and titanomagnetite were abundant at c. 10-50% in the 1 ϕ size range of the Taupō Y2 deposit, however as grain size increased crystal concentration reduced with free crystal being rare in the -1 ϕ size range and absent at larger grain sizes, this corresponds with the findings of this study where crystals were present in the 1-4 mm fraction but absent in the 4-8 mm fraction of Taupō Y2. Research by Tapscott (2023) on the Taupō Y5 deposit indicates that crystal contents increase up the profile between 2 and 1 ϕ before decreasing as grain size increases towards -1 ϕ.

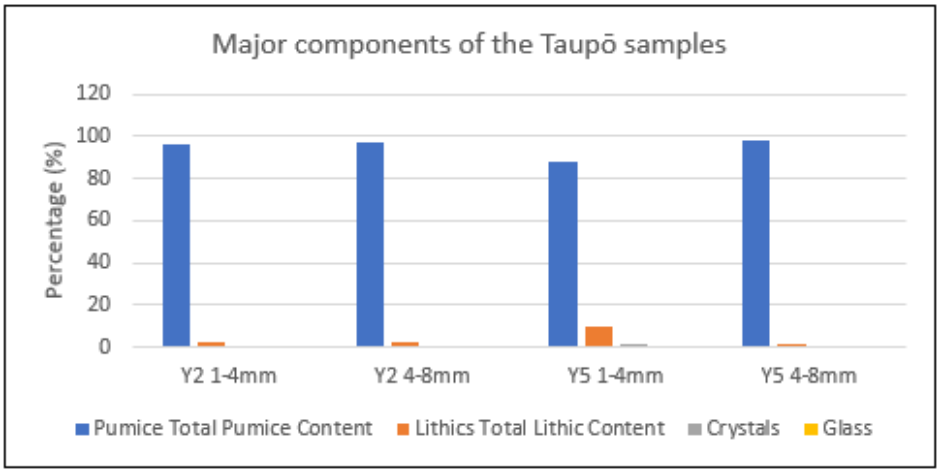

Figure 4.45: Major componentry of the Taupō Pumice samples

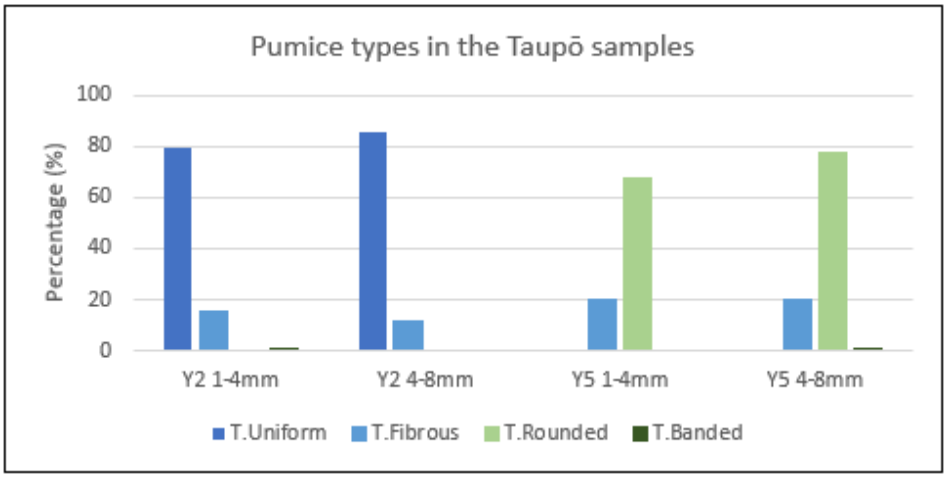

Figure 4.46: Proportions of pumice types in the Taupō samples.

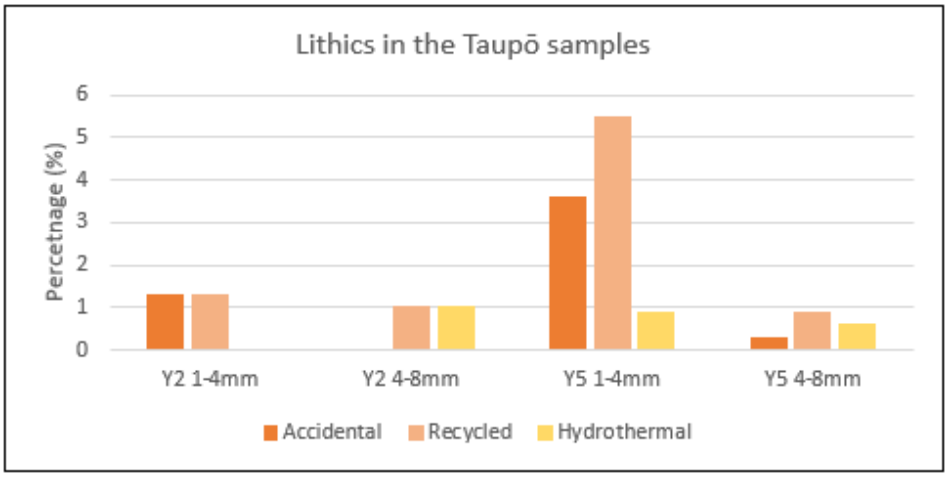

Figure 4.47: Proportions of lithics in the Taupō samples.

Table 4.15: Componentry of the Taupō samples.

Sample	Pumice (%)					Lithics (%)				Crystals (%)	Glass (%)
	T.Uniform	T.Fibrous	T.Rounded	T.Banded	**Total Pumice Content**	Accidental	Recycled	Hydrothermal	**Total Lithic Content**		
Y2 1-4mm	79.7	15.7	0	0.7	**96.1**	1.3	1.3	0	**2.6**	**0.7**	**0.7**
Y2 4-8mm	85.6	11.5	0	0	**97.1**	0	1	1	**2**	**0**	**0.8**
Y5 1-4mm	0	20.1	67.5	0	**87.6**	3.6	5.5	0.9	**10**	**1.4**	**0.9**
Y5 4-8mm	0	19.9	77.6	0.6	**98.1**	0.3	0.9	0.6	**1.8**	**0**	**0**

4.3.2.4 Particle density and porosity

The skeletal and solid densities of the Taupō Y5 sample are higher than those of Taupō Y2, however, the envelope density of Taupō Y2 is higher than that of Taupō Y5 (Figure 4.48, Table 4.16).

The total and isolated porosities of Taupō Y2 are greater than that of Taupō Y5 with the total porosity of Taupō Y2 being 2.74% greater than that of Taupō Y5 and the isolated porosity of Taupō Y2 being 15.67% greater than that of Taupō Y5. However, the connected porosity of Taupō Y5 is 12.93% greater than that found in Taupō Y2 (Figure 4.49, Table 4.16).

As envelope density decreases the connected porosity increases. The Taupō Y5 sample has higher solid and skeletal densities than is found in Taupō Y2, however the isolated and total porosities in Taupō Y5 are lower than those of Taupō Y2 (Figure 4.48 & 50, Table 4.16).

Table 4.16: Mean Particle Densities and Porosities of Taupō Pumice Sample Subsets of 10 Clasts.

	Taupō Y2(4-8 mm)		Taupō Y5(4-8 mm)	
	Mean	SD (σ)	Mean	SD (σ)
Skeletal density (dc)	1.44 g/cm^3	0.173	1.90 g/cm^3	0.145
Envelope density (de)	0.66 g/cm^3	0.151	0.62 g/cm^3	0.138
Solid Density (ds)	2.12 g/cm^3	0.255	2.58 g/cm^3	0.166
Total porosity (Φt)	88.10%	2.24	85.36%	2.95
Connected porosity (Φc)	54.31%	8.60	67.24%	7.25
Isolated porosity (Φi)	33.79%	9.63	18.12%	7.01

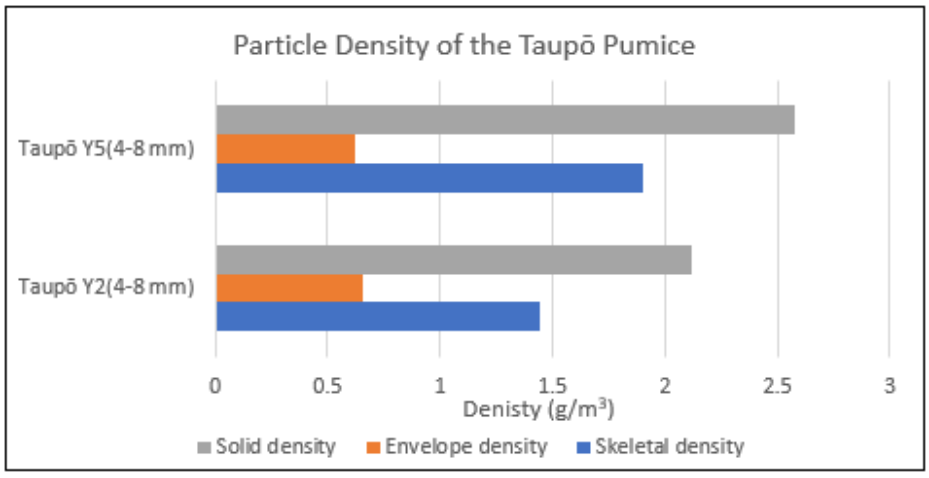

Figure 4.48: Mean Particle Densities of a subset of the Taupō samples.

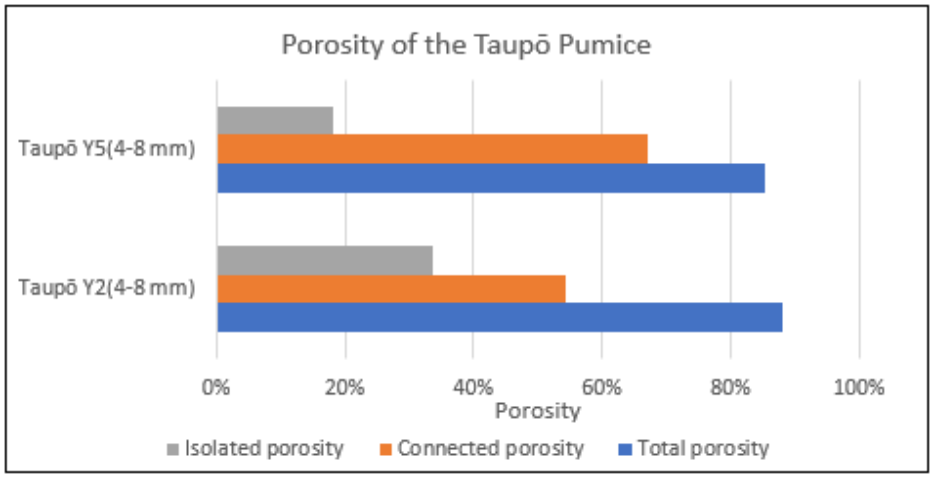

Figure 4.49: Mean Porosities of a subset of the Taupō samples.

4.3.3 Hydroponic Properties

4.3.3.1 Bulk Density, Total Porosity, Free Air Space, pH, and Water Holding Capacity

The bulk density of the 4-8 mm fractions is lower than that of the 1-4 mm fractions in both the Taupō Y2 and Y5 samples. The bulk density is slightly higher in the Y2 fractions than the corresponding Y5 fractions. The bulk density ranges from 0.42 g/cm^3 in Y2 4-8 mm to 0.47 g/cm^3 in Y2 1-2 mm while it ranges from 0.37 g/cm^3 in Y5 4-8 mm to 0.45 g/cm^3 in Y5 1-4 mm.

Total Porosity of the Taupō pumice fractions ranged from 49.49% in Taupō Y2 1-4 mm to 81.09% in Taupō Y5 4-8 mm. The largest difference between fractions in a sample was 22.31% in the Taupō Y5 (Figure 4.50).

Free Air Space of the Taupō pumice ranged from 17.64% in Y5 1-4 mm to 59.61% in the Y5 4-8 mm. The Y2 fractions were within this range (Figure 4.50).

The volumetric WHC (q) of Y5 1-4 mm and Y2 1-4 mm and the gravimetric WHC (ω) of the Y2 1-4 mm were higher than the corresponding 4-8 mm fractions. However, the gravimetric WHC (ω) of Y5 1-4 mm was lower than that found in Y5 4-8 mm (Figure 4.50, Table 4.17).

Table 4.17: Water holding capacities of a subset of the Taupō samples.

	Taupō Y2	Taupō Y5
Volumetric WHC (q) (1-4 mm)	23.45%	41.14%
Volumetric WHC (q) (4-8 mm)	18.76%	21.48%
Gravimetric WHC (ω) (1-4 mm)	60.76%	33.51%
Gravimetric WHC (ω) (4-8 mm)	34.58%	44.95%

The pH of all the Taupō samples was neutral at pH 7.

As free air space in the sample increases so too does the bulk density of the sample, while total porosity of the sample decreases. As total porosity increases so too does the volumetric WHC of both fractions of the Taupō and gravimetric WHC the Taupō 4-8 mm fractions, however the gravimetric WHC of the Taupō 1-4 mm fractions increases as the free air space increase (Figure 4.50, Table 4.17).

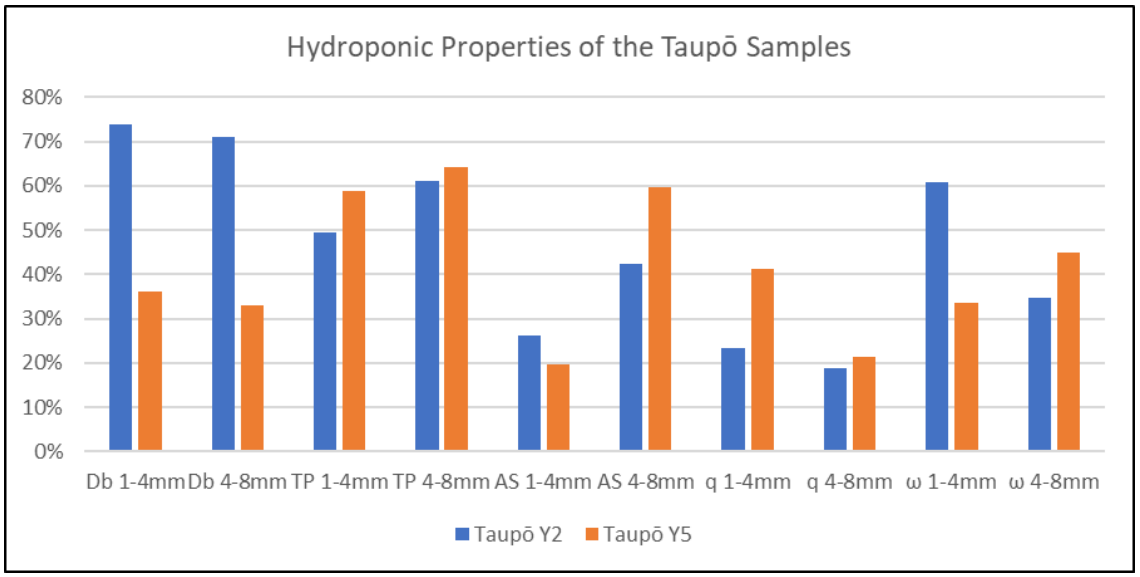

Figure 4.50: The hydroponic properties of a subset of the Taupō samples. Db is bulk density, TP is total porosity, AS is free air space, q is volumetric WHC and ω is gravimetric WHC.

4.3.3.2 Stress Point, Permanent Wilting Point, Total Available Water Holding Capacity and Readily Available Water Holding Capacity

The ωSP, ωPWP, ωt and ωr of Taupō Y2 1-4 mm are higher than those of Taupō Y5 1-4 mm (Table 4.18). The ωt and ωr values for the 4-8 mm fractions are negative, it is thought likely that the larger clasts of these samples had a small contact area with the plate, leading to either extended drain times or the cessation of drainage via the plate when ωPWP was being measured. If this

has occurred, then this is a function of the physical properties of the sample rendering the analytical method unsuitable in this case. (Figure 4.51, Table 4.18).

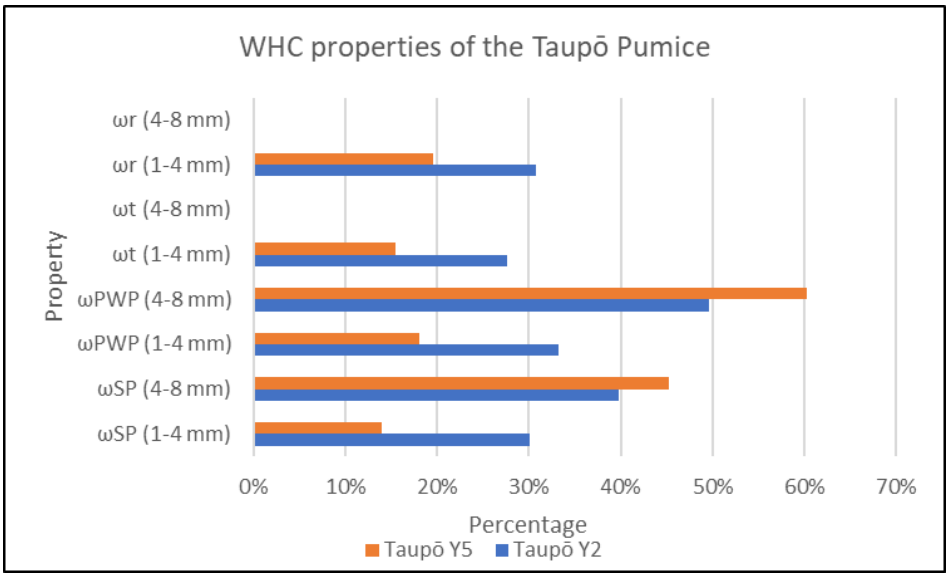

Figure 4.51: WHC properties of a subset of the Taupō samples (the negative ωt and ωr values for Y2 and Y5 4-8 mm have been removed for clarity).

Table 4.18: ωSP, ωPWP, ωt and ωr of a subset of the Taupō samples.

	Taupō Y2	Taupō Y5
Stress point (ωSP) (1-4 mm)	30.04%	13.90%
Stress point (ωSP) (4-8 mm)	39.76%	45.21%
Permanent wilting point (ωPWP) (1-4 mm)	33.18%	18.04%
Permanent wilting point (ωPWP) (4-8 mm)	49.69%	60.33%
Total available water holding capacity (ωt) (1-4 mm)	27.58%	15.47%
Total available water holding capacity (ωt) (4-8 mm)	-15.11%	-16.63%
Readily available water holding capacity (ωr) (1-4 mm)	30.73%	19.61%
Readily available water holding capacity (ωr) (4-8 mm)	-5.17%	-1.52%

4.4 Dalton's Tephra

4.4.1 Sample description

Samples of the commercially available Daltons Fine and Coarse Pumice were purchased from Bunnings Warehouse in Palmerston North on 10 March 2023. Dalton's Coarse Pumice and Dalton's Fine Pumice (Figure 4.53) are a washed and graded (not naturally sorted) by-product of sand quarrying on the outskirts of Matamata (Figure 4.52) that are marketed for use in potting mixes to improve air filled porosity and drainage to the mix (Daltons, n.d.). The pumice in the

Dalton samples is a mix of tephras based on the location of the quarry and isopach maps in Pullar (1967). They likely include the Taupō Pumice (Y5), the Rotoma Ash and the Rotorua Ash and fluvially reworked products from the breakout flood following the 1.8 ka Taupō eruption. A bulk sample was extracted from the Coarse and the Fine Pumice.

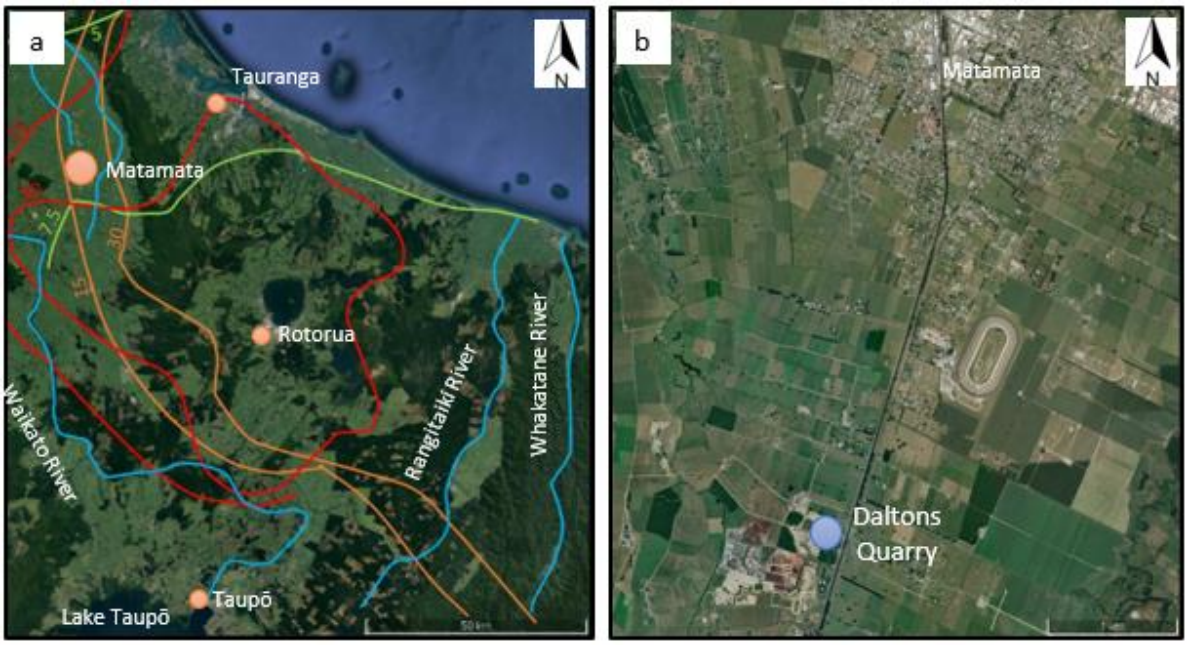

Figure 4.52: a. Location of Matamata in relation to Taupō, Rotorua and Tauranga; Taupō Pumice isopaches shown in green, Rotoma Ash isopach are shown in orange and Rotorua Ash isopaches are shown in red, all isopaches are in cm after (Pullar, 1967);. B. Location of Daltons Sand Quarry where Daltons Coarse and Daltons fine samples were quarried in relation to Matamata (images from Google Earth).

Figure 4.53: Dalton sample collection bags. a. Daltons Coarse; b. Daltons Fine.

4.4.2 Physical Properties

4.4.2.1 Grain size distribution

The Daltons Coarse bulk sample (Figure 4.54a and b) was graded prior to sale to contain grains between 4 mm and 8 mm. The results indicate that it also contains a significant proportion of smaller particles. The sample is poorly sorted with a coarse ash to lapilli dominated distribution. The histogram is unimodal and left skewed with a peak between -2 ϕ and -3 ϕ, a coarse tail extending to -4 ϕ and a long fine tail extending to 8 ϕ. The cumulative curve indicates that there is a steady increase in grain size from -0.3 ϕ to -1 ϕ, at -1 ϕ grain size tapers off to a long tail that extends to 8 ϕ. D_{10} is -2.93 ϕ and D_{90} is 3.16 ϕ.

The Daltons Fine bulk sample (Figure 4.54c and d) was graded prior to sale to contain grains between 1 mm and 4 mm. The results indicate that it also contains a significant proportion of both larger and smaller particles. The sample is very poorly sorted with a coarse ash to lapilli dominated distribution. The histogram is unimodal and left skewed with a peak between -1 ϕ and -2 ϕ, an asymmetrical coarse tail extending to -3 ϕ and a long fine tail extending to 8 ϕ. The cumulative curve indicates that there is a steady increase in grain size from -0.2 ϕ to 0 ϕ, at 0 ϕ grain size tapers off to a long tail that extends to 8 ϕ. D_{10} is -1.85 ϕ and D_{90} is 4.77 ϕ.

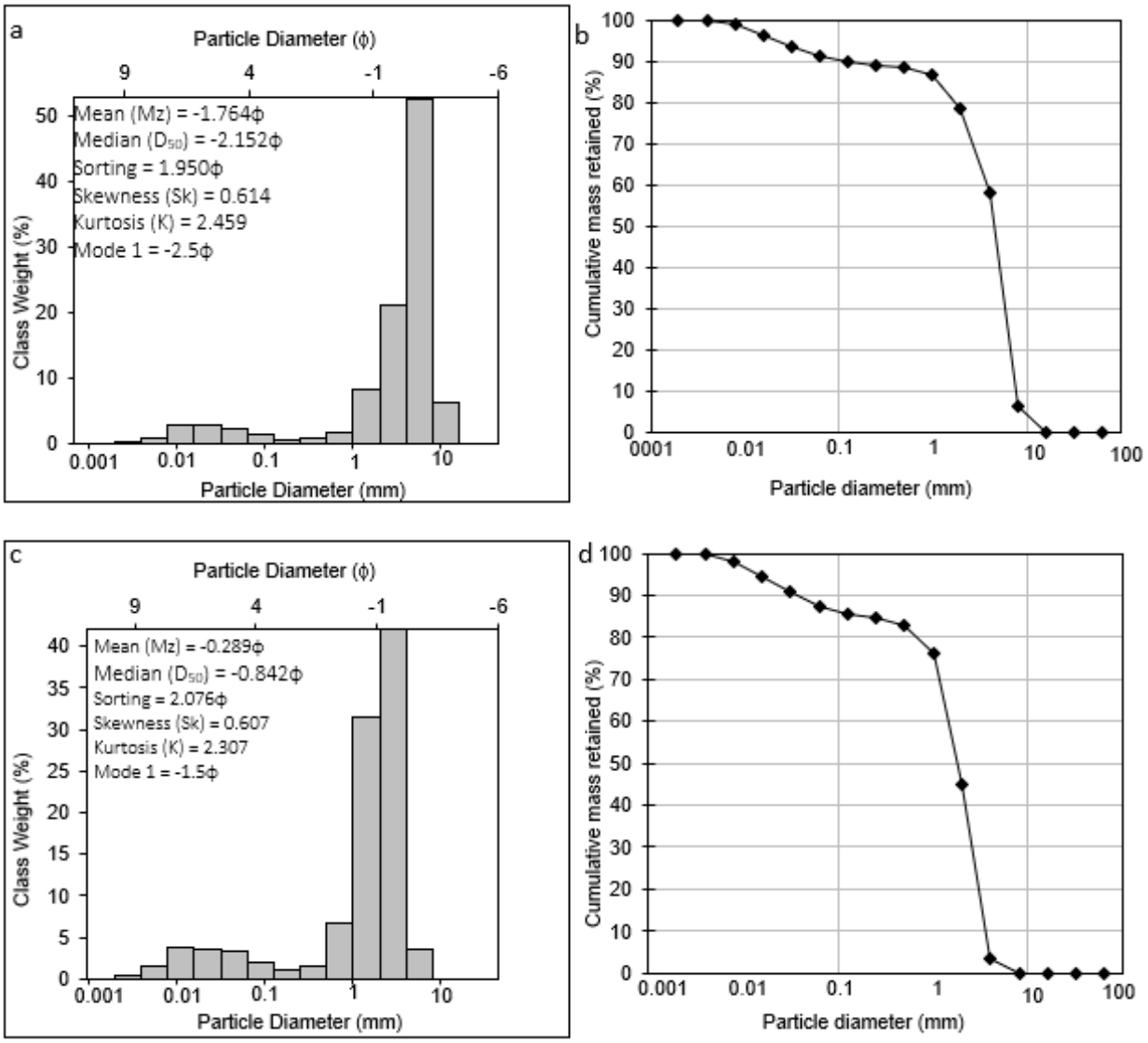

Figure 4.54: Grain size distribution histograms & cumulative curves of Daltons Coarse (a, b) and Daltons Fine (c, d).

4.4.2.2 Pumice Morphologies and Textures

Between 304 and 413 pumice clasts were visually assessed to determine their morphology and textures.

4.4.2.2.1 Pumice types

The pumice clasts were separated into five types. D.Rounded pumice clasts (Figure 4.55a) are rounded to subrounded with a uniform texture and are poorly to moderately vesiculated with equant to slightly elongated vesicles. D.Frothy pumice clasts (Figure 4.55b) are subrounded to subangular with a frothy texture and are highly vesiculated with generally elongated vesicles. D.Dense pumice clasts (Figure 4.55c) are angular with a uniform texture and are incipiently to

poorly vesiculated with equant to slightly elongated vesicles. D.Fibrous pumice clasts (Figure 4.55d) are subangular to angular with a fibrous texture and are highly to extremely vesiculated with elongated vesicles. D.Banded pumice clasts have a banded texture.

Figure 4.55: Pumice types identified in the Dalton Pumice samples, the black lines at the bottom of the photos are at 1mm intervals. a. D.Rounded, b. D.Frothy, c. D.Dense and d. D.Fibrous.

4.4.2.2.2 Clast Shapes

Visual observations of the Dalton pumice clast shapes indicate that the 4-8 mm fractions are more rounded than the 1-4 mm fraction. Except the Coarse 1-4 mm sample which contained predominantly Subrounded pumice clasts the dominant clast shape was rounded. Minor amounts of clasts were more angular in each sample (Figure 4.56, Table 4.19).

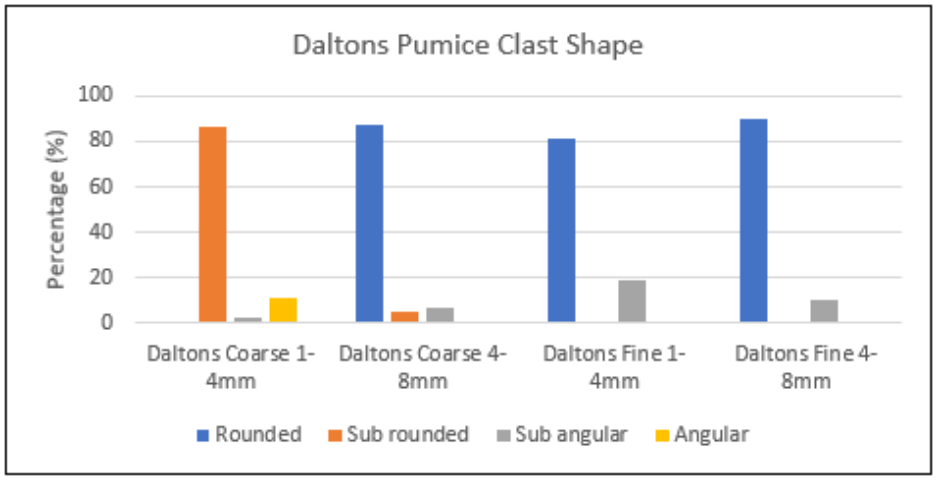

Figure 4.56: Clast shape proportions of the Daltons samples.

Table 4.19: Morphologies and textures of Daltons pumice clasts.

Sample	Clast Shape (%)				Clast Texture (%)			Clast Vesicularity (%)					Vesicle Shape (%)		
	Rounded	Sub rounded	Sub angular	Angular	Uniform	Frothy	Fibrous	Incipiently	Poorly	Moderately	Highly	Extremely	Equant	Slightly Elongate	Elongated
Coarse 1-4mm	0.0	86.3	2.3	11.3	70.1	17.5	12.4	1.3	68.8	0	19.9	10.1	68.8	1.3	29.9
Coarse 4-8mm	87.2	5.0	6.7	1.1	88.3	11.7	0	0	88.3	0	11.7	0	93.3	0	6.7
Fine 1-4mm	81.1	0	18.9	0	81.1	18.9	0	0	0	81.1	18.9	0	0	81.1	18.9
Fine 4-8mm	90.0	0	10.0	0	90.0	10.0	0	0	0	90.0	10.0	0	0	90.0	10.0

4.4.2.2.3 Clast Textures

The dominant texture in all samples is uniform with minor amounts of frothy clasts. Daltons Coarse 104 mm contained minor amounts of fibrous clasts (Table 4.19).

4.4.2.2.4 Clast Vesicularities

The Daltons Coarse samples are predominantly poorly vesiculated with remaining clasts being either highly or extremely vesiculated (Figure 4.57, Table 4.19).

The Daltons Fine samples are predominantly moderately vesiculated with the remaining clasts being highly vesiculated (Figure 4.57, Table 4.19).

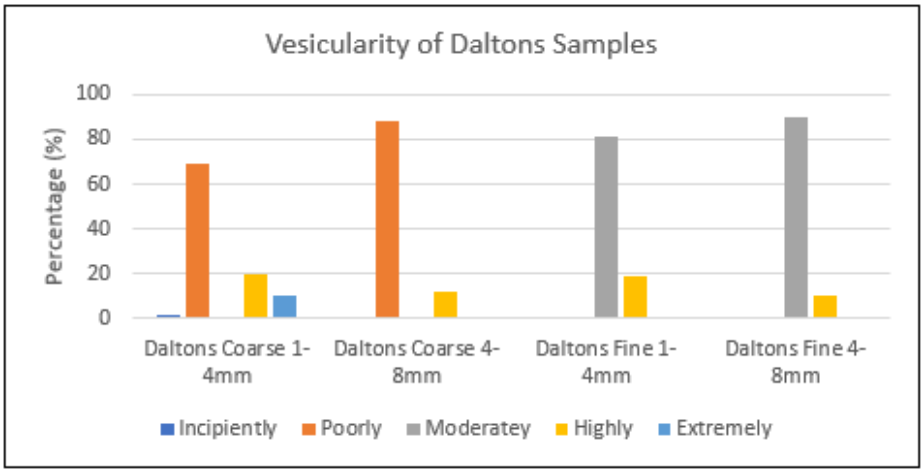

Figure 4.57: Clast vesicularity proportions of the Daltons samples.

4.4.2.2.5 Vesicle Shapes

The Daltons Coarse clasts contain predominantly equant vesicles with remaining clasts containing elongated vesicles (Figure 4.58, Table 4.19).

The Daltons Fine clasts contain predominantly slightly elongated vesicles with remaining clasts containing elongated vesicles (Figure 4.58, Table 4.19).

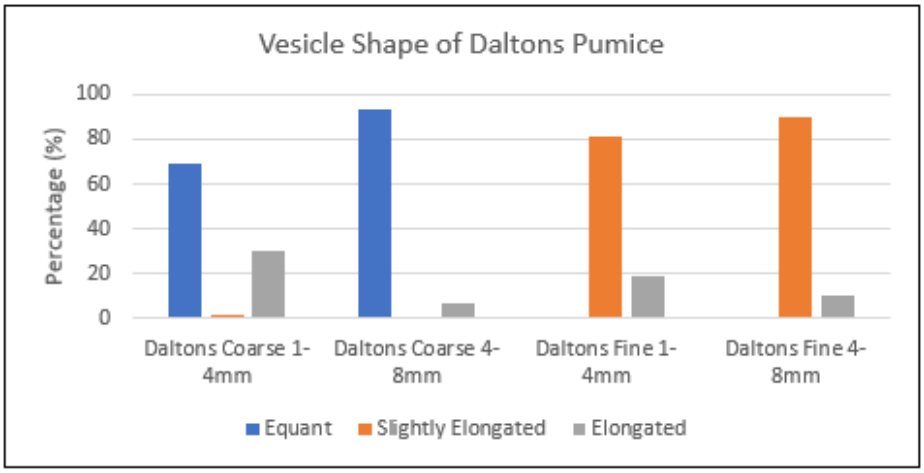

Figure 4.58: Vesicle shape of Daltons pumice clasts.

4.4.2.3 Componentry

Pumice clasts ≥ 90% of the Daltons samples with the remainder of the samples comprised of lithics and a small proportion of glass. No crystals were present in the samples (Figure 4.59, Table 4.9).

The dominant pumice type in the Daltons samples was D.Rounded (Section 4.4.2.2.1) and minor amounts of D.Frothy, D.dense and D.Fibrous clasts. A single D.Banded clast was found in the Daltons Coarse 1-4 mm sample (Figure 4.60, Table 4.9).

Lithic contents of the Coarse samples were higher than that found in the Fine samples with the 4-8 mm grade containing a higher proportion than that found in the corresponding 1-4 mm grade (Figure 4.61, Table 4.9).

A single glass shard was found in each of the Coarse and the Fine 1-4 mm samples (Figure 4.59, Table 4.9).

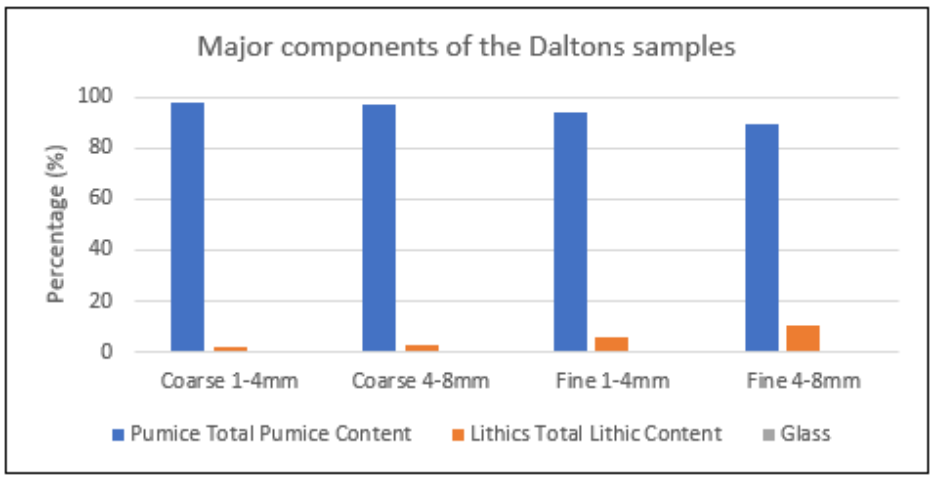

Figure 4.59: Major componentry of the Daltons Pumice samples

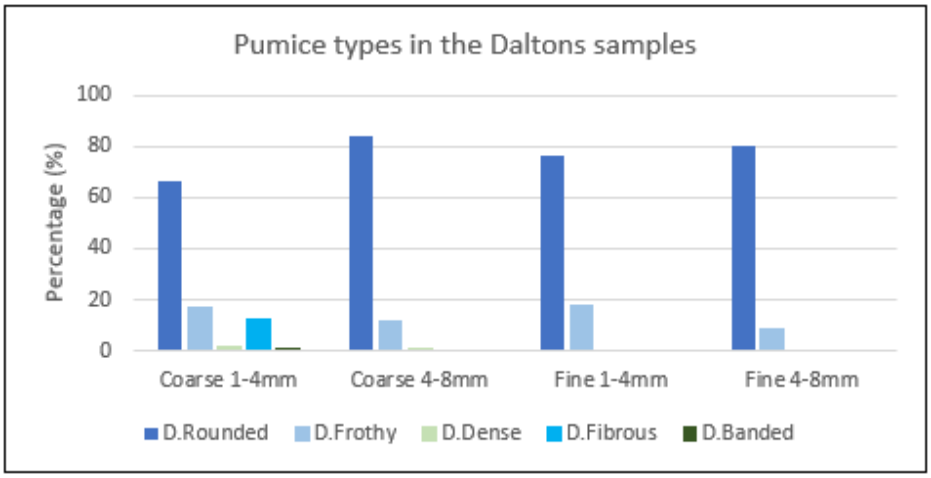

Figure 4.60: Proportions of pumice types in the Daltons samples.

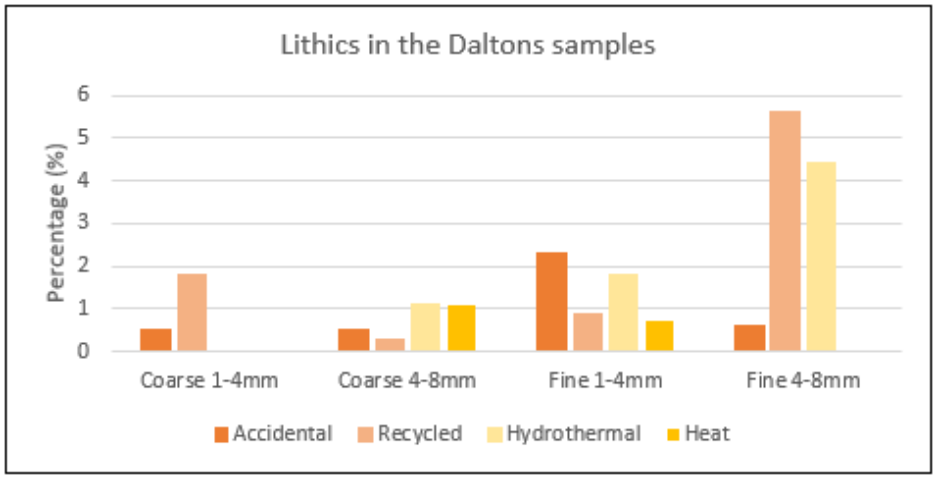

Figure 4.61: Proportions of lithics in the Daltons samples.

Table 4.20: Componentry of the Daltons samples.

Sample	Pumice (%)					Lithics (%)					Glass (%)
	D.Rounded	D.Frothy	d.Dense	D.Banded	**Total Pumice Content**	Accidental	Recycled	Hydrothermal	Heat	**Total Lithic Content**	
Coarse 1-4mm	66.8	17.1	1.3	12.1	0.3	**97.6**	0.5	1.8	0	0	**2.3**
Coarse 4-8mm	84.3	11.4	1.1	0	0	**96.8**	0.5	0.3	1.1	1.1	**3**
Fine 1-4mm	76.4	17.5	0	0	0	**93.9**	2.3	0.9	1.8	0.7	**5.7**
Fine 4-8mm	80.6	8.8	0	0	0	**89.4**	0.6	5.6	4.4	0	**10.6**

4.4.2.4 Particle density and porosity

Due to the large variability of tephra sources represented in the Daltons pumice mix that were not investigated in detail, particle densities and porosities were not calculated.

4.4.3 Hydroponic Properties

4.4.3.1 Bulk Density, Total Porosity, Free Air Space, pH, and Water Holding Capacity

The bulk density of the 4-8 mm fractions is lower than that of the 1-4 mm fractions in both Daltons Coarse and Daltons Fine. The bulk density is slightly higher in the Daltons Fine size fractions than the corresponding Daltons Coarse fractions. The bulk density of Daltons Coarse ranged from 0.34 g/cm^3 in Daltons Coarse 4-8 mm to 0.44 g/cm^3 in Daltons Coarse 1-4 mm fraction. The bulk density of Daltons Fine ranged from 0.42 g/cm^3 in Daltons Fine 4-8 mm to 0.45 g/cm^3 in Daltons Fine 1-4 mm.

Total Porosity of the Dalton's pumice ranged from 18.31% in the Coarse 1-4 mm to 39.47% in the Coarse 4-8 mm sample.

Free Air Space of the Dalton's pumice fractions ranged from 26.98% in the Daltons Fine to 39.47% in the Daltons Coarse.

Both the volumetric WHC (q) and gravimetric WHC (ω) of the Daltons Fine pumice were higher than those of the Daltons Coarse pumice (Table 4.21).

Table 4.21: Mean water holding capacities of a subset of the Daltons samples.

	Daltons Coarse	Daltons Fine
Volumetric WHC (q) (1-4 mm)		33.06%
Volumetric WHC (q) (4-8 mm)	34.10%	
Gravimetric WHC (ω) (1-4 mm)		58.01%
Gravimetric WHC (ω) (4-8mm)	75.6%	

The pH of all the Dalton samples was neutral at pH 7.

No discernable relationship was found between the hydroponic properties of the Daltons pumices (Figure 4.62).

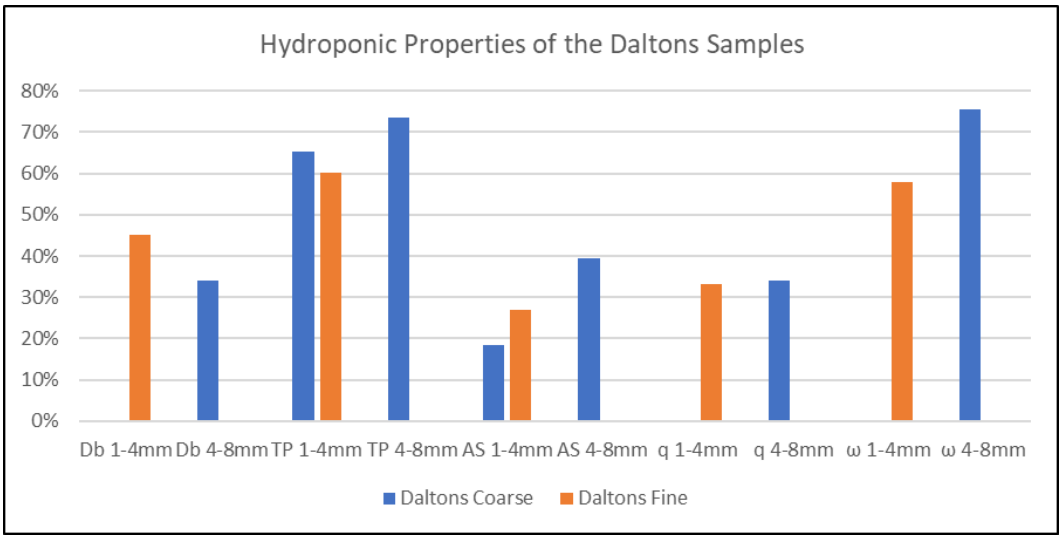

Figure 4.62: The hydroponic properties of a subset of the Dalton samples. Db is bulk density, TP is total porosity, AS is free air space, q is volumetric WHC and ω is gravimetric WHC.

4.4.3.2 Stress Point, Permanent Wilting Point, Total Available Water Holding Capacity and Readily Available Water Holding Capacity

The ωSP and ωr of the Daltons Coarse sample is higher than that of the Daltons Fine (Figure 4.63,

Table 4.22). The ωt of the Daltons Fine sample was unable to be calculated as ωPWP was not measured on the Daltons Fine sample.

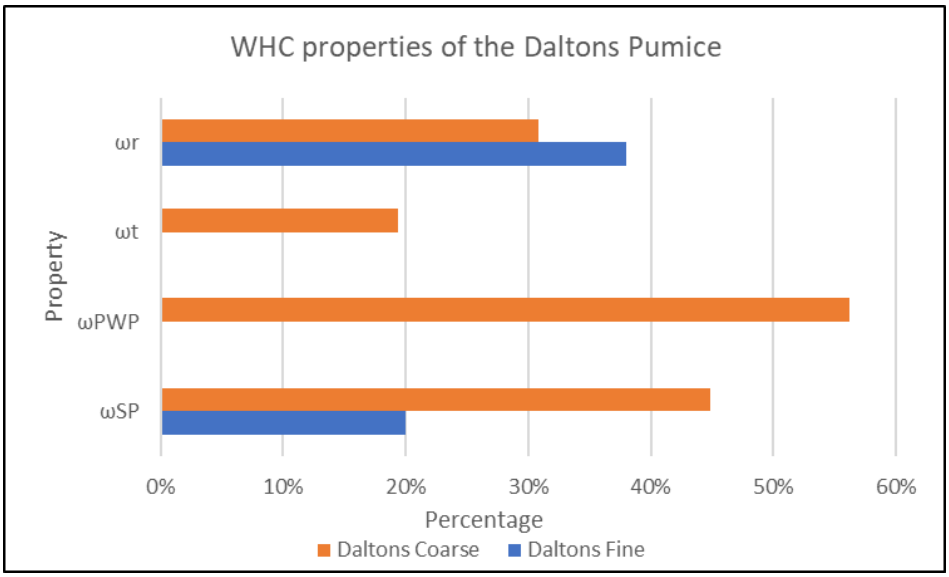

Figure 4.63: WHC properties of a subset of the Daltons samples.

Table 4.22: ωSP, ωPWP, ωt and ωr of a subset of the Daltons samples.

	Daltons Fine	Daltons Coarse
Stress point (ωSP)	20.02%	44.80%
Permanent wilting point (ωPWP)	-	56.18%
Total available water holding capacity (ωt)	-	19.42%
Readily available water holding capacity (ωr)	37.99%	30.80%

4.5 Hydroponic Media

4.5.1 Sample Collection

Samples of the Coir, Coir/Pumice mix, Harakeke/Pumice mix and Inpro Pumice (herein referred to as Ausperl for clarity) used in the Whenua Fruits raspberries trials at Massey University (Zhao et al., 2023 (in revision)) were supplied by the School of Agriculture and Environment at Massey University. The Harakeke was sourced from Whenua Fruits and the Coir is an imported product that is commercially available. The Ausperl was originally sourced from a sand and pumice quarry near Atiamuri, within 50 km of Lake Taupō where it was deposited by the Waikato River 80 km downstream of Taupō (Ausperl, n.d.). The Ausperl sample is a washed and graded (not naturally sorted) by-product of sand quarrying. The pumice in the Ausperl sample is a fluvially reworked product from the Taupō eruption.

Figure 4.64: Map indicating the Location of the Ausperl Quarry where the Ausperl sample was originally sourced from in relation to Lake Taupō and the Waikato River (image courtesy of Google Earth).

4.5.2 Description

Coir

The supplied coir sample (Figure 4.65) was made up of pieces of plant/coconut fibre up to c. 2 cm square in size with individual fibres making up 10-20% of the sample. When examined under the microscope the fibres were supported in a grainy matrix. The sample was very light and loosely packed.

Figure 4.65: Coir sample.

Ausperl Pumice

Clasts in the supplied hydroponic pumice sample (Figure 4.66) were on average 1-2 mm in size with some clasts up to 10 cm. The sample was lithic-rich with grey to red fragments. The pumice clasts appear to be of two types. Type 1 was subrounded, poorly vesiculated with rounded vesicles and a uniform texture; Type 2 was subangular, highly vesiculated with elongated vesicles and a fibrous texture.

Figure 4.66: Hydroponic pumice sample.

Coir and Pumice Mix

The supplied pumice and coir mix (Figure 4.67) contained equal proportions of the above coir and Ausperl pumice. It was noted that much of the pumice in the sample had migrated to the bottom of the sample container.

Figure 4.67: Coir/Pumice sample.

Harakeke and Pumice Mix

The supplied pumice and Harakeke mix (Figure 4.68) contained equal proportions of Harakeke and Ausperl pumice. It was noted that much of the pumice in the sample had migrated to the bottom of the sample container. The Harakeke was cut into fibres c. 6 cm long, these fibres were often in clumps and the clumps easily pulled apart. When examined under the microscope the fibres were clean and smooth.

Figure 4.68: Harakeke/Pumice sample.

4.5.3 Hydroponic Properties

4.5.3.1 Bulk Density, Total Porosity, Free Air Space, pH, and Water Holding Capacity

Bulk density of the hydroponic media ranged from 0.09 g/cm^3 for Coir to 0.71 g/cm^3 for Ausperl pumice with the coir/pumice and harakeke/pumice mixes falling between these values.

Total porosity of the Hydroponic Media had a ranged from 47.09% in the Ausperl pumice to 82.31% in the Coir with the Coir/Pumice mix and the Harakeke/Pumice mix lying between these values.

Free air space of the Hydroponic Media ranged from 11.18% in the Ausperl pumice to 42.18% in the Harakeke/Pumice mix, the Coir was similar to the Harakeke/Pumice mix at 41.51% and the Coir/Pumice mix was closer to the Ausperl pumice at 16.84%.

The volumetric WHC (q) of the harakeke/pumice mix is lower at 30.19% than that found in the other hydroponic media which were similar and ranged from 35.91% in the Ausperl to 40.80% of the Coir. The gravimetric WHC (ω) 328.52% of coir exceeded that found in the other hydroponic media (Table 4.23). Coir is superhydrophilic and has been shown to hold 5-10 times its weight in water (Carlile et al., 2019). A ω of 328.52% is below this, however this result is within the 137 – 1100% range found by Minnesota Pollution Control Agency (2023).

Table 4.23: Water holding capacities of a subset of the Hydroponic Medium samples.

	Coir	Coir/pumice	Harakeke/pumice	Ausperl
Volumetric WHC (q)	40.80%	39.58%	30.19%	35.91%
Gravimetric WHC (ω)	328.52%	51.81%	37.26%	28.95%

The pH of water in the hydroponic samples tested immediately after the air space measurements had been conducted were slightly acidic in the Ausperl sample at pH 6.5 and the Coir/Pumice mix and Coir at pH 6. The Harakeke/Pumice mix was neutral at pH 7. Overnight the pH changed in three of the samples; the Ausperl sample increased in acidity to pH 6, while acidity in the Coir/Pumice mix and Coir sample reduced to pH 6.5. The Harakeke/Pumice mix remained neutral at pH 7. The pH of the Ausperl pumice, Coir/Pumice mix or the Coir samples did not change over the following three days. The Harakeke/Pumice sample became slightly basic with a pH of 7.5.

As free air space increases the total porosity increased and the bulk density decreased. As the bulk density increased the gravimetric WHC also increased (Figure 4.69).

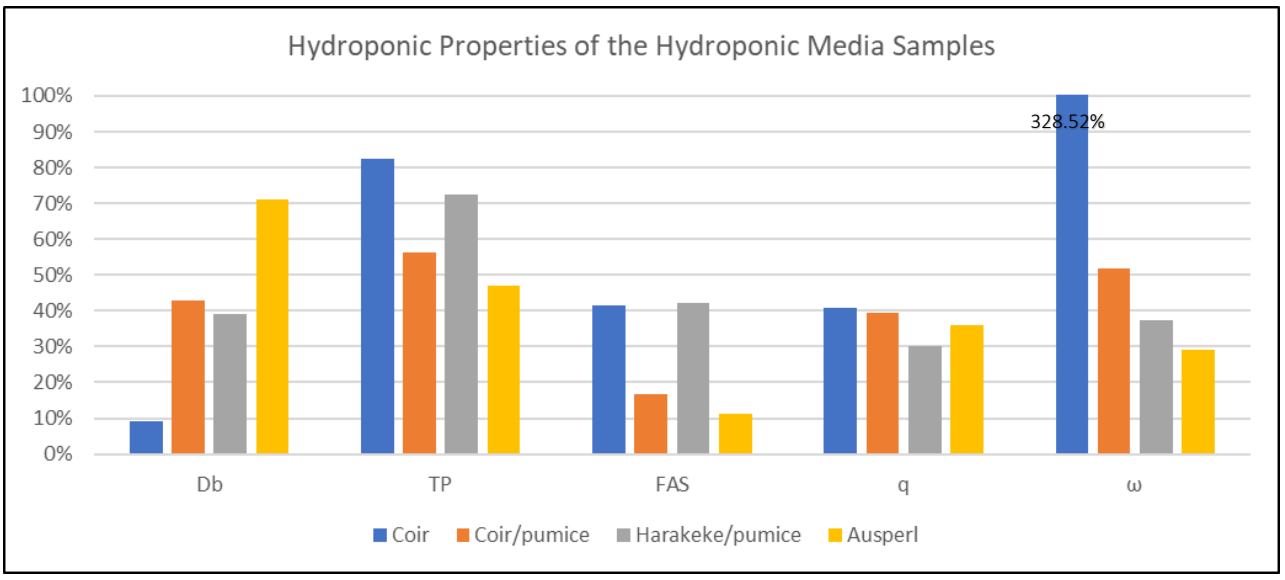

Figure 4.69: The hydroponic properties of a subset of the Hydroponic Media samples. Db is bulk density, TP is total porosity, FAS is free air space, *q* is volumetric WHC and ω is gravimetric WHC.

4.5.3.2 Stress Point, Permanent Wilting Point, Total Available Water Holding Capacity and Readily Available Water Holding Capacity

The ωSP, ωPWP, ωt and ωr of coir exceeds those found in the other hydroponic media (Figure 4.70, Table 4.24). These values are high when compared against values found by Londra et al. (2018) in their study of hydrological behaviours of peat and coir.

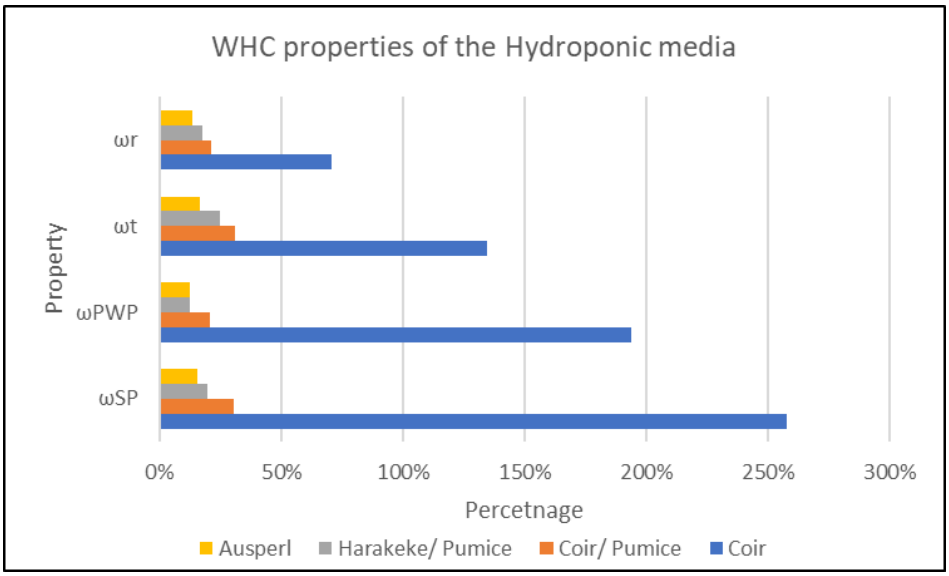

Figure 4.70: WHC properties of a subset of the Hydroponic media samples.

Table 4.24: ωSP, ωPWP, ωt and ωr of a subset of the Hydroponic Medium samples.

	Coir	Coir/ Pumice	Harakeke/ Pumice	Ausperl
Stress point (ωSP)	257.89%	30.51%	19.72%	15.36%
Permanent wilting point (ωPWP)	193.98%	20.58%	12.62%	12.57%
Total available water holding capacity (ωt)	134.54%	31.23%	24.65%	16.38%
Readily available water holding capacity (ωr)	70.62%	21.30%	17.54%	13.59%

5 Discussion

5.1 Tephras

In hydroponics the physical properties of a growth media are important to plant growth. The hydroponic properties of pumice deposits are influenced by their volcanological characteristics such as grain size distribution, componentry, clast morphology and textures, particle densities and porosities.

Grain size distribution and shape determine the internal geometry, porosity, and fluid interaction of the medium and thus its behaviour (Wallach, 2019). For pumice this is influenced by eruption type and explosivity, and particle fragmentation, transport, and deposition (Jutzeler et al., 2012). Grain size distributions of Plinian fall deposits typically vary laterally with distance from the volcano and vertically as eruption parameters may change during an eruption.

There are three main components in tephra deposits which occur in different but overlapping grain sizes in deposits (Fisher & Schmincke, 1984). These are (1) crystals (2) juvenile pyroclastic components including glass shards, pumices of different textures, lava and scoria; and (3) foreign lithics of earlier erupted products such as glass shards, pumices of different textures, lava, scoria and crystals and country rock of non-volcanic fragments that have been incorporated during magma ascent, and conduit and vent erosion (Fisher & Schmincke, 1984; Jurado-Chichay & Walker, 2001).

Clast shape is defined by the relative lengths of its three axes while roundness describes the curvature of the edges (Benn, 2013) and is influenced by transport mechanisms. Manga et al. (2011) found in a study of examples from 4 eruptions around the world that volcanic clasts in PDC deposits exhibit more rounding than corresponding fall deposits. This is due to abrasion during transport in a PDC, whereas clasts which break up due to collision increase in angularity (Manga et al., 2011).

Vesicularity is the relative amount of gas bubbles trapped in magma fragments when they cooled (Gardner et al., 1996). Vesicularity influences particle densities, porosities, and the bulk density of pumice deposits (von Lichtan et al., 2016). The size and shape of pumice vesicles is determined

by the amount of gas involved, the rate of cooling and the type of eruption (Thomas et al., 1994). A change in fragmentation conditions during an eruption will alter clast vesicularity (Thomas et al., 1994).

5.1.1 Rotorua Tehpra

The Rotorua samples showed variations in grain size distribution, componentry, vesicularity, clast density and clast porosity through time/stratigraphic position. Samples are better sorted, have lower average grain size, higher crystal and glass contents and lower lithic contents towards the top of the profile. Pumice clasts within the samples also showed more variation and increased density towards the top of the stratigraphic profile. These changes are interpreted to be the result of changes in gas content as the eruption progressed as suggested by Kilgour and Smith (2008).

Differences in grain size, componentry and clast morphology between the Rotorua samples are similar to Kilgour and Smith (2008) Units A (RQ-L1-03), B (RQ-L1-02) and C (RQ-L1-01). These changes are interpreted to be the result of hotter, gas-rich (T1) magma (RQ-L1-02 and RQ-L1-03) reactivating a cooler gas-poor (T2) magma (RQ-L1-01) by magmatic injection (Smith et al., 2004). The changes in bedding and sorting through the stratigraphic profile are likely due to rapid buoyancy changes within the eruption plume resulting in varying plume heights (13-20 km) and intensities which occurred sporadically during phase 1 of the eruption (Kilgour & Smith, 2008). Changes in degree of vesiculation and vesicle shape indicate changes in gas content, bubble nucleation and shear of the magma as it ascends through the conduit (Rotella et al., 2014).

Componentry variations observed in the Rotorua samples are consistent with Kilgour and Smith (2008) who found that as clast size decreases towards the top of the phase 1 (T2 magma) deposit the combined proportion of lithics and crystals increases. Nairn (1980) also found that lithic contents vary with proportions of essential lithics (glassy and pumiceous lava) increasing up the Rotorua profile. The 1-4 mm fraction of the RQ-L1-01 bulk sample was crystal rich, while free crystals in the remainder of the Rotorua sample fractions were either rare or not present. Kilgour and Smith (2008) identified free crystals of plagioclase, quartz, hypersthene, hornblende, and

biotite in Unit A (RQ-L1-03), this differs from this study as crystals were not identified in RQ-L1-03.

Circa 7.7% of RQ-L1-01 1-4 mm was glass shards, the proportion of glass shards in other fractions were lower ranging from 0.6% in RQ-L1-02 4-8 mm to 3.6% in RQ-L1-02 1-4 mm.

A model by Hammer et al. (1999) showed that eruption variability at Mt Pinatubo caused rapid and frequent small amounts of magma to degas and cool in the conduit, allowing plagioclase growth and resulting in inhibited vesicle expansion. The degassed magma is then deposited on the wall or forms a cap on the magma (Kilgour & Smith, 2008). The componentry changes between RQ-L1-01, RQ-L1-02 and RQ-L1-03 in this study are likely due to the incorporation and fragmentation of cooled degassed magma from earlier phases of the eruption.

5.1.2 Kaharoa Tephra

In contrast to the Rotorua samples which show temporal changes as the eruption progressed, in the Kaharoa samples medial – proximal relationships of the physical properties were investigated. The samples varied in grain size distribution, componentry, vesicularity, clast density and clast porosity between medial (KA01) and distal (KR01) sites. The more distal KR01 had a lower mean particle size, mode and was better sorted than the medial KA01 sample.

Deposit componentry changed over distance. Samples indicate significantly higher proportions of lithic clasts of lithoidal rhyolite from earlier eruptions, sparse basaltic and rare grandiorite, diorite, gabbro, and olivine clinopyroxenite clasts (Leonard et al., 2002) and glass shards in the medial sample compared to that in the distal sample. This corresponds with findings by Nairn et al. (2001) where although sections as distant as KR01 from the vent were not investigated stratigraphic logs of Koa Valley and Ashpit Road Quarry already indicate a reducing proportion of lithics with distance from the vent.

A single crystal was found in both the KA01 and KR01 1-4 mm fractions in this study, this differs from Nairn et al. (2001) who found crystal contents at Koa Gully c. 5 km north of KA01 to be between 6 and 25%.

Vesicularity and angularity of Kaharoa pumice clasts increase with distance from the vent from predominantly moderately vesiculated sub rounded clasts to predominantly highly or extremely vesiculated particles. This is consistent with Nairn et al. (2001) who found Kaharoa pumice clasts to be slightly to moderately vesiculated at the proximal Koa Gully (K291) site located c. 5 km north of KA01 sample location.

Deposition of pyroclasts from an eruption plume depends on settling velocities that are determined by clast density, shape, and size (Fisher & Schmincke, 1984; Taddeucci & Palladino, 2002). Available particle sizes and their settling velocities determine the grain size distribution and sorting of a deposit with clasts of lower settling velocities being transported further by the eruption cloud and atmospheric winds (Fisher & Schmincke, 1984). Clast density in KR01 was lower and vesicularity higher than that found in KA01 clasts as expected due to denser clasts settling first and lighter clasts being transported over greater distances from the vent. Similarly, the pumice content of both size fractions increases as contents of denser lithics decrease with distance from the vent. This observation agrees with Nairn et al. (2001) who found that lithic contents reduce with distance from the vent due to the lower density of pumice when compared to the higher density of lithics.

5.1.3 Taupō Tephra

The Taupō samples reflect differences between the two Plinian phases of the Taupō eruption. The Taupō samples ranged in grain size distribution, componentry, vesicularity, clast density and clast porosity with the sample of the earlier Plinian phase (Y2) having a lower mean particle size and mode than the sample of the later Plinian phase (Y5). Both samples were poorly sorted with similar proportions of pumice grains and minor lithics, crystals and / or glass shards.

The only pumice types common to both samples was T.Fibrous which made up a minor proportion of the samples. The Y5 sample had a higher porosity and skeletal density than the Y2 sample.

The morphology, texture and vesicle shape of pumice clasts from both fractions of the Taupō Y2 and Y5 samples are similar. However, vesicularity of the Taupō Y5 pumice clasts is higher and clast density is lower than in the Taupō Y2 sample. This matches the observation of Wilson (1993)

and Wilson and Walker (1985) who found the Y2 deposit to be highly to extremely vesiculated. Additionally, Houghton et al. (2010) found that the Y5 unit had more tube (sheared) and highly expanded (coalesced) pumices with lower densities than the white micro vesicular pumice types that are typically found in Y2. Houghton et al. (2010) suggests the differences can be linked to shallow conduit processes, degassing and volatile exsolution before and during the eruption.

The pumice content of the Y5 sample is similar to Wilson (1993) who found that there were few recycled clasts and to Walker (1980) who found that glass shards were predominantly found in the <1mm grain size which was not investigated in this study.

The presence of lithic clasts in the Taupō samples corresponds with isopleth maps in Walker (1981b) which indicate that lithics up to 15 mm diameter are present in the Taupō Y2 deposit and Figure 3 in Lowe and Pittari (2021b) which indicates that lithics are present in both Taupō Y2 and Taupō Y5 deposits. Additionally, Tapscott (2023) recognises that lithic proportions change through the Taupō Y5 deposit due to the different stages of the eruption of the unit.

The low crystal content of the Taupō Y2 sample is consistent with findings of Wilson (1993) and Wilson and Walker (1985) and from Walters (2020) who found that free crystals of plagioclase, pyroxene, quartz and titanomagnetite were abundant at c. 10-50% in the 1 ϕ size range of the Taupō Y2 deposit and that as grain size increased crystal concentration reduced with free crystals being rare in the -1 ϕ size range and absent at larger grain sizes, this corresponds with the findings of this study where crystals were present in the 1-4 mm fraction but absent in the 4-8 mm fraction of Taupō Y2. Research by Tapscott (2023) on the Taupō Y5 deposit indicates that crystal contents increase up the profile between 2 and 1 ϕ before decreasing as grain size increases towards -1 ϕ. As crystals and glass shards are denser than pumice grains of the same size they will generally settle closer to the source than similar sized pumice clasts due to aeolian fractionation in the plume (Tapscott, 2023), this was observed when comparing the glass shard proportions of KA01 (which contained significantly higher proportions of glass shards) than KR01.

5.1.4 Comparison of Tephra properties

5.1.4.1 Grain size distribution

The Gradistat program used to calculate grain-size distribution and statistics uses sedimentary grain size terminology which has been carried through to Table 5.1 & Figure 5.1 and the following discussion. Under sedimentary grain size terminology gravel equates to lapilli (-1 ϕ - -6 ϕ or 2 - 64 mm), whereas sand (4 ϕ - -1 ϕ or 0.06 – 2mm) and mud (<4 ϕ or <0.06 mm) equate to ash (<-1 ϕ or <2 mm).

Grains in the bulk samples range from mud / ash (9 ϕ to 10 ϕ) to gravel (-5 ϕ to -6 ϕ), in addition RQ-L1-03 contained a bomb (-6 ϕ and -7 ϕ) The relative combinations of gravel, sand and ash in a sample define the textural group of the sample (Table 5.1 & Figure 5.1). The very poorly sorted RQ-L1-02, RQ-L1-03 and Daltons Fine and the poorly sorted Dalton Coarse samples are muddy sandy gravel, the poorly sorted RQ-L1-01, KA01, KR01 and Taupō Y2 samples are sandy gravels and the poorly sorted Taupō Y5 sample is classified as gravel (Figure 5.1).

Table 5.1: Grain size distribution of bulk samples.

Sample	Textural Group	Gravel (lapilli -1 ϕ - -6 ϕ or 2 - 64 mm) (%)	Sand (ash 4 ϕ - -1 ϕ or 0.06 - 2 mm) (%)	Mud (ash <4 ϕ or <2 mm) (%)
RQ-L1-01	Sandy Gravel	52	44	4
RQ-L1-02	Muddy Sandy Gravel	73	22	5
RQ-L1-03	Muddy Sandy Gravel	75	20	5
KA01	Sandy Gravel	65	32	3
KR01	Sandy Gravel	44	54	2
Taupō Y2	Sandy Gravel	69	29	2
Taupō Y5	Gravel	88	10	2
Daltons Coarse	Muddy Sandy Gravel	79	12	9
Daltons Fine	Muddy Sandy Gravel	45	42	13

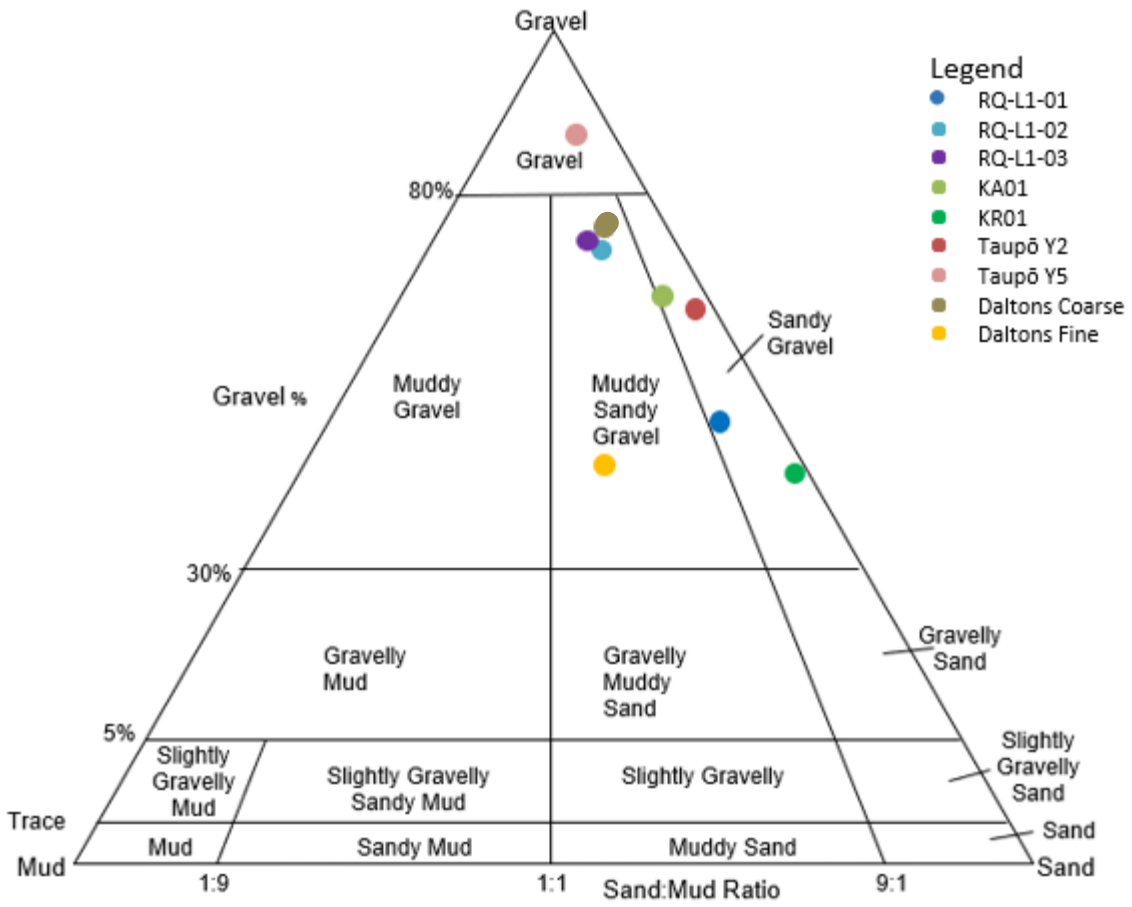

Figure 5.1: Gravel Sand Mud diagram showing the grain-size distribution of the Rotorua, Kaharoa, Taupō and Daltons samples.

Most cumulative curves followed a similar curve with steep slopes between c. D_{10} and c. D_{90} and long fine tails. As a result of being collected from a graded bag the Daltons Fine sample follows a similar curve as other samples, however, the overall grain size is smaller. The Taupō Y5 has a larger mean particle size and coarser cumulative curve than other samples (Figure 5.2).

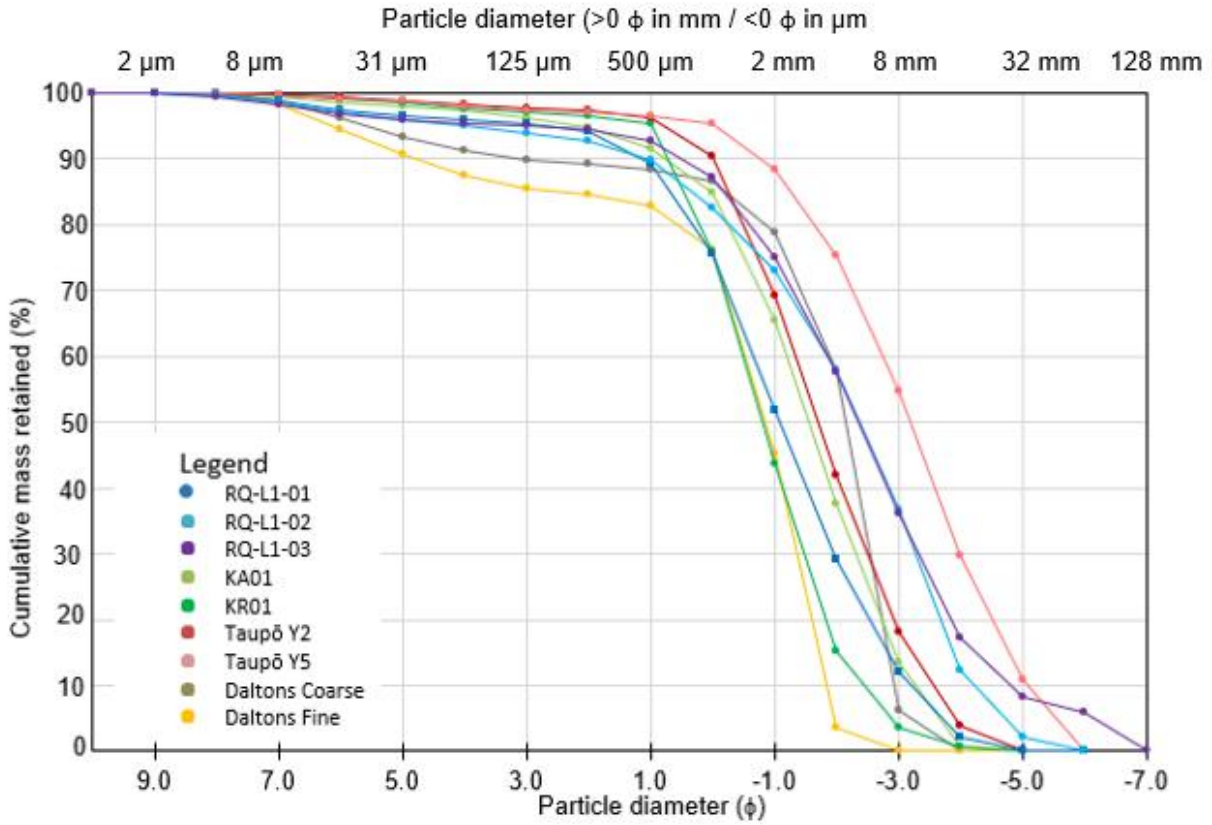

Figure 5.2: Combined Cumulative Curves of the Rotorua, Kaharoa, Taupō and Daltons Samples.

5.1.4.2 Components

Pumice clasts are the dominant component in both size fractions of all samples, however RQ-L1-01 1-4 mm contains significantly less pumice than other samples. The remainder of the samples are comprised of lithics, crystals and/or glass (Figure 5.3). The number of pumice types and characteristics of dominant pumice types varies between fractions and tephras.

The Rotorua, Kaharoa and Taupō pumice clasts are predominantly subrounded while the Daltons samples were rounded. Clast textures in the Rotorua, Taupō and Daltons samples were predominantly uniform while the Kaharoa clasts change from frothy in the medial location to fibrous in the distal location. The Rotorua and Daltons clasts are incipiently or poorly to moderately vesicular. The Kaharoa clasts change from moderately vesicular in the medial location to highly vesicular in the distal location while the Taupō samples change from highly vesicular in the earlier Y2 phase to moderately vesicular in the Y5 phase of the eruption.

The lithic content of the samples ranged from 0% in KR01 1-4 mm to 11.11% in RQ-L1-02 1-4 mm (Figure 5.3) similar to earlier findings (Kilgour & Smith, 2008; Leonard et al., 2002; Lowe & Pittari, 2021a; Nairn et al., 2001; Walker, 1981b).

Crystals make up a significant proportion of the 1-4 mm fraction of the RQ-L1-01 sample, however they were not identified in the 4-8 mm fractions and were rare or not present in other 1-4 mm fractions (Figure 5.3).

Glass results when magma cools and solidifies rapidly without crystallization. Glass ranged from 0% in the KR01 fractions, Taupō Y5 4-8 mm and Daltons Fine 4-8 mm to 7.74% in RQ-L1-01 1-4 mm (Figure 5.3).

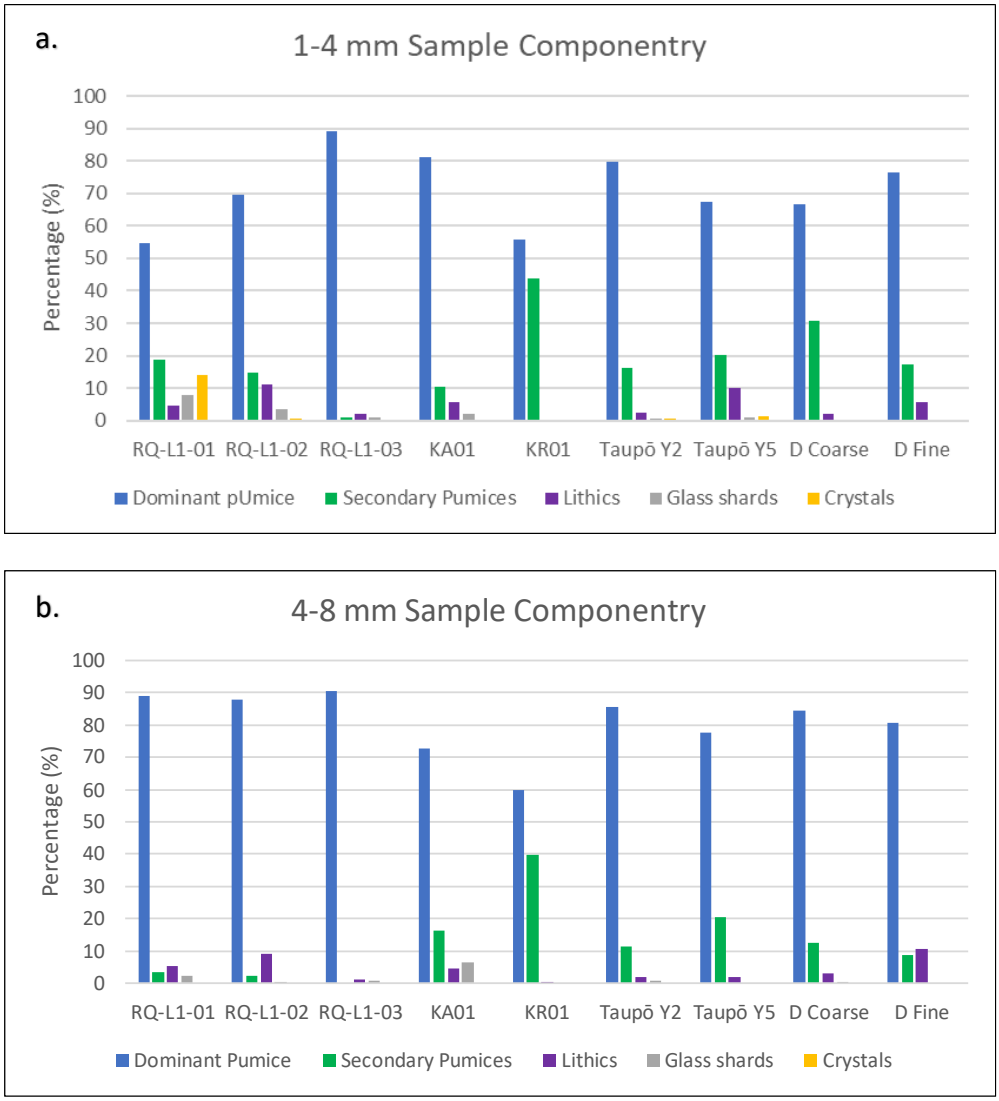

Figure 5.3: Main Components of the Pumice Sample Fractions a. 1-4 mm fractions and b. 4-8 mm fractions.

5.1.4.3 Particle density and porosity

In hydroponics particle density influences pedotransfer functions (Ruehlmann, 2020). And envelope density of pumice is related to total porosity, although solid density is used in porosity calculations for pumice as it contains closed pores (Wallach, 2019).

The Taupō Y2, Taupō Y5 and KR01 samples which have the lowest envelope densities also had moderate to high vesicularity, while samples KA01 and RQ-L1-01 which have the highest envelope density also have poor to moderate vesicularity. With the exception of RQ-L1-01 and KA01 the envelope density of the pumices tested in this study correspond with Fisher and Schmincke (1984) who found that silicic pumice generally has a density of <1.0 g/cm^3 due to its vesicularity.

Total and isolated porosity increase as the envelope density of the pumice clasts increases (Figure 5.4a and c). In contrast to this connected porosity decreases as envelope density increases (Figure 5.4e). The most extreme case are clasts from the Kaharoa distal KR01 sample, which shows the highest envelope density and total and isolated porosities but the lowest connected porosity, in contrast to this is the Kaharoa medial KA01 which has a significantly lower envelope density and total and isolated porosities and a high connected porosity (Figure 5.4a, b and e). The distance of the deposit from the Kaharoa eruption vent has a significant influence on particle density and porosity parameters.

The envelope density of the Rotorua and Taupō Y5 samples fall between the extremes of the Kaharoa samples, however the total porosity of these samples is lower than the Kaharoa samples (Figure 5.4a). The total porosity of the Taupō Y2 sample is similar to that of the Kaharoa medial (KA01) sample (Figure 5.4a).

As isolated porosity increases total porosity also increases, however, the reverse is seen in connected porosity which increases as total porosity decreases (Figure 5.4b and d). A direct relationship is seen between isolated and connected porosity with isolated porosity decreasing as connected porosity increases (Figure 5.4f).

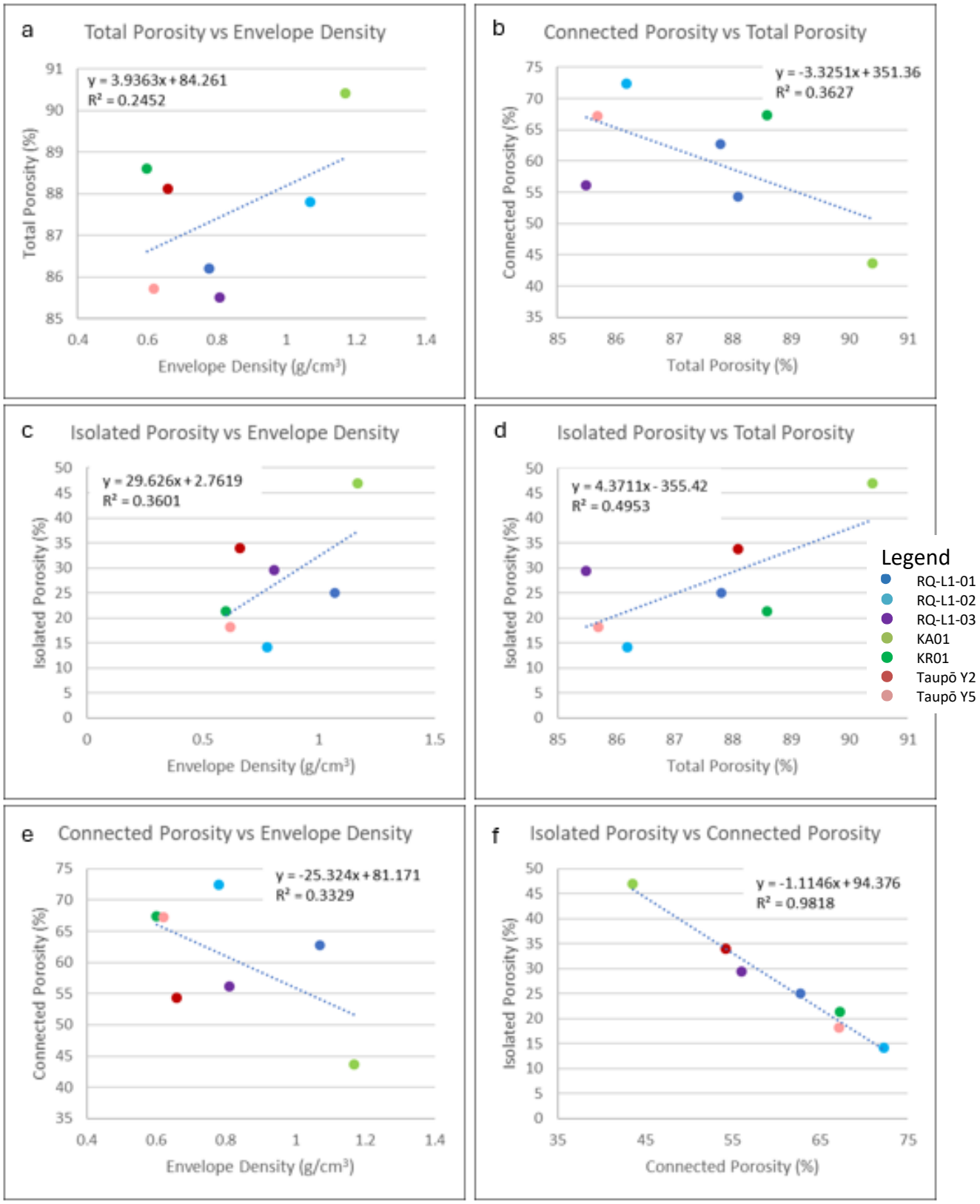

Figure 5.4: Particle density and porosity comparisons of the 4-8 mm grains.

5.2 Relationship of material and hydroponic properties

5.2.1 Total porosity, free air space and bulk density

Testing was undertaken to determine the hydroponic parameters of the pumice fractions and how they relate to the physical properties of the deposits. Hydroponic parameters include bulk density, pH, total porosity, free air space and water holding capacity of the two hydroponic grades. These are compared with each other and against the skeletal and envelope densities and connected porosities of the 4-8 mm fractions. Additionally, the stress point, permanent wilting point, and the total and readily available water holding capacities were calculated from the gravimetric WHC for all sample fractions excluding KR01 4-8 mm, Taupō Y2 4-8 mm, Taupō Y 4-8 mm and Daltons Fine 1-4 mm.

Free air space of the bulk sample shows a slight correlation with bulk density in the 1-4 mm fractions. In the 1-4 mm grade as the free air space increases the bulk density increases slightly. In the 4-8 mm fractions as the free air space remains constant as bulk density changes (Figure 5.5a & b). The free air space in the 1-4 mm fractions is lower than that found in the 4-8 mm fraction and the bulk density of the 4-8 mm fractions is generally lower than that found in the 1-4 mm fractions. This is similar to findings in previous studies. Sahin et al. (2005) also found that the 2-4 mm grade of pumice had a lower bulk density than the larger 4-8 mm grade. Results from Gizas and Savvas (2007) on different grades of pumice indicate a relationship between bulk density and free air space in which as the grade size increases the free air space increases and bulk density decreases.

The results of this study indicate that the 4-8 mm grade samples contain more free air space due to the larger grains not packing together as tightly as the smaller grains of the 1-4 mm grades. The higher free air space in the 4-8 mm grade corresponds with lower bulk densities than found in the corresponding 1-4 mm fraction (Figure 5.5a and b). This agrees with Bar-Tal et al. (2019) who found that the physical properties of pumice are affected by the aggregate size. Furthermore, all components in a sample influence the bulk density and free air space, this includes lithics, crystals and glass shards which have higher densities than pumice (Bar-Tal et al., 2019; Wallach, 2019).

The RQ-L1-01 1-4 mm sample which has a high proportion of crystals, lithics and glass shard compared to pumice clasts which has resulted in a higher bulk density. The Taupō Y2 samples also had a high bulk density, however componentry does not indicate a high proportion of lithics, crystals or glass shards, clast bulk density and porosity measurements are not unusually high or low, thus it is possible that the shape of the clasts may result in a tightly packed sample.

The Kaharoa and Daltons low bulk densities and relatively low proportions of lithics, crystals and glass shards, additionally both Kaharoa and the Daltons Fine samples are moderately to highly vesiculated indicating that vesicularity reduces bulk density.

The Taupō Y5 sample is an outlier with comparatively high free air space in the 4-8 mm grade and low free air space in the 1-4 mm grade. However, both grades have a low bulk density (Figure 5.5a and b). The Y5 sample is shown on the graphs but is excluded from the regression line calculations and discussion.

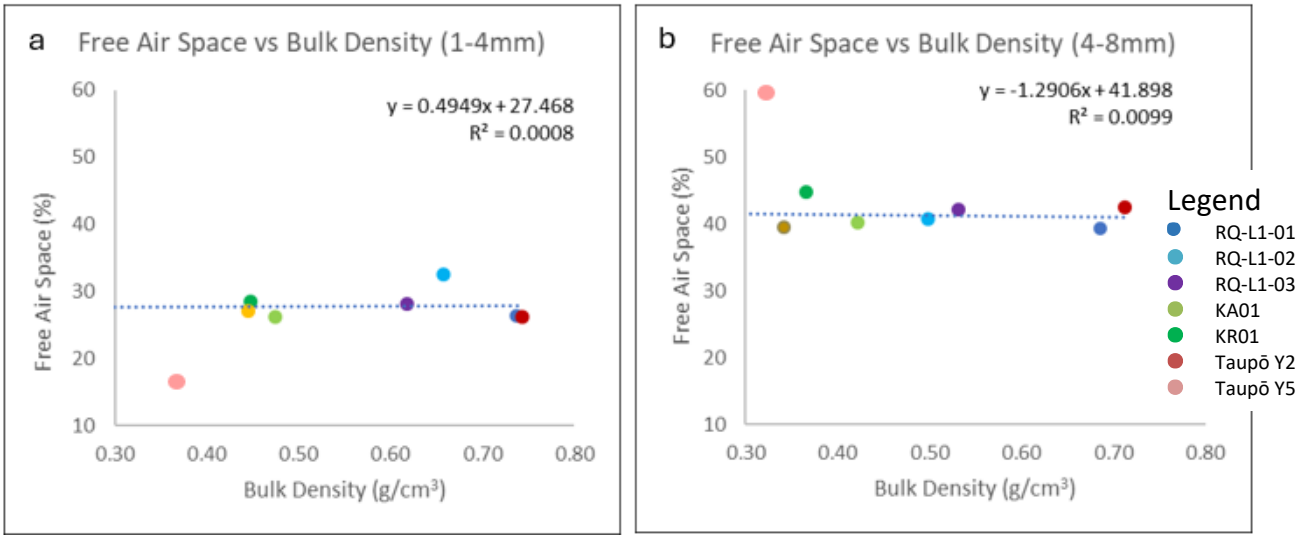

Figure 5.5: Free air space and bulk density comparison of a. the 1-4 mm fraction and b. the 4-8 mm fraction.

Free air space and total porosity of the bulk medium increase with decreasing envelope and skeletal density of the particles that make up the medium (Figure 5.6a, b, d, and e). Densities describe the mass of the particles compared to pores space. Therefore, samples with more pore spaces between particles (inter-clast pore space) and accessible pore space within the clasts (intra-clast pore spaces) within the clasts are likely to have lower densities. This also applied to total porosity as free air space and total porosity are related.

Free air space and total porosity increase with increasing connected porosity of the particles (Figure 5.6c and f). As connected porosity is the accessible intra-clast pore space, particles with a higher connected porosity have more free air space and thus higher total porosity.

Although free air space and total porosity which describe volumes are related, the bulk densities which describe mass of the particle as well as sample volume do not appear to have any clear trends when compared against connected porosity which also describes a volume (Figure 5.6i).

No clear trend is seen when comparing bulk density of the sample to the envelope and skeletal densities or connected porosity of the clasts (Figure 5.6g and h). However, this is expected as bulk density describes the mass and volume of the sample and envelope and skeletal densities describe the mass and volume of the clasts.

The Taupō Y5 4-8 mm sample is an outlier with comparatively high total porosity and free air space. One likely reason for overestimating the total porosity and thus free air space is that pumice clasts might have unknowingly floated to the surface due to their high vesicularity and thus low density. The Y5 sample is shown on the graphs but is excluded from the regression line calculations and discussion.

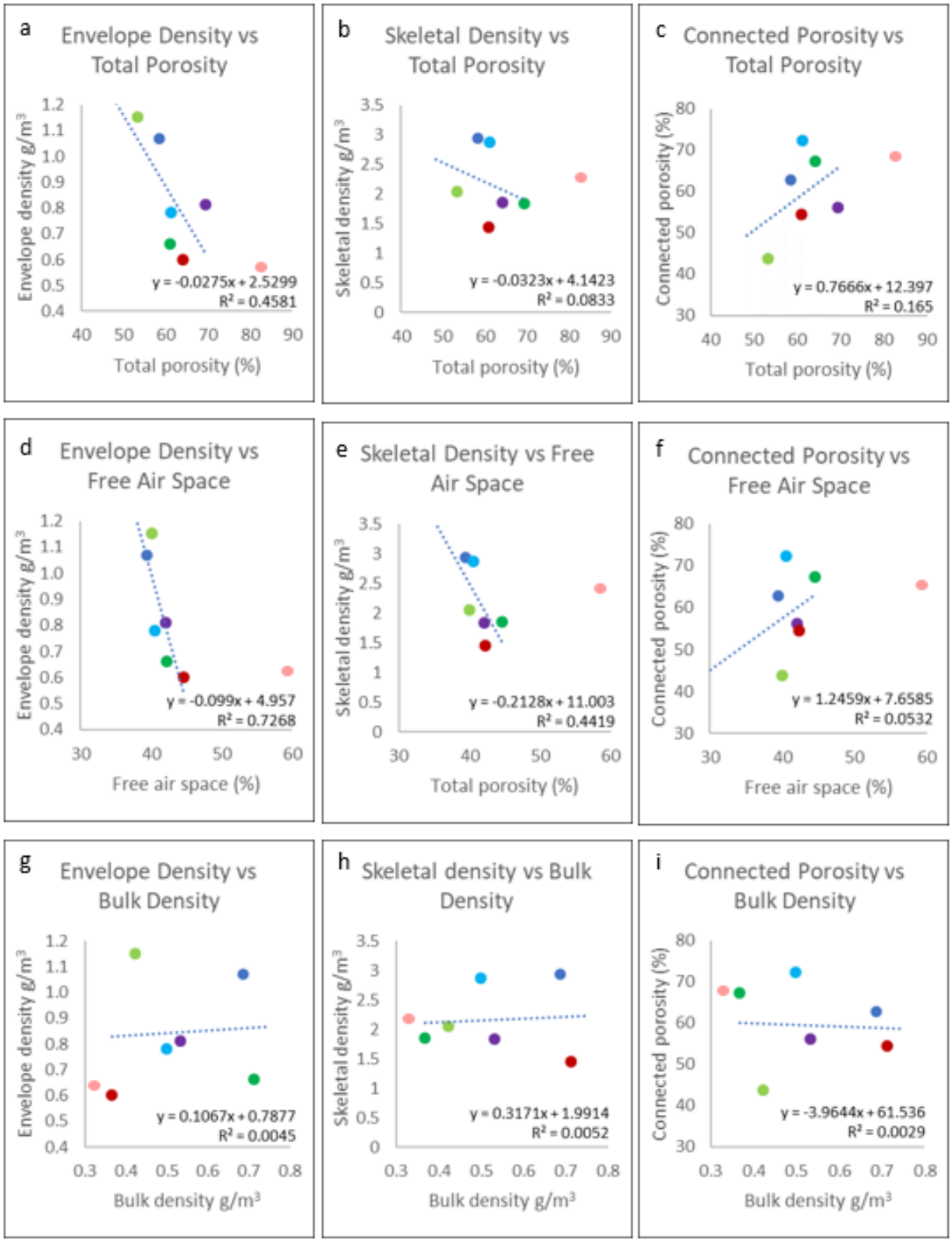

Figure 5.6: Relationships between bulk samples and 4-8 mm clast properties. a. total porosity and envelope density; b. total porosity and skeletal density; c. total porosity and connected porosity; d. free air space and envelope density; e. free air space and skeletal density; f. free air space and connected porosity; g. bulk density and envelope density; h. bulk density and skeletal density; i. total and connected porosity.

5.2.2 Water Holding Capacity of Bulk Media

The 1-4 mm fractions of the studied tephra samples generally had a higher volumetric WHC than the 4-8 mm fractions except in RQ-L1-03. Finer particles create smaller inter-clast pore spaces and therefore a higher WHC due to capillary action, while coarse particles create larger inter-clast pore spaces which helps with roots aeration (Gizas & Savvas, 2007; Raviv et al., 1999; Raviv et al., 2002).

In both fractions the Daltons Coarse sample has the highest volumetric WHC and KA01 has the lowest (Figure 5.7a and b). The sample with the largest difference WHC between fractions was Taupō Y5, however the Taupo Y5 4-8 mm is an outlier. The Daltons Coarse sample also has a large difference in WHC between the grades, this may be a function of being graded prior to sale. RQ-L1-03 had no significant difference in WHC between the fractions.

Total porosity of the samples is higher than the corresponding WHC, however except in the Taupō Y5 4-8 mm grade total porosity increases as WHC increases (Figure 5.7a and b), this is due to increased total porosity indicating an increase in available inter- and intra-clast pore space for water to be stored.

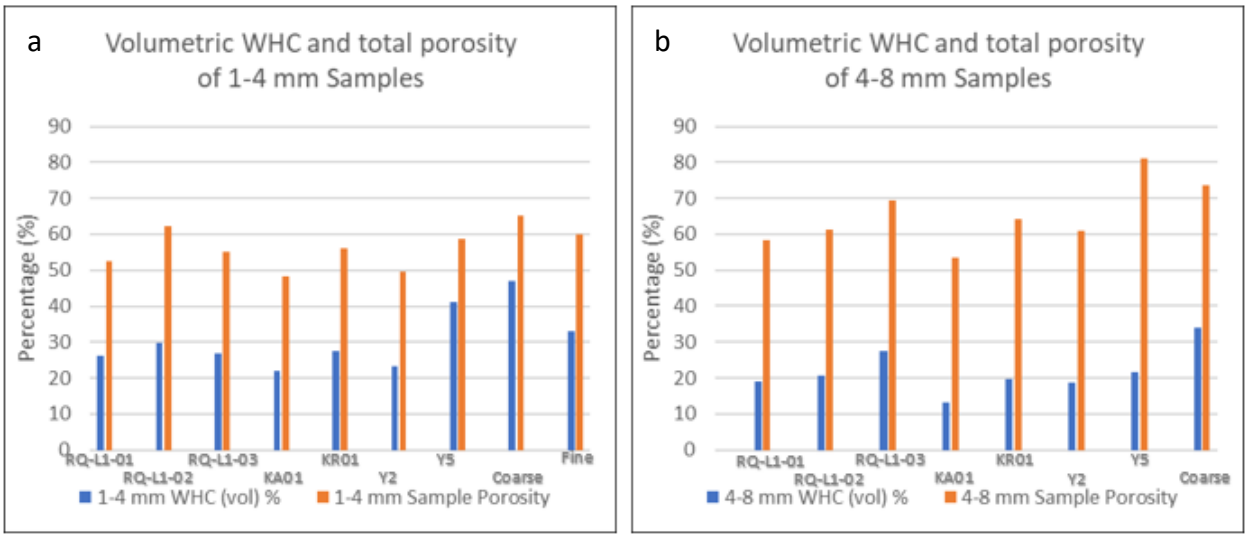

Figure 5.7: Volumetric WHC and total porosity of the a. 1-4 mm and b. 4-8 mm fractions of the bulk sample fractions.

The results of this study suggest that clast shape does not influence the volumetric WHC of the pumice fractions (Figure 5.8).

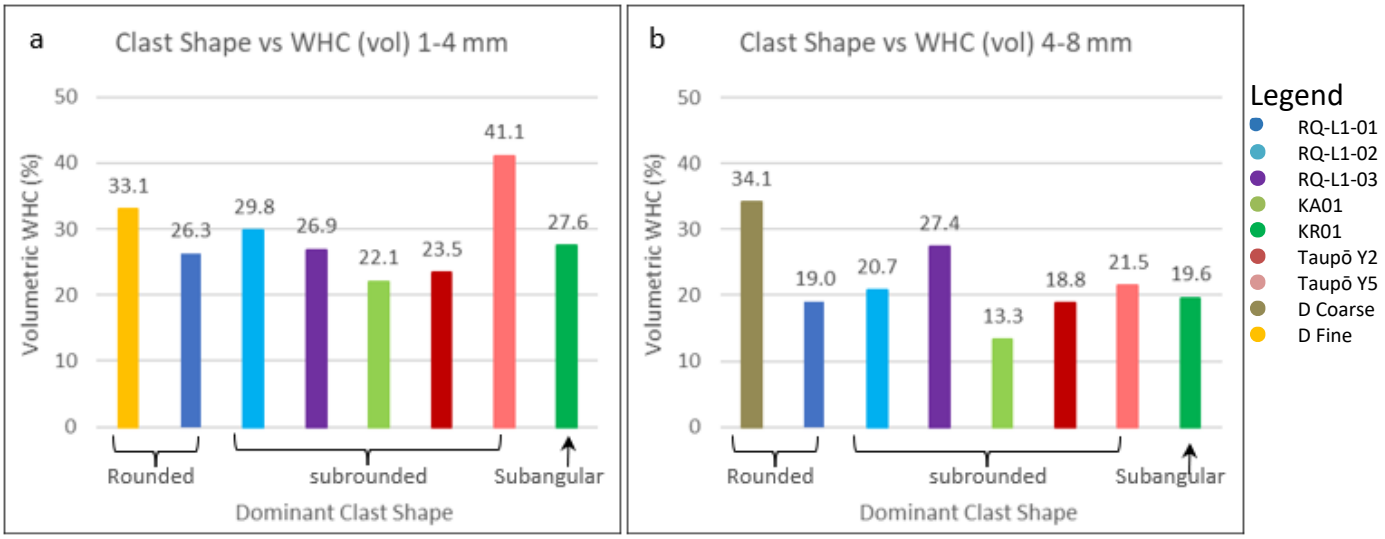

Figure 5.8: Effect of dominant clast shape on the volumetric water holding capacity of a. the 1-4 mm fraction and b. the 4-8 mm fraction of the pumice samples.

The volumetric WHC increases with increasing connected porosity and decreasing envelope density of the pumice particles (Figure 5.9a and b) due to more intra clast space being available for particle with higher connected porosities.

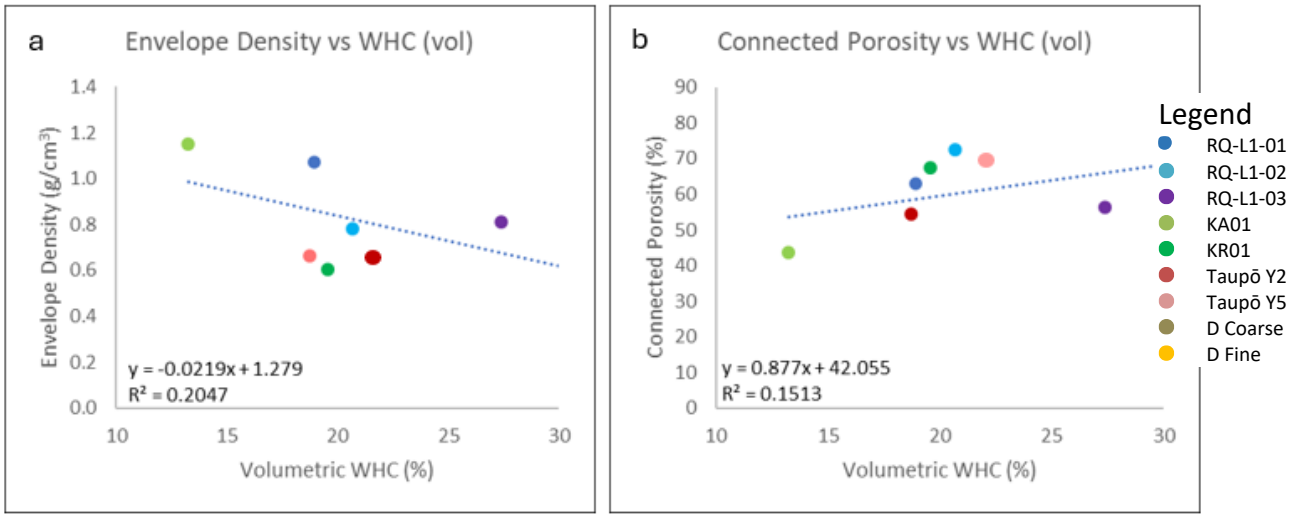

Figure 5.9: Clast property relationship with volumetric water holding capacity of the 4-8 mm samples. a. envelope density and b. connected porosity.

The permanent wilting point, stress point, total available water holding capacity (TAWHC) and readily available water holding capacity (RAWHC) of the KR01, Taupō Y2 and Taupō Y5 4-8 mm

samples are not included as when these were calculated using the measured data negative readings were produced. This is likely due to the larger clasts having had a small contact area with the plate, leading to either extended drain times or the cessation of connected drainage via the plate. If this is the case, then this is a function of the physical character of the medium. The 4-8 mm fractions of KR01, Taupō Y2 and Taupō Y5 where positive are included in Figure 5.11 and Figure 5.12 for information, however, are not included in the discussion below.

Both volumetric WHC (q) and gravimetric WHC (ω) in both grades was lowest in KA01. Volumetric WHC (q) was highest in the Daltons Coarse and Gravimetric WHC (ω) was highest in RQ-L1-02. Gravimetric WHC (ω) shows a slight correlation with volumetric WHC (q) in the 1-4 mm grade (Figure 5.10a), the Taupō Y5 1-4 mm q is particularly high, this may be an outlier or an undetected error in measurement. If this value were to be removed the correlation between q and ω would be stronger. In the 4-8 mm grade there is a correlation between q and ω (Figure 5.10b). In both grades q values being generally lower than ω, this is due to different measurement techniques with q being volume based and ω being weight based. The 4-8 mm fractions generally have lower q and ω than that found in the 1-4 mm fractions (Figure 5.10a and b).

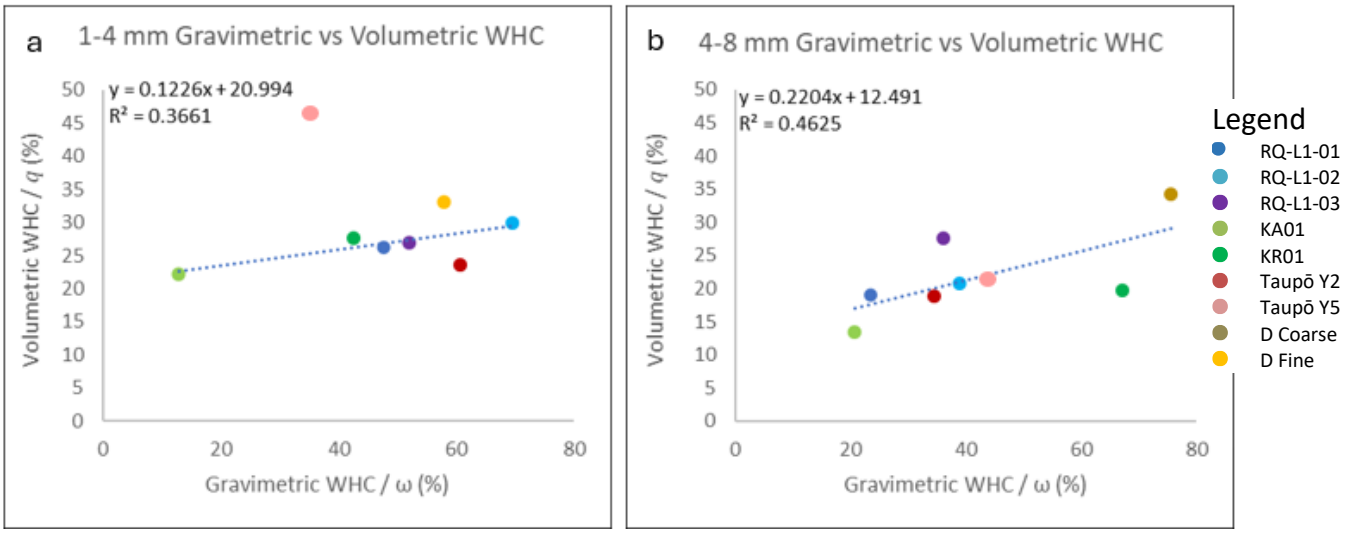

Figure 5.10: Comparison of volumetric and gravimetric water holding capacities of the a. 1-4 mm and b. 4-8 mm fractions.

Stress point (ωSP) in the 1-4 mm fraction was lowest in KA01 and highest in KR01 and in the 4-8 mm fraction. It was lowest in RQ-L1-01 and highest in KRO1. Permanent wilting point (ωPWP) in the 1-4 mm fraction was lowest in RQ-L1-01 and highest in Taupō Y2 and in the 4-8 mm fraction.

It was lowest in RQ-L1-01 and highest in KR01. In the 1-4 mm fraction there is a grouping of samples with lower ωSP and ωPWP, while the remaining Y2 and KR01 have higher ωSP and ωPWP. In the 4-8 mm fraction the samples are spread more evenly along the trendline. The ωSP and ωPWP in the 4-8 mm fraction is generally higher than found in the 1-4 mm fraction. As expected there is a strong correlation between ωSP and ωPWP, as ωSP is the point at which the plant has to work to extract water and generally correlates to a water content between -40 and -100kPa (-0.4 and -1bar) while ωPWP is the point where no further water can be extracted and generally correlates to a water content of -1,500 kPa (-15bar) (Scotter, n.d.).

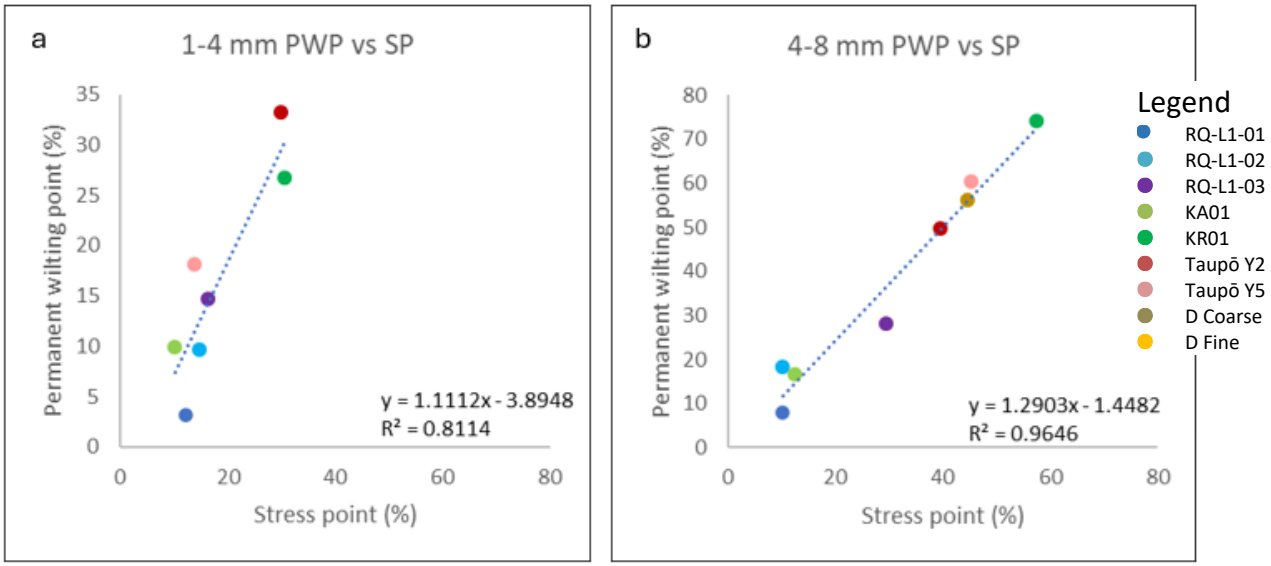

Figure 5.11: Comparison of permanent wilting point and stress point of the a. 1-4 mm and b. 4-8 mm fractions.

Total available water holding capacity (TAWHC) and RAWHC in both grades was lowest in KA01 and highest in RQ-L1-02. However, the TAWHC and RAWHC range in the 4-8 mm fractions is significantly narrower than that found in the 1-4 mm fractions with TAWHC showing a larger variation between sample fractions than that seen for RAWHC. Both the TAWHC and the RAWHC of the fractions increased as the gravimetric WHC increased (Figure 5.12a and b) similarly TAWHC increased as RAWHC increased (Figure 5.12c) .This is expected as gravimetric WHC measures the amount of water held in a sample at atmospheric pressure while RAWHC and TAWHC is the amount of which can be extracted from the sample under higher pressures.

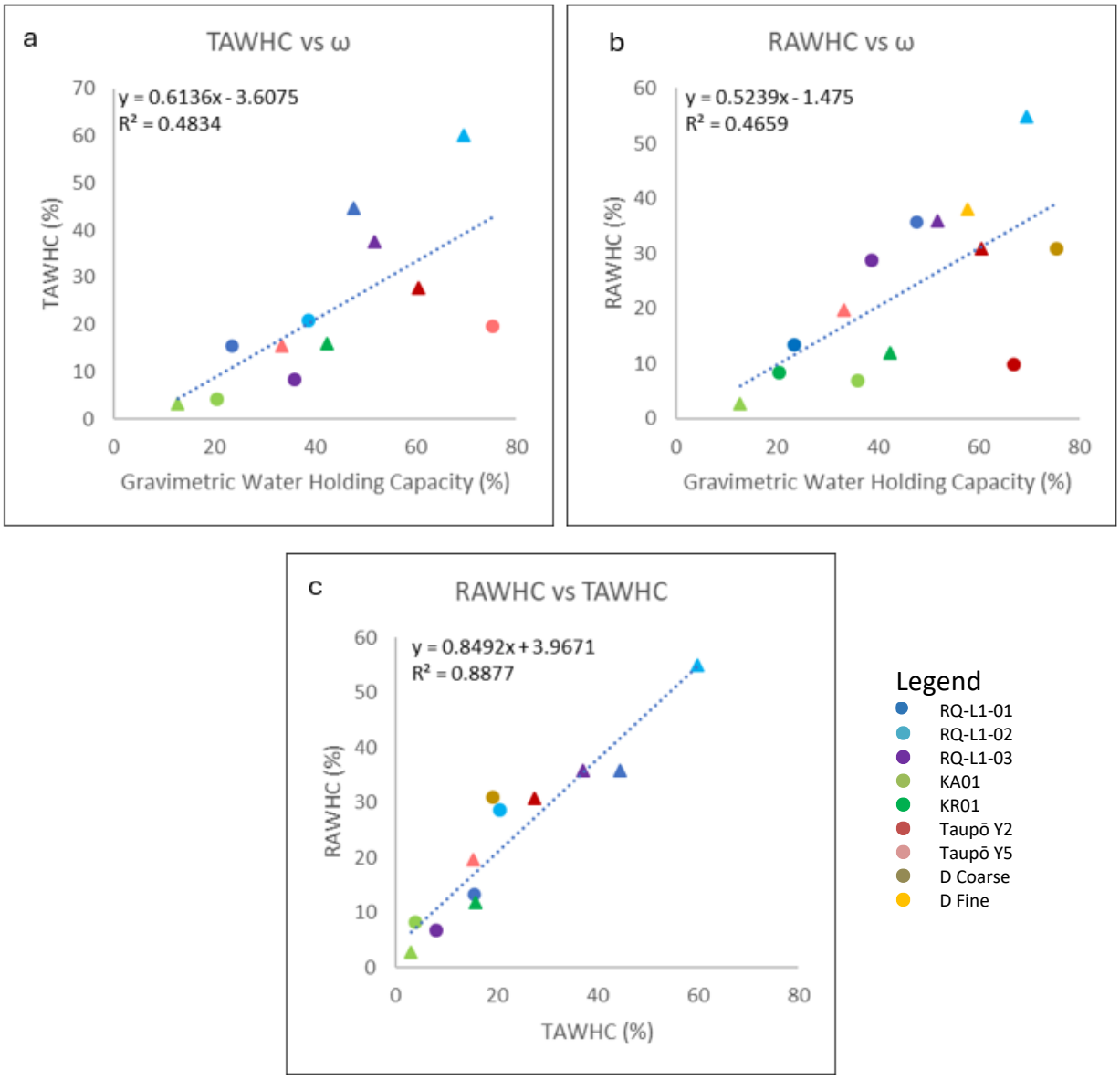

Figure 5.12: a. Gravimetric water holding capacity relationship with total available water holding capacity; b. gravimetric water holding capacity relationship readily available water holding capacity and c. relationship between RAWHC and TAWHC. Triangles are the 1-4 mm fractions and circles are the 4-8 mm fractions.

5.3 Influence of material properties on their potential performance as hydroponic growth media

Here, the different types of pumice investigated in this project will be assessed for their suitability as hydroponic growth substrates. The pumice is compared against published (Gizas & Savvas, 2007; Marinou et al., 2013; Pérez-Urrestarazu et al., 2019; Sahin et al., 2005) and unpublished (Zhao et al., 2023) studies which assessed various material properties in relation to yield and growth.

5.3.1 Grain size

Grain sizes of 1-4 mm and 4-8 mm were selected for this project as they represent commonly used grades used in hydroponics. Grain size influences hydroponic parameters including bulk density, total porosity and free air space as discussed in the following sections. Growth trials have been previously undertaken with pumice grain sizes of 0-2 mm, 0-5 mm, 0-8 mm, and 4-8 mm by Gizas and Savvas (2007) and grain sizes of 2-4 mm and 4-8 mm by Sahin et al. (2005), while Marinou et al. (2013) and Pérez-Urrestarazu et al. (2019) conducted growth trials with hydroponic substrates including pumice.

The effect of pumice particle size on the growth of cucumbers, lettuce, rose and gypsophila was studied by Gizas and Savvas (2007) who found that gypsophila and cucumber gave the highest yields when grown in the 0-2 mm and 0-5-mm grade whereas lettuce and rose showed a weaker response to the different size grades. Sahin et al. (2005) investigated the effect of adding pumice (2-4 mm and 4-8 mm) in different ratios to soil on strawberry plant growth and found that the best plant growth was obtained using 4-8 mm pumice at a 45% ratio to soil.

Marinou et al. (2013) investigated the effect of differing ratios of sawdust, coco soil and/or pumice mixtures on hydroponically grown strawberries and found that the leaf numbers doubled on plants grown in 100% sawdust and runner growth increased by 70% when plants were grown in coco soil over those grown in pumice, however fruit numbers on plants grown in pumice increased by 50% over those grown in sawdust. Additionally, yield increased by 50% in a 50/50 mix of sawdust and pumice compared to those grown in sawdust. A study by Pérez-Urrestarazu et al. (2019) into substrates for use in living walls found that pumice produced slightly better green cover and biomass production of Soleirolia soleirolii (Req.) Dandy (SO) and Spathiphyllum wallisii Regel (SP) over plants grown in perlite and expanded clay.

5.3.2 pH

The pH range of media identified in Table 5.2 ranges from pH 4.71 for sawdust (Marinou et al., 2013) to pH 8.2 – 9.6 for biochar and hydrochar (Belda et al., 2016). The pH of the pumice (pH 6.5-7) and hydroponic media (pH 6-7) assessed during this study and in Zhao et al. (2023) (Table 5.2) are within the range of those found in other hydroponic materials and are thus considered

to have a suitable pH for use as a hydroponic substrate. The pH results of Zhao et al. (2023) are lower than found in the same materials in this study, however, it is unknown how long the material was left in water prior to pH testing in the Zhao et al. (2023) trail.

Table 5.2: pH of hydroponic media from previous studies (pumice is highlighted).

Source	Medium	pH
Kennard et al. (2020)	Ideal pH	5.2-6.3
	Perlite	6.9
Zhao et al. (2023)	Pumice	6.1
	Coir	5.9
	Harakeke/Pumice	6.0
Belda et al. (2016)	Biochar & hydrochar	8.2-9.6
	Coir	6.5
Papadopoulos et al. (2008)	Perlite & vermiculite	7.0-7.5
Arancon et al. (2015)	Coir	5.6
	Sphagnum Moss	5.7
Marinou et al. (2013)	Pumice	7.87
	Sawdust	4.71

5.3.3 Bulk Density

There is a large range of bulk densities between the tested pumices, the hydroponic media and the pumice mixes with coir having a distinctly lower density and Taupō Y2, RQ-L1-01 and the hydroponic pumice having the highest bulk densities (Figure 5.13).

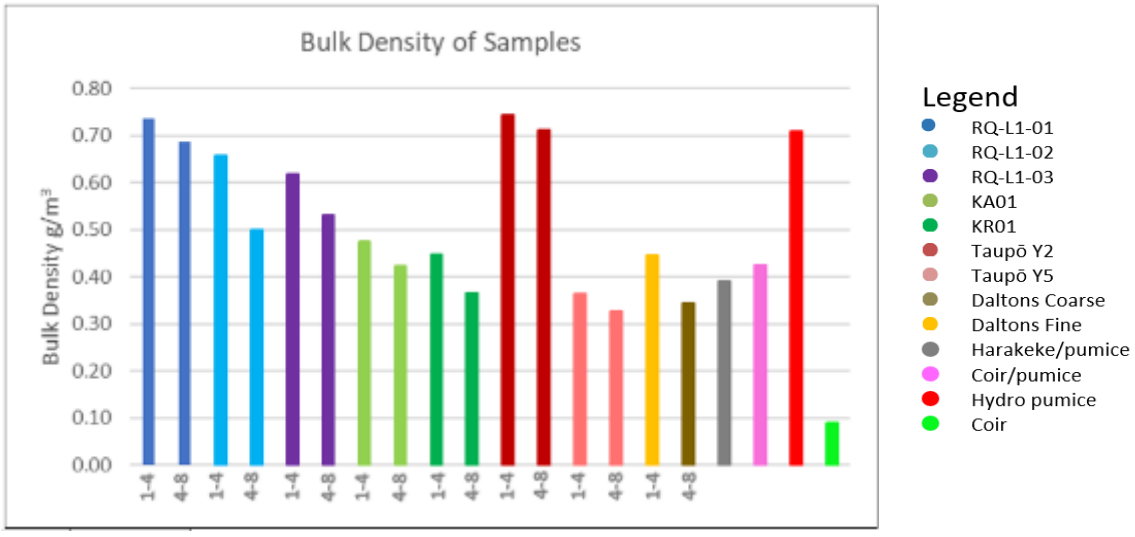

Figure 5.13: Bulk densities of the investigated pumices and hydroponic media tested.

Bulk densities of various growth media show a very large range from 0.05 g/cm^3 to 0.99 g/cm^3 with coir having the lowest and pumice having the highest densities (Figure 5.14, Table 5.3). The studied pumices fall within centre of this range (Figure 5.14) with RQ-L1-01, RQ-L1-02 1-4 mm, RQ-L1-03 1-4 mm and Y2 being comparable to pumices in the studies by Raviv et al. (1999) and Marinou et al. (2013) and Sicily pumice in Papadopoulos et al. (2008), while KA01, KR01 and Y5 are comparable to the biochar/hydrochar in Belda et al. (2016), pumices in Sahin et al. (2005) and Iceland pumice in Papadopoulos et al. (2008). Of the tested hydroponic media the bulk density of coir is at the low end of the range and comparable to the coir in Belda et al. (2016) and perlite in Kennard et al. (2020), while Ausperl pumice is comparable to pumices in studies by Raviv et al. (1999) and Marinou et al. (2013).

The ideal bulk density of any growth medium depends on the species being grown and the type of hydroponic system in which it is being grown. However, Kennard et al. (2020), indicates that an ideal bulk density is <0.4 g/cm^3. Outdoor applications may require higher bulk densities to provide container stability particularly in areas subject to high winds while intensive indoor production of greenhouse crops is likely to require lower bulk densities (Raviv et al., 2002). Additionally, transport and handling are easier for media with low bulk densities (Raviv et al., 2002).

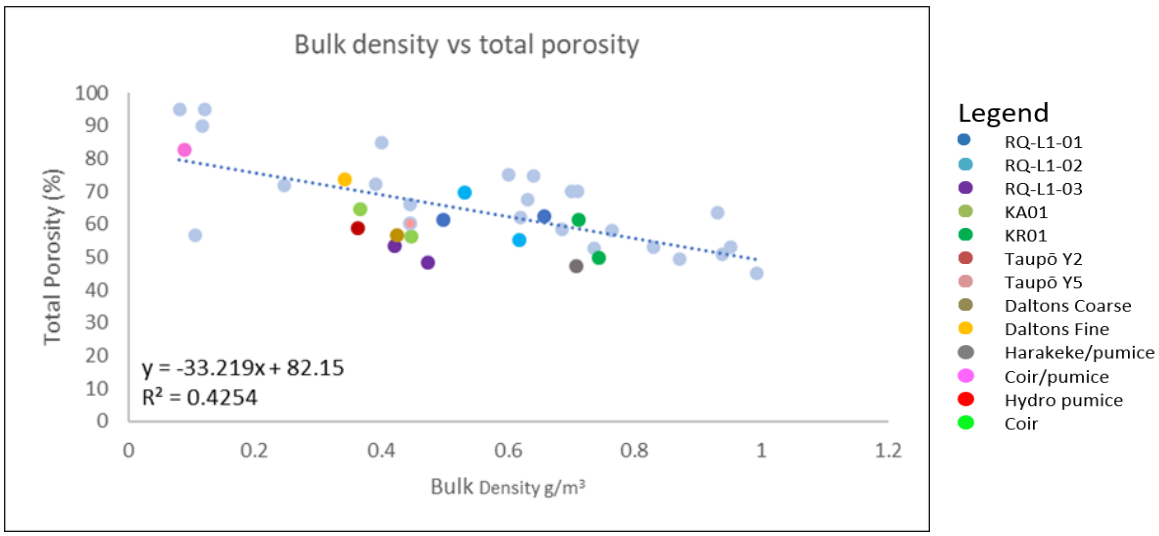

Figure 5.14: Bulk densities and total porosity of the investigated pumice and media of this study with media from previous studies. Light blue dots are media from Belda et al. (2016); Gizas and Savvas (2007); Kennard et al. (2020); Papadopoulos et al. (2008); Raviv et al. (1999); Zhao et al. (2023).

Table 5.3: Bulk density of hydroponic media from previous studies (pumice is highlighted).

Source	Medium	Bulk Density (g/cm^3)
Kennard et al. (2020)	Ideal	<0.4
	Perlite	0.105
Zhao et al. (2023)	Coir	0.446
	Pumice	0.993
	Harakeke / Pumice	0.87
	Coir / Pumice	0.764
Belda et al. (2016)	Biochar & hydrochar	0.247 - 0.444
	Coir	0.081
Papadopoulos et al. (2008)	Iceland pumice	0.4
	Sicily pumice	0.7
	Greece pumice	0.6
Arancon et al. (2015)	Coir	0.05
	Sphagnum Moss	0.15
Raviv et al. (1999)	Yellow tuff	0.93
	Italy pumice	0.71
	Greece Pumice	0.64
Marinou et al. (2013)	Pumice	0.631
	Sawdust	0.117
	Coco soil	0.121
Sahin et al. (2005)	Pumice 2-4 mm	0.38
	Pumice 4-8 mm	0.44
Gizas and Savvas (2007)	Pumice 0-2 mm	0.952
	Pumice 0-5 mm	0.938
	Pumice 0-8 mm	0.829
	Pumice 4-8 mm	0.620

In growth trials by Kennard et al. (2020) oakleaf lettuce (*Lactuca sativa*) produced the highest yields when grown in perlite with a bulk density of 0.11 g/cm^3 over almond shell and recycled plastic planks, both of which had significantly higher bulk densities. Conversely Gizas and Savvas (2007) obtained the best growth of gypsophilia and cucumbers in 0-2 mm pumice grades with a bulk density of 0.95 g/cm^3 whereas lettuce and roses in the same study were less affected by grain size. Except for coir, the bulk densities of the pumices and hydroponic medium tested in this study are within these extremes and Coir is slightly lower at 0.9 g/cm^3.

5.3.4 Total Porosity

There is a large range in the total porosity of the tested pumices, the hydroponic media and the pumice mixes with coir and Taupō Y5 4-8 mm having a distinctly higher total porosity and KA01 1-4 mm, Taupō Y2 1-4 mm and Ausperl pumice having the lowest (Figure 5.15).

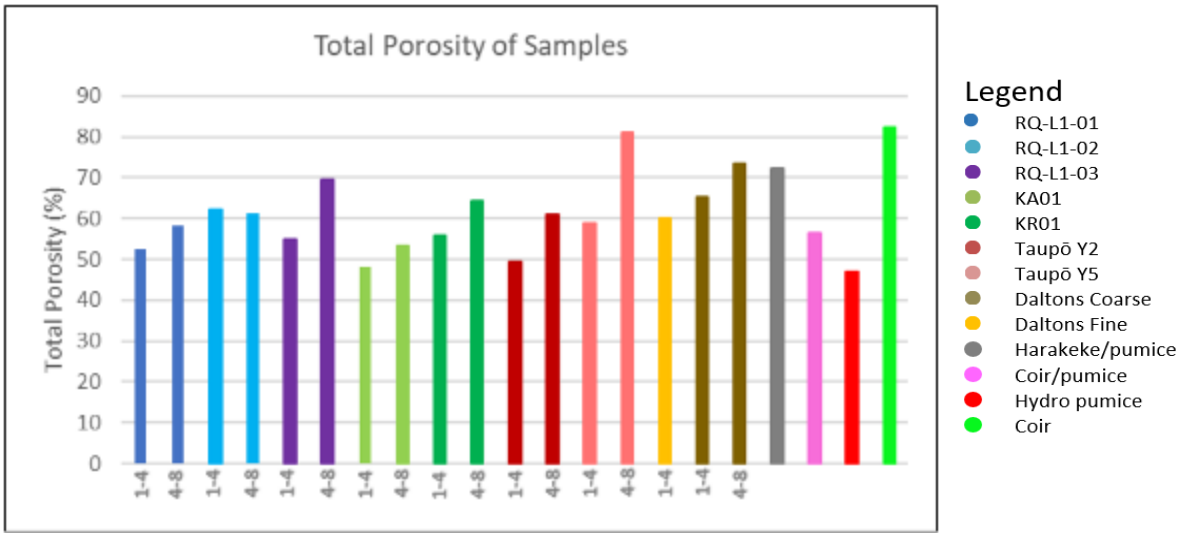

Figure 5.15: Total porosity of investigated pumices and hydroponic media tested.

The total porosity of various growth media show a very large range from 53% to 95% with coir having the highest and 0-8 mm pumice having the lowest (Figure 5.15, Table 5.4). The studied pumices fall within this range; however, most are at the lower end of the range (Figure 5.15 and 5.17). Most pumices in this study are comparable to pumices in studies by Gizas and Savvas (2007); Marinou et al. (2013); Papadopoulos et al. (2008); Raviv et al. (1999), while coir and Y5 4-8 mm are comparable to Iceland pumice in Papadopoulos et al. (2008) and coco soil and sawdust in Marinou et al. (2013).

Total porosity is the total space available for air and water, where larger pores provide space for air exchange and root growth whereas smaller pores can hold more water (Gizas & Savvas, 2007; Nemali, 2018; Raviv et al., 2002). None of the samples tested are within the ideal range of ≥85% indicated by Kennard et al. (2020) although the total porosity of coir (82.3%) is only slightly lower. Gizas and Savvas (2007) found that the total porosity of pumice grades between 0-2 mm and 0-8 mm did not consistently change, however, it was significantly higher in the 4-8 mm grade (Table

5.4). This is consistent with the findings of this study except for RQ-L1-02 for which the 4-8 mm fractions have a higher total porosity than found in the 1-4 mm fractions (Figure 5.16).

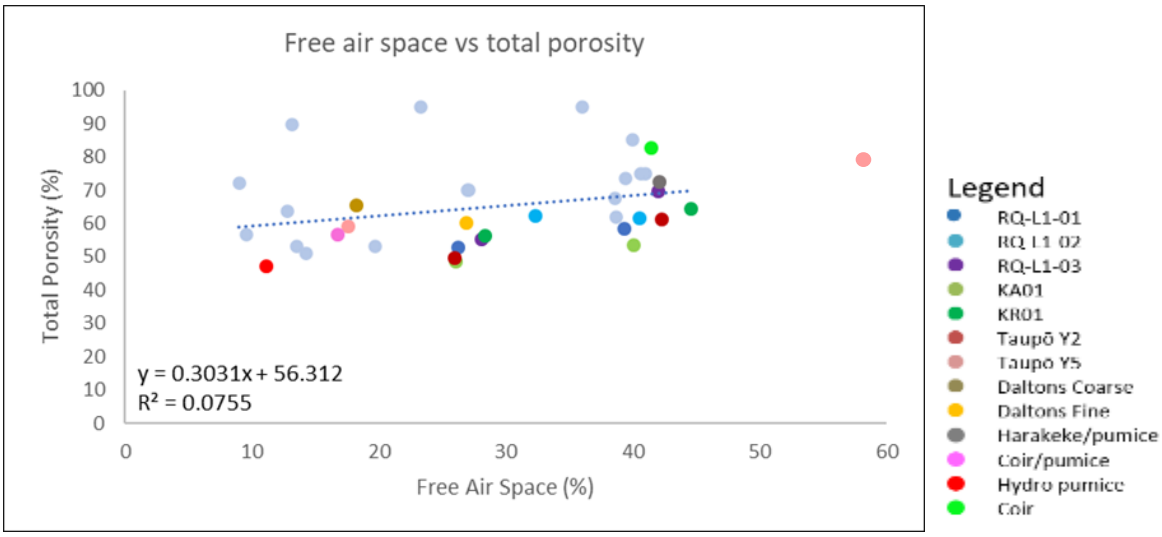

Figure 5.16: Free air space and total porosity of pumice and media of this study with media from previous studies. Light blue dots are media from Belda et al. (2016); Gizas and Savvas (2007); Kennard et al. (2020); Papadopoulos et al. (2008); Raviv et al. (1999).

Table 5.4: Total porosity of hydroponic media from previous studies, (pumice is highlighted).

Source	Medium	Total Porosity (%)
Kennard et al. (2020)	Ideal	≥85
	Perlite	56.8
Zhao et al. (2023)	Coir	66.05
	Pumice	45.03
	Harakeke / Pumice	49.53
	Coir / Pumice	57.95
Belda et al. (2016)	Biochar & hydrochar	72-85
	Coir	95
Papadopoulos et al. (2008)	Iceland pumice	85
	Sicily pumice	70
	Greece pumice	75
Raviv et al. (1999)	Yellow tuff	63.7
	Italy pumice	69.9
	Greece Pumice	74.9
Marinou et al. (2013)	Pumice	67.5
	Sawdust	89.8
	Coco soil	95.1
Gizas and Savvas (2007)	Pumice 0-2 mm	53.1
	Pumice 0-5 mm	51.0
	Pumice 0-8 mm	53.0
	Pumice 4-8 mm	62.0

Gizas and Savvas (2007) obtained the best growth of gypsophilia and cucumbers in pumices with grain sizes of 0-2 mm and 0-5 mm and total porosities of 51-53%. In the same study lettuce and roses were less affected by the grain size of the pumices which had total porosities from 51-62%. Of the tested samples only the KA01 4-8 mm fraction and RQ-L1-01 1-4 mm fractions fell within the 51-53% range that produce the best growth of gypsophilia and cucumber. However, except for KA01 1-4 mm, Y2 1-4 mm, Y5 4-8 mm (outlier) and Daltons Coarse 4-8 mm all the pumices and the coir/pumice mix are within the 51-62% range of the pumice grain sizes investigated by Gizas and Savvas (2007) study.

Strawberry trials by Marinou et al. (2013) found greater leaf numbers of plants grown in sawdust with total porosity of 89.8% over those grown in pumice with a total porosity of 67.5%, However, fruit numbers increased by 50% for the plants grown in pumice over those grown in sawdust or coco soil (95.1% total porosity). Only the 4-8 mm fractions of the RQ-L1-03, Taupō Y5 and Daltons Coarse samples and the harakeke/pumice mix and coir have total porosities within the range of the Marinou et al. (2013) study.

Whether particular pumice types and/or grade would be suitable for hydroponics would depend on the specific species of plant being grown.

5.3.5 Free Air Space

There is a large range of free air space between the tested pumices, the hydroponic media, and the pumice mixes with the Ausperl pumice having the least free air space and Taupō Y5 4-8 mm having distinctly more free air space than seen in other samples, however it is suspected that a measurement error was undetected during testing of this sample (Figure 5.17).

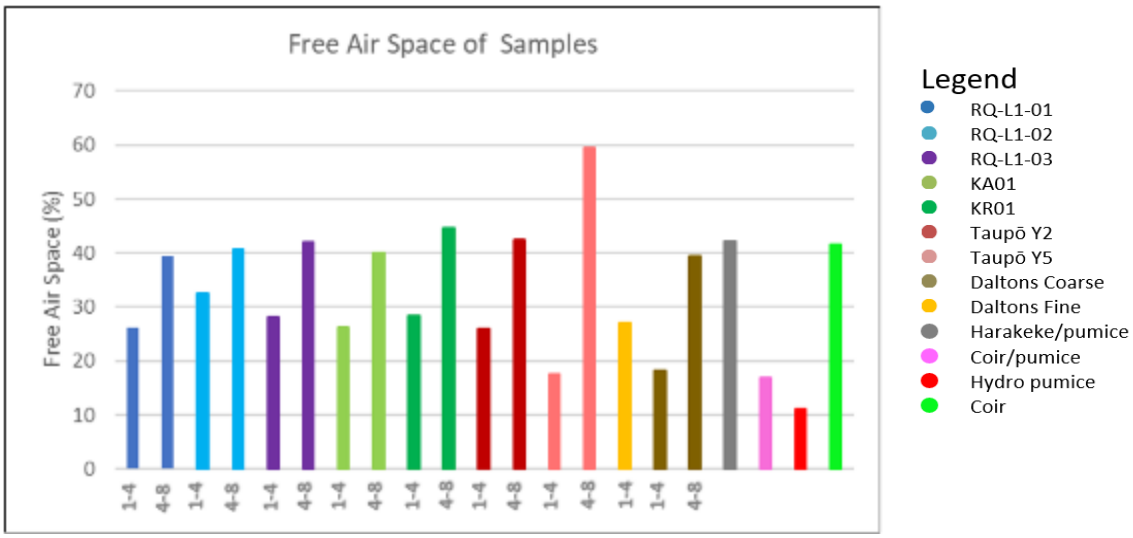

Figure 5.17: Free air space of investigated pumices and hydroponic media tested.

The free air space of the various growth media ranges from 9.5% to 41% with perlite having the lowest and Greece pumice having the highest (Figure 5.17, Table 5.3). Except for RQ-L1-03 4-8 mm, KR01 4-8 mm and Y5 4-8 mm (outlier), the studied pumices fall within this range (Figure 5.16 above). The 4-8 mm fractions are generally comparable to pumice/s in Raviv et al. (1999), Papadopoulos et al. (2008) and Marinou et al. (2013) and the 4-8 mm pumice in Gizas and Savvas (2007). The 1-4 mm fractions are generally comparable to the ideal ranges indicated by Bunt (1988), Kennard et al. (2020) and Nemali (2018). Of the tested hydroponic media tested coir and the harakeke/pumice mix are comparable to pumice/s in Raviv et al. (1999), Papadopoulos et al. (2008) and Marinou et al. (2013) and the 4-8 mm pumice in Gizas and Savvas (2007) and the coir/pumice mix and Ausperl pumice are comparable to perlite in Kennard et al. (2020), yellow tuff in Raviv et al. (1999), sawdust in Marinou et al. (2013) and 0-2 mm and 0-4 mm pumices in Gizas and Savvas (2007) (Figure 5.16 and 5.18, Table 5.3).

An ideal range of free air space is difficult to determine given the widespread exhibited by commonly used media. Ultimately, it will depend on factors such as aeration requirements that are specific to individual plant species, and management and environmental factors specific to the system set up (Bunt, 1988). It is, however, an important parameter to consider in hydroponics as it is an indicator of the space available for air exchange and root growth (Nemali, 2018). While the 1-4 mm pumice fractions, the hydroponic pumice (Ausperl) and the Coir/pumice mix are within an ideal range of 10-30% indicated by Kennard et al. (2020), only the 1-4 mm

fractions of the Daltons Fine and Coarse, the hydroponic pumice (Ausperl) and the coir/pumice mix were within the ideal range of 10-20% proposed by Bunt (1988) of 10-20%. Nemali (2018) indicates a range of 20-25% to be ideal for root growth, the 1-4 mm fractions and the coir/pumice mix are close to this range. The 4-8 mm fractions, Coir and the Harakeke/pumice mix exceeded all proposed ideal ranges.

Table 5.5: Free Air Space of Hydroponic Media from Previous Studies, (pumice is highlighted).

Source	**Medium**	**Free Air Space (%)**
Kennard et al. (2020)	Ideal	10-30
	Perlite	9.52
Bunt (1988)	Ideal	10-20
Nemali (2018)	Ideal	20-25
Belda et al. (2016)	Biochar & hydrochar	8.9-42
	Coir	36
Papadopoulos et al. (2008)	Iceland pumice	40
	Sicily pumice	27
	Greece pumice	41
Raviv et al. (1999)	Yellow tuff	12.8
	Italy pumice	27.1
	Greece Pumice	40.6
Marinou et al. (2013)	Pumice	38.6
	Sawdust	13.2
	Coco soil	23.3
Gizas and Savvas (2007)	Pumice 0-2 mm	13.5
	Pumice 0-5 mm	14.3
	Pumice 0-8 mm	19.7
	Pumice 4-8 mm	38.7

In growth trials by Kennard et al. (2020) oakleaf lettuce (*Lactuca sativa*) produced the highest yields when grown in perlite with air space of 9.5% over almond shell and recycled plastic planks, both of which had higher free air space although still within the proposed ideal range. Strawberry trials by Marinou et al. (2013) found leaf numbers of plants grown in sawdust with free air space of 27.4% over those grown in pumice with free air space of 38.6%; however, fruit numbers increased by 50% for the plants grown in pumice over those grown in sawdust or coco soil. The Ausperl pumice, harakeke/pumice mix, coir/pumice mix and the 1-4 mm pumice fractions are within the 9.5% to 38.6% free air space of media in these studies, furthermore the 4-8 mm fractions and the coir are close to the highest free air space of the above studies. This indicates

that depending on the species, the free air space of the pumice fractions would be suitable for use as hydroponic media.

5.3.6 Volumetric Water Holding Capacity.

Water holding capacity is the amount of water retained by a media once excess water has been drained; this water is held in narrow pores by capillary action, whereas water in larger pores drains away by gravity (Nemali, 2018). Finer particles in a substrate pack more tightly resulting in smaller inter clast pore spaces and therefore a higher volumetric WHC (Gizas & Savvas, 2007; Raviv et al., 2002).

As expected, the volumetric water holding capacity of the coarser materials tested was higher with a narrow range for the hydroponic media between 30.2% for the Harakeke/pumice mix and 40.80% for coir. In contrast the pumice samples had a wider spread with coarser samples having higher values than finer grades and a generally lower volumetric WHC than the harakeke/pumice mix. Only the Daltons Coarse overlapped with the hydroponic media range while the Taupō Y5 1-4 mm (outlier) and Daltons fine grade had higher values.

Trials undertaken by Zhao et al. (2023) measured lower volumetric WHC in all tested hydroponic samples tested (Coir (18.13%), harakeke and pumice mix (21.38%), coir and pumice mix (11.25%) and Ausperl pumice (14.58%) than was found for the same materials during this study. The difference in the results could be due to differences in the sample volumes tested, heterogeneity of the harakeke/pumice and coir/pumice samples or drainage times.

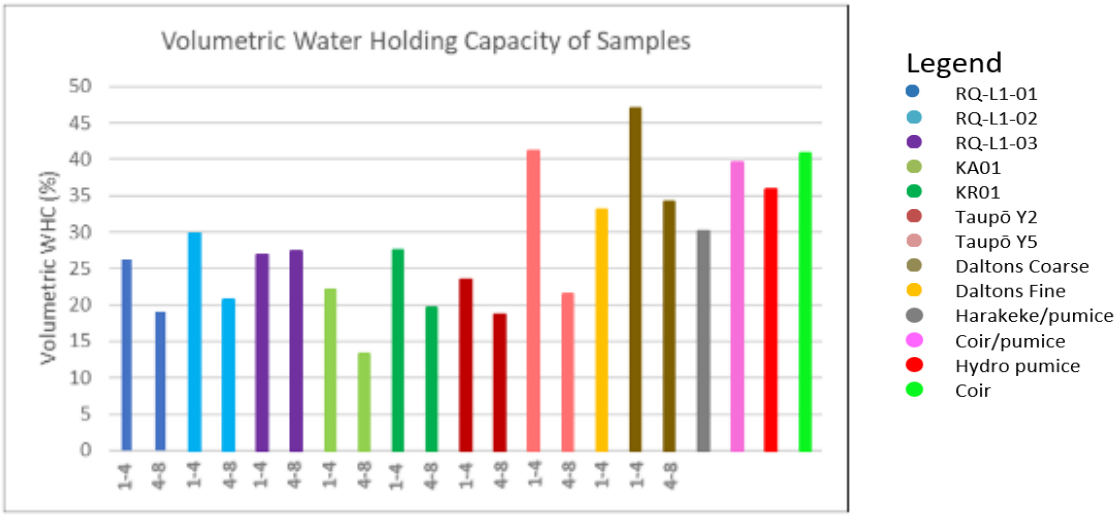

Figure 5.18: Volumetric WHC of investigated pumices and hydroponic media tested.

Kennard et al. (2020) indicates that the ideal range of WHC lies between 6% and 100% and all samples tested fall within this large range. This suggests that the ideal WHC is likely specific to the cultivated species and hydroponic system.

Table 5.6: Volumetric WHC of Hydroponic Media from Previous Studies, (pumice is highlighted).

Source	**Medium**	**Volumetric WHC (%)**
Kennard et al. (2020)	Ideal	6 - 100
	Perlite	47.3
Zhao et al. (2023)	Coir	18.31
	Pumice	15.49
	Harakeke / Pumice	10.95
	Coir / Pumice	22.55
Belda et al. (2016)	Biochar & hydrochar	8.7 – 21.9
	Coir	72.2
Papadopoulos et al. (2008)	Iceland pumice	Total porosity - free air space = 45
	Sicily pumice	Total porosity - free air space = 43
	Greece pumice	Total porosity - free air space = 34
Raviv et al. (1999)	Yellow tuff	Total porosity - free air space = 50.9
	Italy pumice	Total porosity - free air space = 42.8
	Greece Pumice	Total porosity - free air space = 34.3
Marinou et al. (2013)	Pumice	23.2
	Sawdust	33.0
	Coco soil	71.8
Gizas and Savvas (2007)	Pumice 0-2 mm	Total porosity - free air space = 39.6
	Pumice 0-5 mm	Total porosity - free air space = 36.7
	Pumice 0-8 mm	Total porosity - free air space = 33.3
	Pumice 4-8 mm	Total porosity - free air space = 23.3

Except the Daltons grades, RQ-L1-02 1-4 mm and Y5 1-4 mm which are higher, and KA01 4-8 mm which is lower the WHC of all the tested pumices are within 5% of the volumetric WHC (23.2%) of the pumice in Marinou et al. (2013)'s strawberry growth trials (Table 5.6). Additionally, most pumices in this study were within the WHC range (23.3 – 39.6%) of the pumice grades in Gizas and Savvas (2007)'s growth trial on gypsophilia, cucumber, lettuce, and roses (Table 5.6). In contrast to this, except for the coarse Taupō Y5 and Daltons grades the WHC of the pumices in this study are lower than the pumices in Papadopoulos et al. (2008) (34-45%) and in Raviv et al. (1999)'s rose study (34.3-50.9%).

Whether particular pumice types and/or grades are suitable for hydroponics in regard to their volumetric WHC would depend on the specific system and species of plant being grown.

5.3.7 Suitability

The pumice grades were each tested for the hydroponic properties of pH, bulk density, free air space, total porosity and volumetric water holding capacity. The pH of the pumice is considered to be suitable for use as a hydroponic substrate. The bulk density, free air space, total porosity and volumetric WHC indicates that the suitability of the pumice fractions likely depends on the requirements of the species being grown and the type of hydroponic system that is being used.

The Rotorua and Taupō Y2 tephras which have higher bulk densities are likely to more suitable for outdoor applications where wind may be a factor while those with lower bulk densities such as the Kaharoa and Taupō Y5 are likely to be more suited to intensive indoor production.

The 4-8 mm fractions of the pumices provide more free air space, which would benefit plant species that require more root aeration, while the higher volumetric WHC of the 1-4 mm grades would be more suitable for systems needing less irrigation.

Zhao et al. (2023) conducted growth trials on two raspberry cultivars using the hydroponic media assessed for comparison in this study. They found that the Ausperl pumice had a higher bulk density and lower porosity than the other hydroponic media tested resulting in better fruit quality and yield, but lower vegetative growth. The addition of Ausperl pumice to coir increased WHC and bulk density, which improved root anchoring and support. Mixing harakeke with pumice resulted in lower growth and productivity. Furthermore, Ausperl pumice was found to be more suitable for cultivar 8 growth than cultivar 110.

6 Conclusions

The active Taupō and Okataina calderas in the TVZ have produced vast volumes of pyroclastic material during frequent eruptions in the last c. 60,000 years. Among these eruptive products are the Kaharoa tephra from the Tarawera Linear Vent Zone (TLVZ) and the Rotorua Tephra from the Haroharo (HLVZ), both in the OVC, and the Taupō Y2 and Y5 fall deposits from the Y eruption from the TVC.

The investigation of the physical properties of the Rotorua, Kaharoa and Taupō tephras showed that:

- All sampled tephras were very poorly to poorly sorted ash to lapilli pumice dominated deposits.
- The average grain size of the Rotorua Tephra decreased from bottom to top of the studied section and the deposit became better sorted towards the top of the profile; This was accompanied by an increase in the proportion of crystals and glass shards and a decrease in lithic contents particularly in the 1-4 mm fractions.
- The average grain size of the Kaharoa Tephra and lithic content decreased with increased distance from the vent, while sorting improved.
- The Taupō Y2 deposit exhibited a smaller average particle size but similar sorting to the Y5 deposit. However, lithic contents in the Y5 1-4 mm fraction were c. 10% higher and pumice contents were c. 10% lower than for the Y5 4-8 mm and both Y2 grades.
- While commercially available Daltons pumice samples were sold as fine (1-4 mm) and coarse (4-8 mm) grades, sieving revealed that they contained significant proportions of larger clasts in the Daltons Fine and smaller grains in the Daltons Coarse than advised on the bags. The Daltons Fine sample contained more lithics particularly in the 4-8 mm fraction than contained in the Daltons Coarse sample.

Further investigation of representative pumice clasts of the tephra samples revealed that:

- The pumice clasts were predominately rounded to subrounded, with only KR01 fractions containing predominately subangular particles.

- The pumices were poorly to highly vesiculated with clasts of higher vesicularity having lower densities.
- Clast density increases and vesicularity decreases towards the top of the Rotorua profile.
- For the Kaharoa deposit pumice density decreased as vesicularity, and angularity increased with distance from the vent.
- The Taupō Y2 sample was more vesiculated with a higher envelope density and porosity but lower skeletal density than Taupō Y5 sample.

The changes seen within the deposits are due to:

- Buoyancy and intensity changes in the eruption plume during phase 1 and a change to a degassed magma in phase 2 as the Rotorua eruption progressed.
- Clast density, shape and size influencing settling velocities from the Kaharoa eruption plume resulting in changes in the deposit over distance.
- Differences in the Taupō Y2 and Y5 are likely to be related to conduit processes, degassing and volatile exsolution as the eruption progressed.

The physical properties of the pumice clasts appear to have a strong influence on the measured hydroponic properties of i.e. WHC (vol), bulk density and total porosity.

- As envelope density increases so does the bulk density while the WHC (vol) and total porosity decrease.
- As the connected porosity increases so does the WHC (vol).
- Bulk densities of the tephras were within the range of those found in the tested hydroponic media (0.33 to 0.69 g/cm^3), apart from the Taupō Y2 factions and the RQ-L1-01 1-4 mm fraction, which had higher bulk densities.
- Free air space and total porosity measurements of the tephras were within or close to the ranges found in the hydroponic media tested except the Taupō Y5 4-8 mm fraction, which was higher. The finer grades of the tephras typically produced lower values than the corresponding 4-8 mm fractions.
- The WHC (vol) of the tested tephras tested were lower for the hydroponic media including both Daltons grades, the fine fraction of the Taupō Y5 sample being an exception. Apart

from RQ-L1-01 the WHC (vol) of the coarser grades were lower than those of the corresponding 1-4 mm fraction.

- The pH of all tested tephras and hydroponic media tested were similar and ranged from pH 6.5 to pH 7.

Bulk density, total porosity and pH of the hydroponic media; = coir, Ausperl pumice, coir/pumice mix and harakeke/pumice mix that were used in raspberry growth trails by Zhao et al. (2023) were also examined in theis study for comparison.

- The pH of these media was within ideal ranges for hydroponics indicated by Kennard et al. (2020).
- The bulk density of the coir and the harakeke/pumice mix were within ideal ranges for hydroponics indicated by Kennard et al. (2020) while the bulk density measurement of the coir/pumice mix was slightly lower and those of the Ausperl pumice was higher than this ideal range.
- The free air space of the Ausperl pumice and the coir/pumice mix were within the ideal ranges given by Bunt (1988) and Kennard et al. (2020), and the coir/pumice mix was slightly lower than the ideal range given by Nemali (2018). The free air space of coir and the harakeke/pumice mix exceeded the ideal ranges.
- The coir was the only media tested that had a total porosity close to the Kennard et al. (2020) ideal values, while the other media had lower total porosities.
- All media fell within the ideal range for volumetric WHC range identified by Kennard et al. (2020). This reflects that the ideal WHC of a growth substrate is specific to the species to be grown and the system in which it is grown.

Bulk density, free air space and pH of the tested tephras tested generally fall within the range of the studies hydroponic media tested. However, the WHC (vol) of the tephras is generally lower than that found in the hydroponic media.

- It is likely that with respect to pH the tephras included in this study could be used in place of or mixed with the hydroponic materials for use as a hydroponic medium growth substrate for crops which thrive in a pH in this range.

- The lower WHC (vol) of the 4-8 mm fractions of the tephras may limit their usefulness as a growing medium or may lead to the need for more frequent or alternate methods of irrigation.
- The bulk density especially of the 4-8 mm fractions of the tephras make it a relatively light material to use in hydroponics.

The results of this study into the physical characteristics of pumice suggest that the Taupō Y5 1-4 mm and the Dalton pumice grades would be the most suitable for use as a growth substrate in hydroponics due to free air space and WHC being similar to those of the 0-2- and 0-5-mm grades of pumice, which produced high yields in gypsophila and cucumber (Gizas and Savvas, 2007). However, the bulk density of Taupō Y5 1-4 mm might be too low. The Taupō Y2 pumice has a bulk density and total porosity comparable to that of the 0-2- and 0-5-mm grades in the Gizas and Savvas (2007) study, but their WHC is low. The 4-8 mm grades of the tested pumice are unlikely to be suitable for use as hydroponic substrates due to their low WHC. However, their hydroponic parameters are similar to the <8 mm pumice that produced high yields in a study by Marinou et al. (2013) on strawberry growth.

Further research is required into the use of individual tephras from the Central North Island as hydroponic media. In particular, growth trials of potential species would need to be undertaken, testing a range of different pumice types and grades as well as mixes for their suitability of growing of various fruit or vegetables in the appropriate hydroponic system.

7 References

Advantech Mfg. (2001). *Test sieving: Principles and procedures*.

Allan, A. S. R., Barker, S. J., Millet, M. A., Rooyakkers, S. M., Schipper, C. I., Wilson, C. J. N., & Morgan, D. J. (2017). A cascade of magmatic events during the assembly and eruption of a super-sized magma body. *Contributions to Mineralogy and Petrology, 172*(7). https://doi.org/10.1007/s00410-017-1367-8

Altland, J. E., Gabriel, M. Z., & Owen Jr, J. S. (2009). Effect of Peat Moss and Pumice on Douglas Fir Bark based Soilless Substrate Physical and Hydraulic Properties *HortScience, 44*(3), 874-878.

Altland, J. E., Owen Jr, J. S., & Gabriel, M. Z. (2011). Influence of pumice and plant roots on substrate physical properties over time. *HortTechnology, 21*(5), 554-557. https://doi.org/10.21273/horttech.21.5.554

Arculus, R. J. (2021). Igneous processes. In D. Alderton & S. A. Elias (Eds.), *Encyclopedia of Geology (Second Edition)* (pp. 1-15). Academic Press. https://doi.org/https://doi.org/10.1016/B978-0-08-102908-4.00129-6

Ausperl. (n.d.). *Pumice*. https://www.ausperl.com/pumice/

Bar-Tal, A., Saha, U. K., Raviv, M., & Tuller, M. (2019). Inorganic and synthetic organic components of soilless culture and potting mixtures. In J. H. Lieth, M. Raviv, & A. Bar-Tal (Eds.), *Soilless Culture : Theory and Practice* (2nd ed.). Academic Press, an imprint of Elsevier.

Barker, S. J., Wilson, C. J. N., Allan, A. S. R., & Schipper, C. I. (2015). Fine-scale temporal recovery, reconstruction and evolution of a post-supereruption magmatic system. *Contributions to Mineralogy and Petrology, 170*(1), 5. https://doi.org/10.1007/s00410-015-1155-2

Barker, S. J., Wilson, C. J. N., Illsley-Kemp, F., Leonard, G. S., Mestel, E. R. H., Mauriohooho, K., & Charlier, B. L. A. (2021). Taupō: an overview of New Zealand's youngest supervolcano. *New Zealand Journal of Geology & Geophysics, 64*(2/3), 320-346. https://doi.org/10.1080/00288306.2020.1792515

Belda, R. M., Lidón, A., & Fornes, F. (2016). Biochars and hydrochars as substrate constituents for soilless growth of myrtle and mastic. *Industrial Crops & Products, 94*, 132-142. https://doi.org/10.1016/j.indcrop.2016.08.024

Benn, D. I. (2013). Clast Form Analysis. *Encyclopedia of Quaternary Science*, 1-5. https://doi.org/10.1016/B978-0-444-53643-3.00081-9

Blake, S. (2021). Volcanoes. In D. Alderton & S. A. Elias (Eds.), *Encyclopedia of geology* (2nd ed., pp. 258-276). Academic Press. https://doi.org/https://doi.org/10.1016/B978-0-08-102908-4.00057-6

Blok, C., Baumgarten, A., Baas, R., Wever, G., & Lohr, D. (2019). Analytical methods used with soilless substrates. In J. H. Lieth, M. Raviv, & A. Bar-Tal (Eds.), *Soilless Culture : Theory and Practice* (2nd ed.). Academic Press, an imprint of Elsevier.

Blott, S. J., & Pye, K. (2001). Gradistat: A grain size distribution and statistics package for the analysis of unconsolidated sediments. *Earth Surface Processes and Landforms, 26*(11), 1237-1248-1248. https://doi.org/10.1002/esp.261

Branney, M. J., Brown, R. J., & Calder, E. (2021). Pyroclastic rocks. In D. Alderton & S. A. Elias (Eds.), *Encyclopedia of geology* (2nd ed., pp. 277-300). Academic Press. https://doi.org/https://doi.org/10.1016/B978-0-08-102908-4.00103-X

Brooker, M. R., Houghton, B. F., Wilson, C. J. N., & Gamble, J. A. (1993). Pyroclastic phases of a rhyolitic dome-building eruption: Puketarata tuff ring, Taupo Volcanic Zone, New Zealand. *Bulletin of Volcanology, 55*(6), 395-406. https://doi.org/10.1007/bf00301999

Bunt, A. C. (1988). *Media and Mixes for Container-Grown Plants*. Springer Dordrecht.

Capillary Flow. (2023). *Capillary hydroponics*. Retrieved 19/11/2023 from https://www.capillaryflow.com/hydroponics

Carey, R. J., Houghton, B. F., Sable, J. E., & Wilson, C. J. N. (2007). Contrasting grain size and componentry in complex proximal deposits of the 1886 Tarawera basaltic Plinian eruption. *Bulletin of Volcanology, 69*(8), 903-926. https://doi.org/10.1007/s00445-007-0117-6

Carlile, W. R., Raviv, M., & Prasad, R. (2019). Organic soilless media components. In J. H. Lieth, M. Raviv, & A. Bar-Tal (Eds.), *Soilless Culture : Theory and Practice* (2nd ed.). Academic Press, an imprint of Elsevier.

Cas, R. A. F., & Wright, J. V. (1987). *Volcanic successions modern and ancient : a geological approach to processes, products and successions* (1st ed.). Chapman & Hall. http://ezproxy.massey.ac.nz/login?url=https://ebookcentral.proquest.com/lib/massey/detail.action?docID=3101048

Chambefort, I., Lewis, B., Wilson, C. J. N., Rae, A. J., Coutts, C., Bignall, G., & Ireland, T. R. (2014). Stratigraphy and structure of the Ngatamariki geothermal system from new zircon U–Pb geochronology: Implications for Taupo Volcanic Zone evolution. *Journal of Volcanology and Geothermal Research, 274*, 51-70. https://doi.org/10.1016/j.jvolgeores.2014.01.015

Cioni, R., Pistolesi, M., & Rosi, M. (2015). Plinian and subplinian eruptions. In H. Sigurdsson (Ed.), *Encyclopedia of volcanoes.* (2nd ed., pp. 519-535). Academic Press is an imprint of Elsevier. https://ezproxy.massey.ac.nz/login?url=https://ebookcentral.proquest.com/lib/massey/detail.action?docID=1983593

Cole, J. W. (1970a). Petrography of the rhyolite lavas of tarawera volcanic complex. *New Zealand Journal of Geology and Geophysics, 13*(4), 903-924-924. https://doi.org/10.1080/00288306.1970.10418209

Cole, J. W. (1970b). Structure and eruptive history of the tarawera volcanic complex. *New Zealand Journal of Geology and Geophysics, 13*(4), 879-902-902. https://doi.org/10.1080/00288306.1970.10418208

Cole, J. W., Brown, S. J. A., Burt, R. M., Beresford, S. W., & Wilson, C. J. N. (1998). Lithic types in ignimbrites as a guide to the evolution of a caldera complex, Taupo volcanic centre, New Zealand. *Journal of Volcanology and Geothermal Research, 80*(3-4), 217-237-237. https://doi.org/10.1016/S0377-0273(97)00045-0

Cole, J. W., Darby, D. J., & Stern, T. A. (1995). Taupo Volcanic Zone and Central Volcanic Region: Backarc Structures of North Island, New Zealand. In B. Taylor (Ed.), *Backarc Basins: Tectonics and magmatism* (pp. 1-28). Plenum Press.

Cole, J. W., Deering, C. D., Burt, R. M., Sewell, S., Shane, P. A. R., & Matthews, N. E. (2014). Okataina Volcanic Centre, Taupo Volcanic Zone, New Zealand: A review of volcanism and synchronous pluton development in an active, dominantly silicic caldera system. *Earth-Science Reviews, 128*, 1-17. https://doi.org/10.1016/j.earscirev.2013.10.008

Cole, J. W., Spinks, K. D., Deering, C. D., Nairn, I. A., & Leonard, G. S. (2010). Volcanic and structural evolution of the Okataina Volcanic Centre; dominantly silicic volcanism associated with the Taupo Rift, New Zealand. *Journal of Volcanology and Geothermal Research, 190*(1), 123-135. https://doi.org/10.1016/j.jvolgeores.2009.08.011

Daltons. (n.d.). *Materials*. Retrieved 20/05/2023 from https://www.daltons.co.nz/materials

Danišík, M., Evans, N. J., Shane, P., Storm, S., Lindsay, J. M., Schmitt, A. K., Hogg, A. G., Santos, G. M., & Keith Fifield, L. (2012). Re-anchoring the late Pleistocene tephrochronology of New Zealand based on concordant radiocarbon ages and combined 238U/ 230Th disequilibrium and (U-Th)/He zircon ages. *Earth and Planetary Science Letters, 349-350*, 240-250. https://doi.org/10.1016/j.epsl.2012.06.041

Davy, B. W., & Caldwell, T. G. (1998). Gravity, magnetic and seismic surveys of the caldera complex, Lake Taupo, North Island, New Zealand. *Journal of Volcanology and Geothermal Research, 81*(1-2), 69-89. https://doi.org/10.1016/S0377-0273(97)00074-7

De Ronde, C. E. J., Davy, B. W., Stoffers, P., Garbe-Schönberg, D., Botz, R., Christenson, B. W., Jones, B., Manconi, R., Browne, P. R. L., Hissmann, K., Schmitt, M., & Battershill, C. N. (2002). Discovery of active hydrothermal venting in Lake Taupo, New Zealand. *Journal of Volcanology and Geothermal Research, 115*(3-4), 257-275. https://doi.org/10.1016/S0377-0273(01)00332-8

Deligne, N. I., & Sigurdsson, H. (2015). Global rates of volcanism and volcanic episodes. In H. Sigurdsson (Ed.), *Encyclopedia of volcanoes.* (2nd ed., pp. 265-272). Academic Press is an imprint of Elsevier. https://ezproxy.massey.ac.nz/login?url=https://ebookcentral.proquest.com/lib/massey/detail.action?docID=1983593

Dufek, J., Ongaro, T. E., & Roche, O. (2015). Pyroclastic density currents: Processes and models. In H. Sigurdsson (Ed.), *Encyclopedia of volcanoes.* (2nd ed., pp. 599-616). Academic Press is an imprint of Elsevier. https://ezproxy.massey.ac.nz/login?url=https://ebookcentral.proquest.com/lib/massey/detail.action?docID=1983593

Fisher, R. V. (1961). Proposed classification of volcaniclastic sediments and rocks. *Bulletin of the Geological Society of America, 72*(9), 1409-1414-1414. https://doi.org/10.1130/0016-7606(1961)72[1409:PCOVSA]2.0.CO;2

Fisher, R. V., & Schmincke, H. U. (1984). *Pyroclastic rocks*. Springer Berlin Heidelberg. https://ezproxy.massey.ac.nz/login?url=https://link.springer.com/10.1007/978-3-642-74864-6

Folk, R. L., & Ward, W. C. (1957). Brazos River bar [Texas]; a study in the significance of grain size parameters. *Journal of Sedimentary Research, 27*(1), 3-26. https://doi.org/10.1306/74D70646-2B21-11D7-8648000102C1865D

Froggatt, P. C. (1981). Stratigraphy and nature of taupo pumice formation. *New Zealand Journal of Geology and Geophysics, 24*(2), 231-248-248. https://doi.org/10.1080/00288306.1981.10422715

Gardner, J. E., Thomas, R. M. E., Jaupart, C., & Tait, S. (1996). Fragmentation of magma during Plinian volcanic eruptions. *Bulletin of Volcanology: Official Journal of the International Association of Volcanology and Chemistry of the Earth`s Interior (IAVCEI), 58*(2-3), 144-162. https://doi.org/10.1007/s004450050132

Geologyistheway. (2023). *Geology is the way*. Retrieved 09/12/2023 from https://geologyistheway.com/sedimentary/roundness/

Gizas, G., & Savvas, D. (2007). Particle size and hydraulic properties of pumice affect growth and yield of greenhouse crops in soilless culture. *HortScience, 42*(5), 1274-1280-1280. https://doi.org/10.21273/hortsci.42.5.1274

Growace. (2023). *Hydroponics*. Retrieved 19/11/2023 from https://growace.com/collections/hydroponics

Grzelewski, D. (2009). *The Power of Taupo*. New Zealand Geographic. Retrieved 11.12.2022 from https://www.nzgeo.com/stories/the-power-of-taupo/

Hammer, J. E., Cashman, K. V., Hoblitt, R., & Newman, S. (1999). Degassing and microlite crystallization during pre-climactic events of the 1991 eruption of Mt. Pinatubo, Philippines. *Bulletin of Volcanology, 60*, 355-380.

Hodgson, K. A., & Nairn, I. A. (2005). The c. AD 1315 syn-eruption and AD 1904 post-eruption breakout floods from Lake Tarawera, Haroharo caldera, North Island, New Zealand. *New Zealand Journal of Geology and Geophysics, 48*(3), 491-506-506. https://doi.org/10.1080/00288306.2005.9515128

Hogg, A. G., Higham, T. F. G., Lowe, D. J., Palmer, J. G., Reimer, P. J., & Newnham, R. M. (2003). A wiggle-match date for Polynesian settlement of New Zealand. *Antiquity, 77*(295), 116-125. https://doi.org/10.1017/S0003598X00061408

Hogg, A. G., Lowe, D. J., Palmer, J., Boswijk, G., & Ramsey, C. B. (2012). Revised calendar date for the Taupo eruption derived by 14C wiggle-matching using a New Zealand kauri 14C calibration data set. *Holocene, 22*(4), 439-449. https://doi.org/10.1177/0959683611425551

HORIBA Ltd. (2023). *LA-950 Laser Particle Size Analyzer*. Retrieved 14.06.2023 from https://www.horiba.com/details/la-950-laser-particle-size-analyzer-108/

Houghton, B. F., & Carey, R. J. (2015). Pyroclastic fall deposits. In H. Sigurdsson (Ed.), *Encyclopedia of volcanoes.* (2nd ed., pp. 599-616). Academic Press is an imprint of Elsevier. https://ezproxy.massey.ac.nz/login?url=https://ebookcentral.proquest.com/lib/massey/detail.action?docID=1983593

Houghton, B. F., Carey, R. J., Cashman, K. V., Wilson, C. J. N., Hobden, B. J., & Hammer, J. E. (2010). Diverse patterns of ascent, degassing, and eruption of rhyolite magma during the 1.8 ka Taupo eruption, New Zealand: Evidence from clast vesicularity. *Journal of Volcanology and Geothermal Research, 195*(1), 31-47. https://doi.org/10.1016/j.jvolgeores.2010.06.002

Houghton, B. F., Carey, R. J., & Rosenberg, M. D. (2014, 01/01/). The 1800a Taupo eruption: "Ill wind" blows the ultraplinian type event down to Plinian [Article]. *Geology, 42*(5), 459-461-461. https://doi.org/10.1130/G35400.1

Houghton, B. F., & Wilson, C. J. N. (1989). A vesicularity index for pyroclastic deposits. *Bulletin of Volcanology, 51*(6), 451-462-462. https://doi.org/10.1007/BF01078811

Houghton, B. F., Wilson, C. J. N., Del Carlo, P., Coltelli, M., Sable, J. E., & Carey, R. (2004). The influence of conduit processes on changes in style of basaltic Plinian eruptions: Tarawera 1886 and Etna 122 BC. *Journal of Volcanology and Geothermal Research, 137*(1), 1-14. https://doi.org/10.1016/j.jvolgeores.2004.05.009

Jones, J. B., Jr. (2005). *Hydroponics : a practical guide for the soilless grower* (2nd ed.). CRC Press. http://ezproxy.massey.ac.nz/login?url=https://www.taylorfrancis.com/books/9780429122309

Jurado-Chichay, Z., & Walker, G. P. L. (2001). Variability of plinian fall deposits: examples from Okataina Volcanic Centre, New Zealand. *Journal of Volcanology and Geothermal Research, 111*(1-4), 239-263. https://doi.org/10.1016/S0377-0273(01)00229-3

Jutzeler, M., Proussevitch, A. A., & Allen, S. R. (2012, 09/15/September 2012). Grain-size distribution of volcaniclastic rocks 1: A new technique based on functional stereology [Article]. *Journal of Volcanology and Geothermal Research, 239-240*, 1-11. https://doi.org/10.1016/j.jvolgeores.2012.05.013

Kennard, N., Stirling, R., Prashar, A., & Lopez-Capel, E. (2020). Evaluation of recycled materials as hydroponic growing media. *Agronomy, 10*(1092), 1092-1092. https://doi.org/10.3390/agronomy10081092

Kilgour, G. N., & Smith, R. T. (2008). Stratigraphy, dynamics, and eruption impacts of the dual magma Rotorua eruptive episode, Okataina Volcanic Centre, New Zealand. *New Zealand Journal of Geology and Geophysics, 51*(4), 367-378. https://ezproxy.massey.ac.nz/login?url=https://search.ebscohost.com/login.aspx?direct=true&AuthType=sso&db=edswsc&AN=000262811600006&site=eds-live&scope=site&authtype=sso&custid=s3027306

Kriewald, S., Pradhan, P., Costa, L., Ros, A. G. C., & Kropp, J. P. (2019). Hungry cities: How local food self-sufficiency relates to climate change, diets, and urbanisation. *Environmental Research Letters, 14*(9). https://doi.org/10.1088/1748-9326/ab2d56

Leonard, G. S., Begg, J. G., & Wilson, C. J. N. (2010). *Geology of the Rotorua area*. Institute of Geological & Nuclear Sciences. https://ezproxy.massey.ac.nz/login?url=https://search.ebscohost.com/login.aspx?direct=true&AuthType=sso&db=cat09011a&AN=mul.oai.edge.massey.folio.ebsco.com.fs00001086.02c68fef.7e64.5de9.a6f0.b0a450b370db&site=eds-live&scope=site&authtype=sso&custid=s3027306

Leonard, G. S., Cole, J. W., Nairn, I. A., & Self, S. (2002). Basalt triggering of the c. AD 1305 Kaharoa rhyolite eruption, Tarawera Volcanic Complex, New Zealand. *Journal of Volcanology & Geothermal Research, 115*(3/4), 461. https://doi.org/10.1016/S0377-0273(01)00326-2

Likitlersuang, S., Phan, T. N., Boldrin, D., & Leung, A. K. (2022). Influence of growth media on the biomechanical properties of the fibrous roots of two contrasting vetiver grass species. *Ecological Engineering, 178*. https://doi.org/10.1016/j.ecoleng.2022.106574

Londra, P., Paraskevopoulou, A., & Psychogiou, M. (2018). Hydrological Behavior of Peat- and Coir-Based Substrates and Their Effect on Begonia Growth. *Water, 10*(6), 722. https://www.mdpi.com/2073-4441/10/6/722

López, G. (2016). Grain Size Analysis. In (pp. 341-348). https://doi.org/10.1007/978-1-4020-4409-0_18

Lowe, D. J. (1988). Stratigraphy, age, composition, and correlation of late quaternary tephras interbedded with organic sediments in waikato lakes, North Island, New Zealand. *New Zealand Journal of Geology and Geophysics, 31*(2), 125-165-165. https://doi.org/10.1080/00288306.1988.10417765

Lowe, D. J. (2016). *Introduction to tephra-derived soils, North Island, New Zealand: University of Waikato and University of Wisconsin-Platteville post-conference Andisol excursion, 21-23 December, 2016*. U. o. W. School of Science. https://hdl.handle.net/10289/10856

Lowe, D. J. (2021). Introduction to the landscapes and soils of the Hamilton Basin and South Waikato. *Field notes, School of Science, University of Waikato, Hamilton*. https://doi.org/10.13140/RG.2.2.36071.39845These

Lowe, D. J., & Balks, M. R. (2019). *Introduction to tephra derived soils and farming, Waikato-Bay of Plenty, North Islandn New Zealand* University of Wisconsin-Platteville Education Abroad Program: Winterim Field Trip (15-17 January, 2019), Waikato, New Zealand. https://researchcommons.waikato.ac.nz/handle/10289/12297

Lowe, D. J., Blaauw, M., Hogg, A. G., & Newnham, R. M. (2013). Ages of 24 widespread tephras erupted since 30,000 years ago in New Zealand, with re-evaluation of the timing and palaeoclimatic implications of the Lateglacial cool episode recorded at Kaipo bog. *Quaternary Science Reviews, 74*, 170-194. https://doi.org/10.1016/j.quascirev.2012.11.022

Lowe, D. J., McFadgen, B. C., Higham, T. F. G., Hogg, A. G., Froggatt, P. C., & Nairn, I. A. (1998). Radiocarbon age of the Kaharoa Tephra, a key marker for late-Holocene stratigraphy and archaeology in New Zealand. *Holocene, 8*(4), 487-495-495. https://doi.org/10.1191/095968398667037879

Lowe, D. J., & Pittari, A. (2021a). The Taupō eruption sequence of AD 232±10 in Aotearoa New Zealand: A retrospection. *Journal of Geography, 130*(1), 117-141.

Lowe, D. J., & Pittari, A. (2021b). The Taupō eruption sequence of AD 232±10 in Aotearoa New Zealand: A retrospection. *J. Geogr.(Chigaku Zasshi), 130*(1), 117-141.

Macías, J. L., Espíndola, J. M., Capra, L., Costa, J. E., Scott, K. M., & García-Palomo, A. (2004). The 26 May 1982 breakout flows derived from failure of a volcanic dam at El Chichón, Chiapas, Mexico. *Bulletin of the Geological Society of America, 116*(1-2), 233-246. https://doi.org/10.1130/B25318.1

Major, J. J., & Mark, L. E. (2006). Peak flow responses to landscape disturbances caused by the cataclysmic 1980 eruption of Mount St. Helens, Washington. *Bulletin of the Geological Society of America, 118*(7-8), 938-958. https://doi.org/10.1130/B25914.1

Major, J. J., Pierson, T. C., Dinehart, R. L., & Costa, J. E. (2000). Sediment yield following severe volcanic disturbance - A two-decade perspective from Mount St. Helens. *Geology, 28*(9), 819-822. https://doi.org/10.1130/0091-7613(2000)28<819:SYFSVD>2.0.CO;2

Manga, M., Patel, A., & Dufek, J. (2011). Rounding of pumice clasts during transport: field measurements and laboratory studies. *Bulletin of Volcanology: Official Journal of the International Association of Volcanology and Chemistry of the Earth`s Interior (IAVCEI), 73*(3), 321-333. https://doi.org/10.1007/s00445-010-0411-6

Manville, V. (2001). Sedimentology and history of Lake Reporoa: an ephemeral supra-ignimbrite lake, Taupo Volcanic Zone, New Zealand. *Volcaniclastic sedimentation in lacustrine settings*, 109-140.

Manville, V. (2002). Sedimentary and geomorphic responses to ignimbrite emplacement: readjustment of the Waikato River after the AD 181 Taupo eruption, New Zealand. *The Journal of Geology, 110*(5), 519-541.

Manville, V., & Hodgson, K. A. (2010). Paleohydrology of Volcanogenic Lake Break-Out Floods in the Taupo Volcanic Zone, New Zealand. In *Natural and Artificial Rockslide Dams* (pp. 519-541). Springer.

Manville, V., Németh, K., & Kano, K. (2009). Source to sink: A review of three decades of progress in the understanding of volcaniclastic processes, deposits, and hazards. *Sedimentary Geology, 220*(3), 136-161. https://doi.org/10.1016/j.sedgeo.2009.04.022

Manville, V., White, J. D. L., Houghton, B. F., & Wilson, C. J. N. (1999). Paleohydrology and sedimentology of a post-1.8 ka breakout flood from intracaldera Lake Taupo, North Island, New Zealand. *Bulletin of the Geological Society of America, 111*(10), 1435-1447. https://doi.org/10.1130/0016-7606(1999)111<1435:PASOAP>2.3.CO

Manville, V., & Wilson, C. J. N. (2004). The 26.5 ka Oruanui eruption, New Zealand: A review of the roles of volcanism and climate in the post-eruptive sedimentary response. *New Zealand Journal of Geology and Geophysics, 47*(3), 525-547. http://ezproxy.massey.ac.nz/login?url=https://search.ebscohost.com/login.aspx?direct=true&AuthType=ip,cookie,url,uid&db=edo&AN=ejs22238080&site=eds-live&scope=site&authtype=sso&custid=s3027306

Marinou, E., Chrysargyis, A., & Tzortzakis, N. (2013). Use of sawdust, coco soil and pumice in hydroponically grown strawberry. *Plant Soil Environ, 59*(10), 452-459.

Micromeritics Instrument Corporation. (2023). *GeoPyc 1365*. Retrieved 28.04.2023 from https://www.micromeritics.com/geopyc/

Miller, C. A., Barretto, J., Stagpoole, V., Caratori-Tontini, F., Brakenrig, T., & Bertrand, E. (2022). The integrated history of repeated caldera formation and infill at the Okataina Volcanic Centre: Insights from 3D gravity and magnetic models. *Journal of Volcanology and Geothermal Research, 427*. https://doi.org/10.1016/j.jvolgeores.2022.107555

Minnesota Pollution Control Agency. (2023). *Coir and applications of coir in stormwater management*. https://stormwater.pca.state.mn.us/index.php?title=Coir_and_applications_of_coir_in_stormwater_management

Morgan, L. (2021). *Hydroponics and protected cultivation : a practical guide*. CAB International. https://ezproxy.massey.ac.nz/login?url=https://dx.doi.org/10.1079/9781789244830.0000

Muirhead, J. D., Illsley-Kemp, F., Barker, S. J., Villamor, P., Wilson, C. J. N., Otway, P., Mestel, E. R. H., Leonard, G. S., Ellis, S., Savage, M. K., Bannister, S., Rowland, J. V., Townsend, D., Hamling, I. J., Hreinsdóttir, S., Smith, B., McGregor, R., Snowden, M., & Shalla, Y. (2022). Stretching, shaking, inflating: Volcanic-tectonic interactions at a rifting silicic caldera. *Frontiers in Earth Science, 10*. https://doi.org/10.3389/feart.2022.835841

Nairn, I. A. (1980). Source, age, and eruptive mechanisms of Rotorua Ash. *New Zealand Journal of Geology and Geophysics, 23*(2), 193-207. https://doi.org/10.1080/00288306.1980.10424206

Nairn, I. A., & Beanland, S. (1989). Geological setting of the 1987 Edgecumbe earthquake, New Zealand. *New Zealand Journal of Geology and Geophysics, 32*(1), 1-13. https://doi.org/10.1080/00288306.1989.10421383

Nairn, I. A., Hedenquist, J. W., Villamor, P., Berryman, K. R., & Shane, P. A. (2005). The ~AD1315 Tarawera and Waiotapu eruptions, New Zealand: contemporaneous rhyolite and hydrothermal eruptions driven by an arrested basalt dike system? *Bulletin of Volcanology, 67*(2), 186-193. https://doi.org/10.1007/s00445-004-0373-7

Nairn, I. A., Self, S., Cole, J. W., Leonard, G. S., & Scutter, C. (2001). Distribution, stratigraphy, and history of proximal deposits from the c. AD 1305 Kaharoa eruptive episode at Tarawera Volcano, New Zealand. *New Zealand Journal of Geology and Geophysics, 44*(3), 467-484. https://doi.org/10.1080/00288306.2001.9514950

Nairn, I. A., Shane, P. R., Cole, J. W., Leonard, G. J., Self, S., & Pearson, N. (2004). Rhyolite magma processes of the ~AD 1315 Kaharoa eruption episode, Tarawera volcano, New Zealand. *Journal of Volcanology and Geothermal Research, 131*(3), 265-294. https://doi.org/10.1016/S0377-0273(03)00381-0

Nemali, K. (2018). *Purdue horticulture and landscape architecture*. https://www.extension.purdue.edu/extmedia/HO/HO-287-W.pdf

Newhall, C. G., & Punongbayan, R. (1996). *Fire and mud: eruptions and lahars of Mount Pinatubo, Philippines*. Philippine Institute of Volcanology and Seismology Quezon City.

Occupational Safety and Health Service. (1994). *Health and safety guidelines for the selection and safe handling of synthetic mineral fibres*. https://worksafe.govt.nz

Ohashi, M., Ichihara, M., Takeda, S., Hirota, K., Sato, S., Kuwano, O., & Kameda, M. (2020). Formation of tube-pumice structure under pure shear: Insights from extension tests of solidifying foam. *Journal of Volcanology and Geothermal Research, 392*. https://doi.org/10.1016/j.jvolgeores.2020.106772

Papadopoulos, A. P., Bar-tal, A., Silber, A., Saha, U. K., & Raviv, M. (2008). Inorganic and synthetic organic components of soilless culture and potting mixes. *Soilless Culture. Elsevier,* , 505-543. https://doi.org/10.1016/B978-044452975-6.50014-9

Park, C., & Schmincke, H.-U. (2020). Multistage damming of the Rhine River by tephra fallout during the 12,900 BP Plinian Laacher See Eruption (Germany). Syn-eruptive Rhine damming I. *Journal of Volcanology and Geothermal Research, 389*, 106688. https://doi.org/https://doi.org/10.1016/j.jvolgeores.2019.106688

Pérez-Urrestarazu, L., Fernández-Cañero, R., Campos-Navarro, P., Sousa-Ortega, C., & Egea, G. (2019). Assessment of perlite, expanded clay and pumice as substrates for living walls. *Scientia Horticulturae, 254*, 48-54. https://doi.org/10.1016/j.scienta.2019.04.078

Pittari, A., Prentice, M. L., McLeod, O. E., Yousef Zadeh, E., Kamp, P. J. J., Danišík, M., & Vincent, K. A. (2021). Inception of the modern North Island (New Zealand) volcanic setting: spatio-temporal patterns of volcanism between 3.0 and 0.9 Ma [Article]. *New Zealand Journal of Geology & Geophysics, 64*(2/3), 250-272. https://doi.org/10.1080/00288306.2021.1915343

Potter, S. H., Scott, B. J., Jolly, G. E., Johnston, D. M., & Neall, V. E. (2015). A catalogue of caldera unrest at Taupo Volcanic Centre, New Zealand, using the Volcanic Unrest Index (VUI). *Bulletin of Volcanology: Official Journal of the International Association of Volcanology and Chemistry of the Earth`s Interior (IAVCEI), 77*(9), 1-28. https://doi.org/10.1007/s00445-015-0956-5

Prentice, M. L. (2023). *Silicic volcanism of the Tauranga Volcanic Centre and the climactic Waitearikisupereruption at the dawn of the Taupō Volcanic Zone* The University of Waikato]. Hamilton, New Zealand. https://hdl.handle.net/10289/15791

Pullar, W. A. (1967). Volcanic ash beds in the Waikato district. https://hdl.handle.net/10289/9103 (Earth Science Journal)

Pullar, W. A., & Birrell, K. S. (1973). *Age and distribution of late Quaternary pyroclastic and associated cover deposits of the Rotorua and Taupo area, North Island, New Zealand. [map]*. Dept. of Scientific and Industrial Research. https://ezproxy.massey.ac.nz/login?url=https://search.ebscohost.com/login.aspx?direct=true&AuthType=sso&db=cat09011a&AN=mul.oai.edge.massey.folio.ebsco.com.fs00001086.f2398d63.a977.5b8d.8a39.547c112714fc&site=eds-live&scope=site&authtype=sso&custid=s3027306

Pullar, W. A., Birrell, K. S., & New Zealand. Soil Bureau. (1973). *Age and distribution of late Quaternary pyroclastic and associated cover deposits of the Rotorua and Taupo area, North Island, New Zealand*. Wellington, N.Z., Dept. of Scientific and Industrial Research.

PureHydroponics. (2023). *PureHydroponics*. Retrieved 06 May 2023 from https://purehydroponics.com/products/growing-media/

Pyle, D. M. (2015). Sizes of Volcanic Eruptions. In H. Sigurdsson (Ed.), *Encyclopedia of volcanoes.* (2nd ed., pp. 257-264). Academic Press is an imprint of Elsevier. https://ezproxy.massey.ac.nz/login?url=https://ebookcentral.proquest.com/lib/massey/detail.action?docID=1983593

Raviv, M., Silber, A., Medina, S., Krasnovsky, A., & Wallach, R. (1999). The effect of hydraulic characteristics of volcanic materials on yield of roses grown in soilless culture. *Journal of the American Society for Horticultural Science, 124*(2), 205-209-209. https://doi.org/10.21273/jashs.124.2.205

Raviv, M., Wallach, R., Silber, A., & Bar-Tal, A. (2002). Substrates and their analysis. *Hydroponic production of vegetables and ornamentals*, 25-102.

Riggs, N. R., Ort, M., White, J., Wilson, C., Houghton, B. F., & Clarkson, R. (2001). Post-1.8-ka Marginal Sedimentation in Lake Taupo, New Zealand: Effects of Wave Energy and Sediment Supply in a Rapidly Rising Lake. *Volcaniclastic sedimentation in lacustrine settings*, 151-177.

Rotella, M. D., Wilson, C. J. N., Barker, S. J., Cashman, K. V., Houghton, B. F., & Wright, I. C. (2014, 2014/07/12). Bubble development in explosive silicic eruptions: insights from pyroclast vesicularity textures from Raoul volcano (Kermadec arc). *Bulletin of Volcanology, 76*(8), 826. https://doi.org/10.1007/s00445-014-0826-6

Rowe, M. C., Carey, R. J., White, J. D. L., Kilgour, G., Hughes, E., Ellis, B., Rosseel, J.-B., & Segovia, A. (2021). Tarawera 1886: an integrated review of volcanological and geochemical characteristics of a complex basaltic eruption. *New Zealand Journal of Geology and Geophysics, 64*(2-3), 296-319. https://doi.org/10.1080/00288306.2021.1914118

Ruehlmann, J. (2020). Soil particle density as affected by soil texture and soil organic matter: 1. Partitioning of SOM in conceptional fractions and derivation of a variable SOC to SOM conversion factor. *Geoderma, 375*. https://doi.org/10.1016/j.geoderma.2020.114542

Saaid, M. F., Yassin, A. I. M., & Tahir, N. M. (2021). Particle Swarm Optimization (PSO) Model for Hydroponics pH Control System. *TEM Journal, 10*(4), 1694-1699. https://doi.org/10.18421/TEM104-27

Sahetapy-Engel, S., Self, S., Carey, R., & Nairn, I. (2014). Deposition and generation of multiple widespread fall units from the c. AD 1314 Kaharoa rhyolitic eruption, Tarawera, New Zealand. *Bulletin of Volcanology, 76*(8), 1-28. https://doi.org/10.1007/s00445-014-0836-4

Sahin, U., Ors, S., Ercisli, S., Anapali, O., & Esitken, A. (2005). Effect of pumice amendment on physical soil properties and strawberry plant growth. *Journal of Central European Agriculture, 6*(3), 361-366.

Sandiford, A., Alloway, B., & Shane, P. (2001). A 28 000-6600 cal yr record of local and distal volcanism preserved in a paleolake, Auckland, New Zealand. *New Zealand Journal of Geology and Geophysics, 44*(2), 323-336. https://doi.org/10.1080/00288306.2001.9514941

Sas, M., Shane, P., Kuritani, T., Zellmer, G. F., Kent, A. J. R., & Nakagawa, M. (2021). Mush, Melts and Metasediments: a History of Rhyolites from the Okataina Volcanic Centre, New Zealand, as Captured in Plagioclase. *Journal of Petrology, 62*(8), 1-26. https://doi.org/10.1093/petrology/egab038

Saxby, J., Beckett, F., Cashman, K., Rust, A., & Tennant, E. (2018). The impact of particle shape on fall velocity: Implications for volcanic ash dispersion modelling. *Journal of Volcanology and Geothermal Research, 362*, 32-48.

Schafer, E. D. P. D. (2020). *Hydroponics*. Salem Press. https://ezproxy.massey.ac.nz/login?url=https://search.ebscohost.com/login.aspx?direct=true&AuthType=sso&db=ers&AN=89250491&site=eds-live&scope=site&authtype=sso&custid=s3027306

Schmincke, H.-U., Park, C., & Harms, E. (1999). Evolution and environmental impacts of the eruption of Laacher See Volcano (Germany) 12,900 a BP. *Quaternary International, 61*(1), 61-72. https://doi.org/https://doi.org/10.1016/S1040-6182(99)00017-8

Scotter, D. R. (n.d.). *Soil science 189.211*

Segschneider, B., Landis, C., Manville, V., White, J., & Wilson, C. (2002). Environmental response to a large, explosive rhyolite eruption: sedimentology of post-1.8 ka pumice-rich Taupo volcaniclastics in the Hawke's Bay region, New Zealand. *Sedimentary Geology, 150*(3-4), 275-299.

Segschneider, B., Landis, C., White, J., Wilson, C., & Manville, V. (2002). Resedimentation of the 1.8 ka Taupo ignimbrite in the Mohaka and Ngaruroro river catchments, Hawke's Bay, New Zealand. *New Zealand Journal of Geology and Geophysics, 45*(1), 85-101.

Shane, P., & Hoverd, J. (2002). Distal record of multi-sourced tephra in Onepoto Basin, Auckland, New Zealand: implications for volcanic chronology, frequency and hazards. *Bulletin of Volcanology, 64*(7), 441-454. https://doi.org/10.1007/s00445-002-0217-2

Shane, P., Martin, S. B., Smith, V. C., Beggs, K. F., Darragh, M. B., Cole, J. W., & Nairn, I. A. (2007). Multiple rhyolite magmas and basalt injection in the 17.7 ka Rerewhakaaitu eruption episode from Tarawera volcanic complex, New Zealand. *Journal of Volcanology and Geothermal Research, 164*(1), 1-26. https://doi.org/10.1016/j.jvolgeores.2007.04.003

Shane, P., Nairn, I. A., Martin, S. B., & Smith, V. C. (2008). Compositional heterogeneity in tephra deposits resulting from the eruption of multiple magma bodies: Implications for tephrochronology. *Quaternary International, 178*(1), 44-53. https://doi.org/10.1016/j.quaint.2006.11.014

Shane, P., Nairn, I. A., & Smith, V. C. (2005). Magma mingling in the ∼50 ka Rotoiti eruption from Okataina Volcanic Centre: implications for geochemical diversity and chronology of large volume rhyolites. *Journal of Volcanology and Geothermal Research, 139*(3), 295-313. https://doi.org/10.1016/j.jvolgeores.2004.08.012

Siebert, L., Cottrell, E., Venzke, E., & Andrews, B. (2015). Earth's volcanoes and their eruptions: An overview. In H. Sigurdsson (Ed.), *Encyclopedia of volcanoes.* (2nd ed., pp. 239-255). Academic Press is an imprint of Elsevier. https://ezproxy.massey.ac.nz/login?url=https://ebookcentral.proquest.com/lib/massey/detail.action?docID=1983593

Smith, R. C. M. (1991a). Landscape response to a major ignimbrite eruption Taupo Volcanic Center New Zealand.

Smith, R. C. M. (1991b). Post-eruption sedimentation on the margin of a caldera lake, Taupo Volcanic Centre, New Zealand [Article]. *Sedimentary Geology, 74*(1-4), 89-138-138. https://doi.org/10.1016/0037-0738(91)90036-D

Smith, R. T., & Houghton, B. F. (1995). Delayed deposition of Plinian pumice during phreatoplinian volcanism - The 1800 - yr - BP Taupo eruption, New Zealand. *Journal of Volcanology and Geothermal Research, 67*(4), 221-226. https://ezproxy.massey.ac.nz/login?url=https://search.ebscohost.com/login.aspx?direct=true&AuthType=sso&db=edswsc&AN=A1995TA25900001&site=eds-live&scope=site&authtype=sso&custid=s3027306

Smith, V. C., Shane, P., & Nairn, I. A. (2004). Reactivation of a rhyolitic magma body by new rhyolitic intrusion before the 15.8 ka Rotorua eruptive episode: implications for magma storage in the Okataina Volcanic Centre, New Zealand. *Journal of the Geological Society, 161*(5), 757-772.

Smith, V. C., Shane, P., & Nairn, I. A. (2005). Trends in rhyolite geochemistry, mineralogy, and magma storage during the last 50 kyr at Okataina and Taupo volcanic centres, Taupo Volcanic Zone, New Zealand. *Journal of Volcanology and Geothermal Research, 148*(3), 372-406. https://doi.org/10.1016/j.jvolgeores.2005.05.005

Smith, V. C., Shane, P., Nairn, I. A., & Williams, C. M. (2006). Geochemistry and magmatic properties of eruption episodes from Haroharo linear vent zone, Okataina Volcanic Centre, New Zealand during the last 10 kyr. *Bulletin of Volcanology, 69*(1), 57-88. https://doi.org/10.1007/s00445-006-0056-7

Sohn, C., & Sohn, Y. K. (2019). Distinguishing between primary and secondary volcaniclastic deposits. *Scientific Reports, 9*(1). https://doi.org/10.1038/s41598-019-48933-4

Speed, J., Shane, P., & Nairn, I. (2002). Volcanic stratigraphy and phase chemistry of the 11 900 yr BP Waiohau eruptive episode, Tarawera Volcanic Complex, New Zealand. *New Zealand Journal of Geology and Geophysics, 45*(3), 395-410. https://doi.org/10.1080/00288306.2002.9514981

Sutton, A. N., Blake, S., & Wilson, C. J. N. (1995). An outline geochemistry of rhyolite eruptives from Taupo volcanic centre, New Zealand. *Journal of Volcanology and Geothermal Research, 68*(1-3), 153-175. https://doi.org/10.1016/0377-0273(95)00011-I

Szabó, T. (2015). Fluvial Clast. In H. Hargitai & Á. Kereszturi (Eds.), *Encyclopedia of Planetary Landforms* (pp. 788-793). Springer New York. https://doi.org/10.1007/978-1-4614-3134-3_421

Taddeucci, J., & Palladino, D. M. (2002, 2002/05/01). Particle size-density relationships in pyroclastic deposits: inferences for emplacement processes. *Bulletin of Volcanology, 64*(3), 273-284. https://doi.org/10.1007/s00445-002-0205-6

Tapscott, S. (2023). *Re-establishing the beast: An investigation into the spatiotemporal evolution of the Y5 phase of the Taupō 232 ± 10 CE eruption, New Zealand* Massey University].

Thomas, N., Jaupart, C., & Vergniolle, S. (1994). On the vesicularity of pumice. *Journal of Geophysical Research: Solid Earth, 99*(B8), 15633-15644.

Thompson, M. A., Lindsay, J. M., Sandri, L., Biass, S., Bonadonna, C., Jolly, G., & Marzocchi, W. (2015). Exploring the influence of vent location and eruption style on tephra fall hazard from the Okataina Volcanic Centre, New Zealand. *Bulletin of Volcanology: Official Journal of the International Association of Volcanology and Chemistry of the Earth`s Interior (IAVCEI), 77*(5), 1-23. https://doi.org/10.1007/s00445-015-0926-y

Todde, A. (2022). *Intra-caldera rhyolitic eruptions: lithostratigraphy and pyroclast textures to reconstruct the ~1314 CE Kaharoa eruption of Mt Tarawera, New Zealand* Massey University].

Volder, A., & van Iersel, M. (2019). Root growth, physiology, and potential impact of soiless culture on their functioning. In J. H. Lieth, M. Raviv, & A. Bar-Tal (Eds.), *Soilless Culture : Theory and Practice* (2nd ed.). Academic Press, an imprint of Elsevier.

von Lichtan, I. J., White, J. D. L., Manville, V., & Ohneiser, C. (2016). Giant rafted pumice blocks from the most recent eruption of Taupo volcano, New Zealand: Insights from palaeomagnetic and textural data. *Journal of Volcanology & Geothermal Research, 318*, 73-88. https://doi.org/10.1016/j.jvolgeores.2016.04.003

Walker, G. P. L. (1980). The Taupo pumice: Product of the most powerful known (ultraplinian) eruption? *Journal of Volcanology and Geothermal Research, 8*(1), 69-94. https://doi.org/10.1016/0377-0273(80)90008-6

Walker, G. P. L. (1981a). Plinian eruptions and their products. *Bulletin Volcanologique, 44*(3), 223-240. https://doi.org/10.1007/BF02600561

Walker, G. P. L. (1981b). The Waimihia and Hatepe plinian deposits from the rhyolitic Taupo volcanic centre. *New Zealand Journal of Geology and Geophysics, 24*(3), 305-324-324. https://doi.org/10.1080/00288306.1981.10422722

Walker, G. P. L. (1983). Ignimbrite types and ignimbrite problems. *Journal of Volcanology and Geothermal Research, 17*(1-4), 65-88-88. https://doi.org/10.1016/0377-0273(83)90062-8

Walker, G. P. L., Self, S., & Wilson, L. (1984). Tarawera 1886, New Zealand - A basaltic plinian fissure eruption. *Journal of Volcanology and Geothermal Research, 21*(1-2), 61-78. https://doi.org/10.1016/0377-0273(84)90016-7

Wallach, R. (2019). Physical characteristics of soiless media. In J. H. Lieth, M. Raviv, & A. Bar-Tal (Eds.), *Soilless Culture : Theory and Practice* (2nd ed.). Academic Press, an imprint of Elsevier.

Walters, H. (2020). *Vertical and lateral variations of grainsize and pyroclast componentry in the Taupo 232 CE Y2 fall deposit : implications for spatiotemporal deposition and conduit conditions in large Plinian eruptions : a thesis presented in partial fulfilment of the requirements for the degree of Magister Scientiarum in Earth Science at Massey University, Manawatū, New Zealand*. http://hdl.handle.net/10179/16199

Webb, P. A. (2001). Volume and density determinations for particle technologists. *Micromeritics Instrument Corp, 2*(16), 01.

White, J. D. L., & Houghton, B. F. (2006). Primary volcaniclastic rocks. *Geology, 34*(8), 677-680-680. https://doi.org/10.1130/G22346.1

White, J. D. L., Manville, V., Wilson, C. J. N., Houghton, B. F., Riggs, N. R., & Ort, M. (2001). Settling and deposition of AD 181 Taupo pumice in lacustrine and associated environments. *Volcaniclastic sedimentation in lacustrine settings*, 141-150.

Whiteford, P. C. (1996). Heat flow in the sediments of Lake Taupo, New Zealand. *Tectonophysics, 257*(1 SPEC. ISS.), 81-92. https://doi.org/10.1016/0040-1951(95)00122-0

Wilson, C. J. N. (1985). The Taupo Eruption, New Zealand II. The Taupo Ignimbrite. *Philosophical Transactions of the Royal Society of London. Series A, Mathematical and Physical Sciences, 314*(1529), 229-310. https://ezproxy.massey.ac.nz/login?url=https://search.ebscohost.com/login.aspx?direct=true&AuthType=sso&db=edsjsr&AN=edsjsr.37663&site=eds-live&scope=site&authtype=sso&custid=s3027306

Wilson, C. J. N. (1993). Stratigraphy, Chronology, Styles and Dynamics of Late Quaternary Eruptions from Taupo Volcano, New Zealand. *Philosophical Transactions: Physical Sciences and Engineering, 343*(1668), 205-306. https://ezproxy.massey.ac.nz/login?url=https://search.ebscohost.com/login.aspx?direct=true&AuthType=sso&db=edsjsr&AN=edsjsr.54146&site=eds-live&scope=site&authtype=sso&custid=s3027306

Wilson, C. J. N. (2001). The 26.5 ka Oruanui eruption, New Zealand: An introduction and overview. *Journal of Volcanology and Geothermal Research, 112*(1-4), 133-174. https://doi.org/10.1016/S0377-0273(01)00239-6

Wilson, C. J. N., Blake, S., Charlier, B. L. A., & Sutton, A. N. (2006). The 26.5 ka Oruanui eruption, Taupo Volcano, New Zealand: Development, characteristics and evacuation of a large rhyolitic magma body. *Journal of Petrology, 47*(1), 35-69. https://doi.org/10.1093/petrology/egi066

Wilson, C. J. N., Houghton, B. F., McWilliams, M. O., Lanphere, M. A., Weaver, S. D., & Briggs, R. M. (1995). Volcanic and structural evolution of Taupo Volcanic Zone, New Zealand: a review. *Journal of Volcanology and Geothermal Research, 68*(1-3), 1-28. https://doi.org/10.1016/0377-0273(95)00006-G

Wilson, C. J. N., Rhoades, D. A., Lanphere, M. A., Calvert, A. T., Houghton, B. F., Weaver, S. D., & Cole, J. W. (2007). A multiple-approach radiometric age estimate for the Rotoiti and Earthquake Flat eruptions, New Zealand, with implications for the MIS 4/3 boundary. *Quaternary Science Reviews, 26*(13), 1861-1870. https://doi.org/10.1016/j.quascirev.2007.04.017

Wilson, C. J. N., Rogan, A. M., Smith, I. E. M., Northey, D. J., Nairn, I. A., & Houghton, B. F. (1984). Caldera volcanoes of the Taupo volcanic zone, New Zealand. *Journal of Geophysical Research, 89*(B10), 8463-8484. https://doi.org/10.1029/JB089iB10p08463

Wilson, C. J. N., & Rowland, J. V. (2016). The volcanic, magmatic and tectonic setting of the Taupo Volcanic Zone, New Zealand, reviewed from a geothermal perspective. *Geothermics, 59*(Part B), 168-187. https://doi.org/10.1016/j.geothermics.2015.06.013

Wilson, C. J. N., & Walker, G. P. L. (1985). The Taupo Eruption, New Zealand I. General Aspects. *Philosophical Transactions of the Royal Society of London. Series A, Mathematical and Physical Sciences, 314*(1529), 199-228. https://ezproxy.massey.ac.nz/login?url=https://search.ebscohost.com/login.aspx?direct=true&AuthType=sso&db=edsjsr&AN=edsjsr.37662&site=eds-live&scope=site&authtype=sso&custid=s3027306

Wright, H. M. N., Folkes, C. B., Cas, R. A. F., & Cashman, K. V. (2011). Heterogeneous pumice populations in the 2.08-Ma Cerro Galán Ignimbrite: implications for magma recharge and ascent preceding a large-volume silicic eruption. *Bulletin of Volcanology: Official Journal of the International Association of Volcanology and Chemistry of the Earth`s Interior (IAVCEI), 73*(10), 1513-1533. https://doi.org/10.1007/s00445-011-0525-5

Zhao, R., Sofkova-Bobcheva, S., Cartmill, D., Hardy, D., & Zernack, A. (2023). Comparative evaluation of pumice as a soilless substrate for indoor Rubs sp. cultivation [Research Paper]. *New Zealand Journal of Crop and Horticultural Science*. http://mc.manuscriptcentral.com/nzjc

8 Glossary

Connected porosity (or effective porosity) is the intra-clast pore space through which an uninterrupted path exists between the edges of a clast.

Fall Deposits: Sedimentation of pyroclastic material from the eruption plume following an explosive eruption results in a fall deposit (Houghton & Carey, 2015).

Fluvial Reworking: Is the process where primary deposits from an eruption are moved from their original location by flowing water and redeposited elsewhere (Manville et al., 2009; Sohn & Sohn, 2019).

Ignimbrite: Ignimbrites result from large scale concentrated PDCs (Deligne & Sigurdsson, 2015) and represent massive deposits that may be welded or non-welded depending on the viscosity of the non-crystalline juvenile particles during deposition, which is dependent on temperature (Walker, 1983).

Pyroclastic: relating to fragments of rock erupted from a volcano. The term pyroclastic is derived from the Greek words for fire (pyro) and broken (clastic).

Pyroclastic Density Currents (PDCs): These flows are produced during plume collapse, phreatic/phreatomagmatic explosions and lateral blasts; the resulting mix of gas and pyroclastic material is driven along the ground by density contrasts with the surrounding atmosphere or water (Dufek et al., 2015).

Tephra: Tephra is the term used to describe pyroclastic material ejected from a vent (Siebert et al., 2015), and predominantly comprises pumice and glass shards, free crystals (phenocrysts from the magma) and lithics (pre-existing rock fragments) (Walker, 1981a).

APPENDICES

Sample Na	Taupo Y2- connected-1	
0.0114g	δ_{skel}	V_{skel}
Run		
1	1.4506	0.0786
2	1.6064	0.071
3	1.5747	0.0724
4	1.5963	0.0714
5	1.4709	0.0775
6	1.5623	0.073
7	1.5183	0.0751
8	1.4638	0.0779
9	1.5016	0.0759
10	1.4546	0.0784
average	1.51995	0.07512
stdev	0.06061924	0.00297351
stdev %	3.98823877	3.95835024

Sample Na	Taupo Y2- connected-2	
0.180g	δ_{skel}	V_{skel}
Run		
1	1.5639	0.1151
2	1.6558	0.1087
3	1.757	0.1024
4	1.7543	0.1026
5	1.7716	0.1016
6	1.781	0.1011
7	1.8093	0.0995
8	1.7748	0.1014
9	1.7606	0.1022
10	1.7343	0.1038
average	1.73626	0.10384
stdev	0.07272811	0.00464308
stdev %	4.18878	4.47138219

Sample Na	Taupo Y2- connected-3	
0.236g	δ_{skel}	V_{skel}
Run		
1	1.639	0.144
2	1.7175	0.1374
3	1.7353	0.136
4	1.6811	0.1404
5	1.6824	0.1403
6	1.6897	0.1397
7	1.7154	0.1376
8	1.7229	0.137
9	1.6904	0.1396
10	1.6835	0.1402
average	1.69572	0.13922
stdev	0.02786714	0.00230882
stdev %	1.64338082	1.65839941

Sample Na	Taupo Y2- connected-4	
0.131g	δ_{skel}	V_{skel}
Run		
1	1.1567	0.1133
2	1.219	0.1075
3	1.2296	0.1065
4	1.2448	0.1052
5	1.2462	0.1051
6	1.2465	0.1051
7	1.2359	0.106
8	1.2098	0.1083
9	1.2094	0.1083
10	1.1993	0.1092
average	1.21972	0.10745
stdev	0.02789005	0.0025352
stdev %	2.28659479	2.3594199

Sample Na	Tapo Y5 connected_1	
	δ_{skel}	V_{skel}
Run		
1	1.5882	0.1429
2	1.8227	0.1245
3	1.8254	0.1244
4	1.7647	0.1286
5	1.7826	0.1273
6	1.7609	0.1289
7	1.7886	0.1269
8	1.7481	0.1299
9	1.733	0.131
10	1.7327	0.131
average	1.75469	0.12954
stdev	0.06700684	0.00524917
stdev %	3.81872807	4.05216091

Sample Na	Tapo Y5 connected_2	
	δ_{skel}	V_{skel}
Run		
1	1.8454	0.0748
2	1.82122	0.0758
3	1.7873	0.0772
4	1.7793	0.0776
5	1.7822	0.0774
6	1.7803	0.0775
7	1.7554	0.0786
8	1.8196	0.0758
9	1.7675	0.0781
10	1.7825	0.0774
average	1.792072	0.07702
stdev	0.02771571	0.00117644
stdev %	1.54657361	1.52744131

Sample Na	Tapo Y5 connected_3	
	δ_{skel}	V_{skel}
Run		
1	2.0717	0.1435
2	2.0898	0.1421
3	2.1209	0.14
4	2.1408	0.1387
5	2.1337	0.1392
6	2.076	0.1431
7	2.0585	0.1443
8	2.1274	0.1396
9	2.1096	0.1408
10	2.1123	0.1406
average	2.10407	0.14119
stdev	0.02841924	0.00194619
stdev %	1.3506796	1.37842118

Sample Na	Tapo Y5 connected_4	
	δ_{skel}	V_{skel}
Run		
1	1.9763	0.0992
2	1.9616	0.0999
3	1.8972	0.1033
4	1.9728	0.0994
5	1.8422	0.1064
6	1.8744	0.1046
7	1.8013	0.1088
8	1.8096	0.1083
9	1.8377	0.1067
10	1.7807	0.1101
average	1.87538	0.10467
stdev	0.07370083	0.00407105
stdev %	3.92991467	3.88941392 ##

Sample Na	Taupo Y2- connected-5	
0.189g	δ_{skel}	V_{skel}
Run		
1	1.292	0.1463
2	1.3727	0.1377
3	1.3841	0.1366
4	1.3554	0.1394
5	1.3465	0.1404
6	1.3418	0.1409
7	1.323	0.1429
8	1.3319	0.1419
9	1.3144	0.1438
10	1.3196	0.1432
average	1.33814	0.14131
stdev	0.02787329	0.00293275
stdev %	2.08298778	2.07539888

Sample Na	Taupo Y2- connected-6	
0.214g	δ_{skel}	V_{skel}
Run		
1	1.4983	0.1428
2	1.5395	0.139
3	1.5722	0.1361
4	1.5383	0.1391
5	1.5215	0.1407
6	1.5036	0.1423
7	1.4639	0.1462
8	1.4645	0.1461
9	1.4816	0.1444
10	1.4691	0.1457
average	1.50525	0.14224
stdev	0.03696738	0.00346352
stdev %	2.4558964	2.43498609

Sample Na	Taupo Y2- connected-7	
0.128g	δ_{skel}	V_{skel}
Run		
1	1.0952	0.1169
2	1.2068	0.1061
3	1.2412	0.103
4	1.2435	0.1029
5	1.2339	0.1037
6	1.2403	0.1032
7	1.2513	0.1023
8	1.2416	0.1031
9	1.238	0.1034
10	1.2135	0.1055
average	1.22053	0.10501
stdev	0.04614706	0.00434446
stdev %	3.78090345	4.137187

Sample Na	Taupo Y2- connected-8	
0.165g	δ_{skel}	V_{skel}
Run		
1	1.4676	0.1111
2	1.4776	0.1103
3	1.5063	0.1082
4	1.4856	0.1097
5	1.4602	0.1116
6	1.4574	0.1118
7	1.4195	0.1148
8	1.4287	0.1141
9	1.4425	0.113
10	1.4092	0.1157
average	1.45546	0.11203
stdev	0.03068493	0.00237021
stdev %	2.10826332	2.11569099

Sample Na	Tapo Y5 connected_5	
	δ_{skel}	V_{skel}
Run		
1	1.9199	0.1245
2	1.9692	0.1214
3	1.9536	0.1223
4	1.8899	0.1265
5	1.9194	0.1245
6	1.8904	0.1264
7	1.8705	0.1278
8	1.9194	0.1245
9	1.8424	0.1297
10	1.8115	0.1319
average	1.89862	0.12595
stdev	0.04831116	0.00322706
stdev %	2.54454092	2.5621721

Sample Na	Tapo Y5 connected_6	
	δ_{skel}	V_{skel}
Run		
1	1.9672	0.1027
2	1.9708	0.1025
3	1.9079	0.1059
4	1.9442	0.1039
5	1.872	0.1079
6	1.8952	0.1066
7	1.857	0.1088
8	1.8288	0.1105
9	1.8341	0.1101
10	1.8253	0.1107
average	1.89025	0.10696
stdev	0.05601814	0.00315003
stdev %	2.96353059	2.94505091

Sample Na	Tapo Y5 connected_7	
	δ_{skel}	V_{skel}
Run		
1	1.7321	0.1801
2	1.826	0.1826
3	1.7091	0.1791
4	1.7541	0.1779
5	1.724	0.181
6	1.7154	0.1819
7	1.7219	0.1812
8	1.7152	0.1819
9	1.7154	0.1819
10	1.6966	0.1839
average	1.73098	0.18115
stdev	0.03665296	0.00173989
stdev %	2.11746878	0.96047002

Sample Na	Tapo Y5 connected_8	
	δ_{skel}	V_{skel}
Run		
1	1.736	0.0933
2	1.7692	0.0916
3	1.7656	0.0918
4	1.7342	0.0934
5	1.7519	0.0925
6	1.7469	0.0927
7	1.7309	0.0936
8	1.7349	0.0934
9	1.7098	0.0947
10	1.7281	0.0937
average	1.74075	0.09307
stdev	0.01796201	0.00093339
stdev %	1.0318548	1.00289337

Sample Na	Taupo Y2- connected-9	
0.141g	δ_{skel}	V_{skel}
Run		
1	1.3186	0.1069
2	1.4249	0.099
3	1.4226	0.0991
4	1.3986	0.1008
5	1.418	0.0994
6	1.4084	0.1001
7	1.4072	0.1002
8	1.4076	0.1002
9	1.4168	0.0995
10	1.3333	0.1058
average	1.3956	0.1011
stdev	0.03771292	0.00283431
stdev %	2.70227296	2.80347533

Sample Na	Taupo Y2- connected-10	
0.136g	δ_{skel}	V_{skel}
Run		
1	1.2862	0.1057
2	1.3326	0.1021
3	1.3598	0.1
4	1.3605	0.1
5	1.3704	0.0992
6	1.3384	0.1016
7	1.3375	0.1017
8	1.3508	0.1007
9	1.3327	0.102
10	1.3378	0.1017
average	1.34067	0.10147
stdev	0.02324923	0.00178764
stdev%	1.73415022	1.76174512

Sample Na	Tapo Y5 connected_9	
	δ_{skel}	V_{skel}
Run		
1	2.0918	0.196
2	2.0463	0.2004
3	2.1089	0.1944
4	2.2016	0.1862
5	2.1372	0.1918
6	2.082	0.1969
7	2.0872	0.1964
8	2.0879	0.1964
9	2.0994	0.1953
10	2.075	0.1976
average	2.10173	0.19514
stdev	0.04211917	0.00383527
stdev %	2.00402387	1.96539657

Sample Na	Tapo Y5 connected_10	
	δ_{skel}	V_{skel}
Run		
1	2.0227	0.0821
2	2.1252	0.0781
3	2.1339	0.0778
4	2.049	0.081
5	2.0727	0.0801
6	1.9841	0.0837
7	2.0058	0.0828
8	2.002	0.0829
9	2.0059	0.0828
10	1.9931	0.0833
average	2.03944	0.08146
stdev	0.0543891	0.0021402
stdev %	2.66686424	2.62729842

Sample Na	KA01_1	
0.187g	δ_{skel}	V_{skel}
Run		
1	1.918	0.0975
2	1.9432	0.0962
3	1.9381	0.0965
4	1.9328	0.0968
5	1.9477	0.096
6	1.9892	0.094
7	1.9782	0.0945
8	1.9437	0.0962
9	1.9229	0.0972
10	1.8883	0.099
average	1.94021	0.09639
stdev	0.02880472	0.00142941
stdev %	1.48461887	1.48294765

Sample Na	KAO1_2	
0.194g	δ_{skel}	V_{skel}
Run		
1	1.9566	0.0992
2	1.917	0.1012
3	1.8893	0.1027
4	1.8498	0.1049
5	1.8468	0.105
6	1.8089	0.1072
7	1.7879	0.1085
8	1.7763	0.1092
9	1.7574	0.1104
10	1.775	0.1093
average	1.8365	0.10576
stdev	0.06729859	0.00380035
stdev %	3.6645025	3.5933726

Sample Na	KAO1_3	
0.260g	δ_{skel}	V_{skel}
Run		
1	1.5612	0.1665
2	1.6538	0.1572
3	1.7032	0.1527
4	1.7218	0.151
5	1.7083	0.1522
6	1.7128	0.1518
7	1.697	0.1532
8	1.6916	0.1537
9	1.6948	0.1534
10	1.6785	0.1548
average	1.6823	0.15465
stdev	0.04661192	0.00450635
stdev %	2.77072581	2.91390465

Sample Na	KAO1_4	
0.301g	δ_{skel}	V_{skel}
Run		
1	1.7411	0.1729
2	1.8055	0.1667
3	1.8152	0.1658
4	1.8326	0.1642
5	1.8503	0.1627
6	1.8394	0.1636
7	1.8318	0.1643
8	1.8381	0.1638
9	1.828	0.1647
10	1.8236	0.1651
average	1.82056	0.16538
stdev	0.03064562	0.00287549
stdev %	1.68330711	1.73871707

Sample Na	KR01_1	
	δ_{skel}	V_{skel}
Run		
1	2.0013	0.0909
2	2.2805	0.0798
3	2.3364	0.0779
4	2.2221	0.0819
5	2.2497	0.0809
6	2.2327	0.0815
7	2.1479	0.0847
8	2.1119	0.0862
9	2.1134	0.0861
10	2.0631	0.0882
average	2.1759	0.08381
stdev	0.1051474	0.00407907
stdev %	4.83236358	4.86703949

Sample Na	KR01_2	
	δ_{skel}	V_{skel}
Run		
1	1.7429	0.1268
2	1.7446	0.1267
3	1.7383	0.1271
4	1.7332	0.1275
5	1.7109	0.1292
6	1.7383	0.1271
7	1.74	0.127
8	1.7235	0.1282
9	1.7011	0.1299
10	1.7097	0.1293
average	1.72825	0.12788
stdev	0.01581604	0.00118491
stdev %	0.91514788	0.92657574

Sample Na	KR01_3	
	δ_{skel}	V_{skel}
Run		
1	2.0151	0.0829
2	2.03	0.0823
3	1.9517	0.0856
4	2.02	0.0826
5	2.0251	0.0825
6	1.9901	0.0839
7	2.0013	0.0834
8	2.0009	0.0835
9	1.9916	0.0839
10	1.9759	0.0845
average	2.00017	0.08351
stdev	0.02413504	0.0010192
stdev %	1.20664939	1.22045801

Sample Na	KR01_4	
	δ_{skel}	V_{skel}
Run		
1	1.7767	0.1109
2	1.7046	0.1156
3	1.6826	0.1171
4	1.7219	0.1144
5	1.6952	0.1162
6	1.7032	0.1157
7	1.7354	0.1135
8	1.7395	0.1133
9	1.7122	0.1151
10	1.6674	0.1181
average	1.71387	0.11499
stdev	0.03130662	0.00207174
stdev %	1.82666256	1.80167065

Sample Na	KAO1_5	
0.270g	δ_{skel}	V_{skel}
Run		
1	1.6787	0.1608
2	1.8103	0.1491
3	1.8312	0.1474
4	1.8496	0.146
5	1.856	0.1455
6	1.8582	0.1453
7	1.8352	0.1471
8	1.8543	0.1456
9	1.8347	0.1472
10	1.8612	0.1451
average	1.82694	0.14791
stdev	0.05442226	0.0046962
stdev %	2.9788752	3.17504167

Sample Na	KAO1_6	
0.389g	δ_{skel}	V_{skel}
Run		
1	2.2724	0.1712
2	2.4781	0.157
3	2.523	0.1542
4	2.4762	0.1571
5	2.428	0.1602
6	2.4448	0.1591
7	2.4205	0.1607
8	2.3982	0.1622
9	2.415	0.1611
10	2.37	0.1641
average	2.42262	0.16069
stdev	0.06875051	0.00466582
stdev %	2.83785785	2.9036165

Sample Na	KAO1_7	
0.250g	δ_{skel}	V_{skel}
Run		
1	1.8853	0.132
2	2.0216	0.1237
3	2.1152	0.1182
4	2.1266	0.1176
5	2.1236	0.1177
6	2.1089	0.1185
7	2.1049	0.1188
8	2.1193	0.118
9	2.0872	0.1198
10	2.0914	0.1195
average	2.0784	0.12038
stdev	0.07437601	0.00445366
stdev %	3.5785225	3.69966993

Sample Na	KAO1_8	
0.354g	δ_{skel}	V_{skel}
Run		
1	2.0829	0.17
2	2.1993	0.161
3	2.2621	0.1565
4	2.2557	0.1569
5	2.2441	0.1577
6	2.2753	0.1556
7	2.2953	0.1542
8	2.2644	0.1563
9	2.2674	0.1561
10	2.2507	0.1573
average	2.23972	0.15816
stdev	0.06041764	0.00451521
stdev %	2.69755306	2.85483616

Sample Na	KR01_5	
	δ_{skel}	V_{skel}
Run		
1	1.9206	0.0781
2	1.9834	0.075
3	1.907	0.0787
4	1.8733	0.0801
5	1.8849	0.0796
6	1.7949	0.0836
7	1.8886	0.0794
8	1.725	0.087
9	1.8149	0.0827
10	1.8697	0.0802
average	1.86623	0.08044
stdev	0.07220862	0.00330293
stdev %	3.86922396	4.10607657

Sample Na	KR01_6	
	δ_{skel}	V_{skel}
Run		
1	1.8997	0.0737
2	1.8183	0.077
3	1.9104	0.0733
4	1.8897	0.0741
5	1.855	0.0755
6	1.8924	0.074
7	1.8625	0.0752
8	1.89441	0.0739
9	1.8017	0.0773
10	1.8939	0.0739
average	1.871801	0.07479
stdev	0.03675407	0.00141221
stdev %	1.96356694	1.88823195

Sample Na	KR01_7	
	δ_{skel}	V_{skel}
Run		
1	1.6775	0.0924
2	1.6777	0.0924
3	1.6801	0.0923
4	1.6872	0.0919
5	1.6461	0.0942
6	1.6861	0.0919
7	1.6381	0.0946
8	1.6319	0.095
9	1.6445	0.0943
10	1.62	0.0957
average	1.65892	0.09347
stdev	0.02524462	0.00142988
stdev %	1.52175009	1.52977379

Sample Na	KR01_8	
	δ_{skel}	V_{skel}
Run		
1	1.9749	0.1068
2	2.0304	0.1039
3	1.971	0.1071
4	1.946	0.1084
5	1.9066	0.1107
6	1.8836	0.112
7	1.8811	0.1122
8	1.8654	0.1131
9	1.8752	0.1125
10	1.8395	0.1147
average	1.91737	0.11014
stdev	0.06045768	0.00342384
stdev %	3.15315673	3.10862357

Sample Na	KAO1_9	
0.3g	δ_{skel}	V_{skel}
Run		
1	2.2156	0.1354
2	2.3284	0.1288
3	2.3845	0.1258
4	2.364	0.1269
5	2.3989	0.1251
6	2.3749	0.1263
7	2.383	0.1259
8	2.2709	0.1321
9	2.3385	0.1283
10	2.3372	0.1284
average	2.33959	0.1283
stdev	0.05723791	0.00322008
stdev %	2.44649335	2.50980196

Sample Na	KAO1_10	
0.518g	δ_{skel}	V_{skel}
Run		
1	2.1081	0.2457
2	2.2342	0.2319
3	2.2506	0.2302
4	2.2242	0.2329
5	2.2253	0.2328
6	2.2415	0.2311
7	2.2254	0.2328
8	2.207	0.2347
9	2.2021	0.2352
10	2.1996	0.2355
average	2.2118	0.23428
stdev	0.04004153	0.004367
stdev %	1.81035962	1.86400779

Sample Na	KR01_9	
	δ_{skel}	V_{skel}
Run		
1	1.8907	0.0852
2	1.8763	0.0858
3	1.9142	0.0841
4	1.9331	0.0853
5	1.8823	0.0855
6	1.852	0.0869
7	1.844	0.0873
8	1.8414	0.0874
9	1.8258	0.0882
10	1.8115	0.0889
average	1.86713	0.08646
stdev	0.03896751	0.00151379
stdev %	2.08702711	1.75085413

Sample Na	KR01_10	
	δ_{skel}	V_{skel}
Run		
1	1.697	0.0872
2	1.6666	0.0888
3	1.741	0.085
4	1.7343	0.0853
5	1.7674	0.0837
6	1.7764	0.0833
7	1.7005	0.087
8	1.7101	0.0865
9	1.5999	0.0925
10	1.6778	0.0882
average	1.7071	0.08675
stdev	0.05214593	0.00270935
stdev %	3.05464986	3.12316538

Sample Na	RQ-L1_01_1	
	δ_{skel}	V_{skel}
Run		
1	3.5806	0.0792
2	3.5082	0.0744
3	3.464	0.0753
4	3.4894	0.0748
5	3.404	0.0767
6	3.4878	0.0748
7	3.5171	0.0742
8	3.4903	0.0748
9	3.4401	0.0759
10	3.5148	0.0743
average	3.48963	0.07544
stdev	0.04767364	0.0015313
stdev %	1.36615163	2.02982901

Sample Na	RQ_L1_01_2	
	δ_{skel}	V_{skel}
Run		
1	3.1056	0.1465
2	3.0764	0.1479
3	3.0651	0.1484
4	3.0037	0.1515
5	3.0856	0.1475
6	3.0037	0.1515
7	2.9309	0.1552
8	3.0123	0.151
9	2.9072	0.1565
10	2.9169	0.156
average	3.0002	0.1512
stdev	0.06880489	0.00367967
stdev %	2.29334335	2.43364676

Sample Na	RQ_L1_01_3	
	δ_{skel}	V_{skel}
Run		
1	3.3711	0.1095
2	3.2645	0.113
3	3.3314	0.1108
4	3.2719	0.1128
5	3.1744	0.1162
6	3.1676	0.1165
7	3.3268	0.1109
8	3.3228	0.1111
9	3.0873	0.1195
10	3.2077	0.115
average	3.25255	0.11353
stdev	0.09060279	0.00318121
stdev %	2.78559244	2.8020895

Sample Na	RQ_L1_01_4	
	δ_{skel}	V_{skel}
Run		
1	3.539	0.0641
2	3.5029	0.0648
3	3.4725	0.0654
4	3.3172	0.0684
5	3.4156	0.0665
6	3.4534	0.0657
7	3.3575	0.0676
8	3.2441	0.07
9	3.4628	0.0656
10	3.1335	0.0724
average	3.38985	0.06705
stdev	0.12700103	0.00258554
stdev %	3.74650872	3.85613228

Sample Na	RQ_L1_02_1	
	δ_{skel}	V_{skel}
Run		
1	2.896	0.105
2	2.8669	0.106
3	2.8499	0.1067
4	2.8467	0.1068
5	2.7693	0.1098
6	2.7322	0.1113
7	2.7326	0.1112
8	2.6911	0.113
9	2.6599	0.1143
10	2.8826	0.1055
average	2.79272	0.10896
stdev	0.08578047	0.0033702
stdev %	3.07157418	3.09305816

Sample Na	RQ-L1_02_2	
	δ_{skel}	V_{skel}
Run		
1	3.0566	0.1031
2	3.0301	0.104
3	3.0665	0.1027
4	2.9703	0.1061
5	3.0927	0.1019
6	2.9555	0.1066
7	3.0508	0.1033
8	2.9104	0.1082
9	3.1005	0.1016
10	2.9769	0.1058
average	3.02103	0.10433
stdev	0.06395094	0.00221412
stdev %	2.11685872	2.12222884

Sample Na	RQ-L1_02_3	
	δ_{skel}	V_{skel}
Run		
1	2.8427	0.0855
2	2.8594	0.085
3	2.9053	0.0836
4	2.742	0.0886
5	2.7845	0.0873
6	2.8161	0.0863
7	2.7649	0.0879
8	2.7023	0.0899
9	2.8502	0.0853
10	2.8199	0.0862
average	2.80873	0.08656
stdev	0.0607677	0.00187865
stdev %	2.16352945	2.17034658

Sample Na	RQ-L1_02_4	
	δ_{skel}	V_{skel}
Run		
1	2.7599	0.1004
2	2.7293	0.1015
3	2.7827	0.0995
4	2.8197	0.0982
5	2.7074	0.1023
6	2.7454	0.1009
7	2.6923	0.1029
8	2.6769	0.1035
9	2.7359	0.1012
10	2.7492	0.1008
average	2.73987	0.10112
stdev	0.04234249	0.00157042
stdev %	1.54541981	1.55302713

Sample Na	RQ_L1_01_5	
	δ_{skel}	V_{skel}
Run		
1	2.6573	0.111
2	2.6267	0.1123
3	2.6408	0.1117
4	2.6432	0.1116
5	2.6176	0.1127
6	2.5965	0.1136
7	2.6542	0.1111
8	2.6497	0.1113
9	2.6069	0.1132
10	2.5773	0.1142
average	2.62702	0.11227
stdev	0.02691323	0.00111759
stdev %	1.02447742	0.99544552

Sample Na	RQ_L1_01_6	
	δ_{skel}	V_{skel}
Run		
1	2.7709	0.1833
2	2.7126	0.1873
3	2.7786	0.1855
4	2.8123	0.1806
5	2.7917	0.182
6	2.8368	0.1791
7	2.7983	0.1815
8	2.8366	0.1791
9	2.8171	0.1803
10	2.7417	0.1846
average	2.78966	0.18233
stdev	0.04011448	0.00278131
stdev %	1.43797024	1.52542459

Sample Na	RQ_L1_01_7	
	δ_{skel}	V_{skel}
Run		
1	3.1006	0.1658
2	3.1135	0.1651
3	3.1411	0.1636
4	3.1389	0.1638
5	3.0243	0.17
6	3.0889	0.1664
7	3.1673	0.1623
8	3.1236	0.1646
9	3.0584	0.1681
10	3.0432	0.1684
average	3.09998	0.16581
stdev	0.04628628	0.00242828
stdev %	1.49311538	1.46449697

Sample Na	RQ_L1_01_8	
	δ_{skel}	V_{skel}
Run		
1	2.5586	0.1546
2	2.7357	0.1616
3	2.8233	0.1566
4	2.8129	0.1571
5	2.8312	0.1561
6	2.7922	0.1583
7	2.7537	0.1605
8	2.7572	0.1603
9	2.7413	0.1671
10	2.75	0.1607
average	2.75561	0.15929
stdev	0.07772353	0.00358994
stdev %	2.82055638	2.25371313

Sample Na	RQ-L1_02_5	
	δ_{skel}	V_{skel}
Run		
1	2.5539	0.1163
2	2.543	0.1168
3	2.4602	0.1207
4	2.4555	0.121
5	2.5339	0.1172
6	2.4471	0.1214
7	2.4019	0.1237
8	2.4147	0.123
9	2.4331	0.1221
10	2.4322	0.1221
average	2.46755	0.12043
stdev	0.05548598	0.00268496
stdev %	2.24862634	2.22947613

Sample Na	RQ-L1_02_6	
	δ_{skel}	V_{skel}
Run		
1	3.0499	0.0879
2	2.9049	0.0923
3	2.95	0.0908
4	3.0458	0.088
5	2.994	0.0895
6	2.9415	0.0911
7	2.9259	0.0916
8	2.869	0.0925
9	2.8099	0.0954
10	2.9496	0.0909
average	2.94405	0.091
stdev	0.07424873	0.00222561
stdev %	2.52199283	2.44572366

Sample Na	RQ-L1_02_7	
	δ_{skel}	V_{skel}
Run		
1	2.6639	0.1396
2	2.6212	0.1419
3	2.6117	0.1424
4	2.5814	0.1441
5	2.5581	0.1454
6	2.5497	0.1459
7	2.5528	0.1457
8	2.5632	0.1451
9	2.5672	0.1449
10	2.5433	0.1463
average	2.58125	0.14413
stdev	0.03895636	0.00215873
stdev %	1.5092054	1.49776525

Sample Na	RQ-L1_02_8	
	δ_{skel}	V_{skel}
Run		
1	2.7393	0.0964
2	2.7445	0.0962
3	2.7556	0.0958
4	2.6177	0.1009
5	2.6635	0.0991
6	2.7066	0.0975
7	2.6921	0.0981
8	2.6877	0.0982
9	2.6874	0.0982
10	2.6099	0.1012
average	2.69043	0.09816
stdev	0.04982171	0.00184343
stdev %	1.85181199	1.87798162

Sample Na	RQ_L1_01_9	
	δ_{skel}	V_{skel}
Run		
1	2.6939	0.1192
2	2.6067	0.1231
3	2.68	0.1198
4	2.6501	0.1211
5	2.6501	0.1211
6	2.7054	0.1187
7	2.6732	0.1201
8	2.7173	0.1181
9	2.7106	0.1184
10	2.6658	0.1204
average	2.67531	0.12
stdev	0.03391959	0.00151804
stdev %	1.26787523	1.26503306

Sample Na	RQ_L1_01_10	
	δ_{skel}	V_{skel}
Run		
1	2.346	0.1087
2	2.3428	0.1088
3	2.307	0.1105
4	2.3985	0.1063
5	2.2549	0.1131
6	2.2598	0.1128
7	2.2882	0.1114
8	2.2822	0.1117
9	2.2191	0.1149
10	2.279	0.1119
average	2.29775	0.11101
stdev	0.05243028	0.00251195
stdev %	2.28180944	2.26281346

Sample Na	RQ-L1_02_9	
	δ_{skel}	V_{skel}
Run		
1	4.0816	0.0649
2	3.999	0.0663
3	4.0337	0.0657
4	4.3188	0.0614
5	4.1758	0.0635
6	4.157	0.0637
7	3.862	0.0686
8	3.8968	0.068
9	3.8566	0.0687
10	4.004	0.0655
average	4.03853	0.06563
stdev	0.14922448	0.00238097
stdev %	3.69501983	3.62786255

Sample Na	RQ-L1_02_10	
	δ_{skel}	V_{skel}
Run		
1	2.6401	0.1049
2	2.6752	0.1035
3	2.6778	0.1034
4	2.6683	0.1038
5	2.6203	0.1057
6	2.6641	0.104
7	2.64	0.1049
8	2.6376	0.105
9	2.6068	0.1063
10	2.6405	0.1049
average	2.64707	0.10464
stdev	0.02367859	0.00095242
stdev %	0.89452077	0.91019095

Sample Na	RQ_L1_03_1	
	δ_{skel}	V_{skel}
Run		
1	1.9051	0.1958
2	1.9031	0.196
3	1.8899	0.1974
4	1.9066	0.1956
5	1.9078	0.1955
6	1.8983	0.1965
7	1.9261	0.1937
8	1.8586	0.2007
9	1.8771	0.1978
10	1.904	0.1959
average	1.89766	0.19649
stdev	0.01863612	0.0018526
stdev %	0.98205779	0.94284481

Sample Na	RQ_L1_03_2	
	δ_{skel}	V_{skel}
Run		
1	1.9509	0.1476
2	1.9853	0.1451
3	1.9242	0.1497
4	1.9423	0.1483
5	1.922	0.1498
6	1.9618	0.1468
7	1.9257	0.1496
8	1.9638	0.1466
9	1.9266	0.1495
10	1.9315	0.1491
average	1.94341	0.14821
stdev	0.02142566	0.00162512
stdev %	1.10247745	1.0964951

Sample Na	RQ_L1_03_3	
	δ_{skel}	V_{skel}
Run		
1	1.8736	0.1815
2	1.8267	0.1861
3	1.8569	0.1831
4	1.8172	0.1871
5	1.8407	0.1847
6	1.8484	0.1839
7	1.8755	0.1813
8	1.8186	0.187
9	1.8127	0.1876
10	1.8217	0.1866
average	1.8392	0.18489
stdev	0.02350967	0.00234921
stdev %	1.27825506	1.2705976

Sample Na	RQ_L1_03_4	
	δ_{skel}	V_{skel}
Run		
1	1.6793	0.128
2	1.7213	0.1249
3	1.7103	0.1257
4	1.7264	0.1245
5	1.7162	0.1253
6	1.6293	0.132
7	1.6108	0.1335
8	1.6907	0.1272
9	1.6613	0.1294
10	1.7004	0.1264
average	1.6846	0.12769
stdev	0.03960295	0.00307117
stdev %	2.35088128	2.40517991

Sample Na	RQ_L1_03_5	
	δ_{skel}	V_{skel}
Run		
1	1.8557	0.1466
2	1.8387	0.1479
3	1.8141	0.1499
4	1.8378	0.148
5	1.8187	0.1496
6	1.8188	0.1495
7	1.8077	0.1505
8	1.7936	0.1517
9	1.7809	0.1527
10	1.8198	0.1495
average	1.81858	0.14959
stdev	0.02194917	0.00180705
stdev %	1.20694023	1.2080046

Sample Na	RQ_L1_03_6	
	δ_{skel}	V_{skel}
Run		
1	1.6085	0.0976
2	1.6441	0.0955
3	1.5712	0.0999
4	1.6518	0.095
5	1.6273	0.0965
6	1.666	0.0942
7	1.6534	0.095
8	1.5594	0.1007
9	1.6307	0.0963
10	1.5325	0.1025
average	1.61449	0.09732
stdev	0.04537509	0.00279913
stdev %	2.81049061	2.87620926

Sample Na	RQ_L1_03_7	
	δ_{skel}	V_{skel}
Run		
1	1.4287	0.1141
2	1.4594	0.1117
3	1.4757	0.1105
4	1.4666	0.1111
5	1.421	0.1147
6	1.4445	0.1128
7	1.4555	0.112
8	1.4287	0.1141
9	1.4825	0.11
10	1.3873	0.1175
average	1.44499	0.11285
stdev	0.02900159	0.00228339
stdev %	2.00704421	2.02338871

Sample Na	RQ_L1_03_8	
	δ_{skel}	V_{skel}
Run		
1	1.8907	0.1148
2	1.8386	0.118
3	1.8778	0.1156
4	1.8598	0.1167
5	1.8462	0.1175
6	1.8833	0.1152
7	1.8735	0.1158
8	1.8355	0.1182
9	1.8776	0.1156
10	1.8676	0.1162
average	1.86506	0.11636
stdev	0.01927763	0.00119089
stdev %	1.03361996	1.02345424

Sample Na	RQ_L1_03_9	
	δ_{skel}	V_{skel}
Run		
1	2.1105	0.1237
2	2.1273	0.1227
3	2.1867	0.1194
4	2.1237	0.1229
5	2.1137	0.1235
6	2.1177	0.1232
7	2.0899	0.1249
8	2.0915	0.1248
9	2.0947	0.1246
10	2.1102	0.1237
average	2.11659	0.12334
stdev	0.02786716	0.00158409
stdev %	1.31660657	1.28432588

Sample Na	RQ_L1_03_10	
	δ_{skel}	V_{skel}
Run		
1	2.1274	0.1621
2	2.0585	0.1676
3	2.0415	0.169
4	2.1067	0.1638
5	2.0492	0.1684
6	2.0523	0.1681
7	2.0948	0.1647
8	2.0563	0.1678
9	2.0481	0.1684
10	2.069	0.1668
average	2.07038	0.16667
stdev	0.02908603	0.00232429
stdev %	1.40486448	1.39454731

Sample Nam	Y2-1	
Run	δ_{bulk}	V_{bulk}
1	0.482	
2	0.504	
3	0.497	
4	0.507	
5	0.512	
average	0.5004	0.2276
stdev	0.01163185	0.0053
stdev %	2.32451096	2.32864675
Dry weight	0.114	

Sample Nam	Y2-2	
Run	δ_{bulk}	V_{bulk}
1	0.917	
2	0.967	
3	0.917	
4	1.004	
5	0.959	
average	0.9528	0.189
stdev	0.03682662	0.0072
stdev %	3.86509454	3.80952381
Dry weight	0.18	

Sample Nam	Y2-3	
Run	δ_{bulk}	V_{bulk}
1	0.746	
2	0.757	
3	0.75	
4	0.772	
5	0.761	
average	0.7572	0.3115
stdev	0.0101341	0.0042
stdev %	1.33836514	1.34831461
Dry weight	0.236	

Sample Nam	
Run	
1	
2	
3	
4	
5	
average	
stdev	
stdev %	
Dry weight	

Sample Nam	Y5-1	
Run	δ_{bulk}	V_{bulk}
1	0.514	
2	0.501	
3	0.491	
4	0.508	
5	0.506	
average	0.504	0.4499
stdev	0.00863134	0.0075
stdev %	1.71256711	1.66703712
Dry weight	0.227	

Sample Nam	Y5-2	
Run	δ_{bulk}	V_{bulk}
1	0.37	
2	0.37	
3	0.371	
4	0.373	
5	0.37	
average	0.3708	0.3716
stdev	0.00130384	0.001
stdev %	0.35162904	0.26910657
Dry weight	0.138	

Sample Nam	Y5-3	
Run	δ_{bulk}	V_{bulk}
1	0.697	
2	0.703	
3	0.709	
4	0.713	
5	0.707	
average	0.7058	0.4205
stdev	0.00609918	0.7062
stdev %	0.86415136	167.942925
Dry weight	0.297	

Sample Nam	
Run	
1	
2	
3	
4	
5	
average	
stdev	
stdev %	
Dry weight	

Y2-4	
δ_{bulk}	V_{bulk}
0.54	
0.528	
0.532	
0.528	
0.53	
0.5316	0.2466
0.00497996	0.0022
0.93678703	0.89213301
0.133	

Sample Nam	Y2-5	
Run	δ_{bulk}	V_{bulk}
1	0.819	
2	0.832	
3	0.803	
4	0.827	
5	0.816	
average	0.8194	0.2305
stdev	0.01114899	0.0032
stdev %	1.36062863	1.38828633
Dry weight	0.189	

Sample Nam	Y2-6	
Run	δ_{bulk}	V_{bulk}
1	0.762	
2	0.756	
3	0.777	
4	0.772	
5	0.783	
average	0.770	0.2778
stdev	0.01097725	0.0042
stdev %	1.42561678	1.51187905
Dry weight	0.214	

Sample Nam	Y2-7
Run	δ_{bulk}
1	0.554
2	0.543
3	0.536
4	0.552
5	0.556
average	0.5482
stdev	0.00843801
stdev %	1.53922095
Dry weight	0.128

Y5-4	
δ_{bulk}	V_{bulk}
0.53	
0.544	
0.543	
0.548	
0.538	
0.5406	0.3622
0.00691375	0.0044
1.27890389	1.21479845
0.196	

Sample Nam	Y5-5	
Run	δ_{bulk}	V_{bulk}
1	0.623	
2	0.617	
3	0.614	
4	0.606	
5	0.612	
average	0.6144	0.3622
stdev	0.00626897	0.0039
stdev %	1.02034037	1.07675318
Dry weight	0.239	

Sample Nam	Y5-6	
Run	δ_{bulk}	V_{bulk}
1	0.596	
2	0.59	
3	0.583	
4	0.588	
5	0.59	
average	0.5894	0.3622
stdev	0.00466905	0.0027
stdev %	0.7921695	0.74544451
Dry weight	0.202	

Sample Nam	Y5-7
Run	δ_{bulk}
1	0.728
2	0.736
3	0.716
4	0.717
5	0.719
average	0.7232
stdev	0.00858487
stdev %	1.18706726
Dry weight	0.312

	Sample Name	Y2-8	
V_{bulk}	***Run***	δ_{bulk}	V_{bulk}
	1	0.676	
	2	0.678	
	3	0.709	
	4	0.68	
	5	0.705	
0.2332	***average***	0.6896	0.2405
0.0035	***stdev***	0.01600937	0.0055
1.50085763	***stdev %***	2.3215447	2.28690229
	Dry weight	0.166	

	Sample Name	Y2-9	
	Run	δ_{bulk}	V_{bulk}
	1	0.702	
	2	0.705	
	3	0.678	
	4	0.71	
	5	0.691	
	average	0.6972	0.2405
	stdev	0.01279453	0.0036
	stdev %	1.83513053	1.4968815
	Dry weight	0.141	

	Sample Name	Y2-10	
	Run	δ_{bulk}	V_{bulk}
	1	0.455	
	2	0.46	
	3	0.456	
	4	0.467	
	5	0.472	
	average	0.462	0.2939
	stdev	0.00731437	0.0046
	stdev %	1.58319684	1.56515822
	Dry weight	0.136	

	Sample Name	Y5-8	
V_{bulk}	***Run***	δ_{bulk}	V_{bulk}
	1	0.699	
	2	0.706	
	3	0.699	
	4	0.716	
	5	0.706	
0.4311	***average***	0.7052	0.2295
0.0049	***stdev***	0.00697854	0.0022
1.13662723	***stdev %***	0.98958289	0.95860566
	Dry weight	0.162	

	Sample Name	Y5-9	
	Run	δ_{bulk}	V_{bulk}
	1	0.882	
	2	0.897	
	3	0.885	
	4	0.905	
	5	0.888	
	average	0.8914	0.4597
	stdev	0.00944987	0.0047
	stdev %	1.06011529	1.02240592
	Dry weight	0.41	

	Sample Name	Y5-10	
	Run	δ_{bulk}	V_{bulk}
	1	0.531	
	2	0.539	
	3	0.535	
	4	0.539	
	5	0.534	
	average	0.5356	0.3096
	stdev	0.00343511	0.002
	stdev %	0.64135788	0.64599483
	Dry weight	0.166	

Sample Nam	KA01-1	
Run	δ_{bulk}	V_{bulk}
1	1.085	
2	1.039	
3	1.095	
4	1.08	
5	1.034	
average	1.0666	0.1753
stdev	0.02805887	0.0046
	2.63068317	2.62407302
Dry weight	0.187	

Sample Nam	KA01-2	
Run	δ_{bulk}	V_{bulk}
1	0.894	
2	0.91	
3	0.888	
4	0.92	
5	0.913	
average	0.905	0.2142
stdev	0.01345362	0.0032
stdev %	1.48658829	1.49393091
Dry weight	0.194	

Sample Nam	KA01-3	
Run	δ_{bulk}	V_{bulk}
1	0.946	
2	0.941	
3	0.931	
4	0.923	
5	0.952	
average	0.9386	0.2768
stdev	0.01163185	0.0034
stdev %	1.23927688	1.2283237
Dry weight	0.26	

Sample Nam	
Run	
1	
2	
3	
4	
5	
average	
stdev	
stdev %	
Dry weight	

Sample Nam	KR01-1	
Run	δ_{bulk}	V_{bulk}
1	0.641	
2	0.639	
3	0.641	
4	0.641	
5	0.643	
average	0.641	0.2835
stdev	0.00141421	0.0008
stdev %	0.22062614	0.28218695
Dry weight	0.182	

Sample Nam	KR01-2	
Run	δ_{bulk}	V_{bulk}
1	0.575	
2	0.582	
3	0.574	
4	0.582	
5	0.575	
average	0.5776	0.3821
stdev	0.00403733	0.026
stdev %	0.69898301	6.80450144
Dry weight	0.221	

Sample Nam	KR01-3	
Run	δ_{bulk}	V_{bulk}
1	0.622	
2	0.611	
3	0.606	
4	0.613	
5	0.598	
average	0.61	0.2736
stdev	0.00886002	0.0039
stdev %	1.45246272	1.4254386
Dry weight	0.167	

Sample Nam	
Run	
1	
2	
3	
4	
5	
average	
stdev	
stdev %	
Dry weight	

KA01-4	
δ_{bulk}	V_{bulk}
1.038	
1.049	
1.075	
1.078	
1.105	
1.069	0.2816
0.02633439	0.0069
2.46346007	2.45028409
0.301	

Sample Nam	KA01-5	
Run	δ_{bulk}	V_{bulk}
1	1.038	
2	1.017	
3	1.035	
4	1.029	
5	1.032	
average	1.0302	0.2619
stdev	0.00810555	0.002
stdev %	0.78679418	0.76365025
Dry weight	0.27	

Sample Nam	KA01-6	
Run	δ_{bulk}	V_{bulk}
1	1.296	
2	1.3	
3	1.303	
4	1.3	
5	1.3	
average	1.2998	0.2992
stdev	0.00248998	0.0005
stdev %	0.19156639	0.1671123
Dry weight	0.389	

Sample Nam	KA01-7
Run	δ_{bulk}
1	0.942
2	0.964
3	0.964
4	0.987
5	1
average	0.9714
stdev	0.0225566
stdev %	2.32207077
Dry weight	0.25

KR01-4	
δ_{bulk}	V_{bulk}
0.612	
0.611	
0.615	
0.618	
0.628	
0.6168	0.3196
0.00683374	0.0024
1.10793447	0.75093867
0.197	

Sample Nam	KR01-5	
Run	δ_{bulk}	V_{bulk}
1	0.565	
2	0.573	
3	0.57	
4	0.57	
5	0.563	
average	0.5682	0.2638
stdev	0.00408656	0.0018
stdev %	0.71921213	0.6823351
Dry weight	0.15	

Sample Nam	KR01-6	
Run	δ_{bulk}	V_{bulk}
1	0.501	
2	0.507	
3	0.5	
4	0.511	
5	0.494	
average	0.5026	0.2784
stdev	0.00658027	0.0035
stdev %	1.30924663	1.25718391
Dry weight	0.14	

Sample Nam	KR01-7
Run	δ_{bulk}
1	0.57
2	0.575
3	0.584
4	0.585
5	0.589
average	0.5806
stdev	0.00782943
stdev %	1.348507
Dry weight	0.155

	Sample Name	KA01-8		Sample Name	KA01-9		Sample Name	KA01-10	
V_{bulk}	***Run***	δ_{bulk}	V_{bulk}	***Run***	δ_{bulk}	V_{bulk}	***Run***	δ_{bulk}	V_{bulk}
	1	1.357		***1***	1.266		***1***	1.638	
	2	1.349		***2***	1.274		***2***	1.646	
	3	1.369		***3***	1.242		***3***	1.615	
	4	1.365		***4***	1.246		***4***	1.63	
	5	1.345		***5***	1.23		***5***	1.618	
0.2573	***average***	1.357	0.2607	***average***	1.2516	0.2396	***average***	1.6294	0.3178
0.006	***stdev***	0.01019804	0.0019	***stdev***	0.01802221	0.0034	***stdev***	0.01310725	0.0025
2.33190828	***stdev %***	0.75151356	0.72880706	***stdev %***	1.43993357	1.41903172	***stdev %***	0.80442187	0.78665828
	Dry weight	0.354		***Dry weight***	0.3		***Dry weight***	0.518	

	Sample Name	KR01-8		Sample Name	KR01-9		Sample Name	KR01-10	
V_{bulk}	***Run***	δ_{bulk}	V_{bulk}	***Run***	δ_{bulk}	V_{bulk}	***Run***	δ_{bulk}	V_{bulk}
	1	0.602		***1***	0.724		***1***	0.597	
	2	0.593		***2***	0.721		***2***	0.601	
	3	0.597		***3***	0.716		***3***	0.59	
	4	0.6		***4***	0.737		***4***	0.599	
	5	0.602		***5***	0.729		***5***	0.577	
0.2661	***average***	0.5988	0.3519	***average***	0.7254	0.2218	***average***	0.5928	0.2495
0.0035	***stdev***	0.00383406	0.0022	***stdev***	0.00801873	0.0023	***stdev***	0.00975705	0.004
1.315295	***stdev %***	0.64029023	0.62517761	***stdev %***	1.10542157	1.03697024	***stdev %***	1.6459259	1.60320641
	Dry weight	0.211		***Dry weight***	0.161		***Dry weight***	0.148	

Sample Nam	RQ_L1_01_1	
Run	δ_{bulk}	V_{bulk}
1	0.657	
2	0.653	
3	0.66	
4	0.664	
5	0.655	
average	0.6578	0.3965
stdev	0.00432435	0.0024
stdev %	0.65739581	0.60529634

Dry weight

Sample Nam	RQ_L1_01_2	
Run	δ_{bulk}	V_{bulk}
1	1.398	
2	1.388	
3	1.401	
4	1.398	
5	1.375	
average	1.392	0.367
stdev	0.01070047	0.0025
stdev %	0.76871173	0.68119891

Dry weight

Sample Nam	RQ_L1_01_3	
Run	δ_{bulk}	V_{bulk}
1	1.252	
2	1.255	
3	1.249	
4	1.249	
5	1.259	
average	1.2528	0.2944
stdev	0.00426615	0.001
stdev %	0.34052888	0.33967391

Dry weight

Sample Nam
Run
1
2
3
4
5
average
stdev
stdev %

Dry weight

Sample Nam	RQ-L1_02_1	
Run	δ_{bulk}	V_{bulk}
1	0.784	
2	0.781	
3	0.781	
4	0.768	
5	0.795	
average	0.7818	0.3887
stdev	0.00962808	0.0046
stdev %	1.23152775	1.18343195

Dry weight

Sample Nam	RQ-L1_02_2	
Run	δ_{bulk}	V_{bulk}
1	0.827	
2	0.822	
3	0.846	
4	0.839	
5	0.842	
average	0.8352	0.377
stdev	0.0102323	0.0046
stdev %	1.22513192	1.22015915

Dry weight

Sample Nam	RQ-L1_02_3	
Run	δ_{bulk}	V_{bulk}
1	0.706	
2	0.713	
3	0.73	
4	0.733	
5	0.718	
average	0.72	0.3373
stdev	0.01137981	0.0053
stdev %	1.58052871	1.57130151

Dry weight

Sample Nam
Run
1
2
3
4
5
average
stdev
stdev %

Dry weight

RQ_L1_01_4	
δ_{bulk}	V_{bulk}
0.676	
0.67	
0.673	
0.658	
0.67	
0.6694	0.3387
0.00684105	0.0035
1.02196781	1.03336286

Sample Nam	RQ_L1_01_5	
Run	δ_{bulk}	V_{bulk}
1	0.852	
2	0.839	
3	0.848	
4	0.837	
5	0.842	
average	0.8436	0.3495
stdev	0.00626897	0.0025
stdev %	0.74312129	0.71530758

Dry weight

Sample Nam	RQ_L1_01_6	
Run	δ_{bulk}	V_{bulk}
1	1.583	
2	1.55	
3	1.568	
4	1.565	
5	1.557	
average	1.5646	0.3245
stdev	0.01246194	0.0026
stdev %	0.7964938	0.80123267

Dry weight

Sample Nam	RQ_L1_01_7
Run	δ_{bulk}
1	1.389
2	1.389
3	1.409
4	1.415
5	1.406
average	1.4016
stdev	0.0119499
stdev %	0.85258957

Dry weight

RQ-L1_02_4	
δ_{bulk}	V_{bulk}
0.779	
0.774	
0.769	
0.776	
0.774	
0.7744	0.3575
0.00364692	0.0016
0.47093447	0.44755245

Sample Nam	RQ-L1_02_5	
Run	δ_{bulk}	V_{bulk}
1	0.797	
2	0.781	
3	0.799	
4	0.788	
5	0.784	
average	0.7898	0.3758
stdev	0.00791833	0.0037
stdev %	1.00257447	0.98456626

Dry weight

Sample Nam	RQ-L1_02_6	
Run	δ_{bulk}	V_{bulk}
1	0.714	
2	0.721	
3	0.727	
4	0.719	
5	0.715	
average	0.7192	0.3724
stdev	0.00521536	0.0027
stdev %	0.72516156	0.72502685

Dry weight

Sample Nam	RQ-L1_02_7
Run	δ_{bulk}
1	0.786
2	0.808
3	0.815
4	0.808
5	0.795
average	0.8024
stdev	0.01167476
stdev %	1.45497995

Dry weight

	Sample Nam	RQ_L1_01_8	
V_{bulk}	***Run***	δ_{bulk}	V_{bulk}
	1	1.285	
	2	1.294	
	3	1.303	
	4	1.288	
	5	1.3	
0.3665	***average***	1.294	0.3415
0.0032	***stdev***	0.00764853	0.0019
0.87312415	***stdev %***	0.59107645	0.55636896

Dry weight

	Sample Nam	RQ_L1_01_9	
	Run	δ_{bulk}	V_{bulk}
	1	0.897	
	2	0.899	
	3	0.917	
	4	0.911	
	5	0.927	
	average	0.9102	0.3525
	stdev	0.01253794	0.0048
	stdev %	1.37749312	1.36170213

Dry weight

	Sample Nam	RQ_L1_01_10	
	Run	δ_{bulk}	V_{bulk}
	1	0.874	
	2	0.886	
	3	0.888	
	4	0.881	
	5	0.884	
	average	0.8826	0.2887
	stdev	0.00545894	0.0017
	stdev %	0.61850642	0.58884655

Dry weight

	Sample Nam	RQ-L1_02_8	
V_{bulk}	***Run***	δ_{bulk}	V_{bulk}
	1	0.747	
	2	0.762	
	3	0.762	
	4	0.764	
	5	0.767	
0.4633	***average***	0.7604	0.3468
0.0068	***stdev***	0.00776531	0.0035
1.46773149	***stdev %***	1.0212135	1.00922722

Dry weight

	Sample Nam	RQ-L1_02_9	
	Run	δ_{bulk}	V_{bulk}
	1	0.71	
	2	0.698	
	3	0.71	
	4	0.704	
	5	0.722	
	average	0.7088	0.3736
	stdev	0.00889944	0.0045
	stdev %	1.25556408	1.20449679

Dry weight

	Sample Nam	RQ-L1_02_10	
	Run	δ_{bulk}	V_{bulk}
	1	0.791	
	2	0.793	
	3	0.796	
	4	0.793	
	5	0.807	
	average	0.796	0.3478
	stdev	0.00640312	0.0027
	stdev %	0.80441259	0.77630822

Dry weight

Sample Nam	RQ_L1_03_1	
Run	δ_{bulk}	V_{bulk}
1	1.012	
2	1.029	
3	1.042	
4	1.047	
5	1.047	
average	1.0354	0.3601
stdev	0.01501	0.0052
stdev %	1.44968096	1.44404332
Dry weight	0.373	

Sample Nam	RQ_L1_03_2	
Run	δ_{bulk}	V_{bulk}
1	0.803	
2	0.806	
3	0.789	
4	0.801	
5	0.8	
average	0.7998	0.3598
stdev	0.00645755	0.0029
stdev %	0.80739606	0.80600334
Dry weight	0.288	

Sample Nam	RQ_L1_03_3	
Run	δ_{bulk}	V_{bulk}
1	0.744	
2	0.753	
3	0.76	
4	0.772	
5	0.77	
average	0.7598	0.4473
stdev	0.01171324	0.007
stdev %	1.54162153	1.56494523
Dry weight	0.34	

Sample Nam
Run
1
2
3
4
5
average
stdev
stdev %
Dry weight

RQ_L1_03_4	
δ_{bulk}	V_{bulk}
0.873	
0.876	
0.887	
0.887	
0.884	
0.8814	0.2438
0.00650385	0.0018
0.73789937	0.73831009
0.215	

Sample Nam	RQ_L1_03_5	
Run	δ_{bulk}	V_{bulk}
1	0.85	
2	0.848	
3	0.844	
4	0.842	
5	0.846	
average	0.846	0.3215
stdev	0.00316228	0.0012
stdev %	0.37379169	0.37325039
Dry weight	0.272	

Sample Nam	RQ_L1_03_6	
Run	δ_{bulk}	V_{bulk}
1	0.504	
2	0.5	
3	0.504	
4	0.51	
5	0.51	
average	0.5056	0.3104
stdev	0.0043359	0.0027
stdev %	0.8575745	0.86984536
Dry weight	0.157	

Sample Nam	RQ_L1_03_7
Run	δ_{bulk}
1	0.628
2	0.625
3	0.632
4	0.625
5	0.623
average	0.6266
stdev	0.00350714
stdev %	0.55970884
Dry weight	0.163

	Sample Name	RQ_L1_03_8		Sample Name	RQ_L1_03_9		Sample Name	RQ_L1_03_10	
V_{bulk}	***Run***	δ_{bulk}	V_{bulk}	***Run***	δ_{bulk}	V_{bulk}	***Run***	δ_{bulk}	V_{bulk}
	1	0.714		***1***	0.904		***1***	1.003	
	2	0.717		***2***	0.87		***2***	0.973	
	3	0.714		***3***	0.902		***3***	0.973	
	4	0.719		***4***	0.907		***4***	0.977	
	5	0.708		***5***	0.919		***5***	0.964	
0.2599	***average***	0.7144	0.3035	***average***	0.9004	0.289	***average***	0.978	0.3527
0.0015	***stdev***	0.00415933	0.0017	***stdev***	0.0182291	0.006	***stdev***	0.01476482	0.0052
0.57714506	***stdev %***	0.58221261	0.5601318	***stdev %***	2.02455549	2.07612457	***stdev %***	1.50969561	1.4743408
	Dry weight	0.217		***Dry weight***	0.261		***Dry weight***	0.345	

Sample Na	Taupo Y2-1	
0.109g	δ_{skel}	V_{skel}
Run		
1	2.0767	0.0525
2	2.087	0.0522
3	2.093	0.0521
4	2.076	0.0525
5	2.0283	0.0537
6	2.0909	0.0521
7	2.0348	0.0536
8	2.0632	0.0528
9	2.0779	0.0525
10	2.0403	0.0534
average	2.06681	0.05274
stdev	0.02404304	0.00061319
stdev %	1.16329212	1.16266285

Sample Na	Taupo Y2-2	
0.178g	δ_{skel}	V_{skel}
Run		
1	2.2685	0.0785
2	2.2218	0.0801
3	2.2467	0.0792
4	2.2331	0.0797
5	2.2261	0.08
6	2.2529	0.079
7	2.2159	0.0803
8	2.2007	0.0809
9	2.2244	0.08
10	2.2081	0.0806
average	2.22982	0.07983
stdev	0.02093789	0.00074244
stdev %	0.93899449	0.93003058

Sample Na	Taupo Y2-3	
0.23g	δ_{skel}	V_{skel}
Run		
1	2.1874	0.1051
2	2.2078	0.1042
3	2.2495	0.1022
4	2.2278	0.1032
5	2.2799	0.1009
6	2.2591	0.1018
7	2.2518	0.1021
8	2.1534	0.1068
9	2.2036	0.1044
10	2.1678	0.1061
average	2.21881	0.10368
stdev	0.04174785	0.00196005
stdev %	1.88154249	1.89047584

Sample Na	Taupo Y2-4	
0.128g	δ_{skel}	V_{skel}
Run		
1	2.6971	0.0475
2	2.7038	0.0473
3	2.5737	0.0497
4	2.6254	0.0488
5	2.5726	0.0498
6	2.5982	0.0493
7	2.5852	0.0495
8	2.4895	0.0514
9	2.5383	0.0504
10	2.5575	0.05
average	2.59413	0.04937
stdev	0.06665963	0.00124726
stdev %	2.56963351	2.52635947

Sample Na	Taupo Y5_1	
	δ_{skel}	V_{skel}
Run		
1	2.6081	0.0855
2	2.5431	0.0877
3	2.676	0.0855
4	2.5747	0.0866
5	2.5721	0.0867
6	2.6029	0.0857
7	2.4988	0.0892
8	2.5712	0.0867
9	2.4092	0.0926
10	2.4847	0.0898
average	2.55408	0.0876
stdev	0.07467654	0.00229637
stdev %	2.92381382	2.62143145

Sample Na	Taupo Y5_2	
	δ_{skel}	V_{skel}
Run		
1	3.2396	0.0423
2	3.0761	0.0445
3	3.0654	0.0447
4	3.0106	0.0455
5	3.0114	0.0455
6	2.9002	0.0472
7	2.79	0.0491
8	2.8726	0.0477
9	2.9171	0.047
10	2.7278	0.0502
average	2.987	0.04594444
stdev	0.1338661	0.00203231
stdev %	4.48162367	4.4234042

Sample Na	Taupo Y5_3	
	δ_{skel}	V_{skel}
Run		
1	2.519	0.1159
2	2.4883	0.1174
3	2.5461	0.1147
4	2.4451	0.1194
5	2.43	0.1202
6	2.4797	0.1178
7	2.4575	0.1188
8	2.4631	0.1185
9	2.5041	0.1166
10	2.4991	0.1168
average	2.4832	0.11761
stdev	0.03545307	0.00167561
stdev %	1.42771696	1.42471673

Sample Na	Taupo Y5_4	
	δ_{skel}	V_{skel}
Run		
1	2.5665	0.074
2	2.5463	0.0746
3	2.4475	0.0776
4	2.4688	0.077
5	2.4519	0.0775
6	2.4656	0.0771
7	2.4608	0.0772
8	2.5524	0.0744
9	2.3961	0.0793
10	2.6282	0.0723
average	2.49841	0.0761
stdev	0.07093046	0.00214631
stdev %	2.83902394	2.82038722

Sample Na	Taupo Y2-5	
0.181g	δ_{skel}	V_{skel}
Run		
1	2.2313	0.0811
2	2.3323	0.0811
3	2.1622	0.0837
4	2.134	0.0848
5	2.1444	0.0844
6	2.0931	0.0865
7	2.2581	0.0802
8	2.2162	0.0817
9	2.2987	0.0787
10	2.1509	0.0842
average	2.20212	0.08264
stdev	0.07784057	0.00243411
stdev %	3.53480169	2.9454374

Sample Na	Taupo Y2-6	
0.206g	δ_{skel}	V_{skel}
Run		
1	2.1055	0.0978
2	2.0542	0.1003
3	2.1119	0.0975
4	2.0944	0.0984
5	2.055	0.1002
6	2.0535	0.1003
7	2.1245	0.097
8	2.0606	0.1
9	2.0439	0.1008
10	2.0331	0.1013
average	2.07366	0.09936
stdev	0.03218969	0.0015313
stdev %	1.55231271	1.54116647

Sample Na	Taupo Y2-7	
0.122g	δ_{skel}	V_{skel}
Run		
1	2.1	0.0581
2	2.1409	0.057
3	2.0842	0.0585
4	2.1126	0.0577
5	2.0324	0.06
6	2.0587	0.0593
7	1.9802	0.0616
8	2.0589	0.0593
9	1.9966	0.0611
10	2.0044	0.0609
average	2.05689	0.05935
stdev	0.05337926	0.00154506
stdev %	2.59514415	2.60330889

Sample Na	Taupo Y2-8	
0.163g	δ_{skel}	V_{skel}
Run		
1	2.1133	0.0653
2	2.0927	0.0659
3	2.0531	0.0672
4	2.0894	0.066
5	2.0722	0.0666
6	2.0904	0.066
7	2.0617	0.0669
8	2.0895	0.066
9	2.0561	0.0671
10	2.0685	0.0667
average	2.07869	0.06637
stdev	0.01932928	0.00061833
stdev %	0.92987787	0.93164244

Sample Na	Taupo Y5_5	
	δ_{skel}	V_{skel}
Run		
1	2.6587	0.088
2	2.6336	0.0889
3	2.5436	0.092
4	2.5351	0.0923
5	2.5651	0.0912
6	2.5556	0.0916
7	2.516	0.093
8	2.4412	0.0959
9	2.4361	0.0961
10	2.4309	0.0963
average	2.53159	0.09253
stdev	0.07894384	0.00289062
stdev %	3.11835013	3.12397817

Sample Na	Taupo Y5_6	
	δ_{skel}	V_{skel}
Run		
1	2.9293	0.0686
2	2.8295	0.071
3	2.8601	0.0703
4	2.9344	0.0685
5	2.69	0.0746
6	2.7018	0.0744
7	2.7083	0.0742
8	2.7413	0.0733
9	2.7053	0.0743
10	2.6712	0.0752
average	2.77712	0.07244
stdev	0.1017538	0.00258938
stdev %	3.66400431	3.57451687

Sample Na	Taupo Y5_7	
	δ_{skel}	V_{skel}
Run		
1	2.5474	0.1213
2	2.5509	0.1211
3	2.5036	0.1234
4	2.5157	0.1228
5	2.5067	0.1233
6	2.5328	0.122
7	2.5428	0.1215
8	2.488	0.1242
9	2.5058	0.1233
10	2.553	0.121
average	2.52467	0.12239
stdev	0.02345241	0.00114741
stdev %	0.92892983	0.93750515

Sample Na	Taupo Y5_8	
	δ_{skel}	V_{skel}
Run		
1	2.4642	0.0649
2	2.501	0.064
3	2.4922	0.0642
4	2.4078	0.0665
5	2.434	0.0657
6	2.533	0.0632
7	2.4936	0.0642
8	2.5569	0.0626
9	2.5805	0.062
10	2.576	0.0621
average	2.50392	0.06394
stdev	0.05837663	0.0014983
stdev %	2.33140946	2.34328328

Sample Na	Taupo Y2-9	
0.138g	δ_{skel}	V_{skel}
Run		
1	1.4506	0.0786
2	1.6064	0.071
3	1.5747	0.0724
4	1.5963	0.0714
5	1.4709	0.0775
6	1.5623	0.073
7	1.5183	0.0751
8	1.4638	0.0779
9	1.5016	0.0759
10	1.4546	0.0784
average	1.51995	0.07512
stdev	0.06061924	0.00297351
stdev %	3.98823877	3.95835024

Sample Na	Taupo Y2-10	
0.134g	δ_{skel}	V_{skel}
Run		
1	2.1968	0.061
2	2.2124	0.0606
3	2.1929	0.0611
4	2.1665	0.0619
5	2.2182	0.0604
6	2.2134	0.0605
7	2.1918	0.0611
8	2.1959	0.061
9	2.1523	0.0623
10	2.2341	0.06
average	2.19743	0.06099
stdev	0.02427518	0.00069033
stdev %	1.10470795	1.13187413

Sample Na	Taupo Y5_9	
	δ_{skel}	V_{skel}
Run		
1	2.5332	0.1603
2	2.5413	0.1598
3	2.5163	0.1614
4	2.487	0.1632
5	2.4698	0.1644
6	2.4813	0.1636
7	2.4443	0.1661
8	2.455	0.1654
9	2.4656	0.1647
10	2.4123	0.1683
average	2.48061	0.16372
stdev	0.04047876	0.00265865
stdev %	1.63180663	1.62390339

Sample Na	Taupo Y5_10	
	δ_{skel}	V_{skel}
Run		
1	2.6915	0.0606
2	2.6581	0.0613
3	2.6753	0.0609
4	2.6259	0.0621
5	2.6494	0.0615
6	2.569	0.0635
7	2.5869	0.063
8	2.6065	0.0625
9	2.599	0.0627
10	2.5731	0.0633
average	2.62347	0.06214
stdev	0.0433592	0.0010222
stdev %	1.65274231	1.64499206

Sample Na	KA01_1	
	δ_{skel}	V_{skel}
Run		
1	2.7452	0.0659
2	2.6842	0.0674
3	2.6831	0.0675
4	2.6465	0.0684
5	2.688	0.0673
6	2.7051	0.0669
7	2.6665	0.0679
8	2.6255	0.0689
9	2.6467	0.0648
10	2.6404	0.0686
average	2.67312	0.06736
stdev	0.0356694	0.00125627
stdev %	1.33437338	1.86501358

Sample Na	KA01_2	
	δ_{skel}	V_{skel}
Run		
1	2.5481	0.0754
2	2.5561	0.0751
3	2.5628	0.0749
4	2.5218	0.0761
5	2.6207	0.0733
6	2.5842	0.0743
7	2.5538	0.0752
8	2.491	0.0771
9	2.4587	0.0781
10	2.4999	0.0768
average	2.53971	0.07563
stdev	0.04766822	0.00141818
stdev %	1.87691569	1.87514963

Sample Na	KA01_3	
	δ_{skel}	V_{skel}
Run		
1	2.4678	0.1041
2	2.468	0.1041
3	2.5275	0.1017
4	2.5016	0.1027
5	2.4768	0.1038
6	2.448	0.105
7	2.426	0.1059
8	2.4403	0.1053
9	2.4761	0.1038
10	2.4462	0.1051
average	2.46783	0.10415
stdev	0.03021872	0.00126337
stdev %	1.22450586	1.21303208

Sample Na	KA01_4	
	δ_{skel}	V_{skel}
Run		
1	2.9977	0.0994
2	2.8881	0.1032
3	2.8771	0.1036
4	2.8089	0.1061
5	2.8014	0.1064
6	2.7356	0.1089
7	2.7122	0.1099
8	2.7483	0.1084
9	2.687	0.1109
10	2.6244	0.1136
average	2.78807	0.10704
stdev	0.11034425	0.00418548
stdev %	3.95772881	3.91019949

Sample Na	KR01_1	
	δ_{skel}	V_{skel}
Run		
1	2.4242	0.073
2	2.472	0.0716
3	2.3489	0.0754
4	2.444	0.0724
5	2.3936	0.0739
6	2.372	0.0746
7	2.3814	0.0743
8	2.3972	0.0738
9	2.3224	0.0762
10	2.3454	0.0755
average	2.39011	0.07407
stdev	0.04657182	0.00144611
stdev %	1.948522	1.95235032

Sample Na	KR01_2	
	δ_{skel}	V_{skel}
Run		
1	2.6758	0.0796
2	2.6707	0.0798
3	2.616	0.0814
4	2.582	0.0825
5	2.6176	0.0814
6	2.5716	0.0828
7	2.6918	0.0791
8	2.5837	0.0824
9	2.5396	0.0839
10	2.6174	0.0814
average	2.61662	0.08143
stdev	0.04980189	0.00154564
stdev %	1.90329096	1.89811989

Sample Na	KR01_3	
	δ_{skel}	V_{skel}
Run		
1	2.8934	0.0553
2	2.8343	0.0565
3	2.9387	0.0544
4	2.8055	0.057
5	2.8536	0.0561
6	2.7994	0.0572
7	2.7507	0.0582
8	2.8378	0.0564
9	2.9111	0.055
10	2.7515	0.0582
average	2.8376	0.05643
stdev	0.06364703	0.0012798
stdev %	2.24298809	2.26794317

Sample Na	KR01_4	
	δ_{skel}	V_{skel}
Run		
1	2.3636	0.0808
2	2.4134	0.0791
3	2.4226	0.0788
4	2.4057	0.0794
5	2.4284	0.0787
6	2.3949	0.0798
7	2.3256	0.0821
8	2.336	0.0818
9	2.3434	0.0815
10	2.3215	0.0823
average	2.37551	0.08043
stdev	0.04200517	0.00142677
stdev %	1.76825904	1.77392504

Sample Na	KA01_5	
	δ_{skel}	V_{skel}
Run		
1	2.7316	0.0974
2	2.8192	0.0944
3	2.8492	0.0934
4	2.8597	0.093
5	2.888	0.0921
6	2.9217	0.091
7	2.8719	0.0926
8	2.8808	0.0923
9	2.9046	0.0914
10	2.8503	0.0933
average	2.8577	0.09309
stdev	0.05319087	0.00181074
stdev %	1.86131757	1.94514939

Sample Na	KA01_6	
	δ_{skel}	V_{skel}
Run		
1	2.4898	0.1542
2	2.4397	0.1574
3	2.4378	0.1575
4	2.4565	0.1563
5	2.4586	0.1562
6	2.4455	0.157
7	2.4614	0.156
8	2.4768	0.155
9	2.484	0.1546
10	2.531	0.1517
average	2.46811	0.15559
stdev	0.02840366	0.00177479
stdev %	1.15082617	1.14068554

Sample Na	KA01_7	
	δ_{skel}	V_{skel}
Run		
1	3.358	0.0742
2	3.3229	0.0746
3	3.2418	0.0768
4	3.1863	0.0781
5	3.2621	0.0763
6	3.2784	0.076
7	3.2577	0.0764
8	3.277	0.076
9	3.2619	0.0763
10	3.1889	0.0781
average	3.2635	0.07628
stdev	0.05259586	0.0012568
stdev %	1.61163964	1.64761891

Sample Na	KA01_8	
	δ_{skel}	V_{skel}
Run		
1	2.9127	0.1188
2	2.8316	0.1222
3	2.8334	0.1221
4	2.8335	0.1221
5	2.8403	0.1218
6	2.866	0.1207
7	2.8211	0.1226
8	2.8476	0.1215
9	2.8351	0.122
10	2.8256	0.1225
average	2.84469	0.12163
stdev	0.02696526	0.00113142
stdev %	0.94791572	0.93021455

Sample Na	KR01_5	
	δ_{skel}	V_{skel}
Run		
1	3.0207	0.0477
2	3.0597	0.0471
3	2.8869	0.0499
4	2.8122	0.0512
5	2.8559	0.0504
6	2.9883	0.0482
7	2.8156	0.0511
8	2.9073	0.0495
9	2.8952	0.0497
10	2.876	0.0501
average	2.91178	0.04949
stdev	0.08438189	0.00139479
stdev %	2.89794881	2.81833077

Sample Na	KR01_6	
	δ_{skel}	V_{skel}
Run		
1	2.278	0.0588
2	2.3347	0.0574
3	2.3173	0.0578
4	2.3124	0.058
5	2.2467	0.0596
6	2.3272	0.0576
7	2.3127	0.0579
8	2.357	0.0569
9	2.2517	0.0595
10	2.2724	0.059
average	2.30101	0.05825
stdev	0.03684292	0.00091924
stdev %	1.60116311	1.57809239

Sample Na	KR01_7	
	δ_{skel}	V_{skel}
Run		
1	2.7533	0.0534
2	2.8612	0.0514
3	2.7303	0.0538
4	2.867	0.0513
5	2.8368	0.0518
6	2.7546	0.0538
7	2.7802	0.0529
8	2.8026	0.0525
9	2.762	0.0532
10	2.8131	0.0523
average	2.79611	0.05264
stdev	0.04778646	0.00093238
stdev %	1.7090335	1.77123949

Sample Na	KR01_8	
	δ_{skel}	V_{skel}
Run		
1	2.662	0.077
2	2.664	0.0769
3	2.6138	0.0784
4	2.669	0.0768
5	2.6531	0.0773
6	2.7348	0.075
7	2.6175	0.0783
8	2.5753	0.0796
9	2.5323	0.081
10	2.5674	0.0798
average	2.62892	0.07801
stdev	0.05970373	0.00176978
stdev %	2.27103631	2.26865419

Sample Na	KA01_9	
	δ_{skel}	V_{skel}
Run		
1	2.9217	0.101
2	2.7728	0.1064
3	2.8378	0.104
4	2.8662	0.1029
5	2.791	0.1057
6	2.8038	0.1052
7	2.8293	0.1043
8	2.8515	0.1035
9	2.7673	0.1066
10	2.7544	0.1071
average	2.81958	0.10467
stdev	0.05194343	0.00190091
stdev %	1.84223985	1.8160946

Sample Na	KA01_10	
	δ_{skel}	V_{skel}
Run		
1	2.5677	0.1963
2	2.5431	0.1982
3	2.5415	0.1983
4	2.5727	0.1959
5	2.55	0.1976
6	2.542	0.1983
7	2.5392	0.1985
8	2.5038	0.2013
9	2.529	0.1993
10	2.517	0.2002
average	2.5406	0.19839
stdev	0.02084312	0.00162717
stdev %	0.82040139	0.8201851

Sample Na	KR01_9	
	δ_{skel}	V_{skel}
Run		
1	2.3778	0.0635
2	2.3252	0.0649
3	2.3549	0.0641
4	2.2848	0.0661
5	2.4128	0.0626
6	2.3906	0.0632
7	2.2764	0.0663
8	2.2575	0.0669
9	2.2851	0.0661
10	2.2864	0.066
average	2.32515	0.06497
stdev	0.05508588	0.00151954
stdev %	2.3691322	2.33883239

Sample Na	KR01_10	
	δ_{skel}	V_{skel}
Run		
1	2.226	0.0647
2	2.3071	0.0624
3	2.2685	0.0635
4	2.204	0.0653
5	2.3225	0.062
6	2.273	0.0634
7	2.2866	0.063
8	2.2528	0.0639
9	2.1932	0.0657
10	2.2821	0.0631
average	2.26158	0.0637
stdev	0.04261324	0.00120922
stdev %	1.88422442	1.89831053

Sample Na	RQ_L1_01_1	
	δ_{skel}	V_{skel}
Run		
1	4.1375	0.0607
2	4.1991	0.0598
3	3.8441	0.0653
4	3.683	0.0682
5	4.2159	0.0595
6	3.9457	0.0636
7	3.928	0.0639
8	4.123	0.0609
9	3.9338	0.0638
10	4.0825	0.0615
average	4.00926	0.06272
stdev	0.17112256	0.00274461
stdev %	4.26818323	4.37597398

Sample Na	RQ_L1_01_2	
	δ_{skel}	V_{skel}
Run		
1	2.8622	0.1565
2	2.8559	0.1569
3	2.9705	0.1508
4	2.8312	0.1582
5	2.8539	0.157
6	2.9135	0.1538
7	2.8944	0.1548
8	2.8929	0.1549
9	2.8408	0.1577
10	2.9059	0.1542
average	2.88212	0.15548
stdev	0.04191138	0.00223249
stdev %	1.4541859	1.43586789

Sample Na	RQ_L1_01_3	
	δ_{skel}	V_{skel}
Run		
1	2.8507	0.1256
2	2.7522	0.1301
3	2.6292	0.1362
4	2.7255	0.1314
5	2.7945	0.1281
6	2.7623	0.1296
7	2.6681	0.1342
8	2.6836	0.1334
9	2.6373	0.1357
10	2.6778	0.1337
average	2.71812	0.1318
stdev	0.07175353	0.00344028
stdev %	2.63982185	2.61023082

Sample Na	RQ_L1_01_4	
	δ_{skel}	V_{skel}
Run		
1	3.3455	0.0658
2	3.3753	0.0652
3	3.3595	0.0655
4	3.4889	0.0631
5	3.4493	0.0638
6	3.5139	0.0626
7	3.1422	0.07
8	3.2351	0.068
9	3.5713	0.0616
10	3.3426	0.0658
average	3.38236	0.06514
stdev	0.12983199	0.00253298
stdev %	3.83850291	3.88852077

Sample Na	RQ-L1_02_1	
	δ_{skel}	V_{skel}
Run		
1	2.7173	0.1093
2	2.5697	0.1156
3	2.7162	0.1093
4	2.5824	0.115
5	2.7445	0.1082
6	2.6037	0.1108
7	2.7488	0.108
8	2.6807	0.1108
9	2.6102	0.1138
10	2.608	0.1139
average	2.65815	0.11147
stdev	0.07023078	0.00286552
stdev %	2.64209252	2.57066747

Sample Na	RQ-L1_02_2	
	δ_{skel}	V_{skel}
Run		
1	2.3384	0.1326
2	2.4489	0.1266
3	2.4053	0.1289
4	2.4983	0.1241
5	2.4581	0.1261
6	2.4094	0.1287
7	2.3722	0.1307
8	2.3757	0.1305
9	2.3864	0.1299
10	2.2924	0.1352
average	2.39851	0.12933
stdev	0.06004125	0.00324107
stdev %	2.50327301	2.50604903

Sample Na	RQ-L1_02_3	
	δ_{skel}	V_{skel}
Run		
1	2.4844	0.0938
2	2.5163	0.0926
3	2.4259	0.096
4	2.3452	0.0994
5	2.4375	0.0956
6	2.3483	0.0992
7	2.2789	0.1023
8	2.5254	0.0923
9	2.5064	0.093
10	2.4667	0.0945
average	2.4335	0.09587
stdev	0.08389131	0.00338002
stdev %	3.44735177	3.5256316

Sample Na	RQ-L1_02_4	
	δ_{skel}	V_{skel}
Run		
1	2.3636	0.1151
2	2.2778	0.1194
3	2.2955	0.1185
4	2.2396	0.1214
5	2.3189	0.1173
6	2.2696	0.1198
7	2.2159	0.1228
8	2.2271	0.1221
9	2.221	0.1225
10	2.332	0.1166
average	2.2761	0.11955
stdev	0.05102037	0.00266552
stdev %	2.24156963	2.22962826

Sample Na	RQ_L1_01_5	
	δ_{skel}	V_{skel}
Run		
1	2.7884	0.1026
2	2.7845	0.1027
3	2.8318	0.101
4	2.8341	0.1009
5	2.7907	0.1025
6	2.7901	0.1025
7	2.7908	0.1025
8	2.7241	0.1025
9	2.7537	0.1038
10	2.7817	0.1028
average	2.78699	0.10238
stdev	0.03225728	0.00084958
stdev %	1.1574236	0.82982522

Sample Na	RQ_L1_01_6	
	δ_{skel}	V_{skel}
Run		
1	2.8208	0.1755
2	2.8514	0.1736
3	2.8769	0.1721
4	2.7578	0.1795
5	2.8089	0.1762
6	2.9157	0.1698
7	2.7859	0.1777
8	2.792	0.1788
9	2.9423	0.1682
10	2.9449	0.1681
average	2.84966	0.17395
stdev	0.06756207	0.00426751
stdev %	2.37088191	2.45329861

Sample Na	RQ_L1_01_7	
	δ_{skel}	V_{skel}
Run		
1	2.6511	0.1909
2	2.6527	0.1908
3	2.6063	0.1941
4	2.6099	0.1939
5	2.5898	0.1954
6	2.6035	0.1944
7	2.5749	0.1965
8	2.6057	0.1942
9	2.6089	0.194
10	2.618	0.1933
average	2.61208	0.19375
stdev	0.02414985	0.0017684
stdev %	0.92454469	0.9127202

Sample Na	RQ_L1_01_8	
	δ_{skel}	V_{skel}
Run		
1	2.4342	0.1799
2	2.4416	0.1794
3	2.4768	0.1768
4	2.464	0.17778
5	2.4086	0.1818
6	2.4085	0.1819
7	2.395	0.1829
8	2.4309	0.1802
9	2.4081	0.1819
10	2.4548	0.1784
average	2.43225	0.180098
stdev	0.02726105	0.00202518
stdev %	1.12081623	1.12449042

Sample Na	RQ-L1_02_5	
	δ_{skel}	V_{skel}
Run		
1	4.37	0.0663
2	4.567	0.0635
3	4.5726	0.0634
4	4.561	0.0642
5	4.5503	0.0637
6	4.5161	0.0642
7	4.6973	0.0617
8	4.5854	0.0633
9	4.5054	0.0644
10	4.5939	0.0631
average	4.5519	0.06378
stdev	0.08252998	0.00117075
stdev %	1.81308862	1.83561421

Sample Na	RQ-L1_02_6	
	δ_{skel}	V_{skel}
Run		
1	2.8369	0.0913
2	2.7711	0.0935
3	2.7688	0.0935
4	2.7781	0.0932
5	2.699	0.096
6	2.6566	0.0975
7	2.6648	0.0972
8	2.6687	0.0971
9	2.7865	0.0929
10	2.7987	0.0925
average	2.74292	0.09447
stdev	0.06458056	0.00225539
stdev %	2.35444555	2.38741252

Sample Na	RQ-L1_02_7	
	δ_{skel}	V_{skel}
Run		
1	2.6073	0.1396
2	2.73	0.1333
3	2.6838	0.1356
4	2.614	0.1393
5	2.6175	0.1391
6	2.6166	0.1391
7	2.5623	0.1404
8	2.6393	0.1379
9	2.6965	0.135
10	2.5493	0.1428
average	2.63166	0.13821
stdev	0.05732801	0.00282625
stdev %	2.17839719	2.04489258

Sample Na	RQ-L1_02_8	
	δ_{skel}	V_{skel}
Run		
1	2.9467	0.0872
2	2.9066	0.0884
3	2.7452	0.0936
4	2.9381	0.0875
5	2.828	0.0909
6	2.7202	0.0945
7	2.738	0.0939
8	2.6876	0.0956
9	2.9181	0.0881
10	2.9216	0.088
average	2.83501	0.09077
stdev	0.10277595	0.0033153
stdev %	3.62524129	3.65241955

Sample Na	RQ_L1_01_9	
	δ_{skel}	V_{skel}
Run		
1	2.6478	0.1167
2	2.6604	0.1161
3	2.5133	0.1229
4	2.5003	0.1236
5	2.6295	0.1175
6	2.6105	0.1184
7	2.4943	0.1236
8	2.6004	0.1188
9	2.6415	0.117
10	2.545	0.1214
average	2.5843	0.1196
stdev	0.06482925	0.00298217
stdev %	2.5085805	2.49345254

Sample Na	RQ_L1_01_10	
	δ_{skel}	V_{skel}
Run		
1	2.3696	0.103
2	2.3619	0.102
3	2.197	0.1111
4	2.3574	0.1035
5	2.2367	0.1091
6	2.2271	0.1096
7	2.2207	0.1099
8	2.2108	0.1104
9	2.3418	0.1042
10	2.2862	0.1067
average	2.28092	0.10695
stdev	0.07027183	0.00348178
stdev %	3.08085483	3.25551937

Sample Na	RQ-L1_02_9	
	δ_{skel}	V_{skel}
Run		
1	2.9267	0.0871
2	2.928	0.0871
3	2.8019	0.091
4	2.8952	0.0881
5	2.8287	0.0901
6	2.7436	0.0929
7	2.7559	0.0925
8	2.9813	0.0855
9	2.675	0.0953
10	2.9521	0.0864
average	2.84884	0.0896
stdev	0.1028638	0.00326258
stdev %	3.61072561	3.64127509

Sample Na	RQ-L1_02_10	
	δ_{skel}	V_{skel}
Run		
1	2.3709	0.1143
2	2.4094	0.1115
3	2.2623	0.1198
4	2.3798	0.1139
5	2.3383	0.1159
6	2.3588	0.1149
7	2.3123	0.1172
8	2.2829	0.1187
9	2.2992	0.1179
10	2.2858	0.1186
average	2.32997	0.11627
stdev	0.04873146	0.00261579
stdev %	2.09150611	2.24975094

Sample Na	RQ_L1_03_1		Sample Na	RQ_L1_03_2		Sample Na	RQ_L1_03_3		Sample Na	RQ_L1_03_4	
	δ_{skel}	V_{skel}		δ_{skel}	V_{skel}		δ_{skel}	V_{skel}		δ_{skel}	V_{skel}
Run			Run			Run			Run		
1	2.3909	0.1548	1	2.4849	0.1135	1	2.4213	0.1384	1	2.3457	0.0891
2	2.3213	0.1594	2	2.4565	0.1148	2	2.4485	0.1368	2	2.2713	0.092
0	2.3325	0.1586	3	2.4818	0.1136	3	2.5112	0.1334	3	2.2856	0.0914
4	2.3556	0.1571	4	2.4136	0.1168	4	2.4902	0.1345	4	2.2548	0.0927
5	2.3231	0.1593	5	2.4343	0.1158	5	2.4346	0.1376	5	2.2139	0.0944
6	2.3017	0.1607	6	2.4241	0.1163	6	2.4281	0.138	6	2.2356	0.0935
7	2.3765	0.1557	7	2.3637	0.1193	7	2.426	0.1381	7	2.2184	0.0942
8	2.298	0.161	8	2.3635	0.1193	8	2.3803	0.1407	8	2.2686	0.0921
9	2.2975	0.161	9	2.439	0.1156	9	2.427	0.138	9	2.2326	0.0936
10	2.3665	0.1563	10	2.4341	0.1159	10	2.4274	0.138	10	2.1744	0.0961
average	2.33636	0.15839	5.5	2.42955	0.11609	5.5	2.43946	0.13735	5.5	2.25009	0.09291
stdev	0.03409931	0.00228544	3.02765	0.04168064	0.00200247	3.02765	0.03691902	0.00206142	3.02765	0.04687538	0.00192091
stdev %	1.45950564	1.44291747	55.04819	1.71557055	1.72492953	55.04819	1.51340938	1.50085043	55.04819	2.08326677	2.06749365

Sample Na	RQ_L1_03_5	
	δ_{skel}	V_{skel}
Run		
1	2.113	0.1264
2	2.1384	0.1249
3	2.0882	0.1279
4	2.0956	0.1274
5	2.0424	0.1307
6	2.0783	0.1285
7	2.0522	0.1301
8	2.0302	0.1315
9	2.027	0.1317
10	2.0248	0.1319
5.5	2.06901	0.1291
3.02765	0.03962032	0.00243903
55.04819	1.91494104	1.88925981

Sample Na	RQ_L1_03_6	
	δ_{skel}	V_{skel}
Run		
1	2.2682	0.0648
2	2.2457	0.0655
3	2.2156	0.0664
4	2.2156	0.0664
5	2.1926	0.067
6	2.2059	0.0666
7	2.1475	0.0685
8	2.2879	0.0643
9	2.1395	0.0687
10	2.1571	0.0681
5.5	2.20756	0.06663
3.02765	0.05025248	0.00149967
55.04819	2.27638108	2.25073785

Sample Na	RQ_L1_03_7	
	δ_{skel}	V_{skel}
Run		
1	2.0866	0.0752
2	2.0699	0.0759
3	2.0276	0.0774
4	2.0091	0.0781
5	2.0167	0.0779
6	2.0919	0.0751
7	1.9802	0.0793
8	2.0809	0.0754
9	1.9831	0.0792
10	1.9926	0.0788
5.5	2.03386	0.07723
3.02765	0.0444308	0.0016879
55.04819	2.18455548	2.1855472

Sample Na	RQ_L1_03_8	
	δ_{skel}	V_{skel}
Run		
1	2.0331	0.1053
2	2.0855	0.1026
3	2.1001	0.1019
4	2.1181	0.101
5	2.1172	0.1011
6	2.0525	0.1043
7	2.0742	0.1032
8	2.0589	0.1039
9	2.0227	0.1058
10	2.0742	0.1032
5.5	2.07365	0.10323
3.02765	0.03269068	0.00163846
55.04819	1.57648012	1.58719494

Sample Na	RQ_L1_03_9	
	δ_{skel}	V_{skel}
Run		
1	2.1873	0.1152
2	2.246	0.1122
3	2.2203	0.1135
4	2.2663	0.1112
5	2.2887	0.1101
6	2.2428	0.1124
7	2.2389	0.1126
8	2.2444	0.1123
9	2.1589	0.1167
10	2.1571	0.1168
5.5	2.22507	0.1133
3.02765	0.04411316	0.00225142
55.04819	1.98255173	1.9871309

Sample Na	RQ_L1_03_10	
	δ_{skel}	V_{skel}
Run		
1	2.2836	0.1498
2	2.3298	0.1468
3	2.2549	0.1517
4	2.2475	0.1522
5	2.174	0.1573
6	2.2547	0.1517
7	2.2253	0.1537
8	2.2119	0.1546
9	2.2007	0.1554
10	2.2267	0.1536
5.5	2.24091	0.15268
3.02765	0.04413886	0.00296903
55.04819	1.96968454	1.94460655

	Vb	Mg		dc		ds			Porosity		
	Input	Input	Input								
			Pycnometer								
	GeoPyc	Scale	Lapilli								
Sample	Bulk volume	dry wt	N-skeletal volume	skeletal density	Solid volume	solid density		ϕconn	ϕbulk	ϕiso	Bulk density
	cm3	g	cm3	g/cm3	cm3	g/cm3	weight of powder				
	Av vbulk	weight of sample	Av vskel	C/D	C/G	Assume av solid density	sample				
Y2-1	0.2276	0.114	0.07512	1.517571885	0.052738278	2.06681	0.109	66.99472759	88.987861	21.99313	0.500879
Taupo Y2_2	0.189	0.18	0.10384	1.733436055	0.079827071	2.22982	0.178	45.05820106	91.52398	46.46578	0.952381
Taupo Y2_3	0.3115	0.236	0.13922	1.695158742	0.103659169	2.21881	0.23	55.30658106	85.960943	30.65436	0.757624
Taupo Y2_4	0.2466	0.131	0.10745	1.219171708	0.049342169	2.59413	0.128	56.42741281	90.493923	34.06651	0.531225
Taupo Y2_5	0.2305	0.189	0.14131	1.337484962	0.082193523	2.20212	0.181	38.69414317	89.532814	50.83867	0.819957
Taupo Y2_6	0.2778	0.214	0.14224	1.504499438	0.099341261	2.07366	0.206	48.79769618	86.603397	37.8057	0.770338
Taupo Y2_7	0.2332	0.128	0.10501	1.21893153	0.059312846	2.05689	0.122	54.96998285	88.662495	33.69251	0.548885
Taupo Y2_8	0.2405	0.165	0.11203	1.47281978	0.078414771	2.07869	0.163	53.41787942	88.430213	35.01233	0.686071
Taupo Y2_9	0.2405	0.141	0.1011	1.394658754	0.09079246	1.51995	0.138	57.96257796	84.177111	26.21453	0.586279
Taupo Y2_10	0.2939	0.136	0.10147	1.340297625	0.060980327	2.19743	0.134	65.47465124	86.625285	21.15063	0.462742
	0.24911	0.1634		1.443403048		2.123831		54.31038533	88.099802	33.78942	0.661638
Taupo Y5_1	0.4499	0.227	0.12954	1.752354485	0.087311282	2.55408	0.223	71.20693487	82.385047	11.17811	0.504557
Taupo Y5_2	0.3716	0.138	0.07702	1.791742405	0.045865417	2.987	0.137	79.27341227	87.559424	8.286012	0.371367
Taupo Y5_3	0.4205	0.297	0.14119	2.10354841	0.117590206	2.4832	0.292	66.42330559	83.066205	16.6429	0.706302
Taupo Y5_4	0.3622	0.196	0.10467	1.87255183	0.076048367	2.49841	0.19	71.10160133	85.50278	14.40118	0.541137
Taupo Y5_5	0.3622	0.239	0.12595	1.897578404	0.092432029	2.53159	0.234	65.22639426	85.692786	20.46639	0.659856
Taupo Y5_6	0.3622	0.202	0.10696	1.88855647	0.07799404	2.57712	0.201	70.46935395	85.945552	15.4762	0.557703
Taupo Y5_7	0.4311	0.312	0.18115	1.722329561	0.122392233	2.52467	0.309	57.9795871	82.924501	24.94491	0.72373
Taupo Y5_8	0.2295	0.162	0.09307	1.740625336	0.063899805	2.50392	0.16	59.44662309	90.834372	31.38775	0.705882
Taupo Y5_9	0.4597	0.41	0.19514	2.101055652	0.16366942	2.48061	0.406	57.55057646	81.468268	23.91769	0.891886
Taupo Y5_10	0.3096	0.166	0.08146	2.037809968	0.062131452	2.62347	0.163	73.68863049	88.198836	14.51021	0.536176
	0.37585	0.2349		1.890815252		2.576407		67.23664194	85.357777	18.12114	0.61986

KA01_1	0.1753	0.187	0.09639	1.940035273	0.067711139	2.67312	0.181	45.01426127	93.44212	48.42786	1.066743
KA01_2	0.2142	0.194	0.10576	1.834341906	0.075599183	2.53971	0.192	50.62558357	91.565966	40.94038	0.905696
KA01_3	0.2768	0.26	0.15465	1.681215648	0.104140074	2.46783	0.257	44.12933526	88.783668	44.65433	0.939306
KA01_4	0.2816	0.301	0.16538	1.820050792	0.106883974	2.78807	0.298	41.27130682	89.899823	48.62852	1.068892
KA01_5	0.2619	0.27	0.14791	1.825434386	0.093081849	2.8577	0.266	43.5242459	90.835287	47.31104	1.030928
KA01_6	0.2992	0.389	0.16069	2.420810256	0.155584638	2.46811	0.384	46.2934492	87.877364	41.58391	1.300134
KA01_7	0.2573	0.25	0.12038	2.076756936	0.076298453	3.2635	0.249	53.21414691	92.115827	38.90168	0.971628
KA01_8	0.2607	0.354	0.15816	2.238239757	0.121630125	2.84469	0.346	39.33256617	90.835557	51.50299	1.357883
KA01_9	0.2396	0.3	0.1283	2.33826968	0.104625512	2.81958	0.295	46.4524207	91.50228	45.04986	1.252087
KA01_10	0.3178	0.518	0.23428	2.211029537	0.198378336	2.5406	0.504	26.28067967	87.491144	61.21046	1.629956
	0.25844	0.3023		2.038618417		2.726291		43.61379955	90.434904	46.8211	1.152325
KR01_1	0.2835	0.182	0.08381	2.171578571	0.074055169	2.39011	0.177	70.43738977	88.138621	17.70123	0.641975
KR01_2	0.3821	0.221	0.12788	1.728182671	0.081402726	2.61662	0.213	66.53232138	85.397192	18.86487	0.578383
KR01_3	0.2736	0.167	0.08351	1.999760508	0.056385678	2.8376	0.16	69.47733918	90.358049	20.88071	0.61038
KR01_4	0.3196	0.197	0.11499	1.713192452	0.080403787	2.37551	0.191	64.02065081	86.546047	22.5254	0.616395
KR01_5	0.2638	0.15	0.08044	1.864743909	0.049454286	2.91178	0.144	69.50720243	90.94025	21.43305	0.568613
KR01_6	0.2784	0.14	0.07479	1.871908009	0.058235297	2.30101	0.134	73.13577586	87.900965	14.76519	0.502874
KR01_7	0.2661	0.155	0.09347	1.658286081	0.052573039	2.79611	0.147	64.87410748	90.483207	25.6091	0.582488
KR01_8	0.3519	0.211	0.11014	1.915743599	0.07797879	2.62892	0.205	68.70133561	86.614275	17.91294	0.599602
KR01_9	0.2218	0.161	0.08646	1.862132778	0.064942047	2.32515	0.151	61.01893598	90.46083	29.44189	0.725879
KR01_10	0.2495	0.148	0.08675	1.706051873	0.0636723	2.26158	0.144	65.23046092	88.96789	23.73743	0.593186
	0.28903	0.1732		1.849158045		2.544439		67.29355194	88.580733	21.28718	0.601978
RQ_L1_01_1	0.3965	0.261	0.07544	3.459703075	0.062605069	4.00926	0.251	80.97351828	90.110394	9.136876	0.65826
RQ_L1_01_2	0.367	0.455	0.1512	3.009259259	0.155441134	2.88212	0.448	58.80108992	87.266318	28.46523	1.239782
RQ_L1_01_3	0.2944	0.369	0.11353	3.250242227	0.131708681	2.71812	0.358	61.43682065	89.168984	27.73216	1.253397
RQ_L1_01_4	0.3387	0.227	0.06705	3.385533184	0.065043343	3.38236	0.22	80.20372011	89.986282	9.782562	0.67021
RQ_L1_01_5	0.3495	0.295	0.11227	2.627594193	0.102619672	2.78699	0.286	67.8769671	87.459589	19.58262	0.844063
RQ_L1_01_6	0.3245	0.508	0.18233	2.786156968	0.173704933	2.84966	0.495	43.81201849	88.612677	44.80066	1.565485
RQ_L1_01_7	0.3665	0.514	0.16581	3.099933659	0.193715353	2.61208	0.506	54.7585266	85.969036	31.21051	1.402456
RQ_L1_01_8	0.3415	0.442	0.15929	2.774813234	0.180080173	2.43225	0.438	53.35578331	85.959503	32.60372	1.29429
RQ_L1_01_9	0.3525	0.321	0.12	2.675	0.119568162	2.5843	0.309	65.95744681	86.359943	20.4025	0.910638

RQ_L1_01_10	0.2887	0.255	0.11101	2.297090352	0.106974379	2.28092	0.244	61.54832006	87.342827	25.79451	0.88327
	0.34198	0.3647		2.936532615		2.853806		62.87242113	87.823555	24.95113	1.072185
RQ_L1_02_1	0.3387	0.304	0.10896	2.790014684	0.114365254	2.65815	0.304	67.829938	87.258055	19.42812	0.897549
RQ_L1_02_2	0.377	0.315	0.10433	3.019265791	0.131331535	2.39851	0.315	72.32625995	84.281908	11.95565	0.835544
RQ_L1_02_3	0.3373	0.243	0.08656	2.807301294	0.099856174	2.4335	0.243	74.33738512	86.139306	11.80192	0.720427
RQ_L1_02_4	0.3575	0.277	0.10112	2.73931962	0.121699398	2.2761	0.277	71.71468531	84.293309	12.57862	0.774825
RQ_L1_02_5	0.3758	0.297	0.12043	2.466162916	0.065247479	4.5519	0.297	67.95369878	91.744107	23.79041	0.790314
RQ_L1_02_6	0.3724	0.268	0.091	2.945054945	0.097706094	2.74292	0.268	75.56390977	86.423228	10.85932	0.719656
RQ_L1_02_7	0.4633	0.372	0.14413	2.581003261	0.141355646	2.63166	0.372	68.89056767	82.395142	13.50457	0.802935
RQ_L1_02_8	0.3468	0.264	0.09816	2.689486553	0.093121365	2.83501	0.264	71.69550173	87.767239	16.07174	0.761246
RQ_L1_02_9	0.3736	0.265	0.06563	4.037787597	0.093020317	2.84884	0.265	82.43308351	86.88589	4.452807	0.709315
RQ_L1_02_10	0.3478	0.277	0.10464	2.647171254	0.118885651	2.32997	0.277	69.91374353	85.072769	15.15903	0.796435
	0.36902	0.2882		2.872256792		2.770656		72.26587734	86.226095	13.96022	0.780825
RQ_L1_03_1	0.3601	0.373	0.19649	1.898315436	0.158366005	2.33636	0.37	45.4346015	84.587136	39.15253	1.035823
RQ_L1_03_2	0.3598	0.288	0.14821	1.943188719	0.116070877	2.42955	0.282	58.80767093	85.190673	26.383	0.800445
RQ_L1_03_3	0.4473	0.34	0.18489	1.838931256	0.137325474	2.43946	0.335	58.66532529	81.663975	22.99865	0.760116
RQ_L1_03_4	0.2438	0.215	0.12769	1.683765369	0.092885173	2.25009	0.209	47.62510254	89.164878	41.53978	0.88187
RQ_L1_03_5	0.3215	0.272	0.14959	1.818303363	0.129047225	2.06901	0.267	53.47122862	84.461167	30.98994	0.846034
RQ_L1_03_6	0.3104	0.157	0.09732	1.61323469	0.066589357	2.20756	0.147	68.64690722	85.939227	17.29232	0.505799
RQ_L1_03_7	0.2599	0.163	0.11285	1.444395215	0.07719312	2.03386	0.157	56.57945364	87.221343	30.64189	0.627164
RQ_L1_03_8	0.3035	0.217	0.11636	1.864902028	0.103199672	2.07365	0.214	61.66062603	85.363972	23.70335	0.714992
RQ_L1_03_9	0.289	0.261	0.12334	2.116101832	0.113254864	2.22507	0.252	57.32179931	87.011645	29.68985	0.903114
RQ_L1_03_10	0.3527	0.345	0.16667	2.069958601	0.152616571	2.24091	0.342	52.7445421	84.260858	31.51632	0.978168
	0.3248	0.2631		1.829109651		2.230552		56.09572572	85.486487	29.39076	0.805353

Solid density	From crushed sample
Bulk density	dry weight/Vbulk

ϕconn	((Vbulk-vskel)/vbulk)	Porosity
ϕbulk	(1-(vbulk/solid density))*1	Porosity
ϕiso	ϕbulk-ϕconn	Porosity